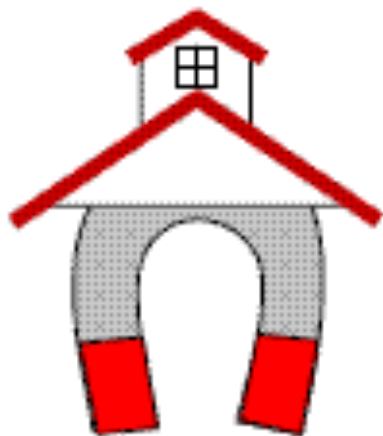




The 7th IEEE Magnetics Society Summer School

August 10-15, 2014

Rio de Janeiro, Brazil



Spintronics

Daniel E. Bürgler

Peter Grünberg Institute, Electronic Properties (PGI-6) and Jülich-Aachen Research Alliance (JARA-FIT)

Forschungszentrum Jülich, Germany

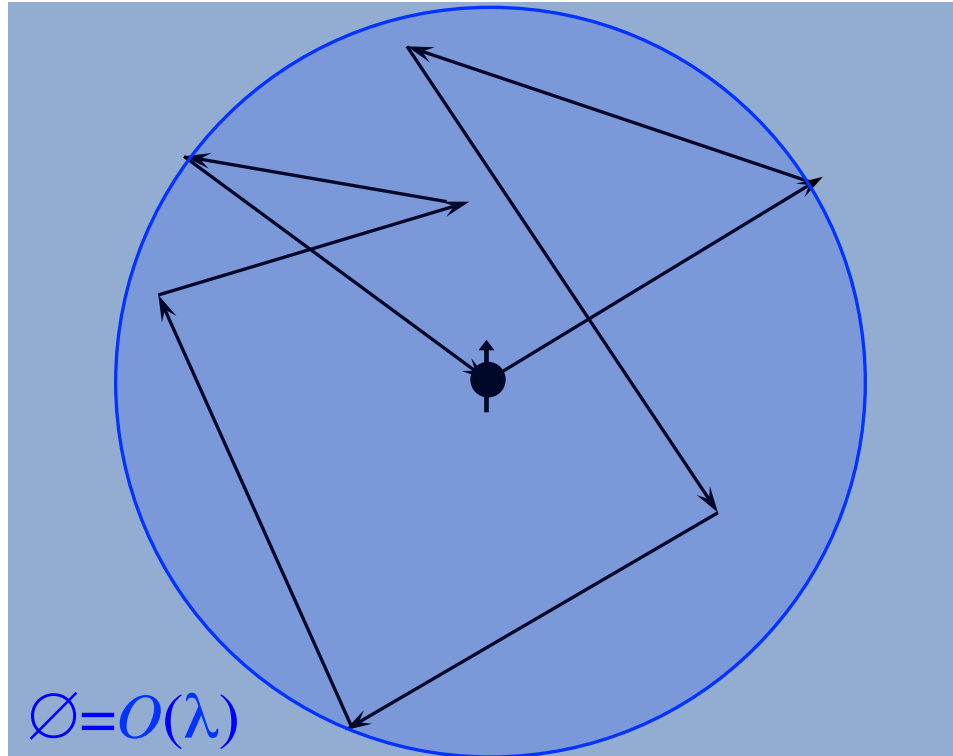
Rio de Janeiro

August 12, 2014

Conduction electrons in a solid

Conduction electrons move with Fermi velocity ($v_F \approx 10^6$ m/s) and undergo random scattering from defects, phonons, electrons

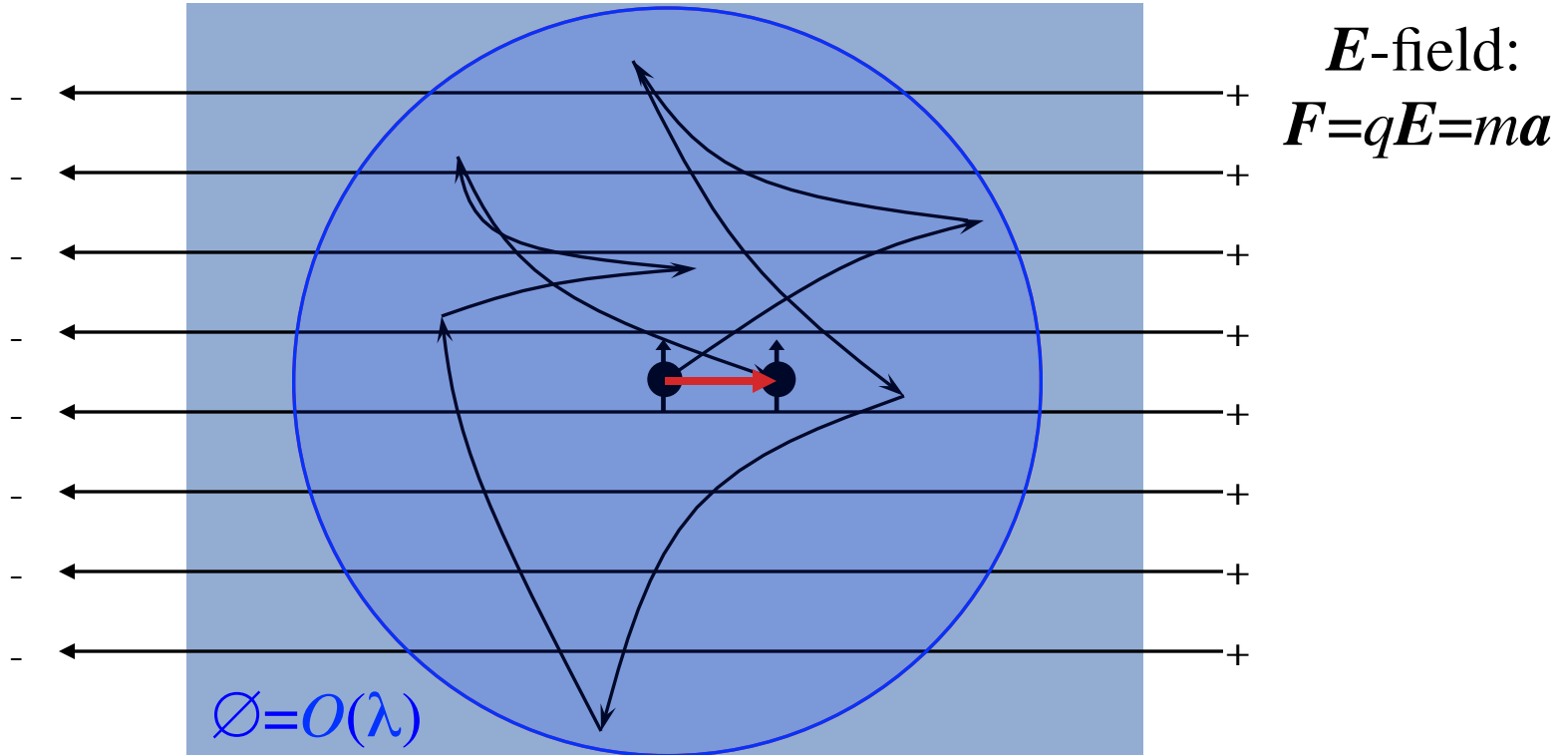
Relaxation time $\tau \approx 10^{-14} - 10^{-15}$ s \Rightarrow Mean free path $\lambda = v_F \tau \approx 1 - 10$ nm



\Rightarrow Conduction electrons experience the environment on a length scale given by the mean free path λ

Drift velocity

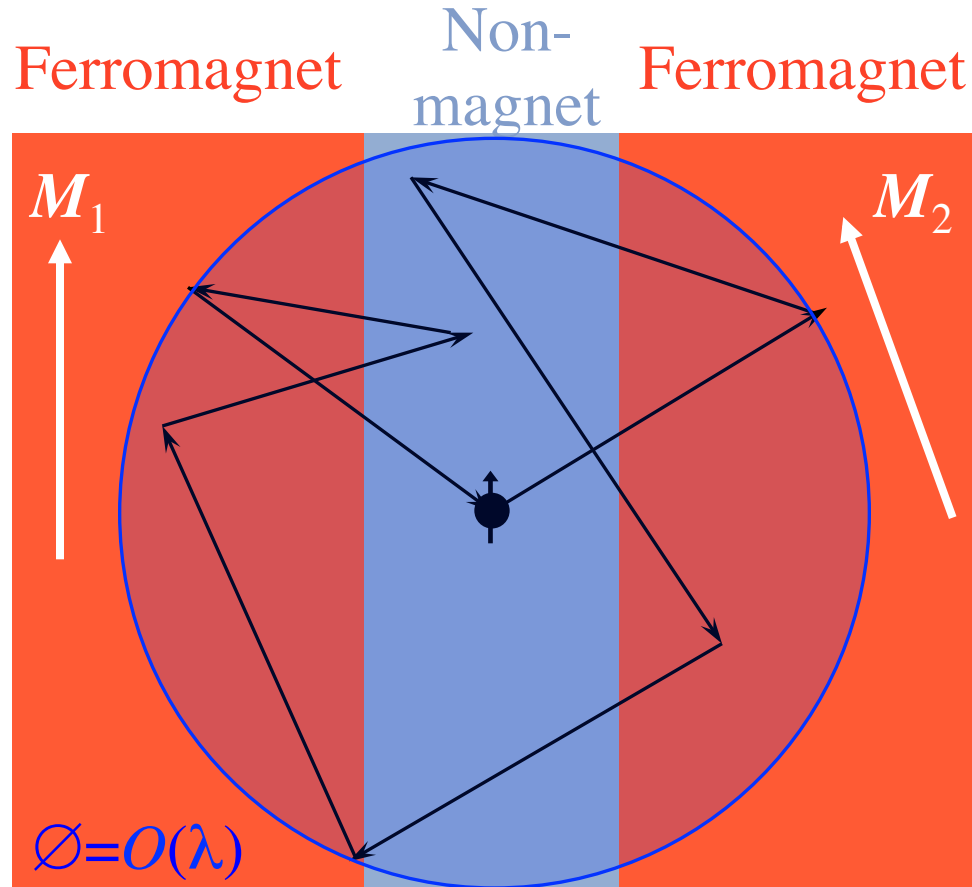
An electric field E superimposes a much lower drift velocity ($v_D \approx 10^3$ - 10^4 m/s) in the direction of the electric field:



$\Rightarrow E$ -field induces net transport of electrons, *i.e.* electrical current
 \Rightarrow Diffusive transport for $d \gg \lambda$ or ballistic transport for $d < \lambda$

Electrons in a multilayer

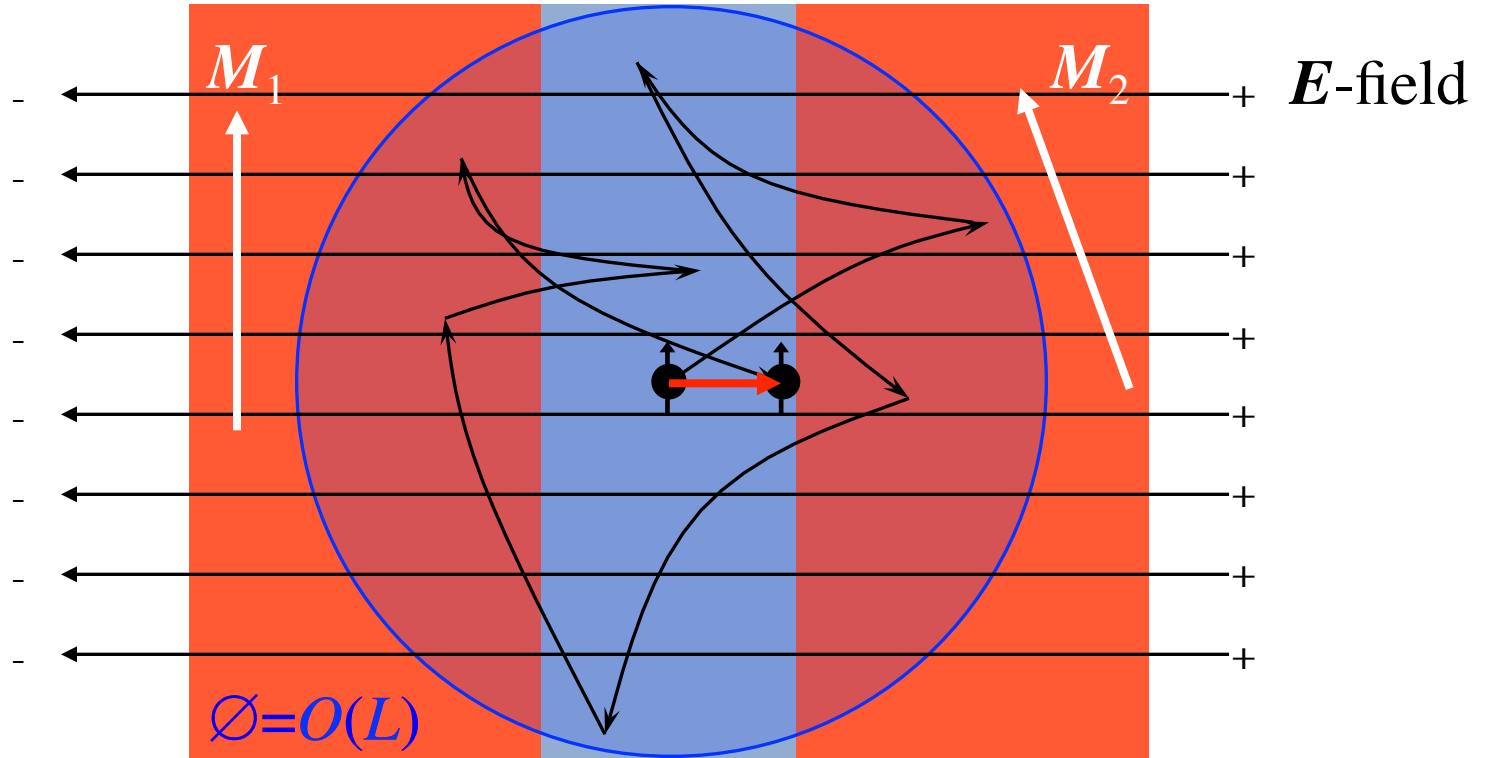
Consider multilayer with layer thicknesses less than λ .



⇒ Conduction electrons experience both magnetic layer
⇒ Static spin-transfer processes

Spin-transfer processes

Spin-flip scattering is less probable than momentum scattering
Spin-flip length exceeds to mean free path L



$\Rightarrow E$ -field gives rise to net charge and/or spin currents
 \Rightarrow Dynamic spin-transfer processes

Definition of spintronics

- Spintronics (magnetoelectronics) comprises all spin-dependent electronic transport phenomena.

⇒ Novel fundamental physics

- Spintronics make use of the spin degree of freedom of the electron in addition to (or instead of) its charge.

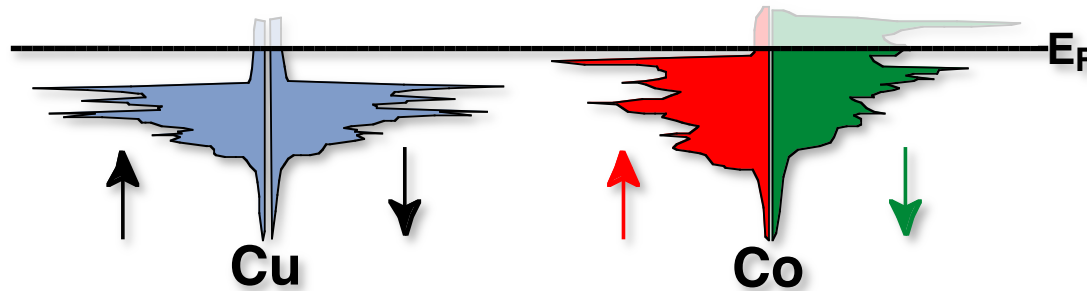
⇒ Spin transport *versus* charge transport

- Spintronics is a new paradigm of electronics based on the spin degree of freedom of the electron.

⇒ Novel prospects for applications in information technology

Spin-resolved density of states (SDOS)

Electrical transport is due to charge carriers close to the Fermi edge E_F



Unequal DOS for spin-up and spin-down in ferromagnets lead to a **polarization of the current**

IMPORTANT: Distinguish

- 1) Total occupation number for the two spin orientations: N_\uparrow and N_\downarrow
 \Rightarrow **Majority and minority spins; magnetization $M \propto (N_\uparrow - N_\downarrow)$**
- 2) Density of states at the Fermi edge E_F : $N_\uparrow(E_F)$ and $N_\downarrow(E_F)$
 \Rightarrow **Polarization P at E_F**

Spin polarization

An imbalance of spin-up and spin-down electrons (*e.g.* in a ferromagnet) can give rise to a spin-polarized current \Rightarrow **Spin-transport**

The **spin polarization** of a current $P_{current}$ is defined as

$$P_{current} = \frac{J^{\uparrow} - J^{\downarrow}}{J^{\uparrow} + J^{\downarrow}} \quad ; \quad |P_{current}| \leq 1 \quad ; \quad J^{\uparrow, \downarrow}: \text{current densities}$$

However, $J^{\uparrow, \downarrow}$ can hardly be measured directly.

\Rightarrow Various, system and experiment dependent “definitions” for the spin polarization of a current are used instead

Various definitions of spin polarization

$$P_{\text{current}} = \frac{J^{\uparrow} - J^{\downarrow}}{J^{\uparrow} + J^{\downarrow}} \quad ; \quad |P_{\text{current}}| \leq 1 \quad ; \quad J^{\uparrow, \downarrow}: \text{current densities}$$

Popular, but only for ground state valid definition (no current) :

$$P = \frac{N^{\uparrow}(E_F) - N^{\downarrow}(E_F)}{N^{\uparrow}(E_F) + N^{\downarrow}(E_F)} \quad ; \quad |P| \leq 1 \quad ; \quad N^{\uparrow, \downarrow}(E_F): \text{SDOS at Fermi edge}$$

$$\text{Ballistic transport: } J \propto \langle Nv \rangle \Rightarrow P_{Nv} = \frac{\langle Nv \rangle^{\uparrow} - \langle Nv \rangle^{\downarrow}}{\langle Nv \rangle^{\uparrow} + \langle Nv \rangle^{\downarrow}}$$

$$\text{Diffusive transport: } J \propto \langle Nv^2 \rangle \Rightarrow P_{Nv^2} = \frac{\langle Nv^2 \rangle^{\uparrow} - \langle Nv^2 \rangle^{\downarrow}}{\langle Nv^2 \rangle^{\uparrow} + \langle Nv^2 \rangle^{\downarrow}}$$

$v^{\uparrow, \downarrow}$: velocity ; $\langle \dots \rangle^{\uparrow, \downarrow}$ integral over Fermi surface of up or down states

\Rightarrow Spin polarization is NOT a uniquely defined quantity

I.I. Mazin, Phys. Rev. Lett. **83**, 1427 (1999)

Spin relaxation

In contrast to the charge the **spin of an electron is not conserved**.

Electrons in a solid undergo random scattering. Most scattering events are spin-conserving but change the electron momentum (direction)

⇒ **momentum scattering**, relaxation time τ

Some (1 in $n \approx 10^3$) scattering events transfer angular momentum (e.g. to the lattice by spin-orbit coupling) and flip the spin

⇒ **spin-flip scattering**, relaxation time $\tau_{\text{SF}} \gg \tau$

⇒ After $n = \tau_{\text{SF}} / \tau$ scattering events the spin-flip occurs. The characteristic length scale is the **spin diffusion length λ_{SF}** :

$$\lambda_{\text{SF}} = v_{\text{F}} \tau_{\text{SF}} \approx 1\text{-}10 \text{ nm for Py}$$

50 nm for Co

100 nm for Cu

(>10 μm for 2-DEG GaAs/GaAlAs or Si)

Decay of spin polarization

An imprinted (injected) **current spin polarization P** decays due to **spin-flip processes** to the equilibrium polarization P_0 :

$$P(x) = P_0 + (P - P_0) \exp(-x/\lambda_{\text{SF}}) \quad ; \quad x \text{ spatial coordinate}$$

Consider a ferromagnet with $P_0 \neq 0$. The unequal density of final states for the two spin directions yields asymmetric spin-flip scattering probabilities. Simple model:

$$\lambda_{\text{SF}}(P_0) = \lambda_{\text{SF}} / (1 - P_0^2)^{1/2} \quad \Rightarrow \quad P = \pm 1: \lambda_{\text{SF}}(P_0) = \infty$$

All electrons are majority electrons. Spin-flip is forbidden because there are no minority states at near the Fermi level.

\Rightarrow Strongly polarized materials show less spin relaxation

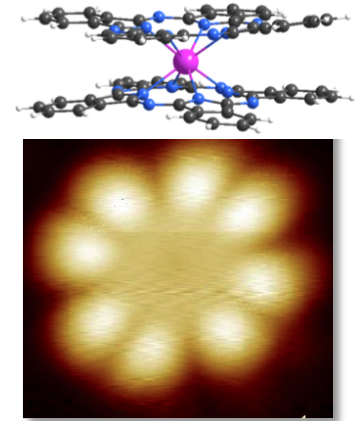
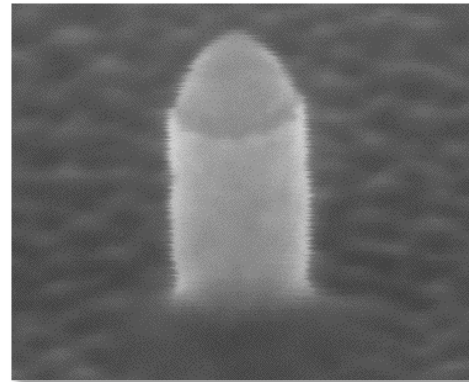
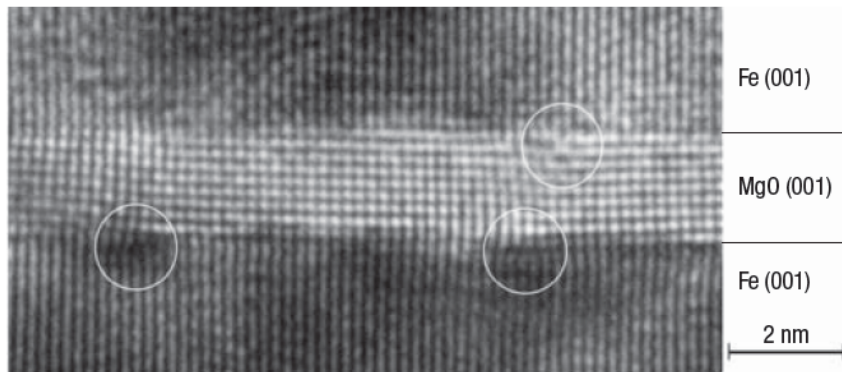
\Rightarrow Intense search for ferromagnetic half-metals (see later)

Spintronics – A nanotechnology

⇒ The spin state of an electron in a solid relaxes within a distance of typically few to several 100 nm (for metals)

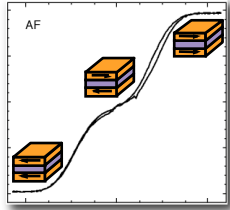
⇒ Need for nanostructures

⇒ Spintronics is intrinsically a nanotechnology

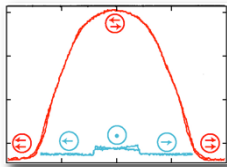


Overview: Spin transfer processes for spintronics

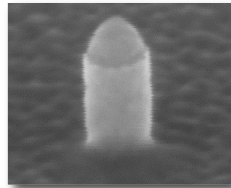
Introduction



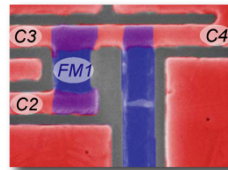
Interlayer exchange coupling



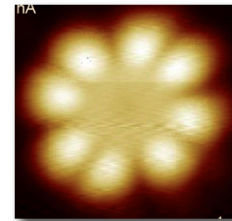
Giant and tunneling magnetoresistance



Current-induced magnetization dynamics



Pure spin current

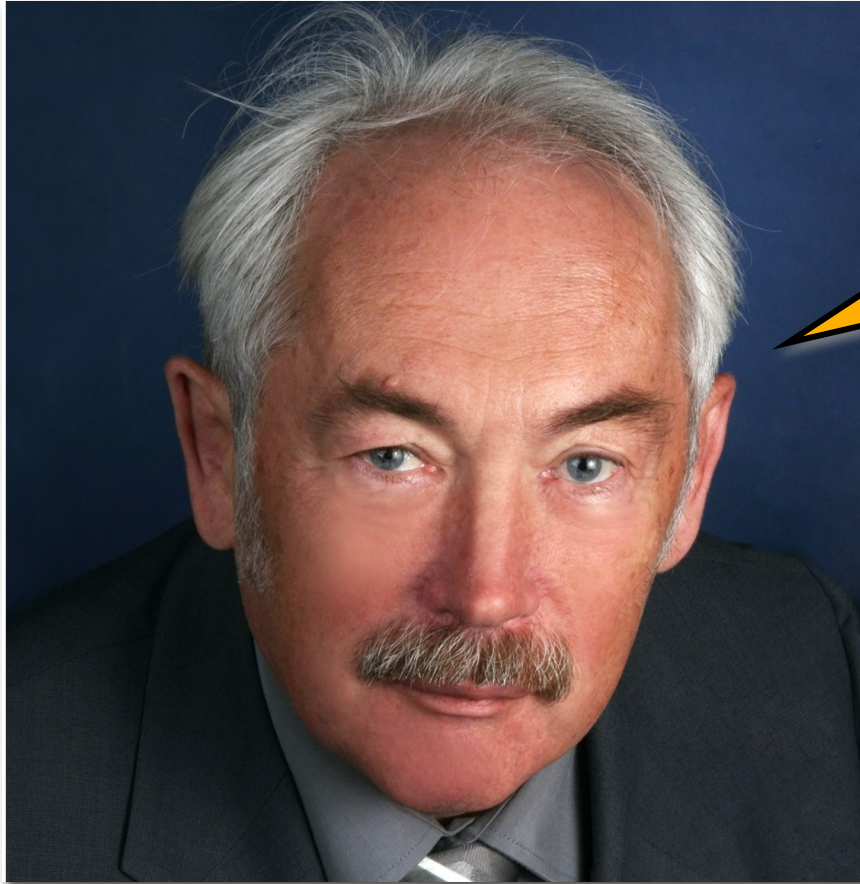


Magnetic molecules
(Time permitting)

Conclusions

Once upon a time, ...

Once upon a time, in the early 1980' s ...



Peter Grünberg

“What happens if I bring two ferromagnets close –I mean *really* close– together?”

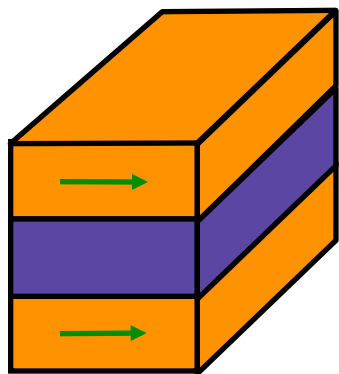


Phenomenology of Magnetic Interlayer Coupling

Consider two ferromagnetic layers separated by a thin spacer layer:

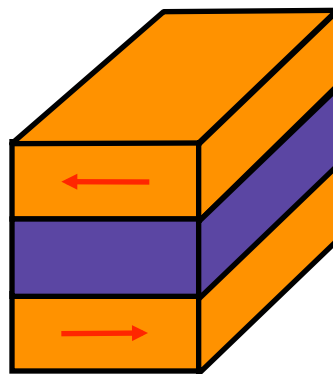
Ferromagnet / Non-Ferromagnet / Ferromagnet

The ferromagnetic layers interact across the spacer and align ...



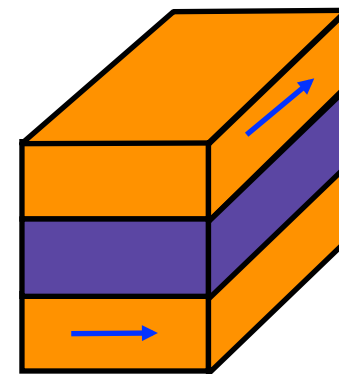
... parallel ...

“ferromagnetic
coupling”



... antiparallel ...

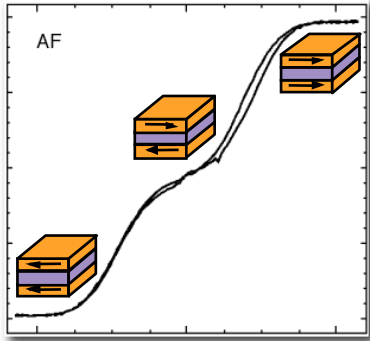
“antiferromagnetic
coupling”



... at 90° ...

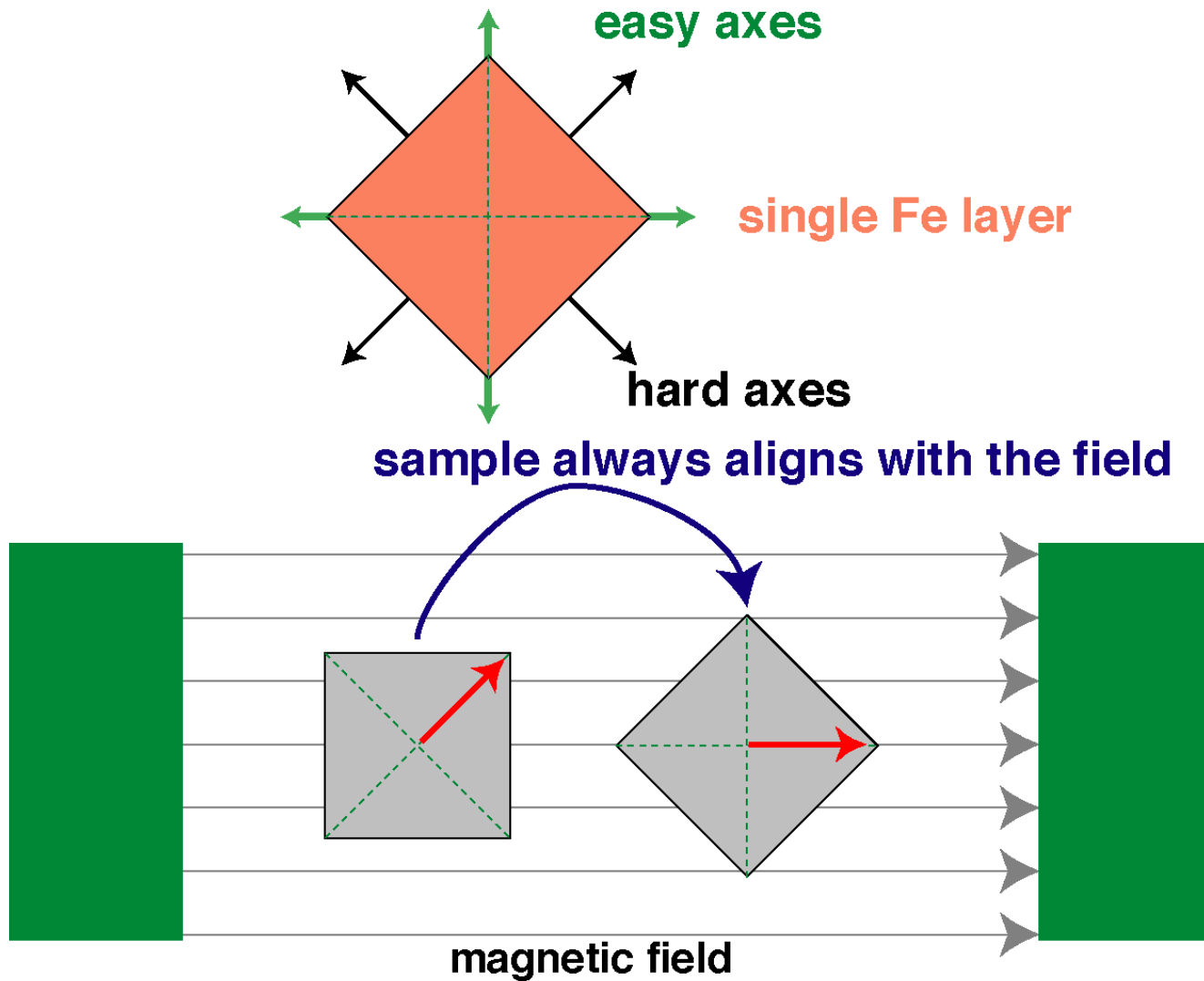
“biquadratic or
90°-coupling”

Outline: Interlayer exchange coupling

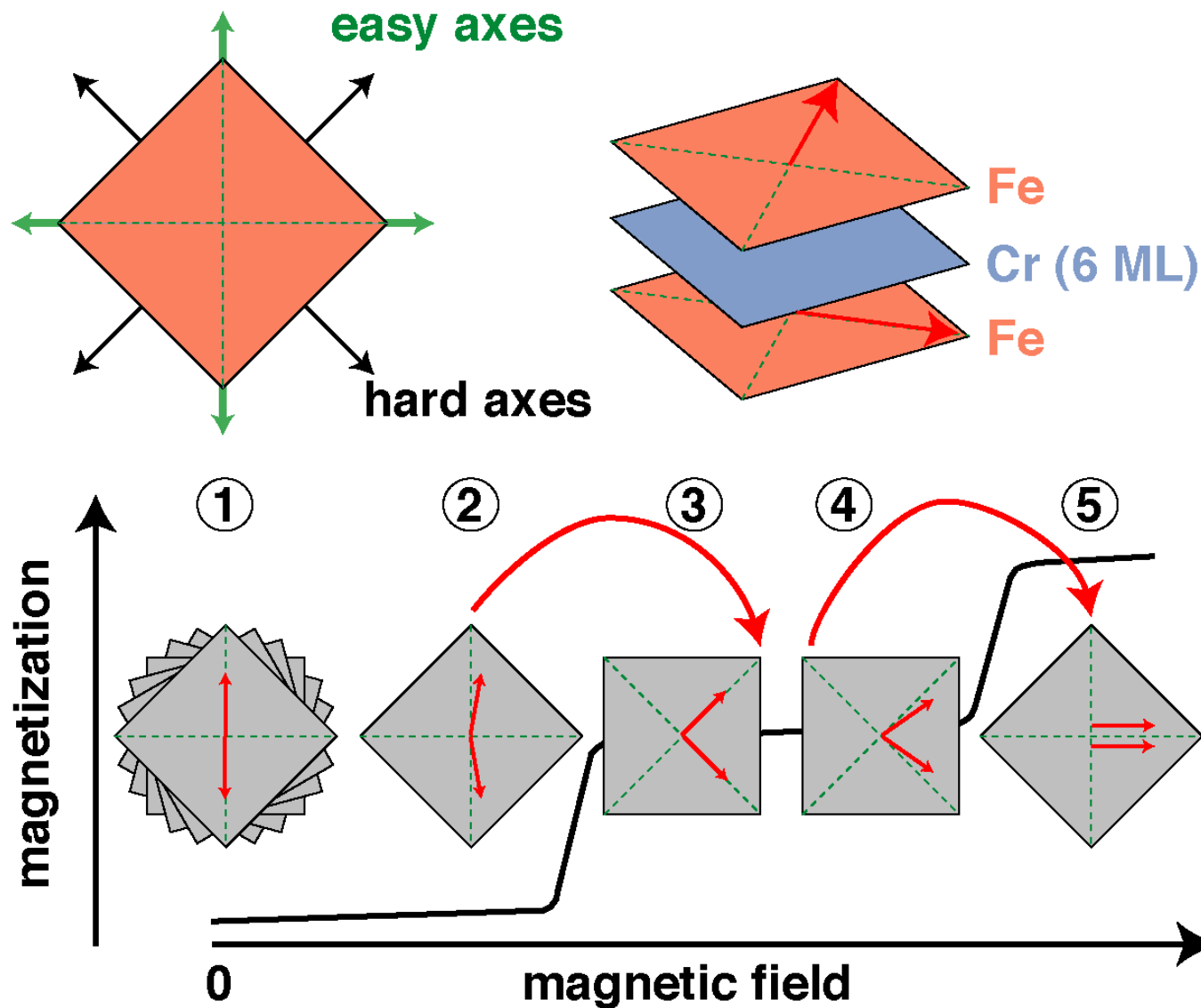


- Phenomenology of interlayer coupling
- Measurement by MOKE
- Physical picture for oscillatory bilinear coupling
- Biquadratic coupling
- Example: Morphology and “Fermiology”
- Applications
- Conclusions

Experiment: Anisotropy (“The normal compass”)



Experiment: Interlayer coupling ("The crazy compass")



Phenomenological description

Contribution of IEC to the areal free energy density:

$$E = -J_1 \cos(\Delta\Theta) - J_2 \cos^2(\Delta\Theta)$$

“bilinear” “biquadratic”

$\Delta\theta$ is the angle between the magnetizations of the two coupled layers.

J_1 and J_2 are parameters describing the coupling type:

$J_1 > 0$: FM coupling

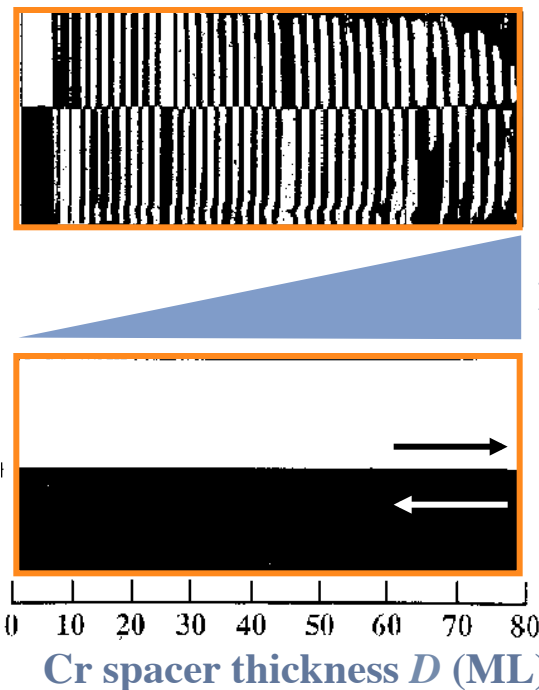
$J_1 < 0$: AF coupling

J_2 dominant and $J_2 < 0$: 90° coupling

Note: $J_1(D)$ oscillates as a function of the spacer thickness D

Oscillatory interlayer exchange coupling

- only occurs for thin spacers with a thickness of a few nm
- is observed for many metallic spacer layers
(see [1] for a “periodic table of interlayer coupling”)
- **oscillates as a function of the spacer thickness D**

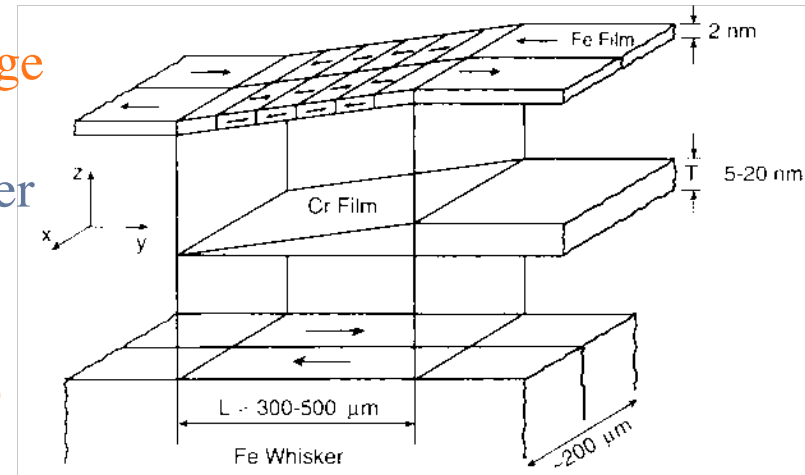


Scanning electron microscopy with spin analysis (SEMPA) [2]:

3) Domain picture of Fe layer grown on Cr wedge

2) Wedge-shaped Cr spacer

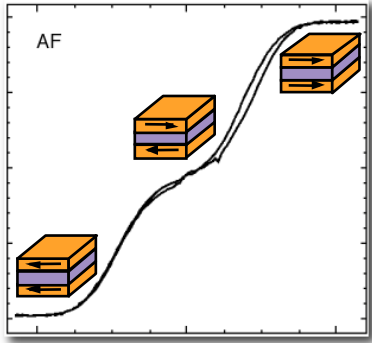
1) Domain picture of Fe single crystal (whisker) with two domains



[1] S.S.P. Parkin, Phys. Rev. Lett. **67**, 3598 (1991)

[2] D.T. Pierce *et al.*, Phys. Rev. B **49**, 14564 (1994)

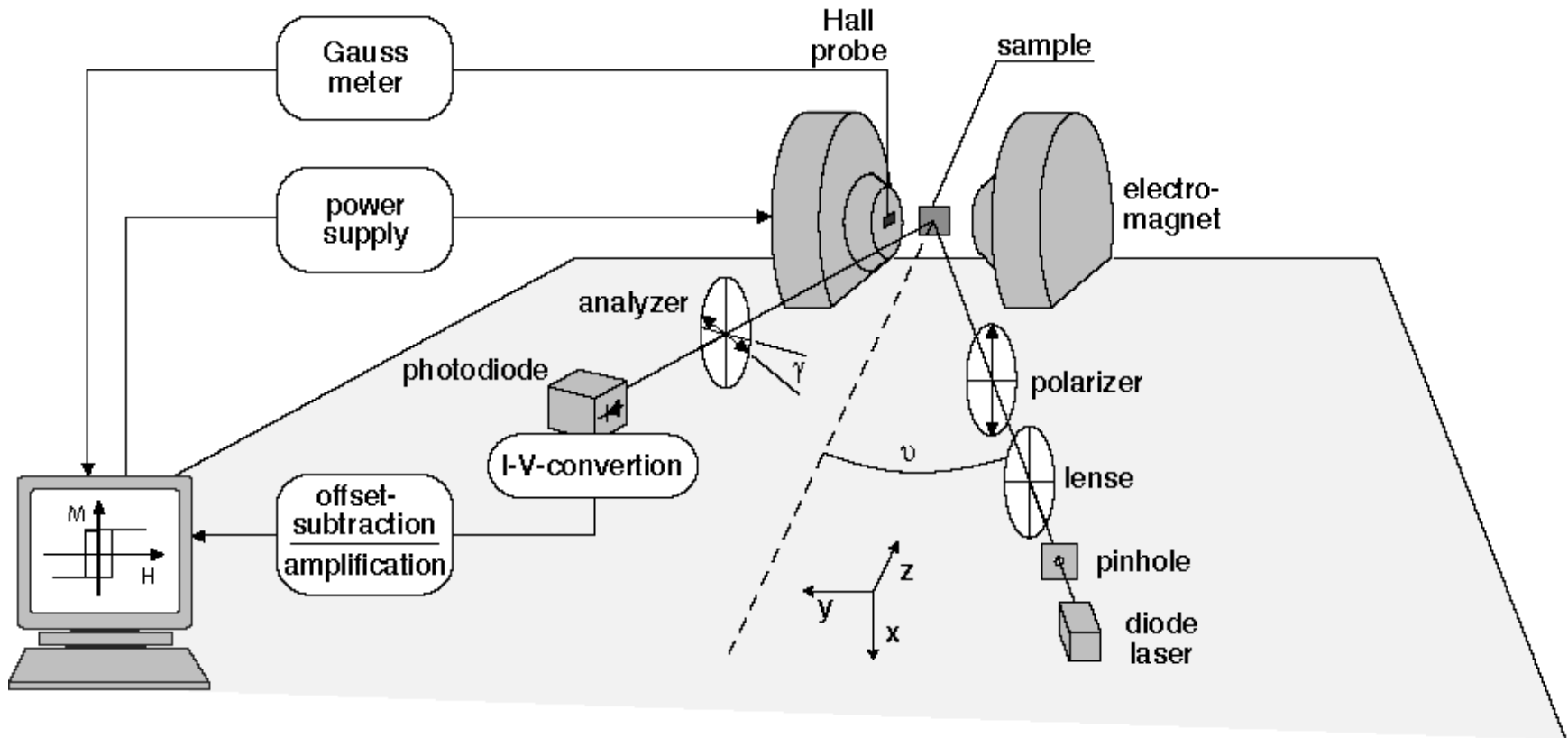
Outline: Interlayer exchange coupling



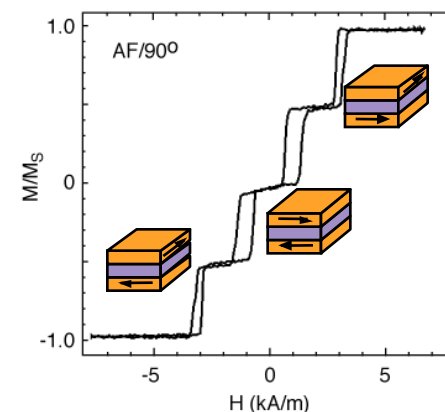
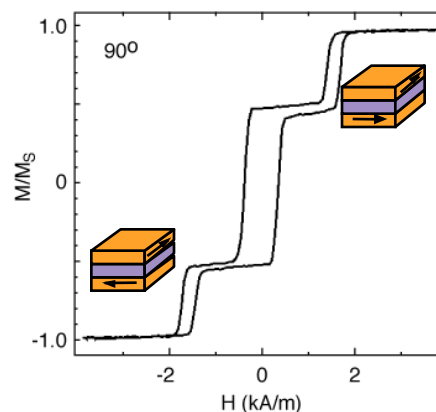
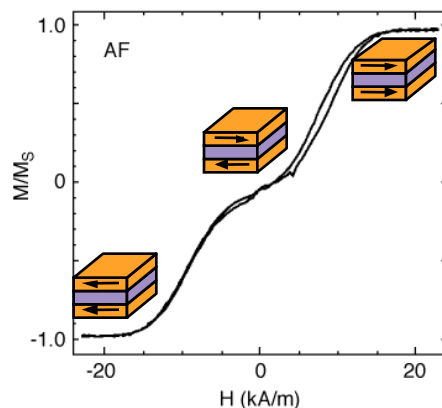
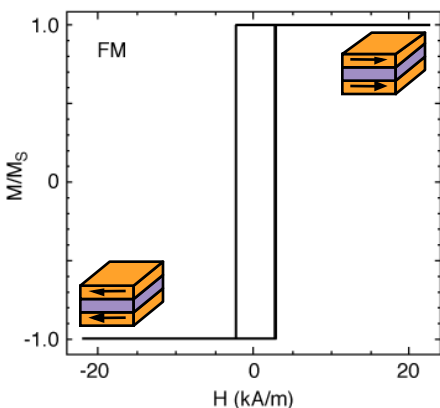
- Phenomenology of interlayer coupling
- **Measurement by MOKE**
- Physical picture for oscillatory bilinear coupling
- Biquadratic coupling
- Example: Morphology and “Fermiology”
- Applications
- Conclusions

MOKE setup

The magneto-optical Kerr effect is a simple means to measure hysteresis loops of thin films and multilayers. Any other method (*e.g.* SQUID, VSM, etc.) yielding hysteresis loops or sensitive to a local effective field (FMR, BLS) can be used to determine interlayer coupling.



Typical hysteresis loops for different types of interlayer coupling



FM coupling
or
decoupled

AF coupling

90° coupling

Dominant
90° plus AF
coupling

The saturation and switching fields are approximate measures for the coupling strength

BUT: A quantitative determination of the coupling needs fitting.

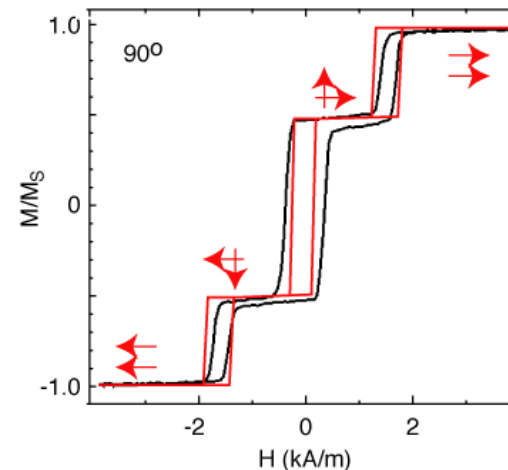
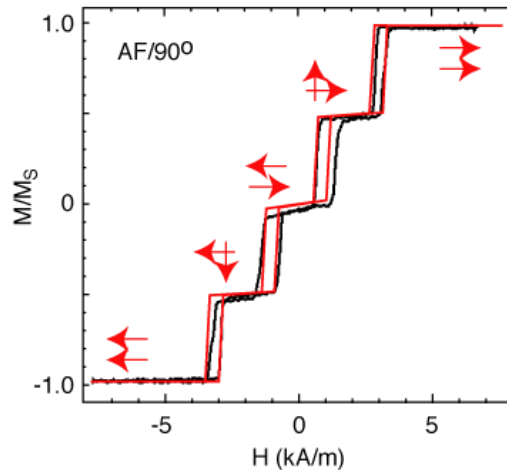
Phenomenological *ansatz* for a coupled trilayer

$$\begin{aligned}
 E(\Theta_1, \Theta_2) = & \\
 & - HM_s [d_1 \cos(\Theta_1) + d_2 \cos(\Theta_2)] \\
 & + \frac{1}{4} [K_1 d_1 \sin^2(2\Theta_1) + K_2 d_2 \sin^2(2\Theta_2)] \\
 & - J_1 \cos(\Theta_1 - \Theta_2) \\
 & - J_2 \cos^2(\Theta_1 - \Theta_2)
 \end{aligned}$$

Free energy per area =
 Zeemann energy
 + in-plane anisotropy
 + bilinear coupling
 + biquadratic coupling

Fitting procedure: Determine for each field H the magnetization alignment (θ_1, θ_2) that minimizes the free energy E . Examples for Fe/Cr/Fe(001):

$$\begin{aligned}
 J_1 &= -0.21 \text{ mJ/m}^2 \\
 J_2 &= -0.10 \text{ mJ/m}^2
 \end{aligned}$$



$$\begin{aligned}
 J_1 + J_2 &= \\
 & -0.16 \text{ mJ/m}^2 \\
 & \text{with} \\
 J_1 &< 2 J_2
 \end{aligned}$$

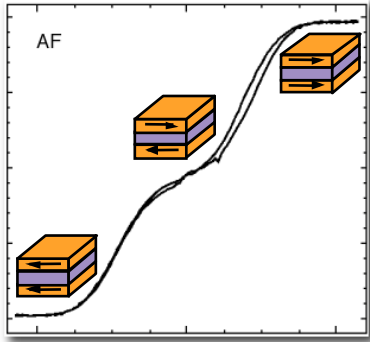
Typical bilinear coupling strengths

Sample	Maximum strength $-J_1$ in mJ/m^2 (at spacer thickness in nm)	Periods in ML and (nm)
Co/Cu/Co (100)	0.4 (1.2)	2.6 (0.47); 8 (1.45)
Co/Cu/Co (110)	0.7 (0.85)	9.8 (1.25)
Co/Cu/Co (111)	1.1 (0.85)	5.5 (1.15)
Fe/Au/Fe (100)	0.85 (0.82)	2.5 (0.51) ; 8.6 (1.75)
Fe/Cr/Fe (100)	> 1.5 (1.3)	2.1 (0.3); 12 (1.73)
Fe/Mn/Fe (100)	0.14 (1.32)	2 (0.33)
Co/Ru/Co (0001)	6 (0.6)	5.1 (1.1)
Co/Rh/Co (111)	34 (0.48) ?	2.7 (0.6)
Fe/Si/Fe (100)	6-8	---

Experimental values are often much smaller than theoretically predicted due to roughness, interdiffusion, etc.

Direct exchange in Fe: $J \approx \frac{k_B T_C}{a^2} = 170 \frac{\text{mJ}}{\text{m}^2} ; T_C = 1040 \text{ K}, a = 2.9 \text{ \AA}$

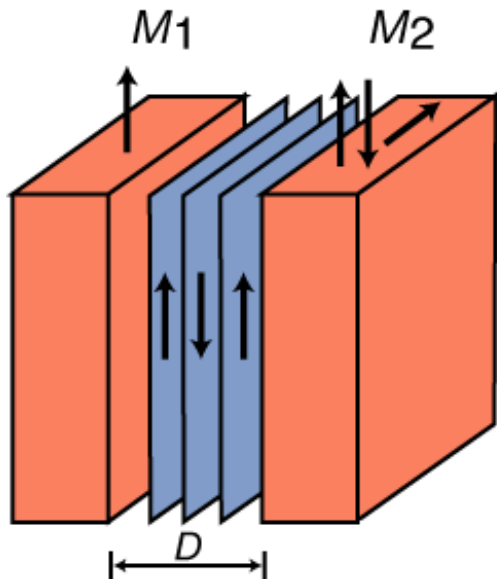
Outline: Interlayer exchange coupling



- Phenomenology of interlayer coupling
- Measurement by MOKE
- Physical picture for oscillatory bilinear coupling
- Biquadratic coupling
- Example: Morphology and “Fermiology”
- Applications
- Conclusions

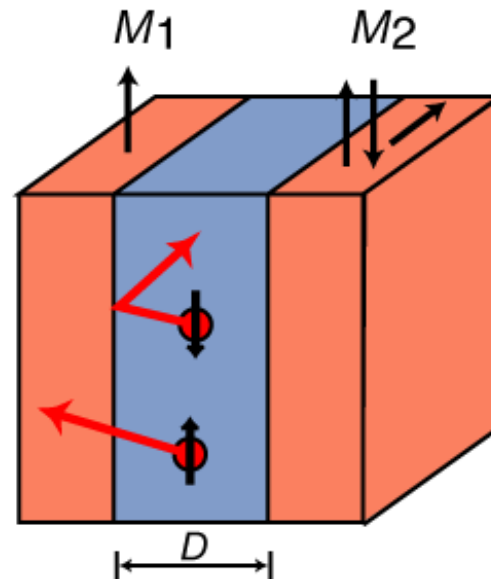
Origin of bilinear coupling

Distinguish antiferromagnetic and paramagnetic/diamagnetic spacers:



Direct exchange from layer to layer gives rise to oscillations with a period of two monolayers.

Possible example: Cr(001) spacers ?

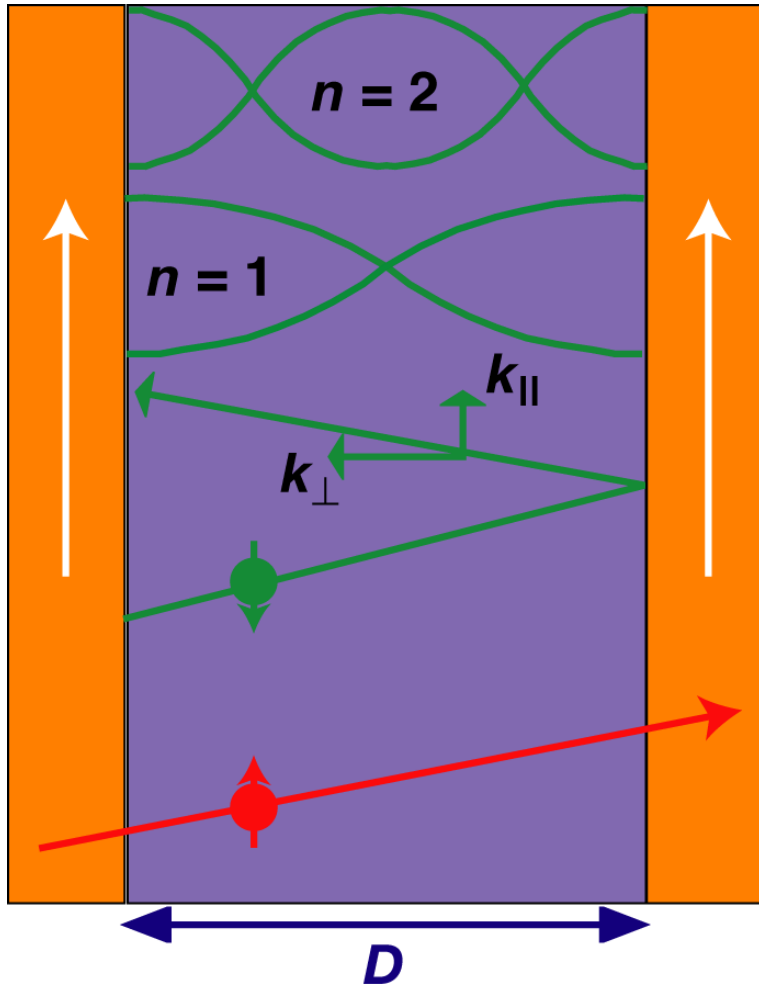


New explanation needed for diamagnetic/paramagnetic spacers without intrinsic magnetic order:

Conduction electrons in the spacer mediate the coupling!

Quantum interference model for bilinear coupling

Consider spin-dependent quantum well states (QWS) due to spin-dependent reflectivities at the interfaces between spacer and FM layers.



For a certain spacer thickness D there is a series of QWS fulfilling the condition:

$$D = n \frac{\lambda}{2} \quad ; \quad n = 1, 2, 3, \dots \quad \lambda = \frac{2\pi}{k_{\perp}}$$

$$\Rightarrow k_{\perp}^{(n)} = n \frac{\pi}{D} \quad ; \quad n = 1, 2, 3, \dots$$

$$\Rightarrow \text{A given } k_{\perp} \text{ yields a period: } \Delta D = \frac{\lambda}{2} = \frac{2\pi}{2k_{\perp}}$$

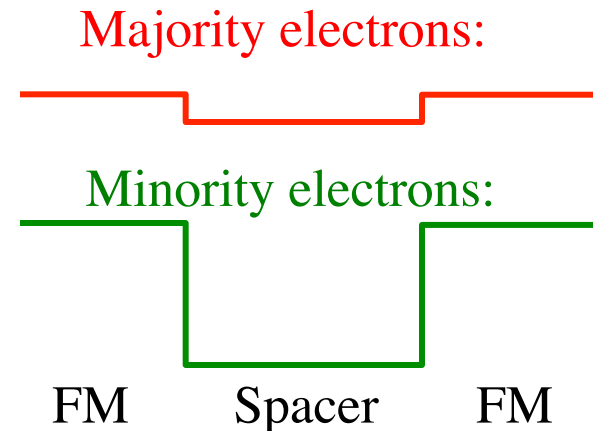
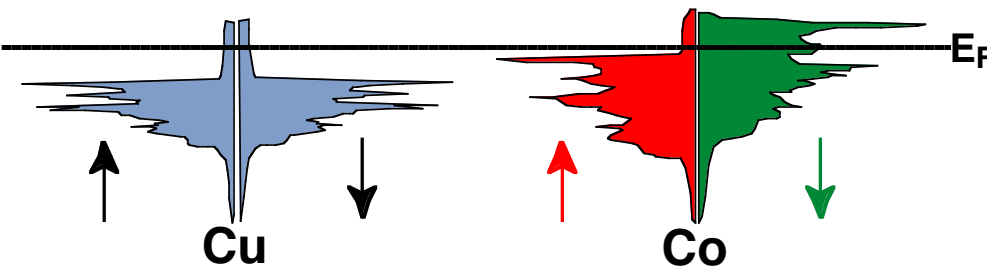
P. Bruno, Phys. Rev. B **52**, 411 (1995)

What is the origin of spin-dependent reflectivity?

Spin-dependent reflectivity arises from the “potential landscape” seen by the electrons due to the layered structure. The two spin channels experience different potential steps at the interfaces between the spacer and the FM layers.

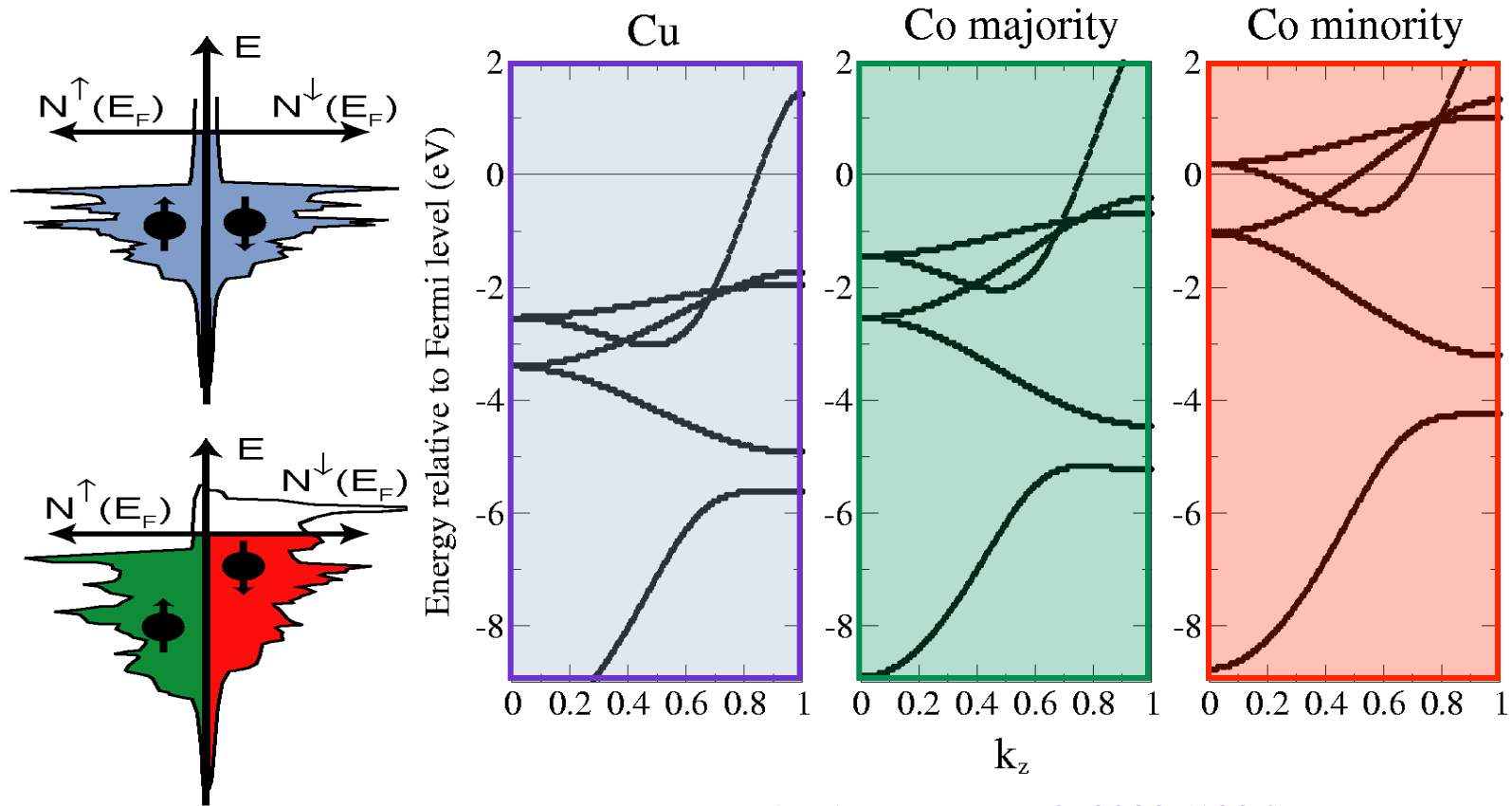
Example Co / Cu / Co:

Similar band structure (low potential steps and low reflectivity) for majority electrons and shifted band structure (high potential step and high reflectivity) for minority electrons:



Spin-dependent “Spaghetti diagrams” of Co and Cu

Example Co / Cu / Co: Similar band structure for Cu and majority electrons; shifted band structure for minority electrons:

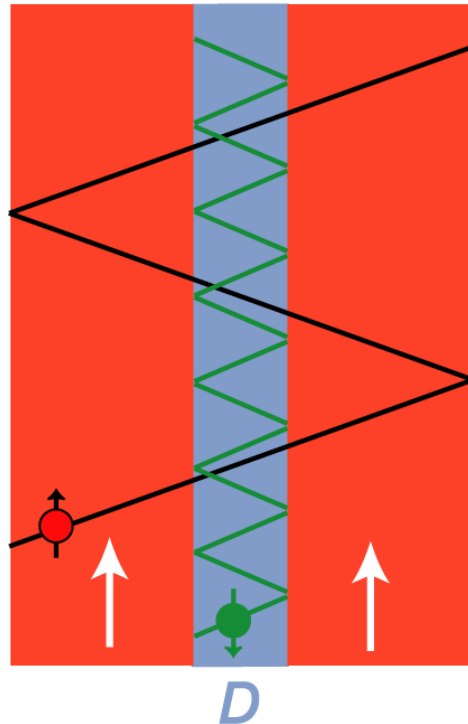


P. Lang *et al.*, Phys. Rev. B **53**, 9092 (1996)

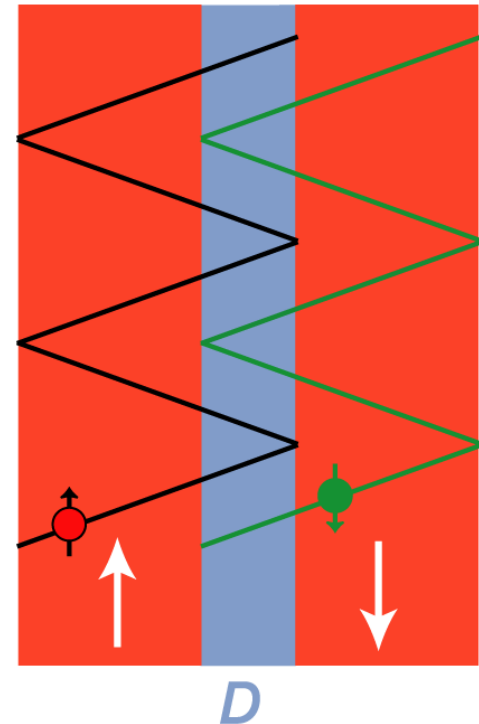
Interlayer exchange coupling

- Consider static case without external E -field
- Assume **spin-dependent interface reflection**

Parallel alignment:



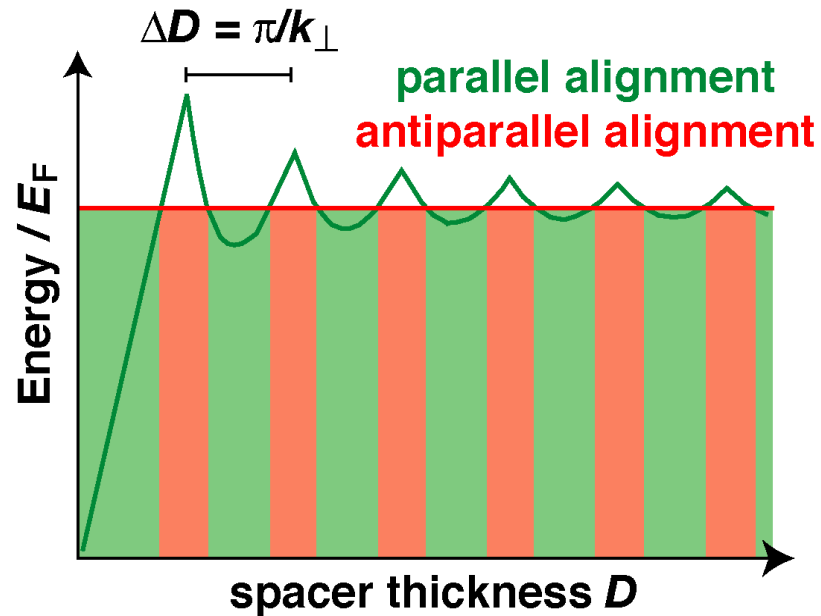
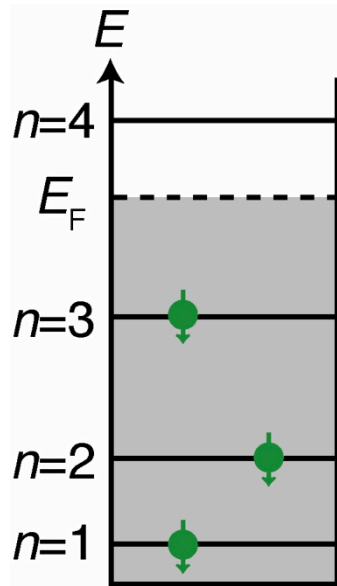
Antiparallel alignment:



⇒ Formation of spin-dependent quantum well states (QWS) for parallel, but not for antiparallel alignment of the FM layers

Quantum well states

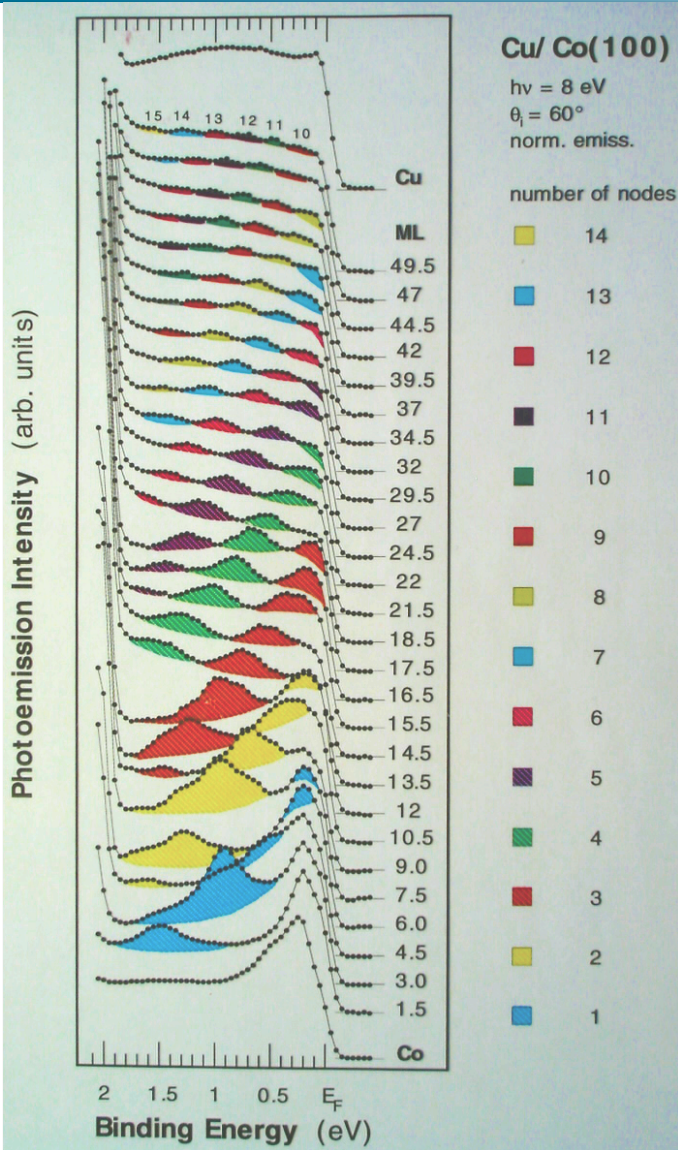
Energy of QWS related to k_{\perp} is quantized. Energy levels shift when the spacer thickness D is varied.



after
M. Stiles

\Rightarrow Interlayer exchange coupling oscillates
as a function of the spacer thickness D

Example: Cu/Co(100)

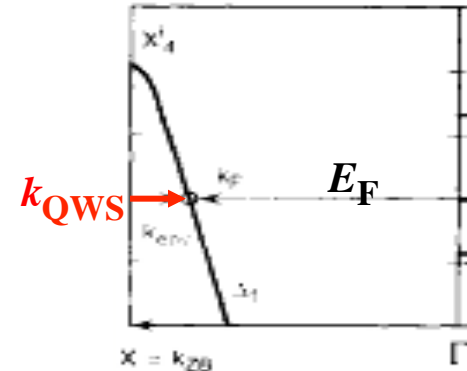


Angle-resolved photoemission:

The QWS **shift up** in energy with increasing D :

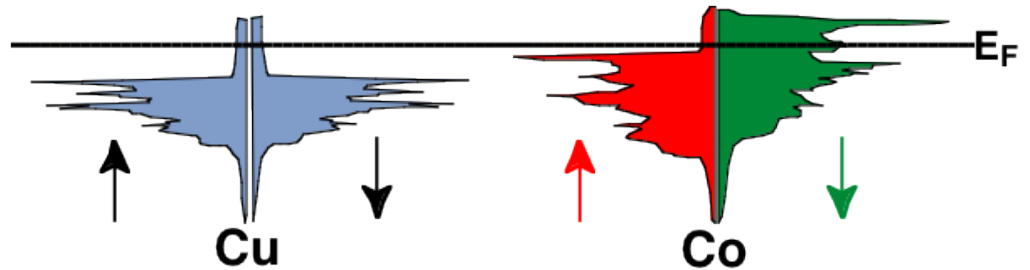
$$E \approx -k_{QWS}^2$$

at upper band edge.



The QWS cross the E_F at regular interval of 5-6 atomic layer, exactly corresponding to the oscillation period of $J(D)$.

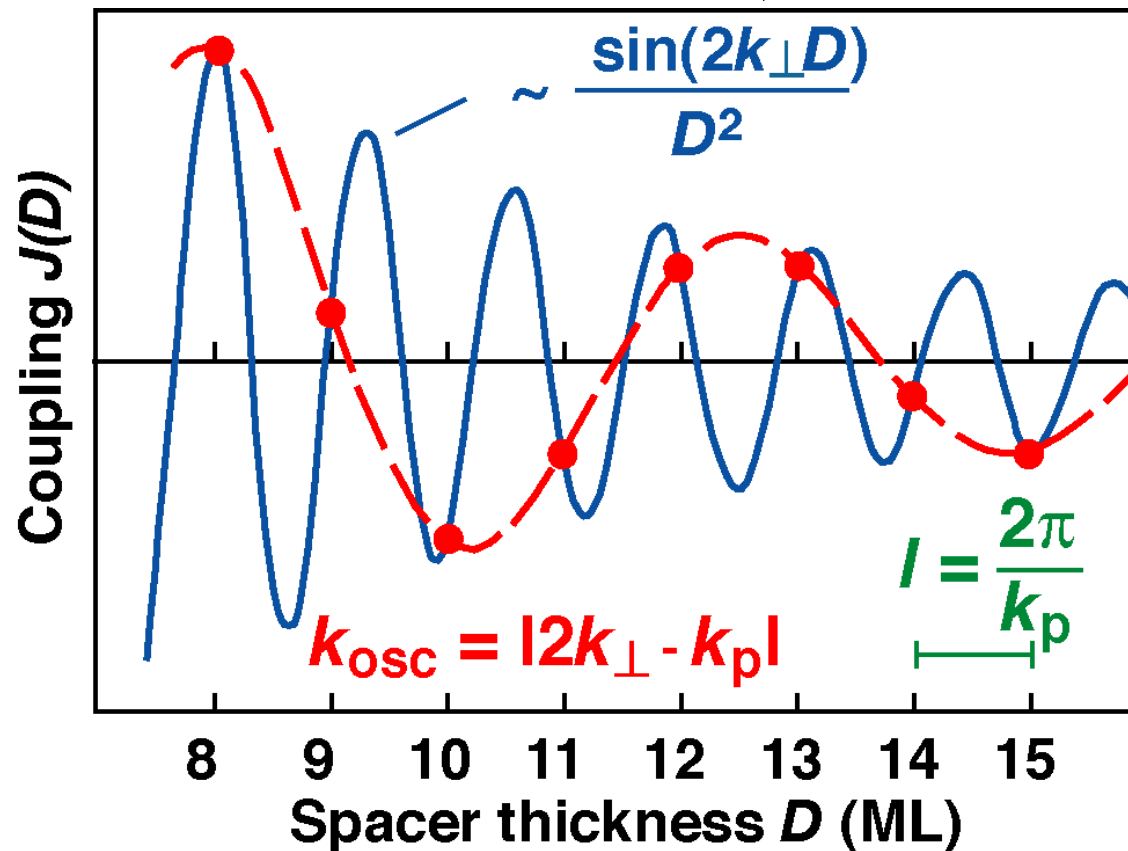
Spin-resolved spectra indicate that the QWS are mainly of minority (spin-down) character:



C. Carbone *et al.*, Solid State Comm. **100**, 749 (1996)

Aliasing (or backfolding into the first Brillouin zone)

Typical ΔD are of the order of a few Å, *i.e.* interatomic distances



⇒ Each k_{\perp} gives rise to an oscillation of $J(D)$ with a periodicity given by

$$k_{osc} = |2k_{\perp} - k_p|$$

R. Coehoorn, Phys. Rev. B **44**, 9331 (1991)

Which k_{\perp} are important?

$J(D)$ is dominated by k_{\perp} with the highest density of states at E_F .

\Rightarrow Consider k_{\perp} at stationary point

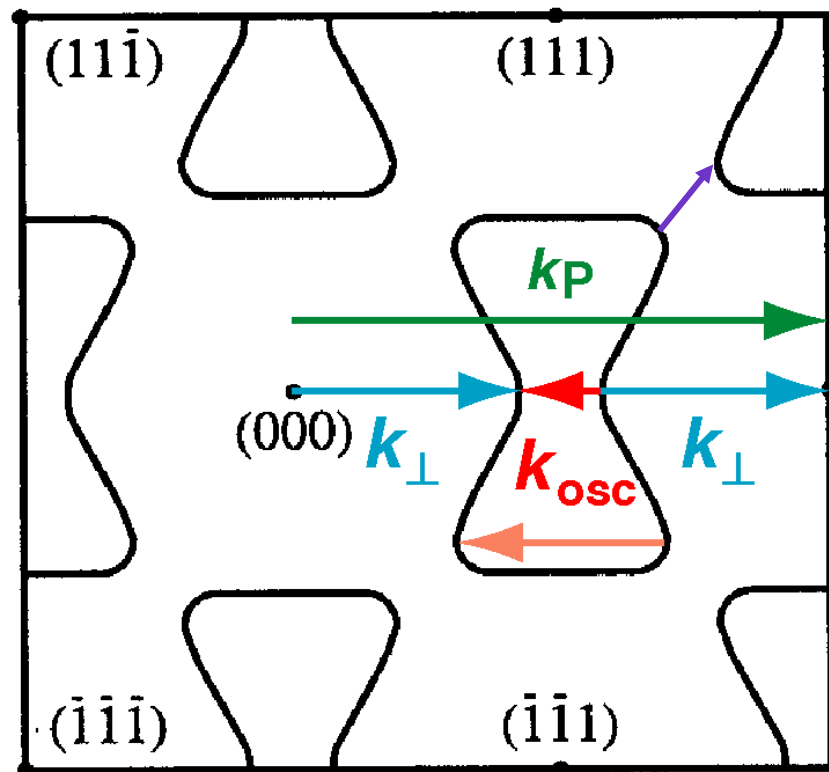
$$k_{\text{osc}} = |2k_{\perp} - k_p|$$

Several stationary points may exist

$\Rightarrow J(D)$ is a superposition of oscillations *e.g.* 2.5 and 8 ML for Au(001)

Real Fermi surfaces are non-spherical

\Rightarrow Oscillation periods depend on growth direction

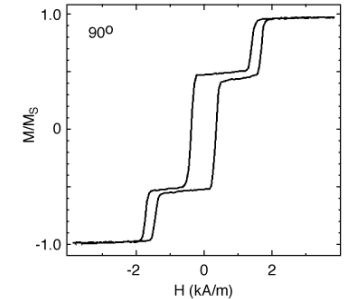
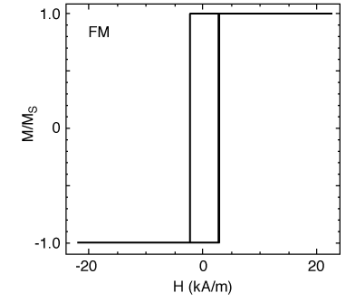
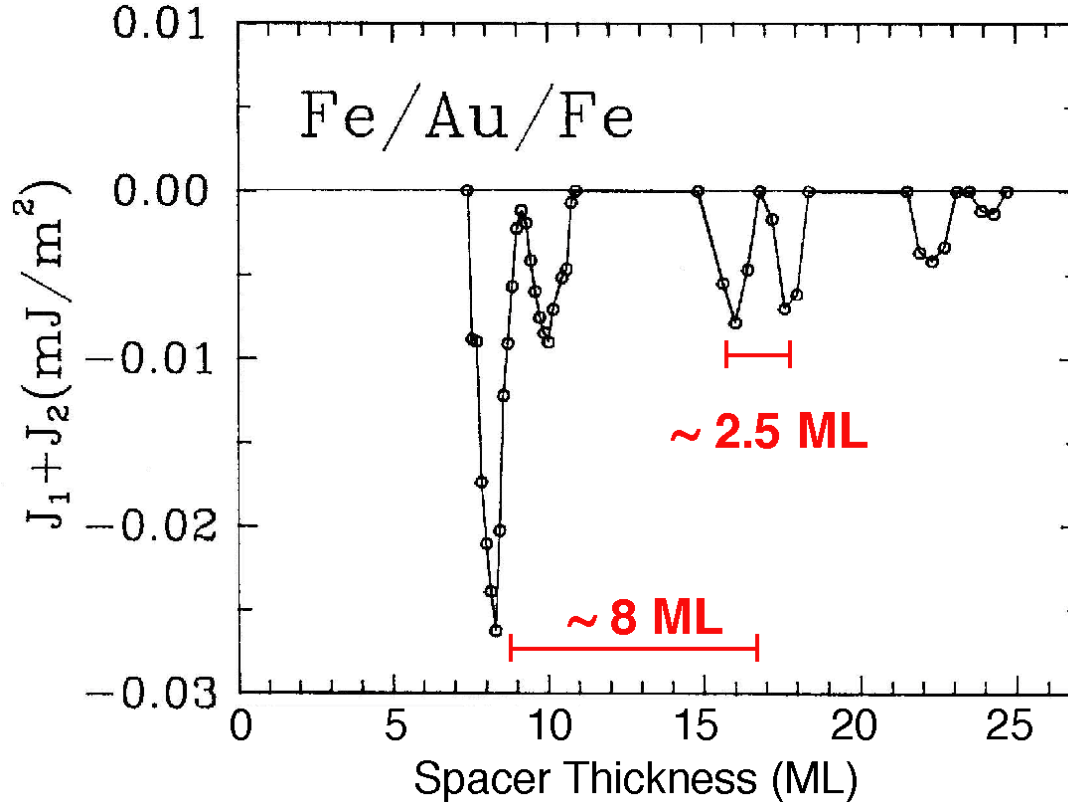


fcc(001) Fermi surface of a noble metal, *e.g.* Au(001)

P. Bruno *et al.*, Phys. Rev. Lett. **67**, 1602(1991)

Example Fe / Au / Fe(001)

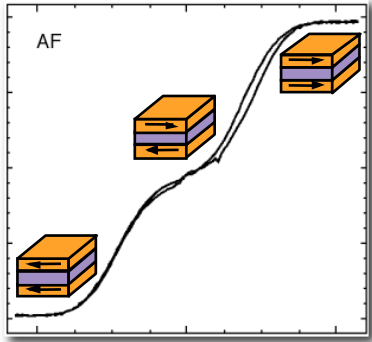
Epitaxially grown Fe/Au/Fe(001)



⇒ Oscillations periods are well described by the quantum interference model

A. Fuss *et al.*, J. Magn. Magn. Mater. **103**, L221 (1992); P. Bruno, Phys. Rev. B **52**, 411 (1995)

Outline: Interlayer exchange coupling



- Phenomenology of interlayer coupling
- Measurement by MOKE
- Physical picture for oscillatory bilinear coupling
- **Biquadratic coupling**
- Example: Morphology and “Fermiology”
- Applications
- Conclusions

Biquadratic or 90°-coupling

Biquadratic coupling is less well understood than bilinear coupling.

Intrinsic higher-order contributions are expected to be small.

Most models relate biquadratic coupling to extrinsic effects like:

- Interface roughness:

 - Fluctuation mechanism

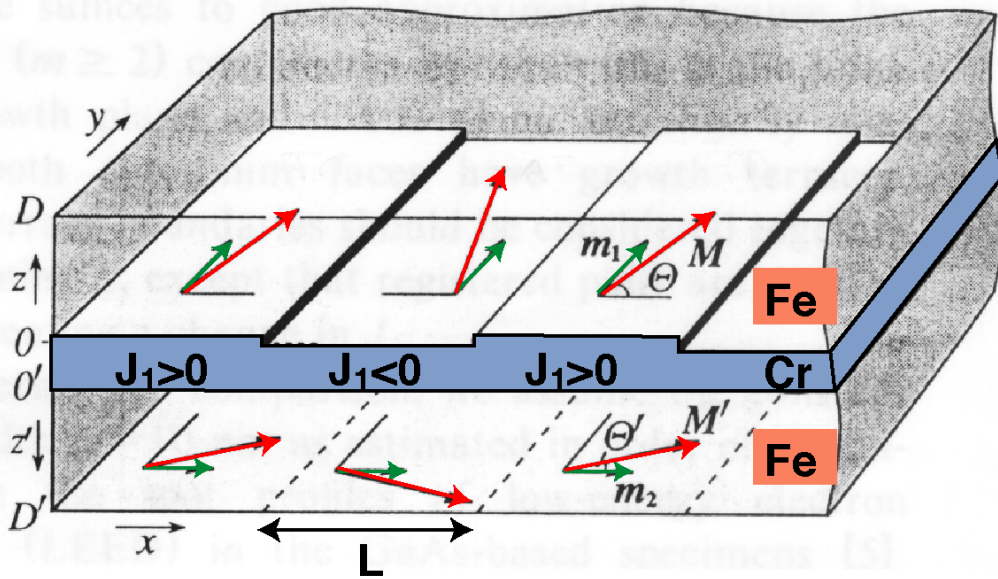
 - Magnetic dipole mechanism

- Pinholes in the spacer

- Chemical intermixing

 - “Loose-spin” mechanism

Fluctuation mechanism



For a oscillation period of $2 ML$
 J_1 locally changes sign at each
step edge!

Examples for short oscillations:

- 2.5 ML for Au(100)
- 2.6 ML for Cu(100)
- 2 ML for Cr(100)
- 2 ML for Mn(100)

Competition between local **fluctuations of the bilinear coupling** due to
spacer thickness fluctuations

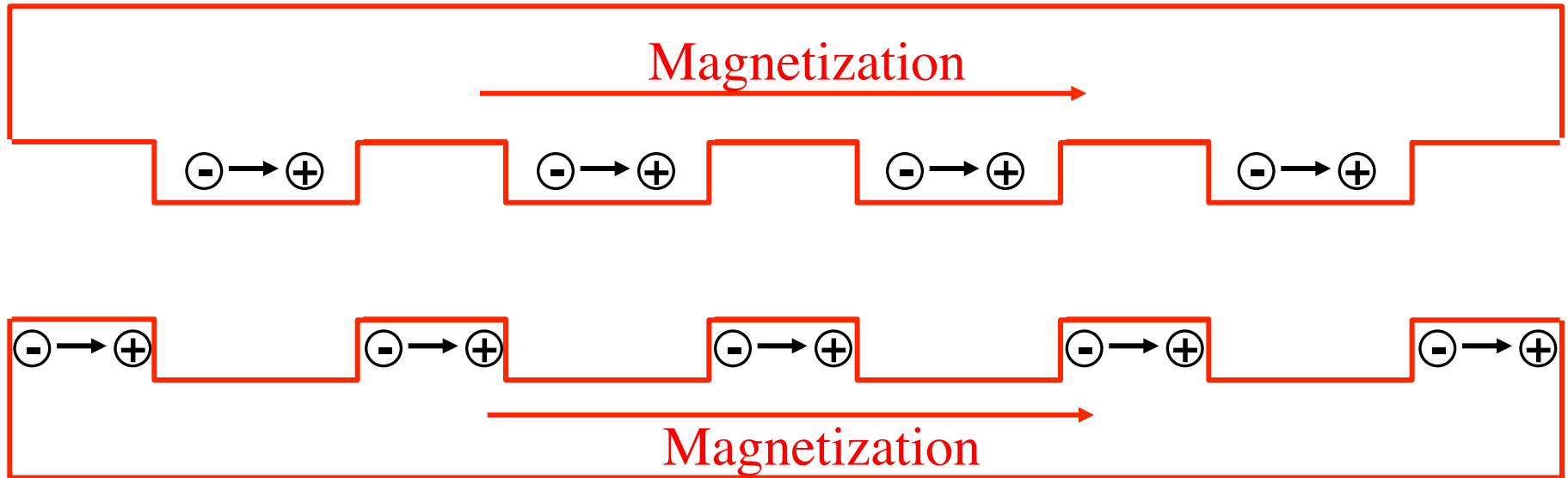
and

direct exchange within the FM layers

on a lateral **length scale** shorter than the FM domain wall width.

Magnetic dipole mechanism

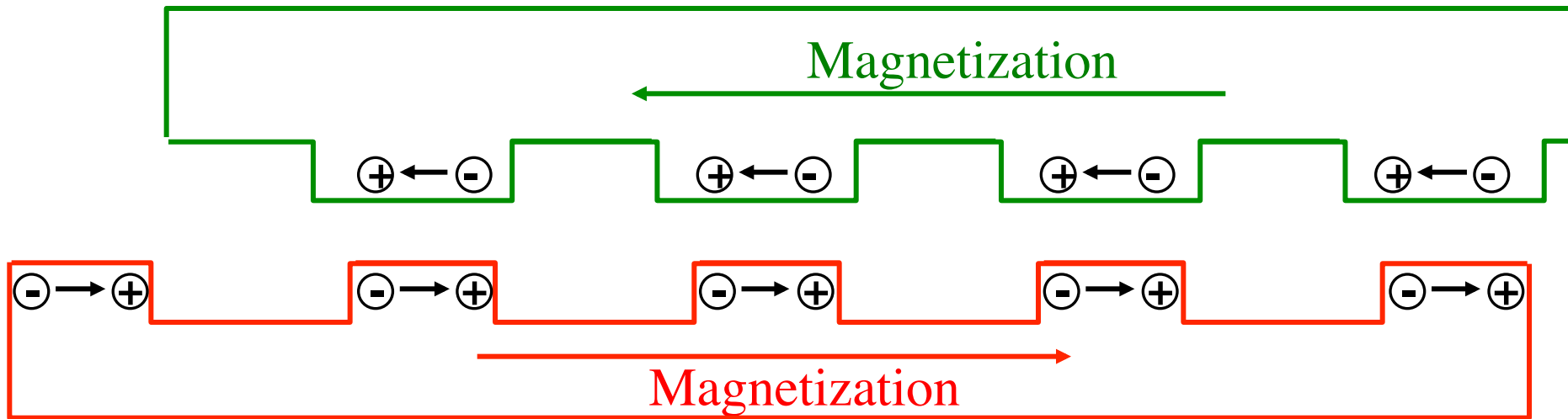
Interface roughness can give rise to interlayer coupling of different types depending on the vertical correlation of the roughness



⇒ Ferromagnetic “orange-peel” coupling for correlated roughness

Magnetic dipole mechanism

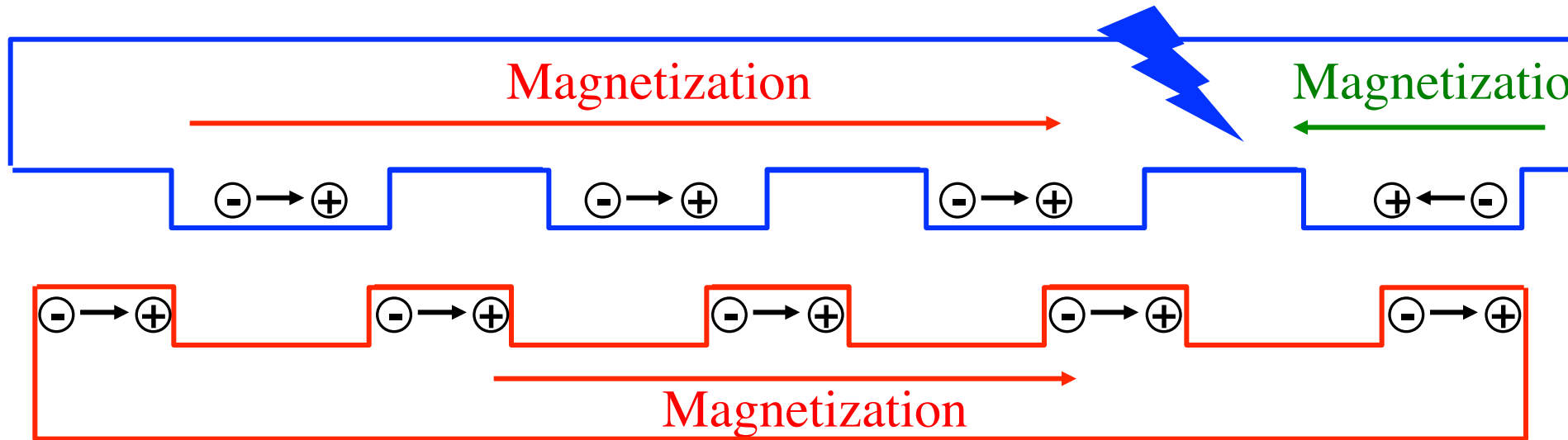
Interface roughness can give rise to interlayer coupling of different types depending on the vertical correlation of the roughness



⇒ Antiferromagnetic “Néel” coupling for anti-correlated roughness

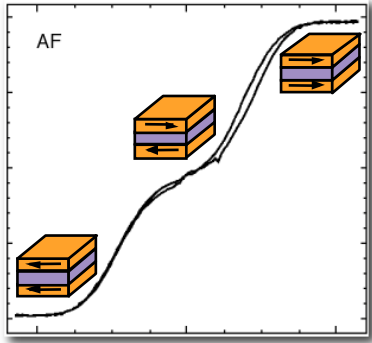
Magnetic dipole mechanism

Interface roughness can give rise to interlayer coupling of different types depending on the vertical correlation of the roughness



⇒ 90°-coupling for uncorrelated (random) roughness

Outline: Interlayer exchange coupling



- Phenomenology of interlayer coupling
- Measurement by MOKE
- Physical picture for oscillatory bilinear coupling
- Biquadratic coupling
- **Example: Morphology and “Fermiology”**
- Applications
- Conclusions

Influence of interface roughness

Epitaxial Fe/Cr-wedge/Fe(001) grown at different substrate temperatures

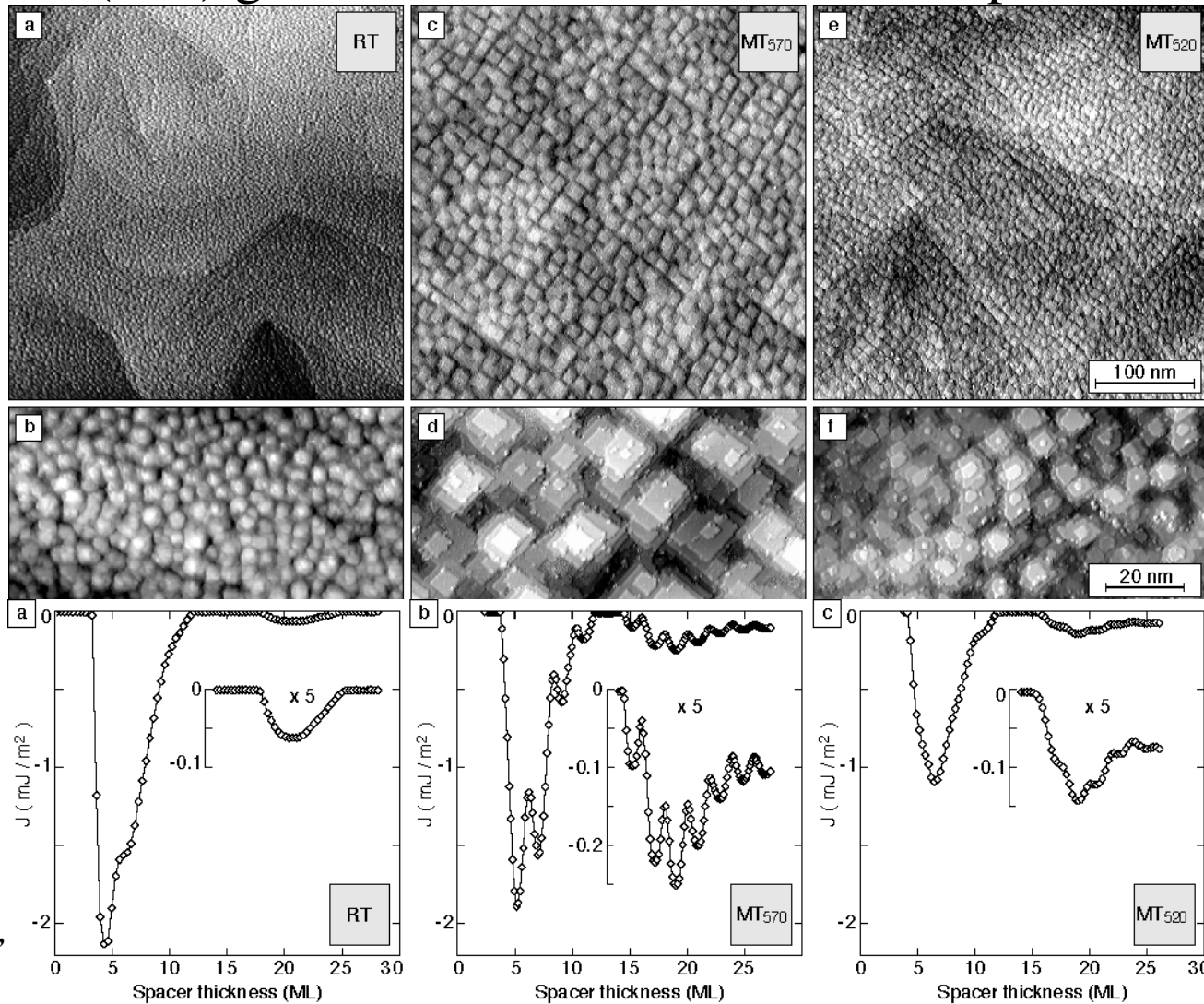
STM images:

400 nm x 400nm

100 nm x 40 nm

Coupling *versus*
spacer thickness
(MOKE)

C.M. Schmidt, D.E. Bürgler *et al.*,
Phys Rev. B **60**, 4158 (1999)

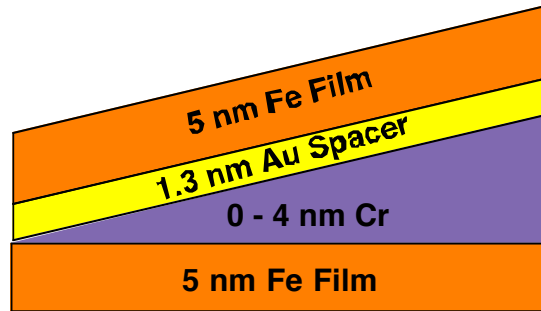


Influence of Fermi surface

Fe / Cr / Fe

compared with

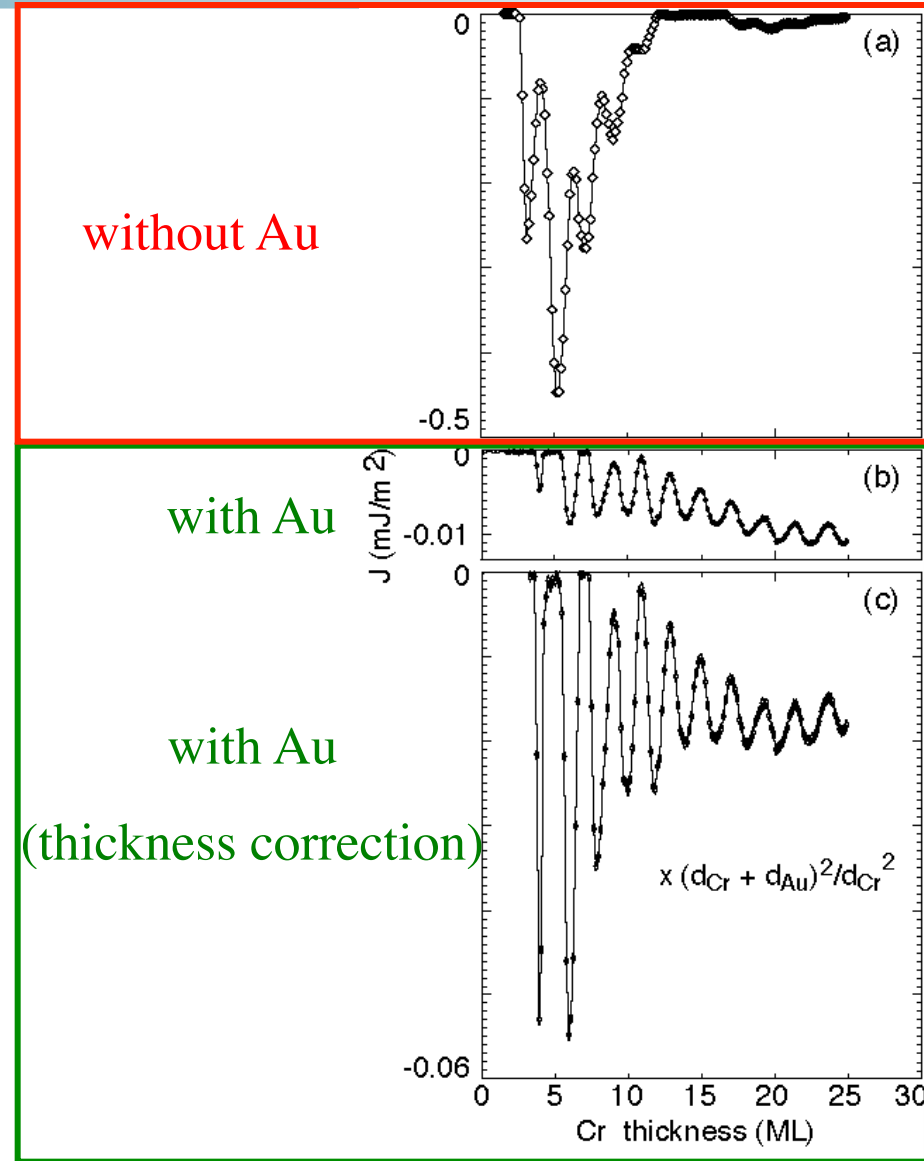
Fe / Cr / Au / Fe(001)



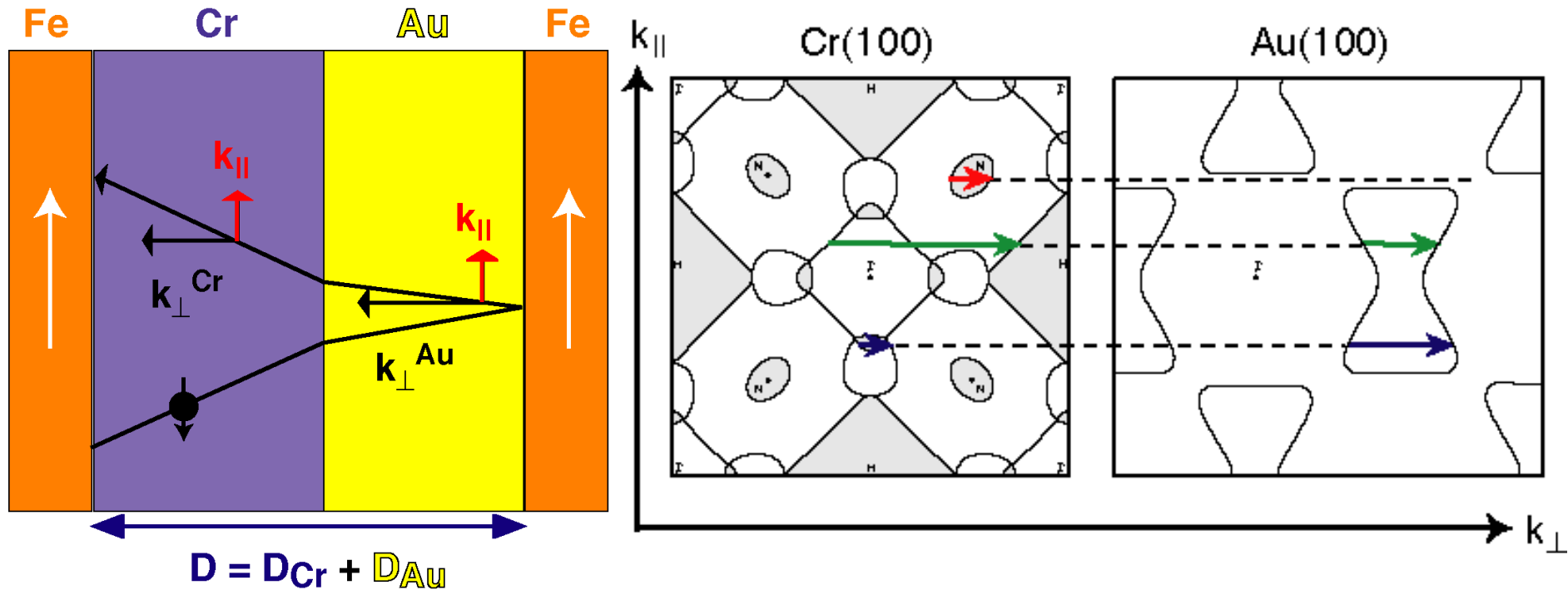
With additional Au layer:

- coupling strength decreases
- short-period oscillations still visible
- long-period oscillation disappeared

D.E. Bürgler *et al.*, Phys. Rev. B **60**, R3732 (1999)



In-plane momentum conservation



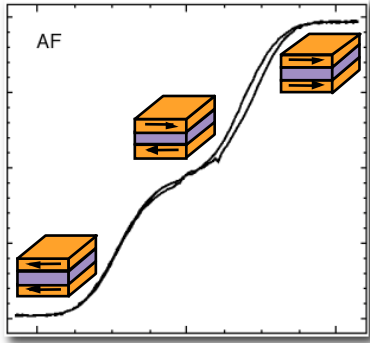
⇒ States giving rise to short-period oscillation can propagate in Au

⇒ States giving rise to long-period oscillation cannot propagate in Au

⇒ States near the X point do not mediate the long-period oscillation

D.E. Bürgler *et al.*, Phys. Rev. B **60**, R3732 (1999)

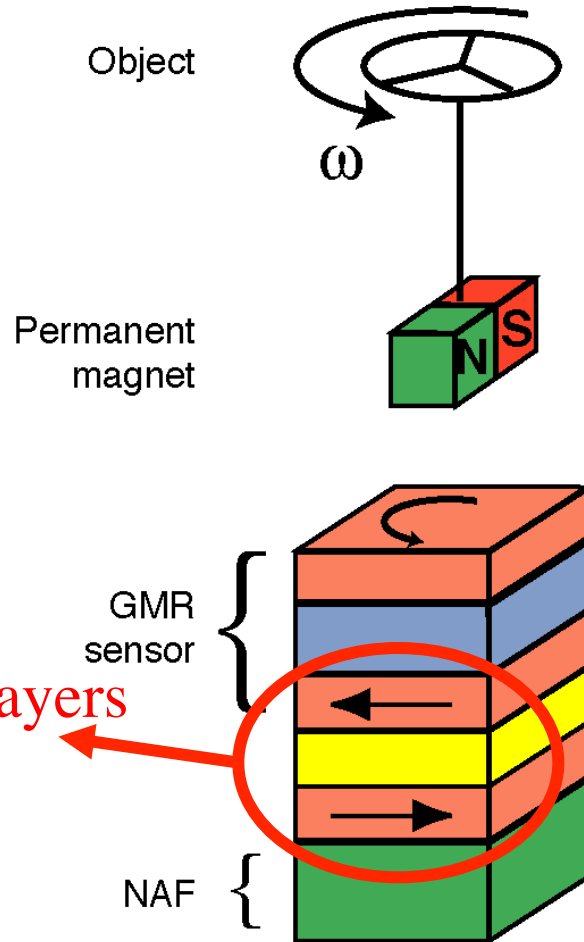
Outline: Interlayer exchange coupling



- Phenomenology of interlayer coupling
- Measurement by MOKE
- Physical picture for oscillatory bilinear coupling
- Biquadratic coupling
- Example: Morphology and “Fermiology”
- **Applications**
- Conclusions

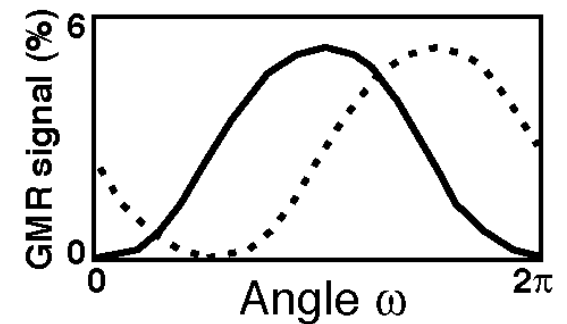
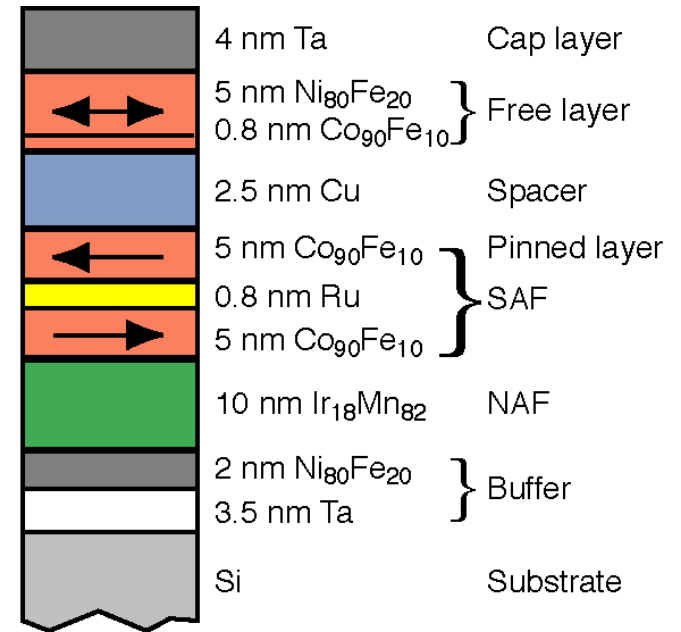
Application: Reference layers in GMR/TMR-sensors

Example: GMR-based angle sensor:



AF-coupled FM layers form a synthetic antiferromagnet

Example of a real layer structure:



K.M.H. Lenssen *et al.*,
J. Appl. Phys. **85**, 5531 (1999)

NAF = natural antiferromagnet, SAF = synthetic antiferromagnet

Application: AFC media for harddisk drives (I)

Application of AF coupling in the disk media in order to push the superparamagnetic limit:

- Condition to increase storage density:

Reduce magnetization density areal $M t$

- Condition to for long-time stability (10 years), *i.e.* to withstand superparamagnetism:

Keep anisotropy energy large enough: $K_U V > 40 k_B T$

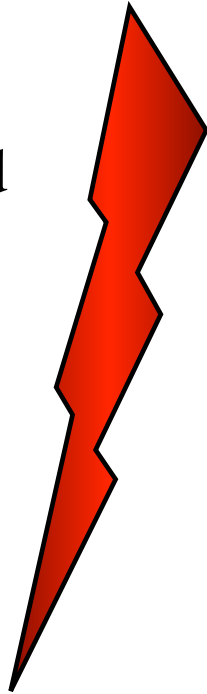
- Condition given by max. field of write-heads:

Keep writing field low enough: $H_{write} \approx K_U/M$

- Condition for sufficient signal-to-noise ratio:

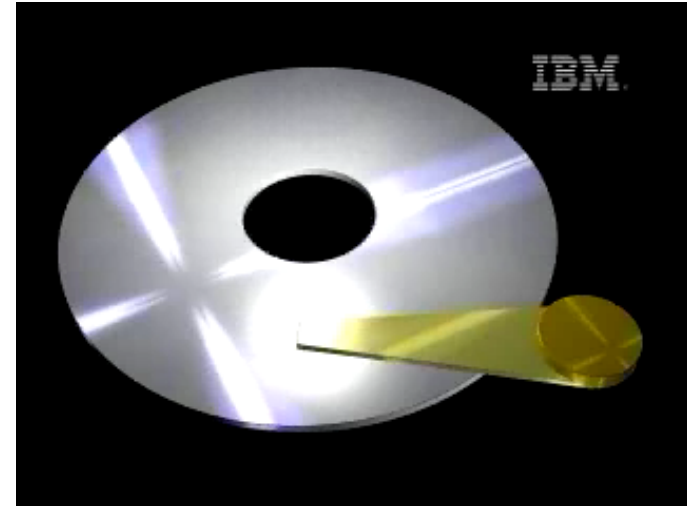
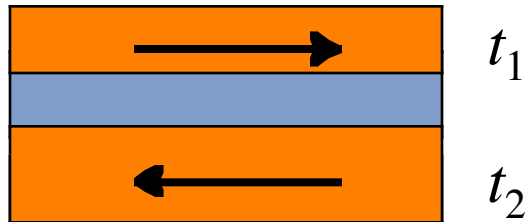
Reduce V in order to keep number of grains per bit constant.

E.E. Fullerton *et al.*, Appl. Phys. Lett. **77**, 3806 (2000)



Application: AFC media for harddisk drives (II)

Idea: Use antiferromagnetically coupled trilayer with different FM layer thicknesses $t_1 < t_2$:



⇒ Reduced effective magnetization density: $M t = M (t_2 - t_1)$

⇒ Anisotropy energy not reduced: $K_U V = K_U (V_1 + V_2) \propto t_1 + t_2$

⇒ Slightly increased writing field: $H_{write} \approx H_c^{(1)} + H_{ex}$

⇒ Grain volume V can be decreased



E.E. Fullerton *et al.*, Appl. Phys. Lett. **77**, 3806 (2000)

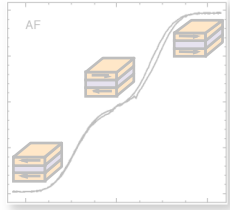
Conclusions on IEC

- **Bilinear** magnetic interlayer exchange coupling across **metallic** spacer layers is **well understood**
- The **quantum interference model** predicts the oscillation periods with high precision
- **Biquadratic** coupling is due to extrinsic effects and, therefore, **less well understood**
- Interlayer exchange coupling has entered **applications** in sensors and harddisk drives
 - Interlayer coupling **paved the way for** the discovery of the **giant magnetoresistance effect** (GMR)

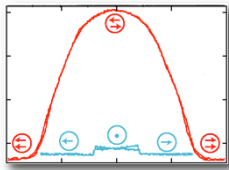
For a review see: D.E. Bürgler *et al.*, in “Handbook of Magnetic Materials”, Vol. 13, ed. by K.H.J. Buschow (Elsevier, 2001).

Overview

Introduction



Interlayer exchange coupling



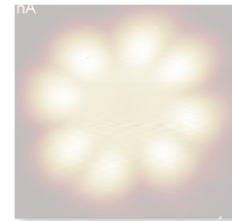
Giant and tunneling magnetoresistance



Current-induced magnetization dynamics



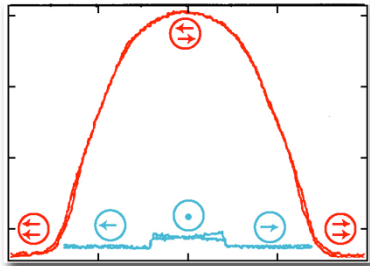
Pure spin current



Magnetic molecules

Conclusions

Outline: Giant and tunneling magnetoresistance (GMR and TMR)



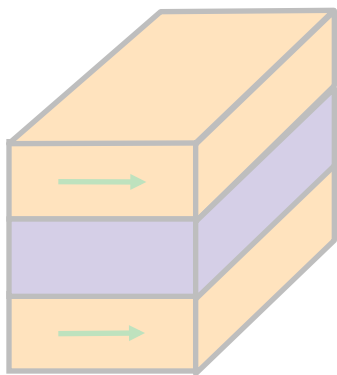
- Phenomenology of GMR
- Intermezzo: Ferromagnetic halfmetals
- Physical picture for GMR
- Applications of GMR
- Phenomenology of TMR
- Physical picture for TMR: Jullière and beyond
- Applications of TMR

Magnetic interlayer exchange coupling (IEC)

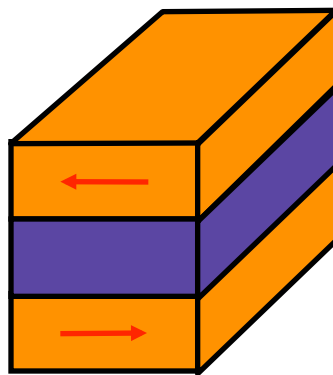
Consider two ferromagnetic layers separated by a thin spacer layer:

Ferromagnet / **Non-Ferromagnet** / **Ferromagnet**

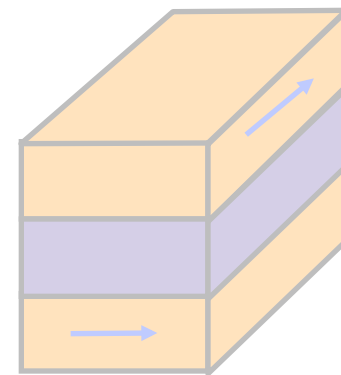
The ferromagnetic layers interact across the spacer and align ...



... parallel ...
“ferromagnetic
coupling”



... antiparallel ...
“antiferromagnetic
coupling”

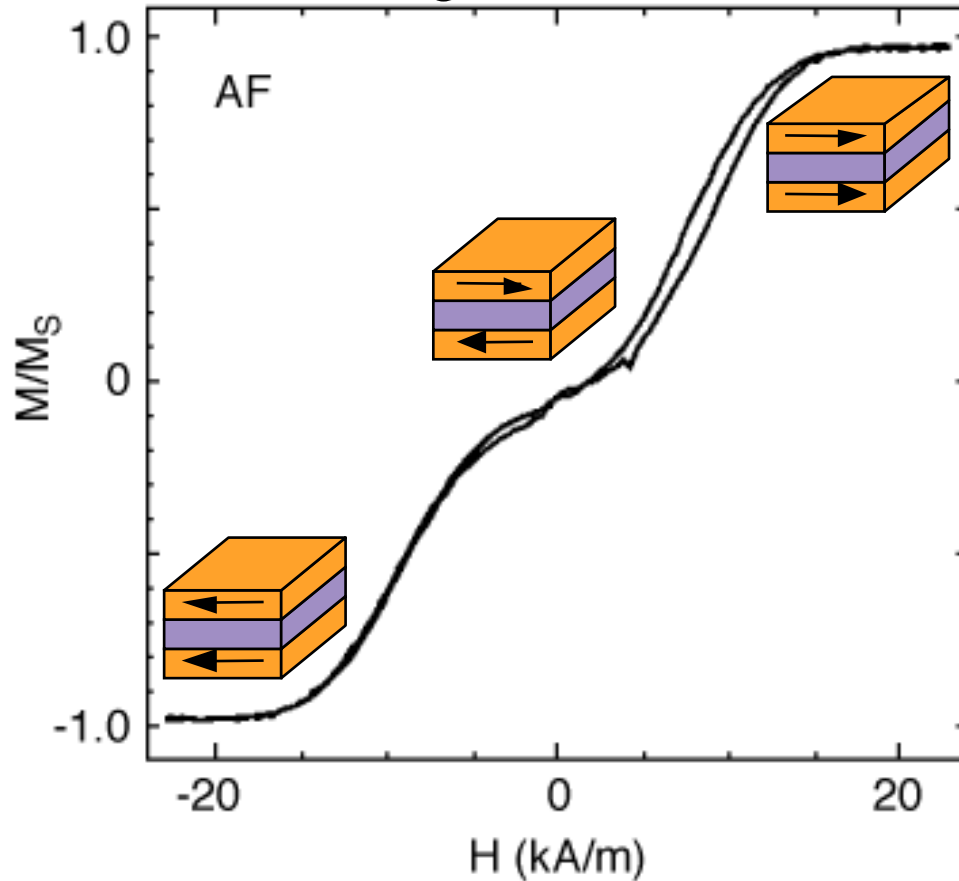


... at 90° ...
“biquadratic or
90°-coupling”

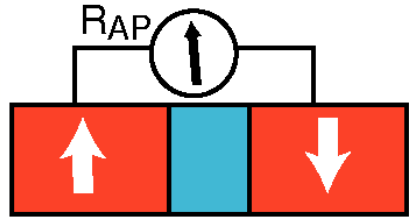
P. Grünberg *et al.*, Phys. Rev. Lett. **57**, 2442 (1986); M. Rührig *et al.*, phys. stat. sol. (a) **125**, 635 (1991)

Control of magnetization alignment

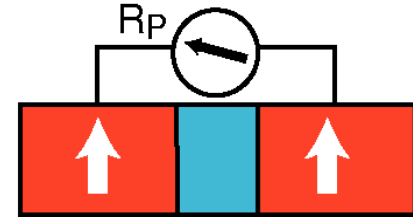
Antiferromagnetic IEC provides a means to reversibly switch between antiparallel and parallel alignment by applying an external magnetic field H



1988: ... simultaneously, but independent ...

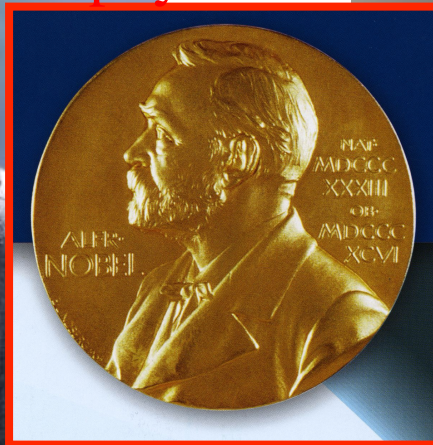


“Does the electrical resistance depend on the magnetization alignment?”



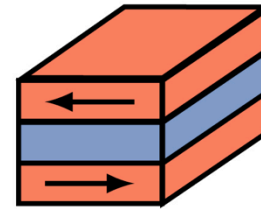
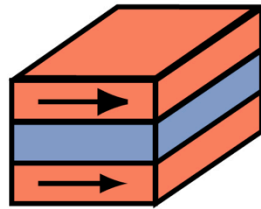
Albert Fert

Nobel prize
in physics 2007



Peter Grünberg

Giant magnetoresistance (GMR)



Ferromagnet
Metal
Ferromagnet

Electrical
resistance:

R_P

$<(>)$

R_{AP}

The electrical resistance depends on
the **relative magnetic alignment** of the ferromagnetic layers

$$\text{GMR} = \frac{R_{AP} - R_P}{R_P}$$

19% for trilayers @RT

80% for multilayers @ RT

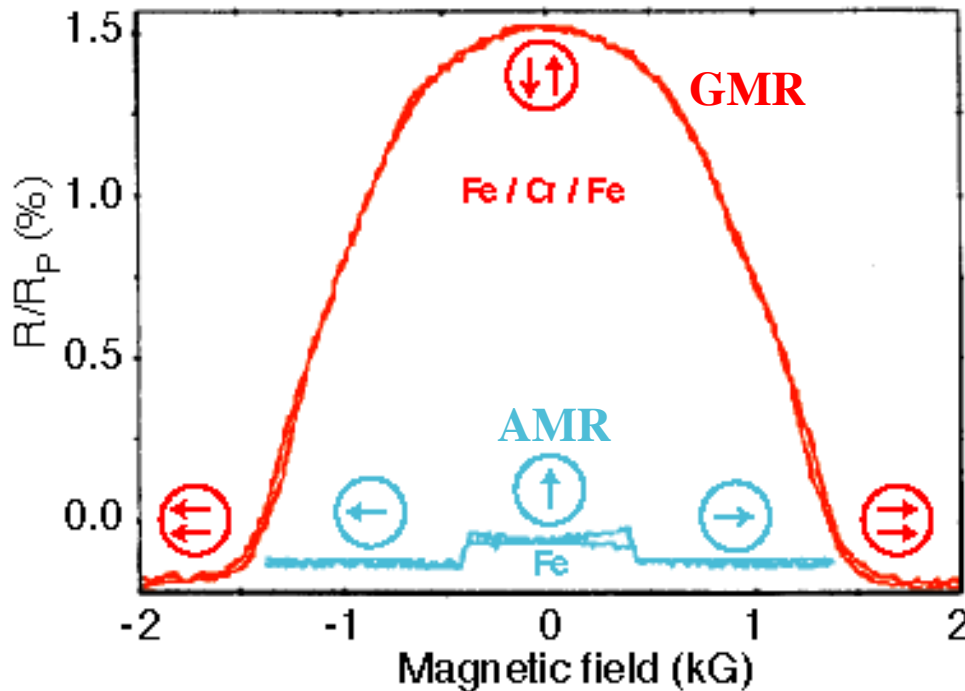
GMR is much **larger than the anisotropic magnetoresistance** (AMR)

First observations of GMR

Both experiments employ **antiferromagnetic interlayer coupling** to achieve the antiparallel alignment

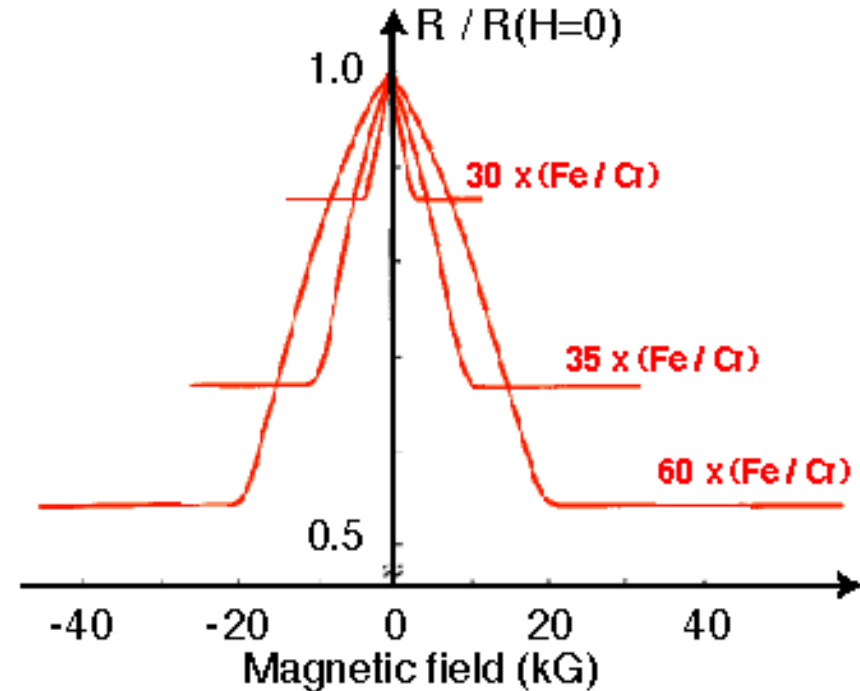
P. Grünberg, FZJ [1]

(a) Fe/Cr/Fe trilayer: 1.5% @ 300 K



A. Fert, Paris-Sud [2]

(b) Fe/Cr multilayers: 80% @ 4.2 K



[1] G. Binasch, P. Grünberg *et al.*, Phys. Rev B **39**, 4828 (1989)

[2] M.N. Baibich, A. Fert *et al.*, Phys. Rev. Lett. **61**, 2472 (1988)

Normal magnetoresistance (MR):

In any metal the Lorentz force due to an applied field acts on the moving electrons and reduces the mean free path
⇒ Resistance increases with field (positive MR)

Spin disorder resistivity and negative MR:

In a ferromagnet spin disorder provides further scattering channels, *e.g.* stronger spin mixing
Especially relevant around T_c
⇒ Resistance decreases with field (negative MR)

Both effects are rather **small** and **isotropic**, *i.e.* they do not depend on the direction of the field with respect to the sample orientation

Retrospect: Anisotropic magnetoresistance (AMR)

Discovered 1857 by Lord Kelvin

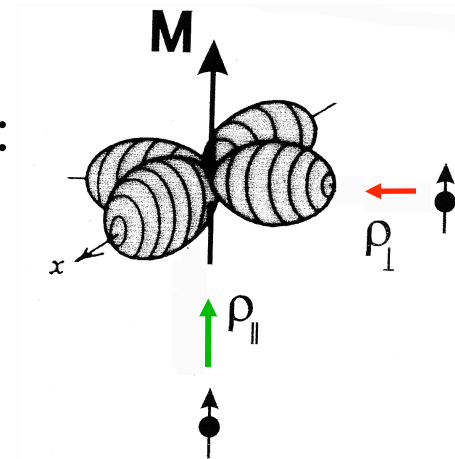
Describes the dependence of the resistance for a current flowing parallel (ρ_{\parallel}) or perpendicular (ρ_{\perp}) to the sample magnetization
 \Rightarrow **Anisotropic** with respect to the sample orientation

$$\text{AMR} = \frac{\rho_{\parallel} - \rho_{\perp}}{\rho_{\parallel}}$$

For a thin film with in-plane magnetization
(θ angle between magnetization and current):

$$\rho(\theta) = \frac{\rho_{\parallel} + \rho_{\perp}}{2} + (\rho_{\parallel} - \rho_{\perp})\left(\cos^2 \theta - \frac{1}{2}\right)$$

$\Rightarrow \pi$ -periodic



AMR originates from spin-orbit coupling and is 3% at most (Py)

Representative GMR ratios

Sample	$\Delta R=R_P$ (%)	Temperature (K)
Fe(4.5)/Cr(12) ₅₀	220	1.5
	42	300
Co(10)/Cu(10) ₁₀₀	80	300
Co(30)/Cu(19)/Co(25)	19	300
Co ₉₀ Fe ₁₀ (40)/Cu(25)/Co ₉₀ Fe ₁₀ (8)...	7	300
NiFe(100)/Cu(25)/Co(22)	4.6	300
...CoFe/AgCu(15)/CoFe...	4–7	300
Co(15)/Cu(12) _n CPP	170	4.2
Co(12)/Cu(11) ₁₈₀ CPP	55	300

Geometry is CIP unless specially marked with CPP. Auxiliary layers which are not directly active in the GMR effect are mostly omitted.

Numbers in brackets indicate the layer thicknesses in Å.

After P. Grünberg, *Sensors and Actuators A* **91**, 153 (2001)

Representative GMR ratios

Sample	$\Delta R=R_P$ (%)	Temperature (K)
Fe(4.5)/Cr(12) 50	220	1.5
	42	300
Co(10)/Cu(10)	80	300
Co(30)/		
Co ₉₀ Fe		
NiFe(10)		
...CoFe		
Co(15)/Cu(12) CIP	170	1.2
Co(12)/Cu(11) 180 CPP	55	300

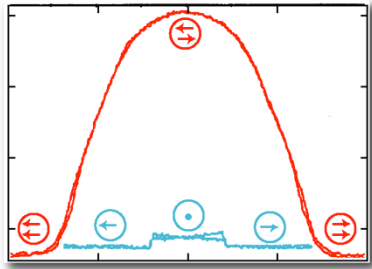
Recent progress with Heusler alloys:
GMR in Co₂Fe_{0.4}Mn_{0.6}Si/Ag/Co₂Fe_{0.4}Mn_{0.6}Si (100)
70% GMR @ RT due to high spin polarization
 Fermi level

Geometry is CIP unless specially marked with CPP. Auxiliary layers which are not directly active in the GMR effect are mostly omitted.

Numbers in brackets indicate the layer thicknesses in Å.

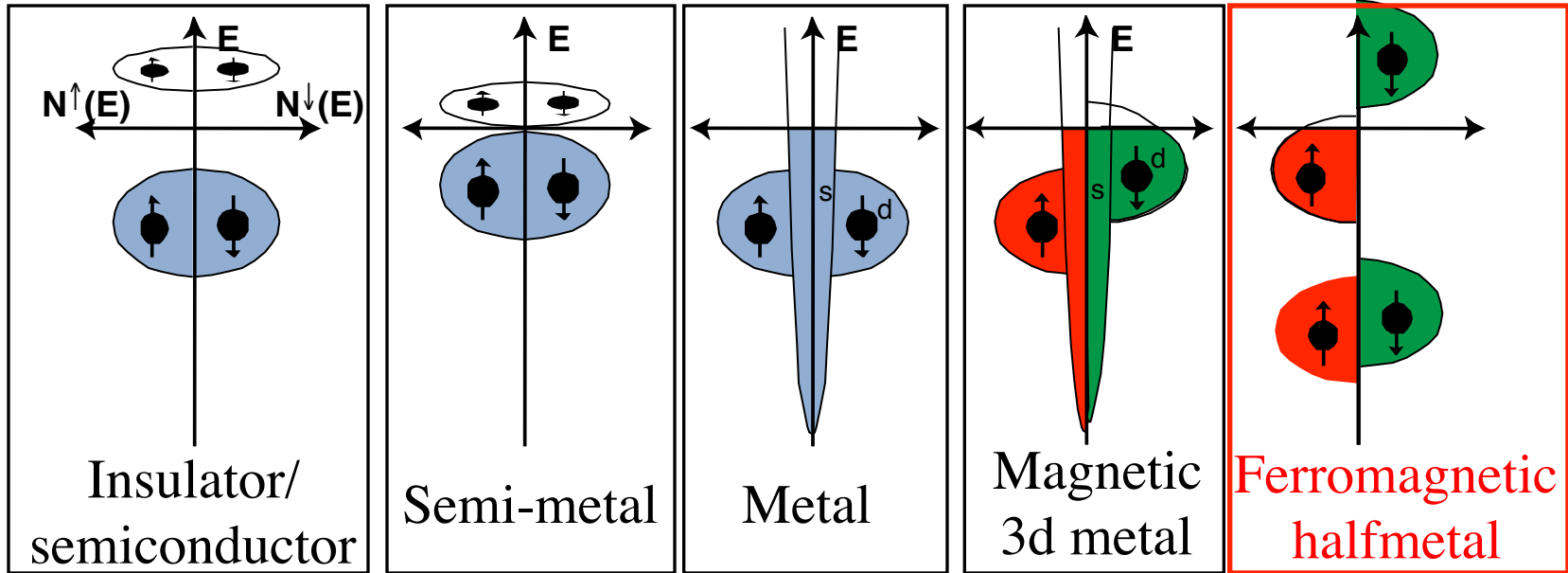
After P. Grünberg, *Sensors and Actuators A* **91**, 153 (2001)

Outline: Giant and tunneling magnetoresistance (GMR and TMR)



- Phenomenology of GMR
- **Intermezzo: Ferromagnetic halfmetals**
- Phenomenology of TMR
- Physical picture for TMR: Jullière and beyond
- Applications of TMR
- Physical picture for GMR
- Applications of GMR

Intermezzo: Properties of ferromagnetic halfmetals



Only electrons of one spin species (spin-up) contribute to transport,
i.e. 100% spin polarization of conduction electrons

⇒ Infinite spin-flip length for spin-up

⇒ Zero spin-flip length for spin-down

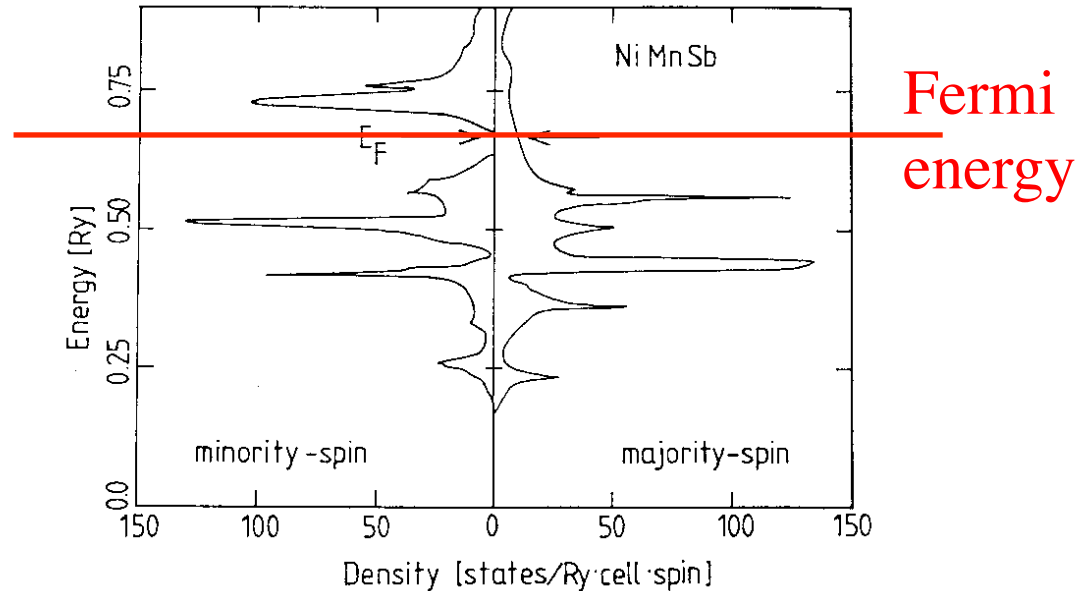
⇒ Ideal electrodes for GMR, TMR, spin-injection, ...

⇒ Ideal spin filter for current-induced magnetic switching

Intermezzo: Ferromagnets halfmetals

Materials:

Some oxides: CrO_2 with $|P| > 95\%$ from experiment at low T
 Fe_3O_4 due to hopping of only one spin species
and **Heusler alloys**



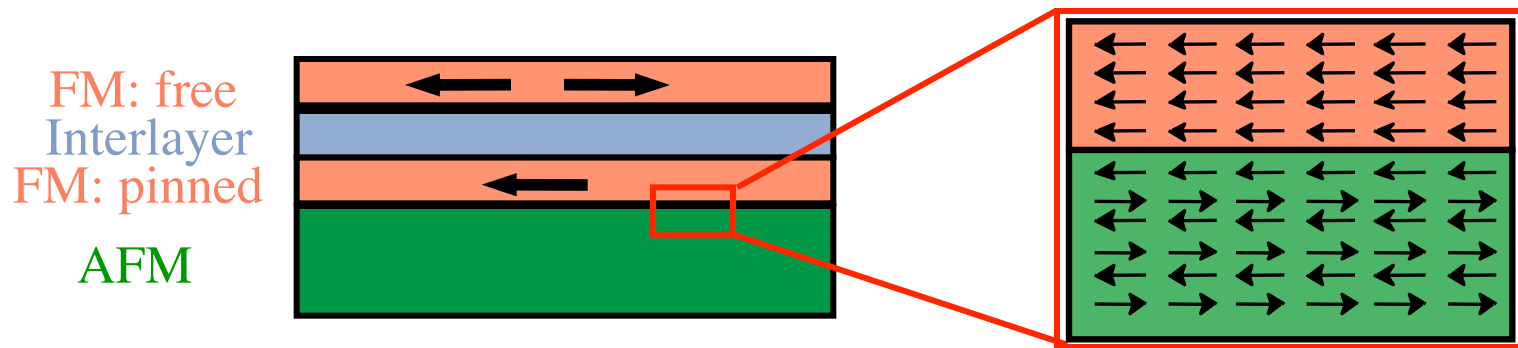
Experimental prove of half-metallicity is lacking for most predicted halfmetals. Problems: Stoichiometry, chemical and structural disorder, interface effects (surface states, bonding), etc.

Back to GMR: Spin-valves

Interlayer coupling is no precondition for GMR.

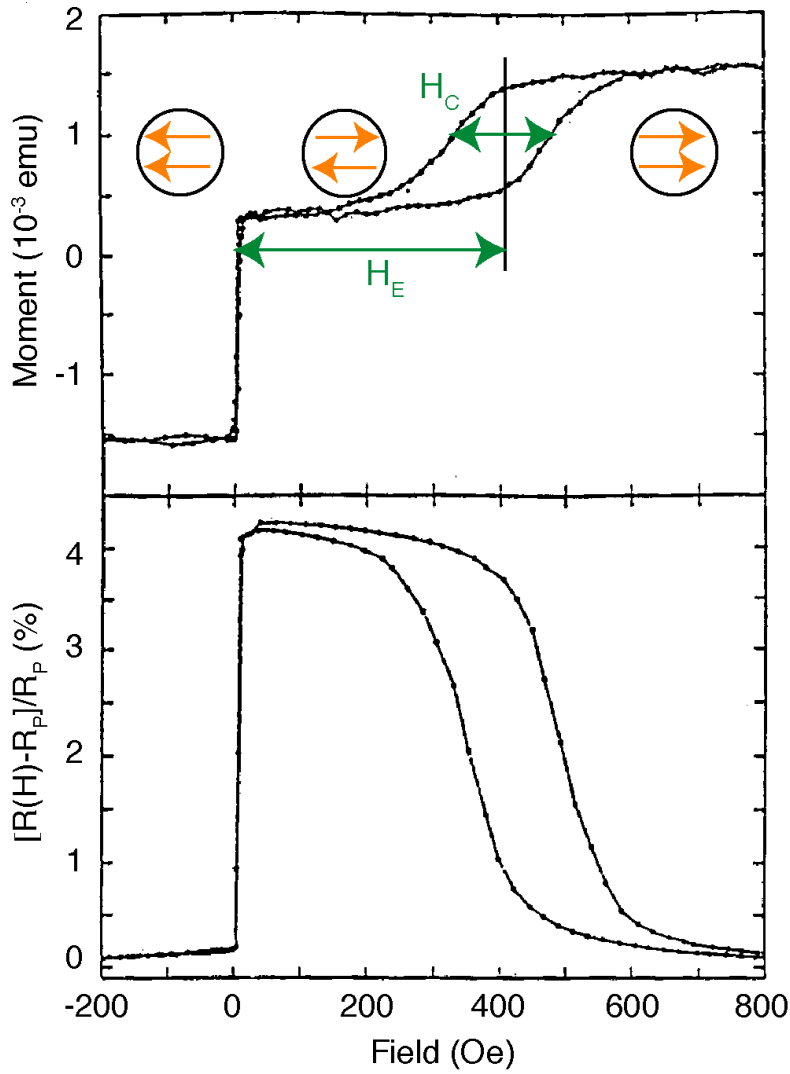
The AP alignment can be achieved by other means, *e.g.* FM layers with **different coercive fields** $H_c^{(1)} < H_c^{(2)} \Rightarrow$ **Pseudo spin-valve**

Exchange bias effect acting at the interface between an antiferromagnet (AFM) and a FM layer \Rightarrow **Spin-valve**

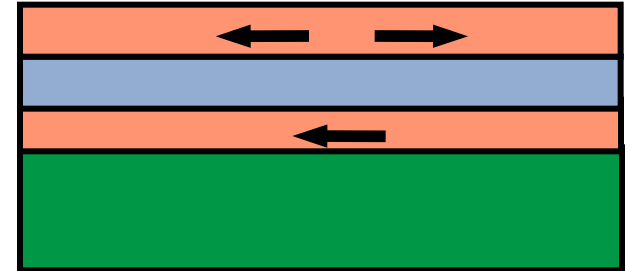


Exchange bias acts on the adjacent FM layer like an additional field H_E and shifts its magnetization loop on the field axis.

GMR of a spin-valve



6 nm $\text{Ni}_{80}\text{Fe}_{20}$
2.2 nm Cu
4 nm $\text{Ni}_{80}\text{Fe}_{20}$
7 nm FeMn

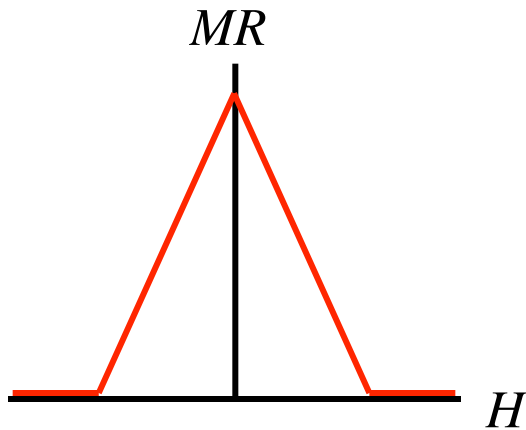
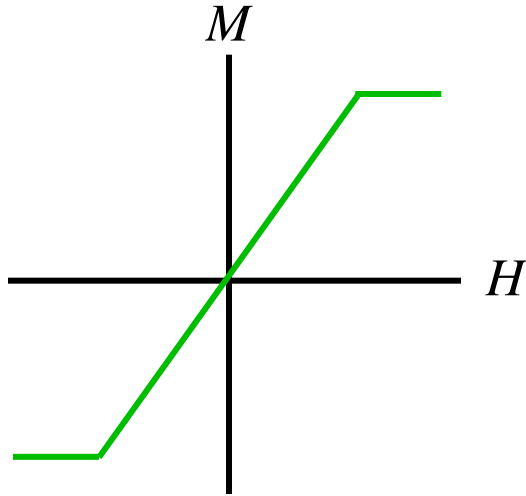


The steep slope at zero field makes spin-valves sensitive field sensors.

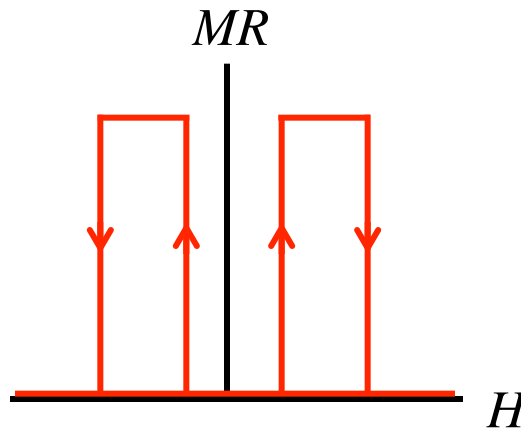
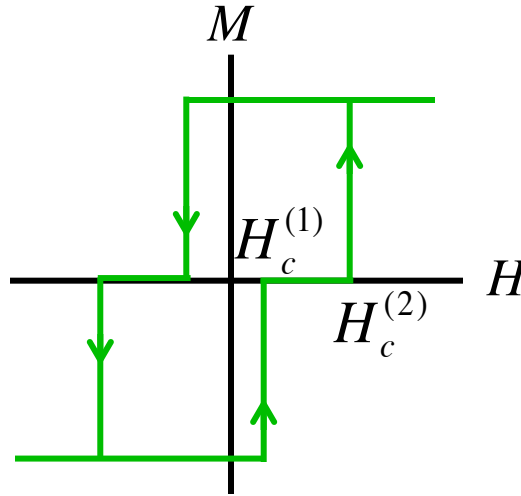
B. Dieny, J. Magn. Magn. Mater. **136**, 335 (1994)

Spin-valves II

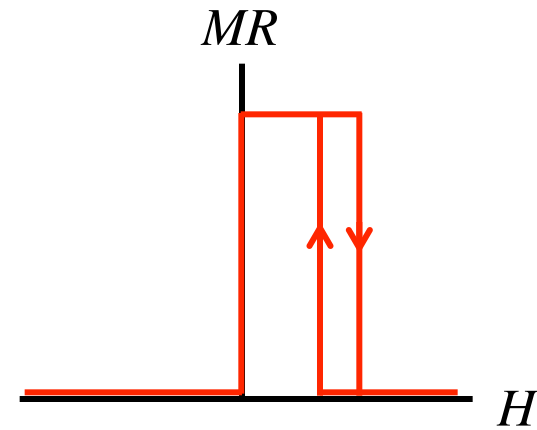
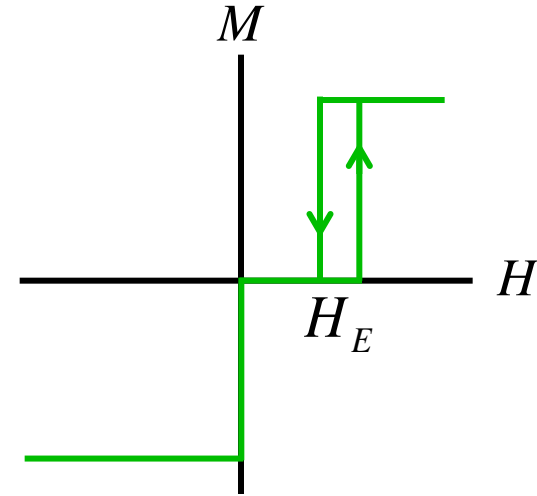
1) AF-coupled system
(multilayer)



2) Pseudo spin-valve
 $H_c^{(1)} < H_c^{(2)}$

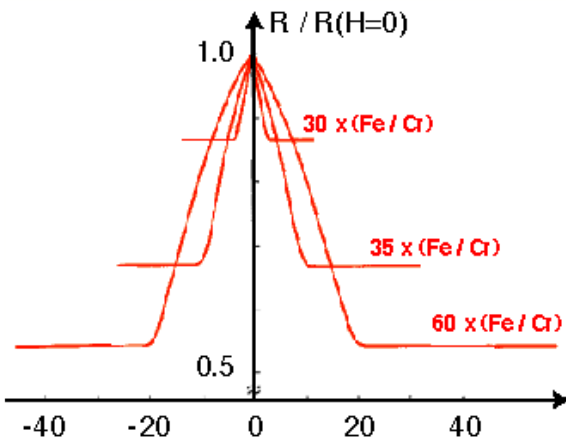
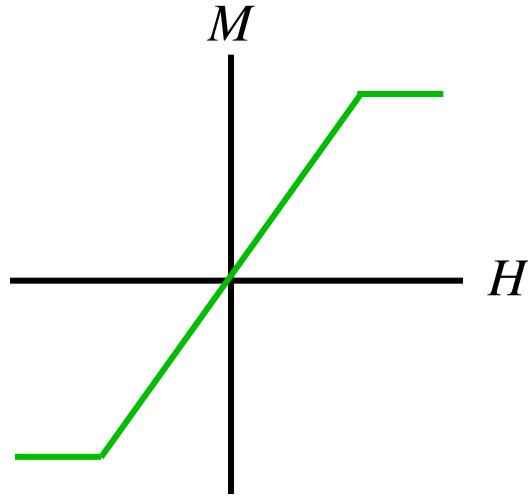


3) Spin-valve
(exchange bias)

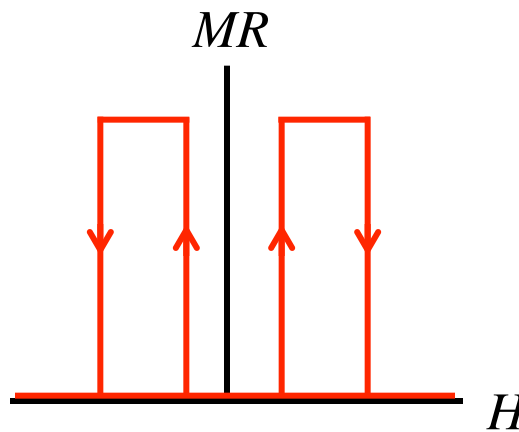
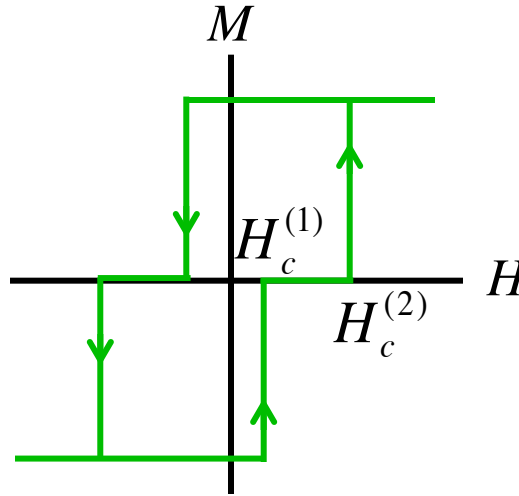


Spin-valves II

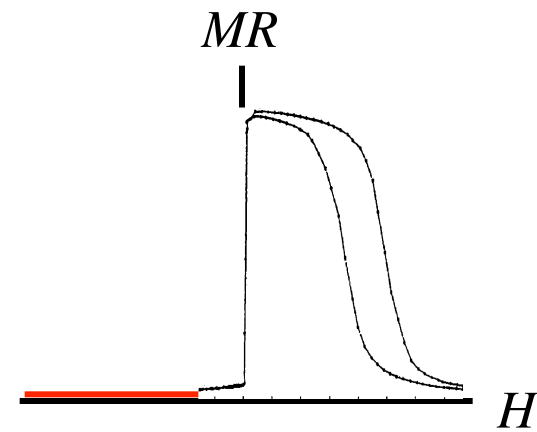
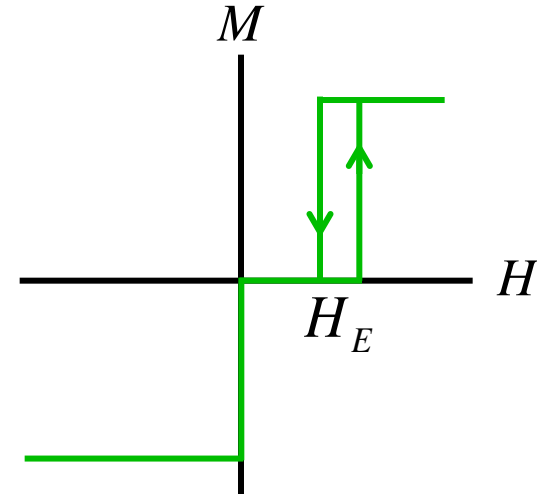
1) AF-coupled system
(multilayer)



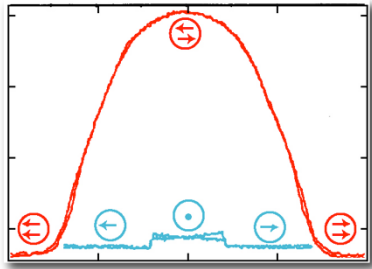
2) Pseudo spin-valve
 $H_c^{(1)} < H_c^{(2)}$



3) Spin-valve
(exchange bias)



Outline: Giant and tunneling magnetoresistance (GMR and TMR)



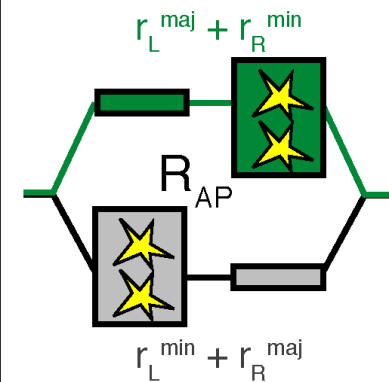
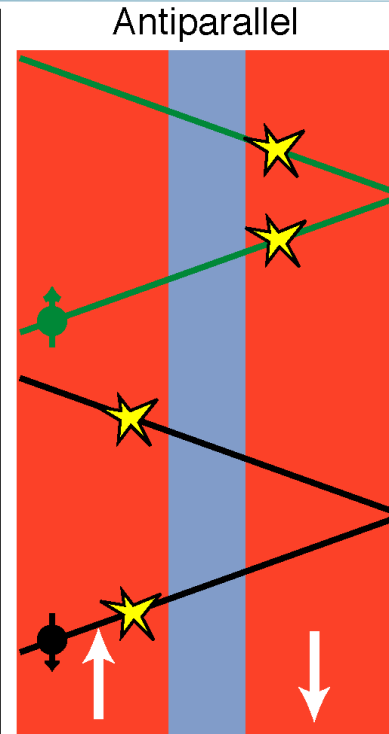
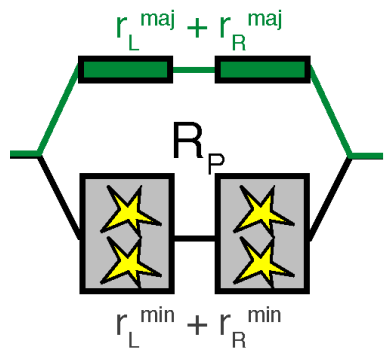
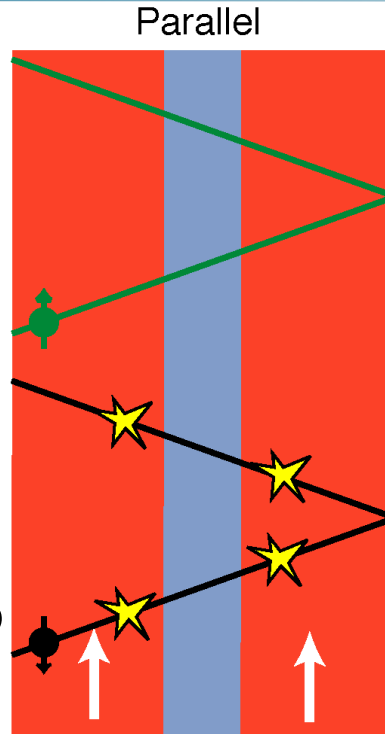
- Phenomenology of GMR
- Intermezzo: Ferromagnetic halfmetals
- Physical picture for GMR
- Applications of GMR
- Phenomenology of TMR
- Physical picture for TMR: Jullière and beyond
- Applications of TMR

Microscopic picture of GMR: Spin-dependent scattering

1) Spin-dependent scattering:

$$r^{min} \neq r^{maj}$$

2) Mott's two current model: independent current channels for spin-up and spin-down (no spin-flip scattering)



CIP and CPP geometry

current direction (CIP)



CIP-GMR requires spacer < mean free path



current direction (CPP)

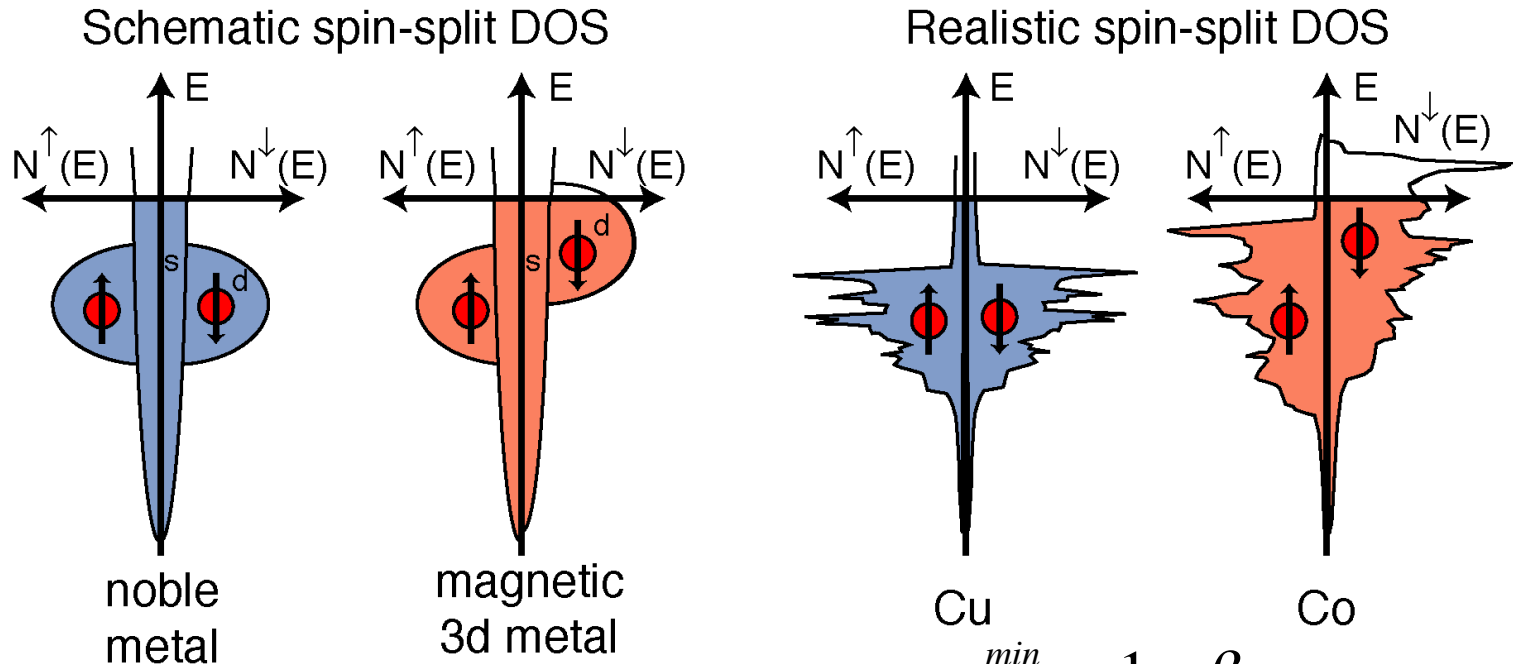
CPP-GMR requires spacer < spin flip length

Microscopic picture of GMR: Scattering spin asymmetry

The origin of the spin-dependent scattering lies in the **spin-split density of states** (DOS) of 3d transition metals:

minority resistance $r^{min} \neq$ majority resistance r^{maj}

$$r^{maj,min} \propto [\text{DOS}^{maj,min}(E_F)]$$



Scattering spin asymmetry parameter β : $\frac{r^{min}}{r^{maj}} = \frac{1 + \beta}{1 - \beta}$; $|\beta| \leq 1$

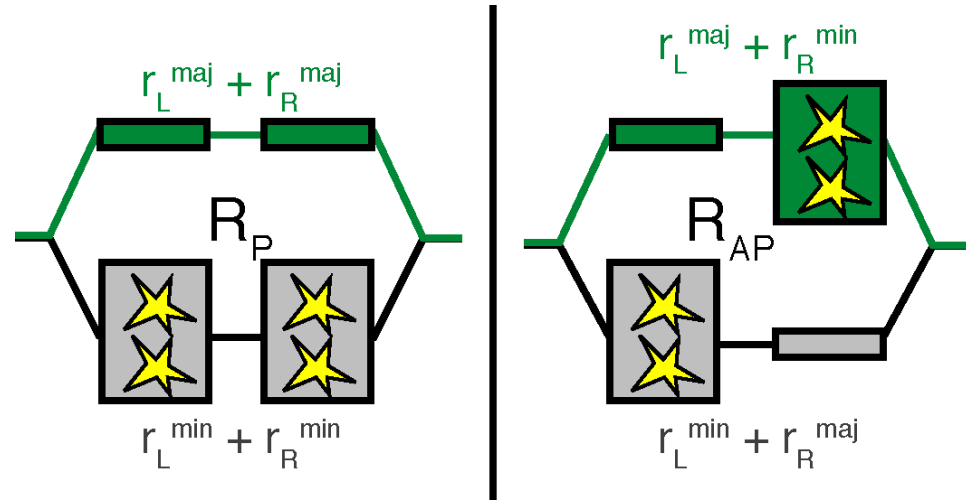
Normal and inverse GMR

Expressing the GMR ratio first by $r_{L,R}^{maj,min}$ and then $\beta_{L,R}$ one obtains:

$$\frac{R_{AP} - R_P}{R_P} = C \beta_L \beta_R \quad ; \quad C > 0$$

\Rightarrow Normal GMR for $\beta_L \beta_R > 0$

Inverse GMR for $\beta_L \beta_R < 0$

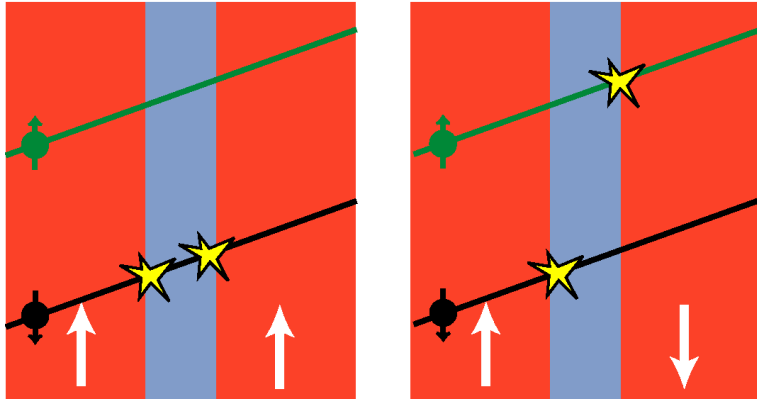


For symmetric systems $\beta_L = \beta_R$, and GMR is always normal

Normal and inverse GMR

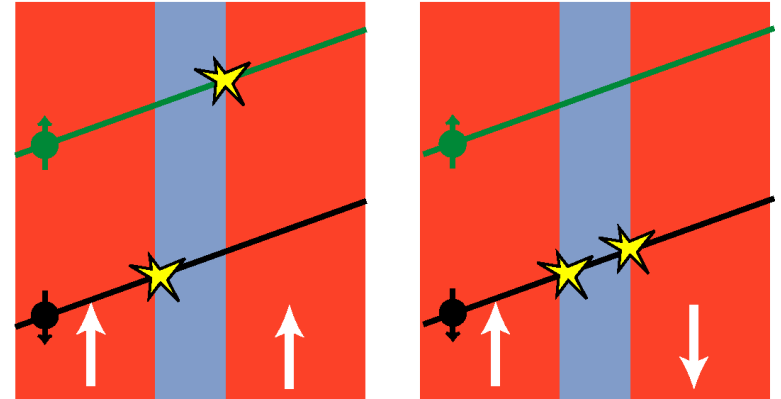
Normal GMR:

$$\beta_{L,R} > 0 \text{ or } \beta_{L,R} < 0$$

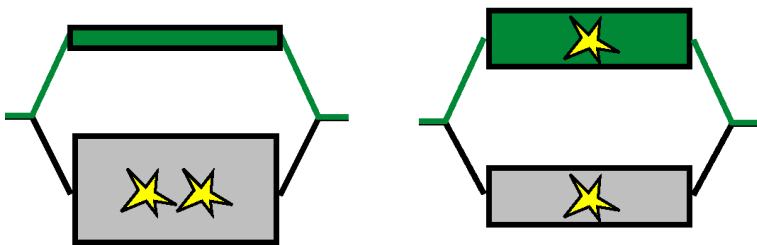


Inverse GMR:

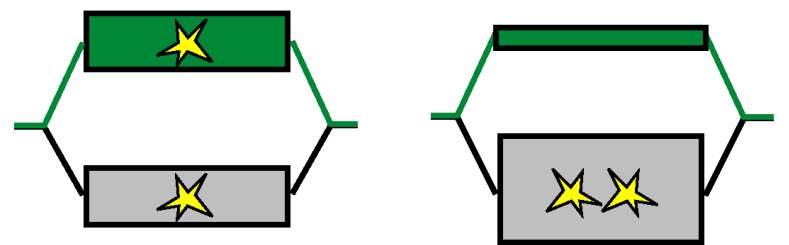
$$\beta_L > 0 \text{ and } \beta_R < 0 \text{ or vice versa}$$



$$\beta_L > 0 \text{ and } \beta_R > 0$$

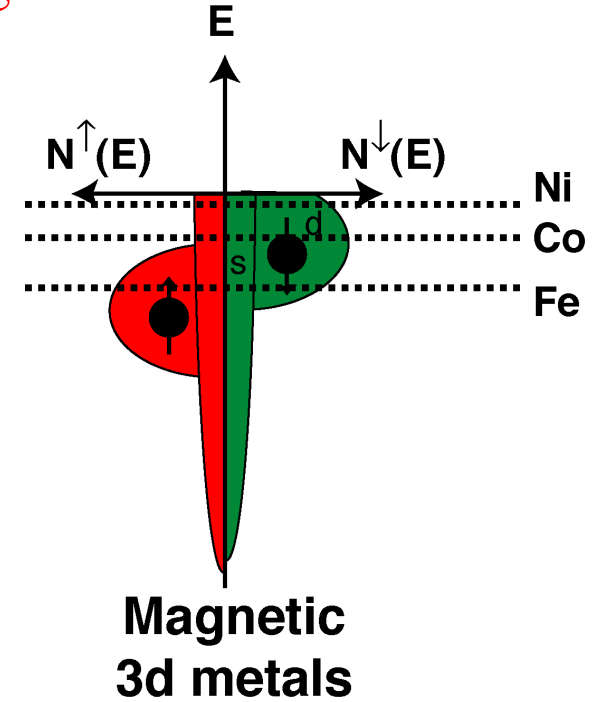
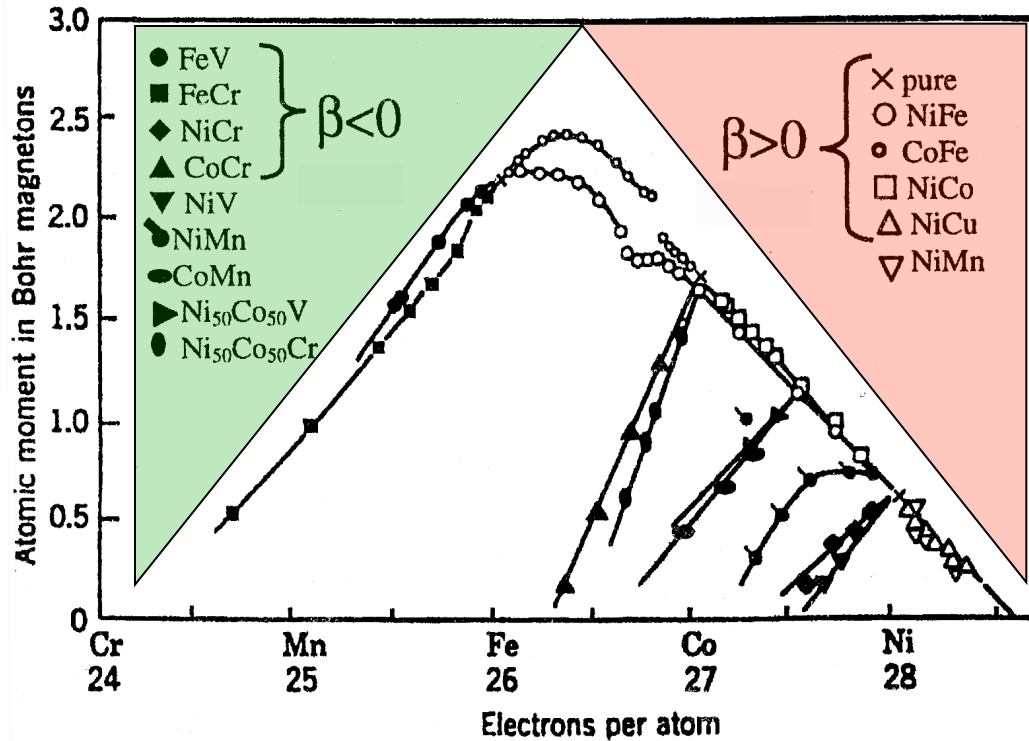


$$\beta_L > 0 \text{ and } \beta_R < 0$$



Relation to Slater-Pauling curve I

The sign of the β' s of 3d transition metals and their alloys can be obtained from the Slater-Pauling curve:



For positive slope: $N^{\uparrow} > N^{\downarrow} \Rightarrow r^{maj} > r^{min} \Rightarrow \beta < 0$

For negative slope: $N^{\uparrow} < N^{\downarrow} \Rightarrow r^{maj} < r^{min} \Rightarrow \beta > 0$

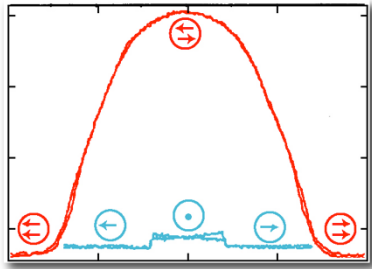
Relation to Slater-Pauling curve II

This rule holds for
bulk scattering spin asymmetries in **AB alloys**
as well as for
interface scattering spin asymmetries at **A/B interfaces**
(*e.g.* $\beta < 0$ for CoCr bulk alloys and Co/Cr interfaces)

This rule is observed in many CIP and CPP
experiments and confirms
spin-dependent scattering
as the
predominant mechanism for GMR.

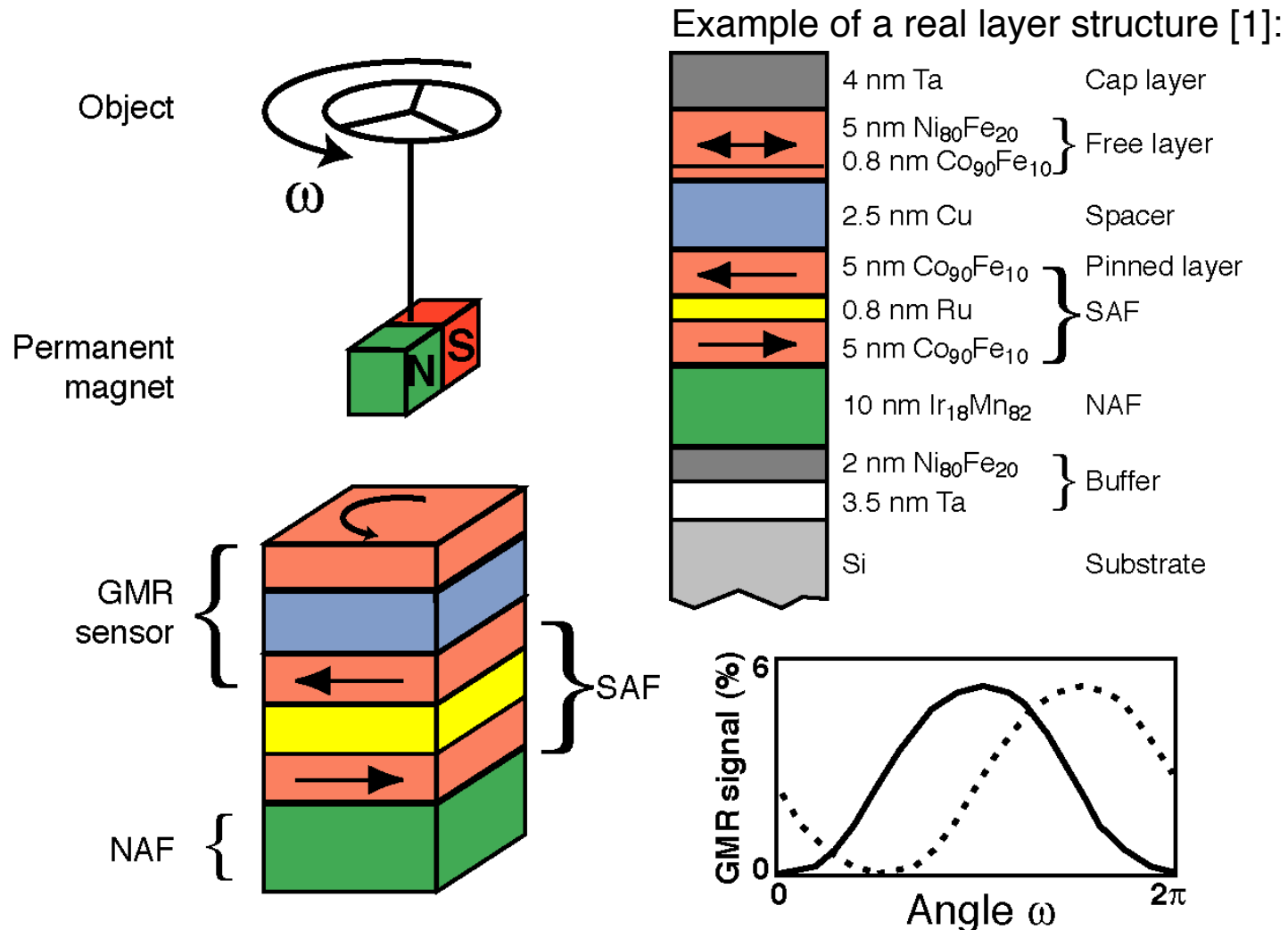
A. Barthélémy *et al.*, Handbook of Magnetic Materials **12** (1999)

Outline: Giant and tunneling magnetoresistance (GMR and TMR)



- Phenomenology of GMR
- Intermezzo: Ferromagnetic halfmetals
- Physical picture for GMR
- **Applications of GMR**
- Phenomenology of TMR
- Physical picture for TMR: Jullière and beyond
- Applications of TMR

Application of GMR: Magnetic field sensor



NAF = natural antiferromagnet, SAF = synthetic antiferromagnet

[1] K.M.H. Lenssen *et al.*, J. Appl. Phys. **85**, 5531 (1999)

Application of GMR in hard-disks

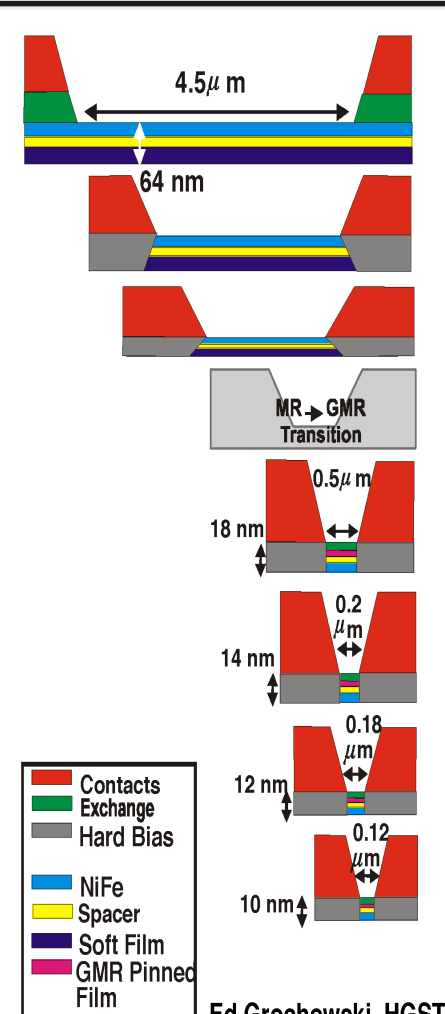
Advantages of GMR-based read heads compared to AMR or inductive read heads:

- 1) **Stronger MR signal**
 - ⇒ Better signal-to-noise
 - ⇒ Smaller bits can be read
- 2) GMR is an **interface effect** (AMR is a bulk effect):
 - ⇒ Thinner MR elements
 - ⇒ Less demagnetization
 - ⇒ Less wide MR elements
 - ⇒ Higher sensitivity

AMR

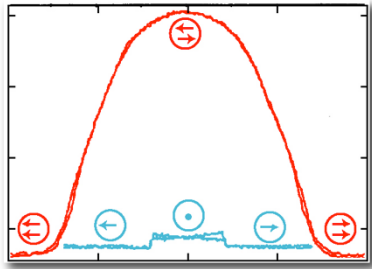
GMR

Year	Areal Density Gbits/in ²	Product
1991	0.132	Corsair
1992	0.260	Allicat
1993	0.354	Spitfire
1994	0.578	Ultrastar XP
1995	0.829	Ultrastar 2XP
	0.923	Travelstar 2LP
1996	1.32	Travelstar 2XP
	1.45	Travelstar VP
1997	2.64	Travelstar 5GS
	2.68	Deskstar 16GP
	3.12	Travelstar 6GN
1998	3.74	Travelstar 6GT
	4.1	Deskstar 25GP
	5.7	Travelstar 6GN
1999	5.3	Deskstar 37GP
	10.1	Travelstar 18GT
2000	7.04	Ultrastar 36LZX
	14.5	Deskstar 40GV
	17.1	Travelstar 30GT
2001	13.2	Ultrastar 73LZX
	25.7	Travelstarr 30GN
	29.7	Deskstar 120GXP
	34.0	Travelstar 40GN
2002	26.3	Ultrastar 146Z10
	45.5	Deskstar 180GXP
	29.7	Deskstar 120GXP
2003	70.0	Travelstar 80GN
2004	>100	
2005	>200	



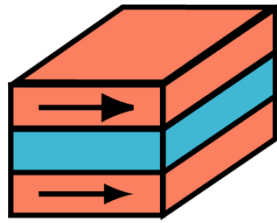
Ed Grochowski, HGST

Outline: Giant and tunneling magnetoresistance (GMR and TMR)



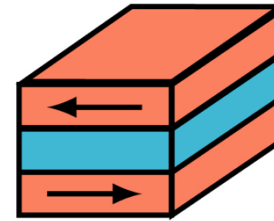
- Phenomenology of GMR
- Intermezzo: Ferromagnetic halfmetals
- Physical picture for GMR
- Applications of GMR
- **Phenomenology of TMR**
- Physical picture for TMR: Jullière and beyond
- Applications of TMR

Tunneling magnetoresistance (TMR)



R_{Par}

$\langle (\rangle$



R_{AP}

Ferromagnet
Insulator
Ferromagnet

Electrical
resistance:

The electrical resistance depends on the **relative magnetic alignment of the ferromagnetic layers**

Only for current perpendicular to the sample plane \Rightarrow Tunneling current

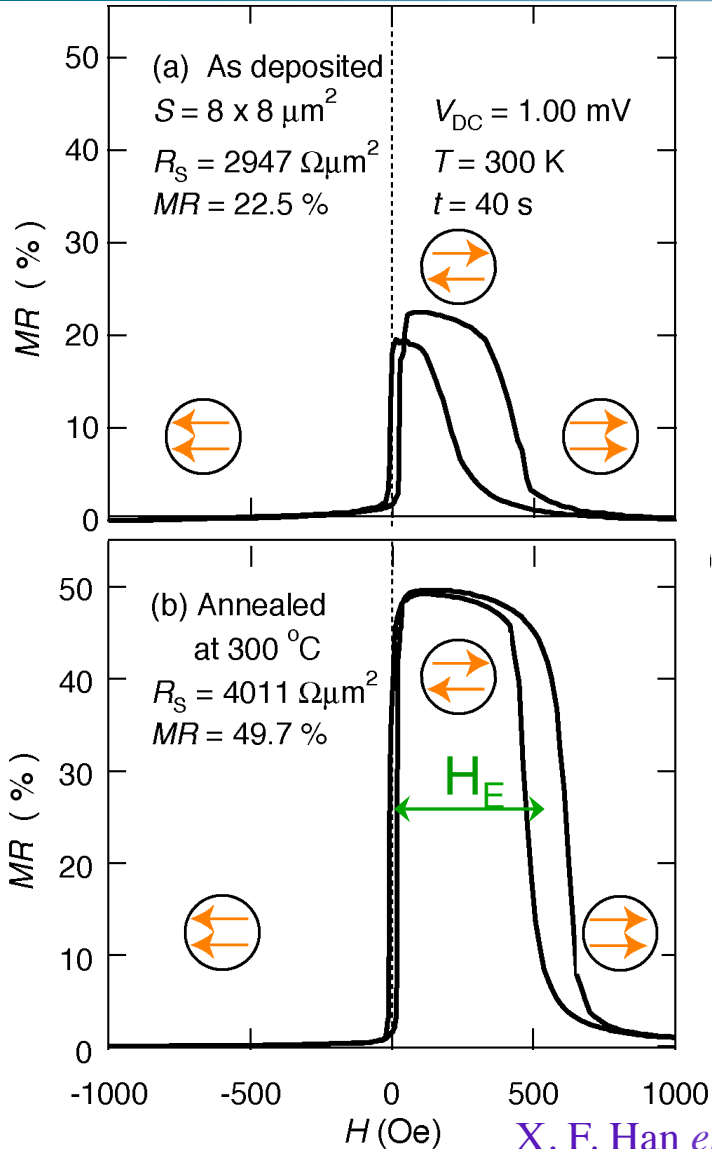
Typical areal resistance: $RA \approx 1 - 10^6 \Omega \mu\text{m}^2$

$$\text{TMR} = \frac{R_{\text{AP}} - R_{\text{P}}}{R_{\text{P}}}$$

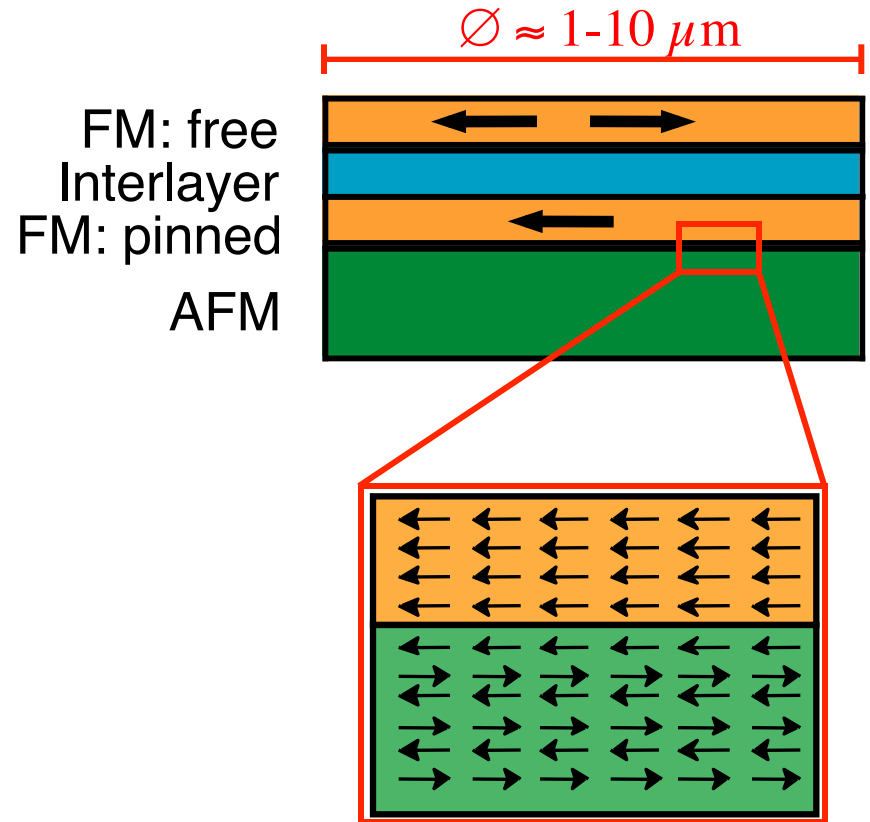
60% for AlO_x barriers @RT

>600% for epitaxial MgO @ RT

Typical TMR structure and measurement



$\text{Co}_{75}\text{Fe}_{25}(4 \text{ nm}) / \text{Al}_2\text{O}_3(0.8 \text{ nm}) / \text{Co}_{75}\text{Fe}_{25}(4 \text{ nm}) / \text{IrMn}(10 \text{ nm})$

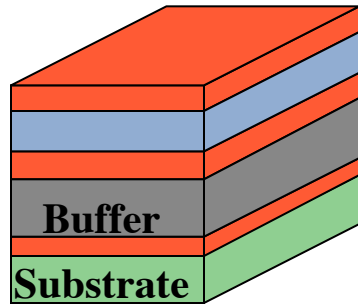


X. F. Han *et al.*, *Jpn. J. Appl. Phys.* **39**, L439 (2000)

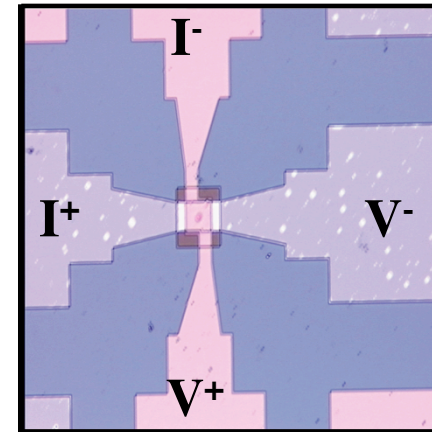
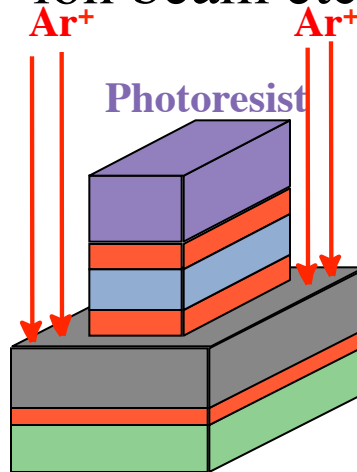
Intermezzo: Optical lithography of TMR junctions

Typical junction areas for TMR: $1 - 10^4 \mu\text{m}^2$

Growth of the layered system

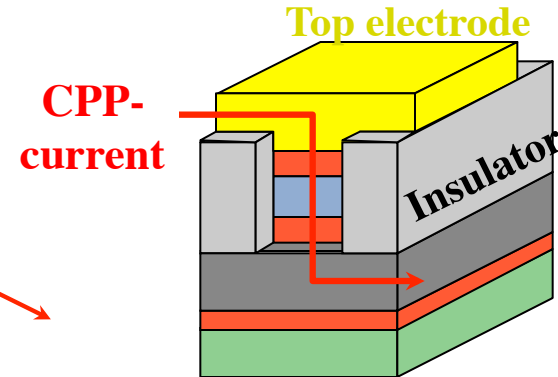


Optical lithography and ion beam etching



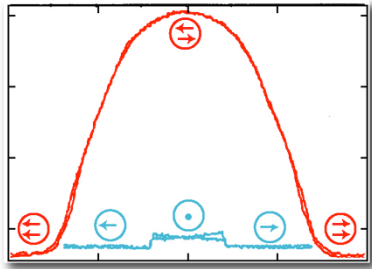
500 μm

Insulator deposition, lift-off, deposition of top electrode



Junctions of layered structures and dimensions on the μm -scale for CPP transport measurements

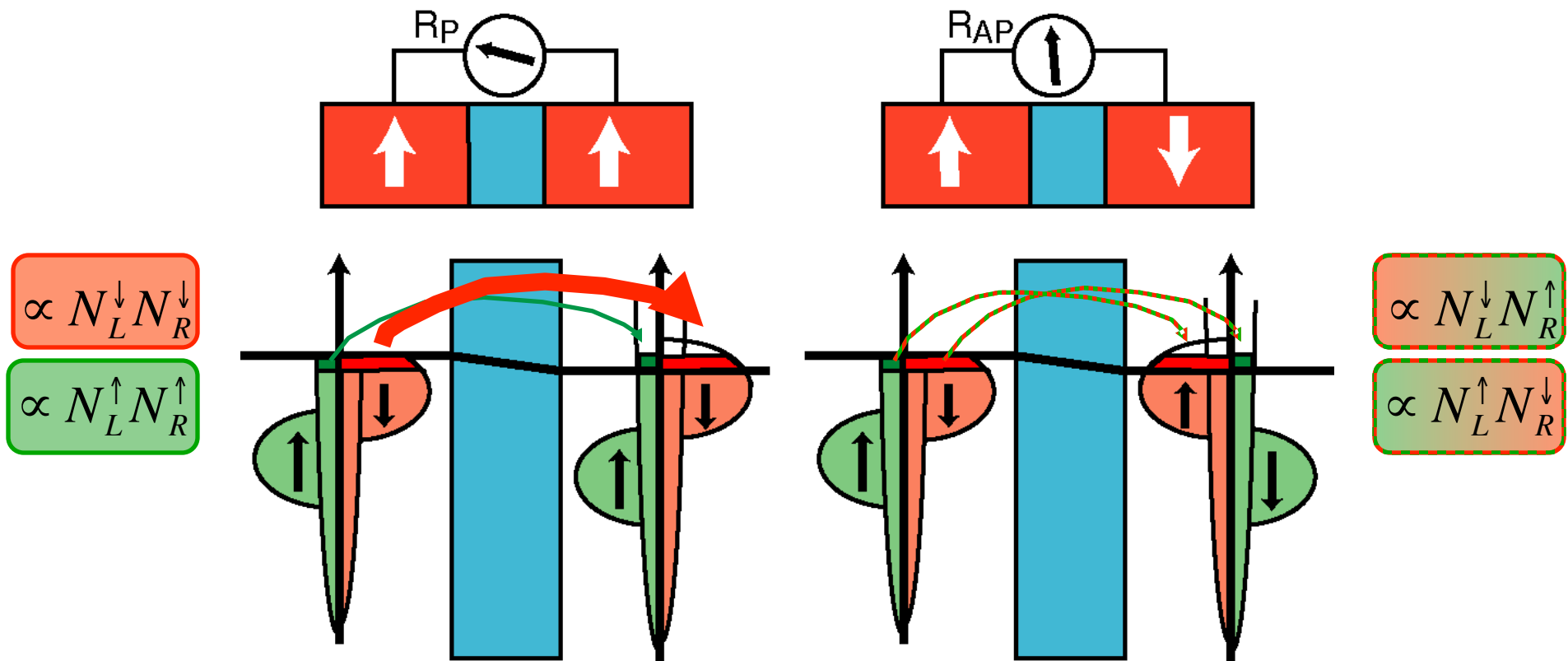
Outline: Giant and tunneling magnetoresistance (GMR and TMR)



- Phenomenology of GMR
- Intermezzo: Ferromagnetic halfmetals
- Physical picture for GMR
- Applications of GMR
- Phenomenology of TMR
- **Physical picture for TMR: Jullière and beyond**
- Applications of TMR

Microscopic picture of TMR: Spin-dependent tunneling

TMR exploits **spin-dependent tunneling probabilities** across an insulator rather than spin-dependent scattering probabilities in metals
 Assumptions: Spin and energy conservation during tunneling



\Rightarrow TMR depends on the spin-split DOS at the Fermi level $N_{L,R}^{\uparrow,\downarrow}$

Jullière's model

$$R_P = \frac{V}{I_P} \propto \frac{V}{N_L^\uparrow N_R^\uparrow + N_L^\downarrow N_R^\downarrow}$$

$$R_{AP} = \frac{V}{I_{AP}} \propto \frac{V}{N_L^\uparrow N_R^\downarrow + N_L^\downarrow N_R^\uparrow}$$

Consider the polarization at the Fermi level: $P_{L,R} = \frac{N_{L,R}^\uparrow - N_{L,R}^\downarrow}{N_{L,R}^\uparrow + N_{L,R}^\downarrow}$

M. Jullière, Phys. Lett. **54A**, 225 (1975)

$$\Rightarrow \text{TMR} = \frac{R_{AP} - R_P}{R_P} = \frac{2P_L P_R}{1 - P_L P_R} \quad \text{Jullière formula}$$

[$P_L P_R > 0$: normal and $P_L P_R < 0$: inverse TMR effect]

BUT: What are the relevant polarizations P_i ? Bulk? Interface?
Are interface states important?
What is the role of barrier material?

Jullière's model

$$R_P = \frac{V}{I_P} \propto \frac{V}{N_L^\uparrow N_R^\uparrow + N_L^\downarrow N_R^\downarrow}$$

$$R_{AP} = \frac{V}{I_{AP}} \propto \frac{V}{N_L^\uparrow N_R^\downarrow + N_L^\downarrow N_R^\uparrow}$$

3d transition metals:

$$P_L = P_R = 40 \dots 50\%$$

$$\Rightarrow \text{TMR} = 38 \dots 67\%$$

Consider the polarization at the Fermi level

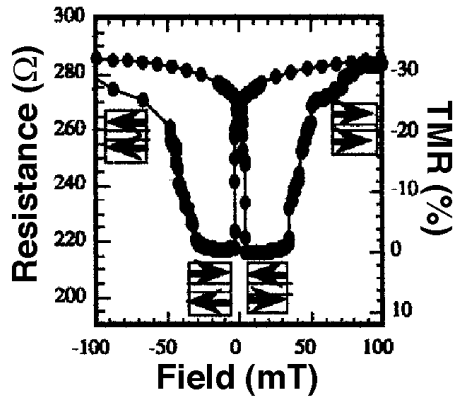
M. Jullière, Phys. Lett. **54A**, 225 (1975)

$$\Rightarrow \text{TMR} = \frac{R_{AP} - R_P}{R_P} = \frac{2P_L P_R}{1 - P_L P_R} \quad \text{Jullière formula}$$

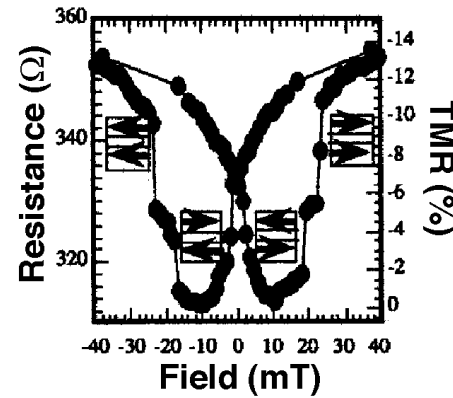
[$P_L P_R > 0$: normal and $P_L P_R < 0$: inverse TMR effect]

BUT: What are the relevant polarizations P_i ? Bulk? Interface?
Are interface states important?
What is the role of barrier material?

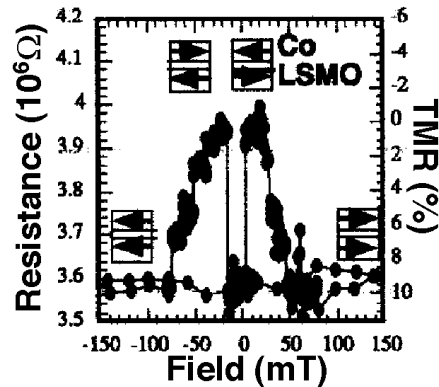
Beyond Jullière's model: Importance of barrier material



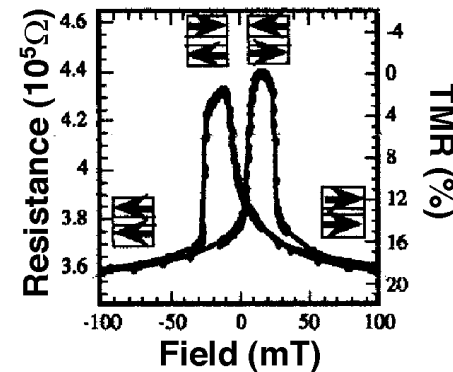
$\text{X} = \text{SrTiO}_3$
Inverse TMR



$\text{X} =$
 $\text{Ce}_{0.7}\text{La}_{0.3}\text{TiO}_{1.85}$
Inverse TMR



$\text{X} = \text{Al}_2\text{O}_3$
Normal TMR



$\text{X} =$
 $\text{Al}_2\text{O}_3 / \text{SrTiO}_3$
Normal TMR

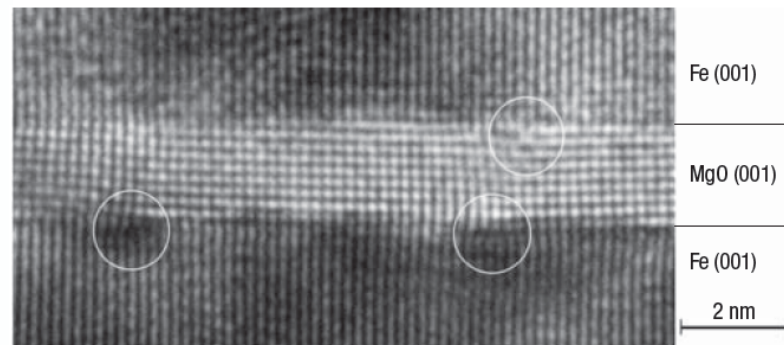
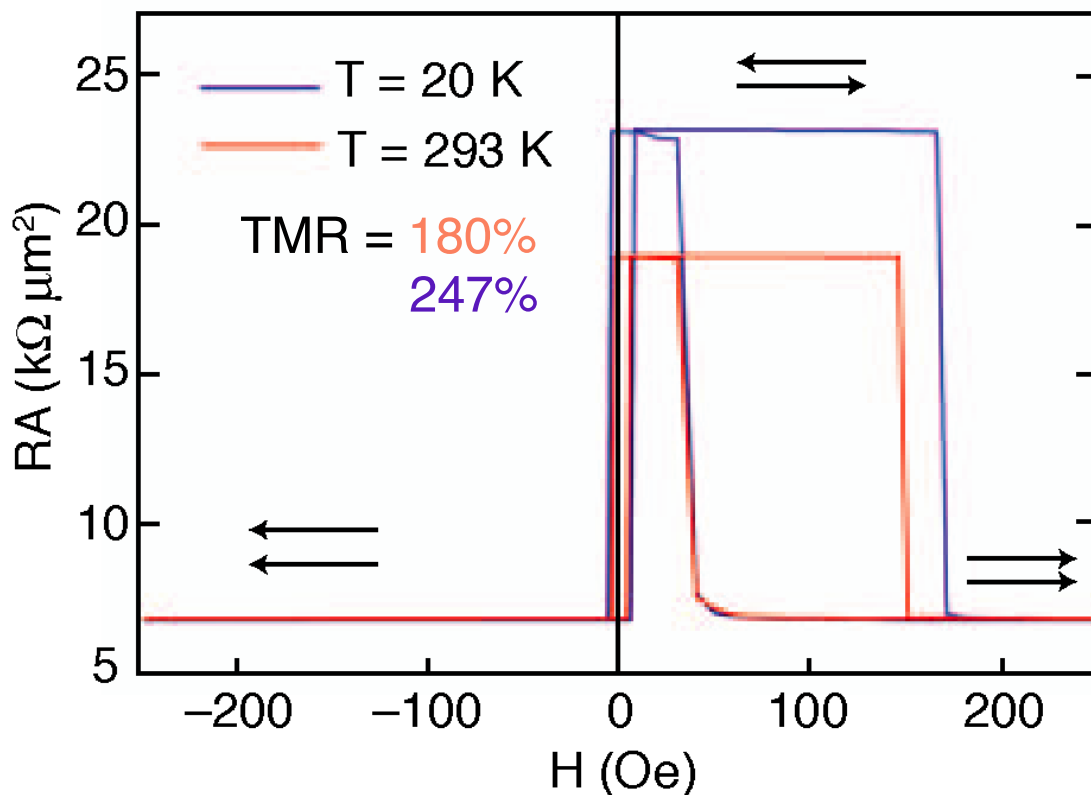
The **strength and sign** of TMR depend on the **barrier material**

P_L and P_R are related to the bonding details at the interface

J.M. de Teresa *et al.*, Science **286**, 507 (1999)

Beyond Jullière's model: Epitaxial MgO barriers

Epitaxial [1] or highly oriented [2] MgO(001) barriers yield very high TMR ratios of up to 220% at RT.

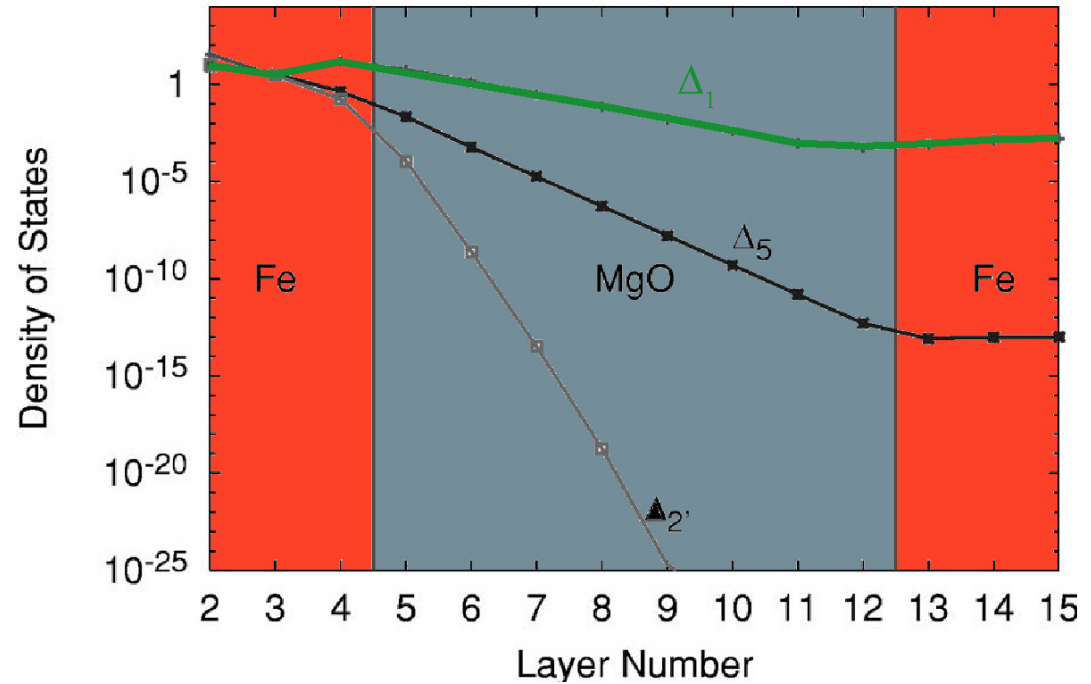
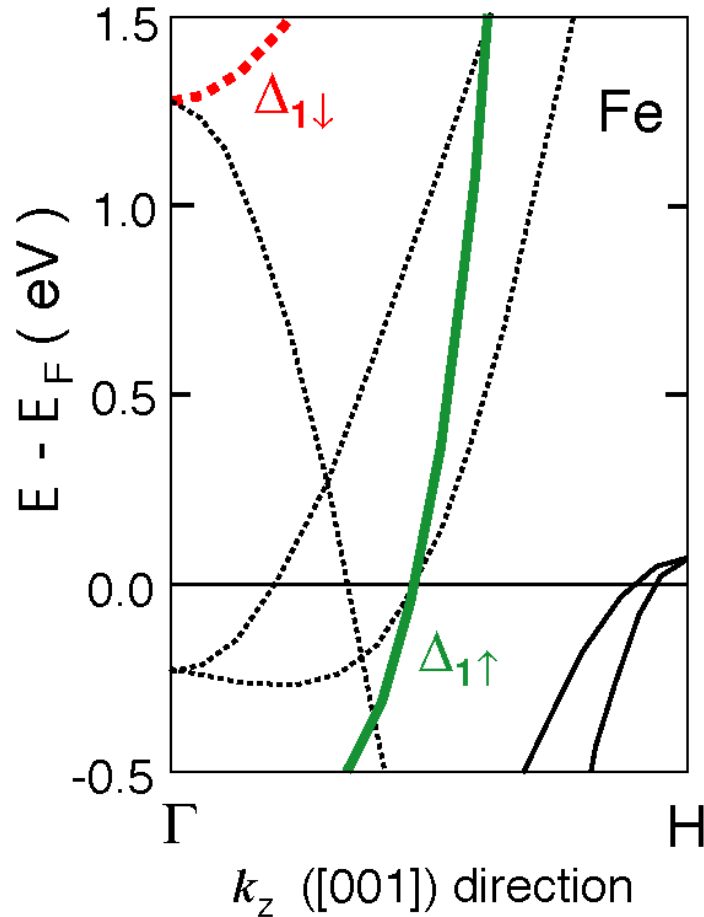


TEM of epitaxial MgO barrier [1]

High TMR ratios beyond what is expected from the Jullière's model
 \Rightarrow More realistic description of tunneling required

[1] S. Yuasa *et al.*, Nature Materials 3, 868 (2004), [2] S.S.P. Parkin *et al.*, Nature Materials 3, 862 (2004)

Beyond Jullière's model: Epitaxial MgO barriers



Δ_1 majority states decay slower and couple to propagating states in Fe

The high TMR is due to **predominant and coherent tunneling** of highly symmetric Fe Δ_1 majority states.

W.H. Butler et al., Phys. Rev. B 63, 054416 (2001)

“History” of TMR

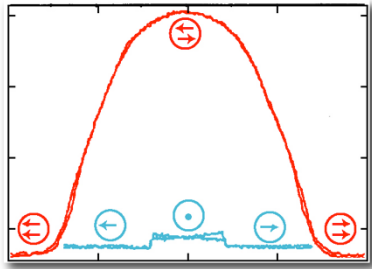
There is always more to come...

1975 **First observation of TMR** in Fe/Ge/Co by Jullière
14% but only at low temperature

1995 **Rediscovery of TMR** by Miyasaki and Moodera
up to the “theoretical Jullière limit” for 3d ferromagnets
and AlO_x barriers of about 60% at RT in the following years

2004 **Epitaxial structures with MgO barriers** yield TMR
ratios of up to 600% at RT

Outline: Giant and tunneling magnetoresistance (GMR and TMR)

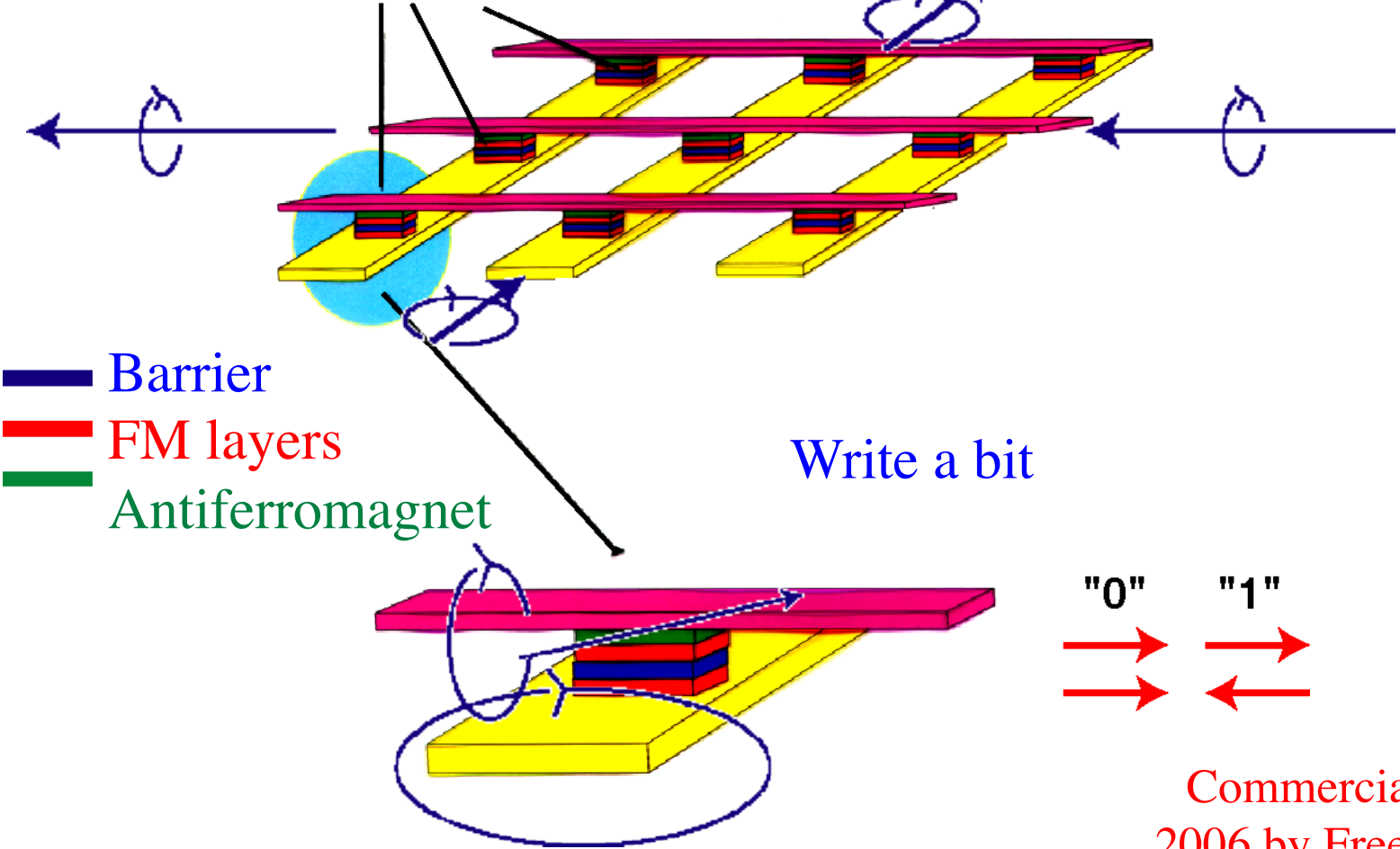


- Phenomenology of GMR
- Intermezzo: Ferromagnetic halfmetals
- Physical picture for GMR
- Applications of GMR
- Phenomenology of TMR
- Physical picture for TMR: Jullière and beyond
- Applications of TMR

Application of TMR: Magnetic RAM

Non-volatile, highly integrated solid-state device

Each TMR element represents one bit

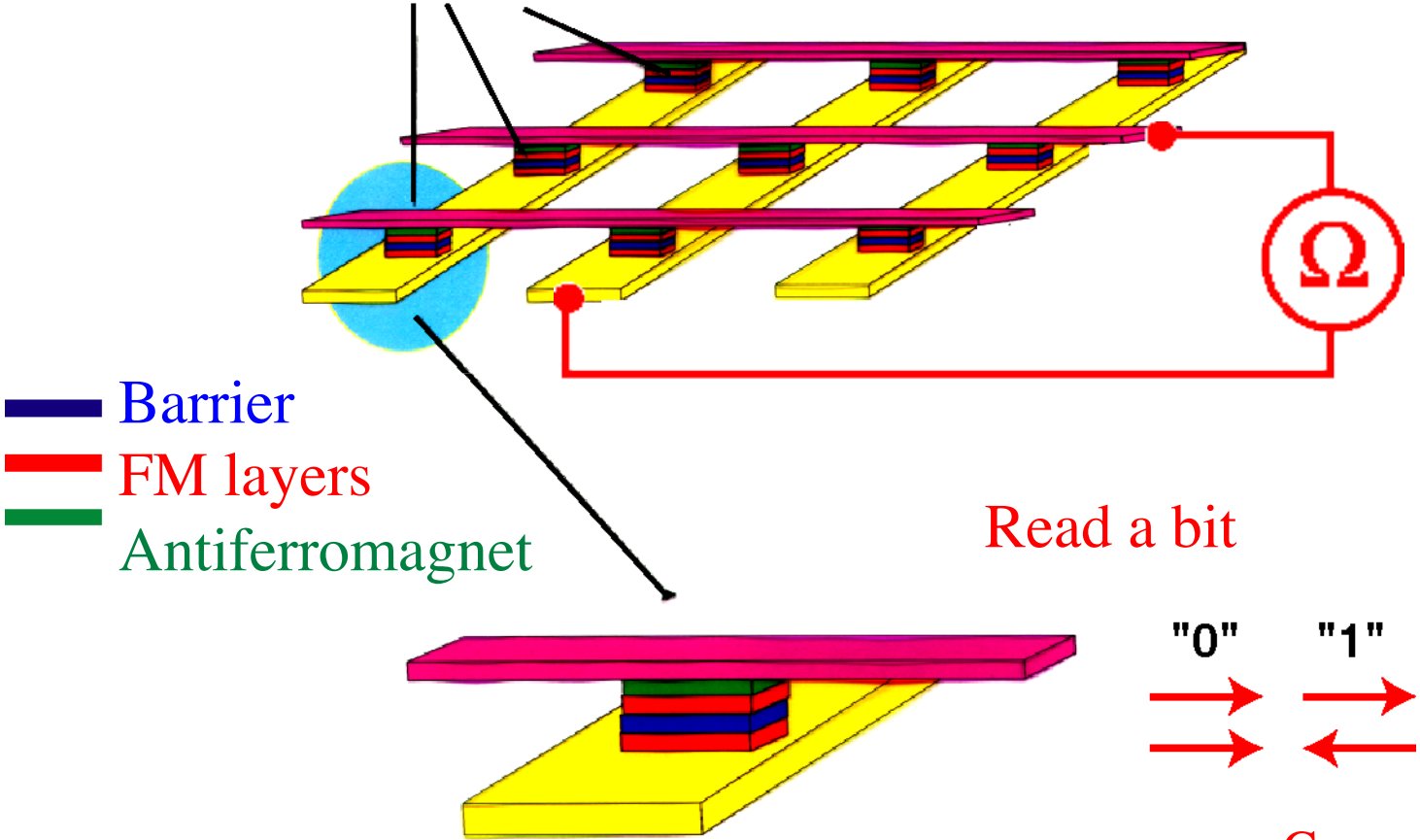


Commercialized
2006 by Freescale

Application of TMR: Magnetic RAM

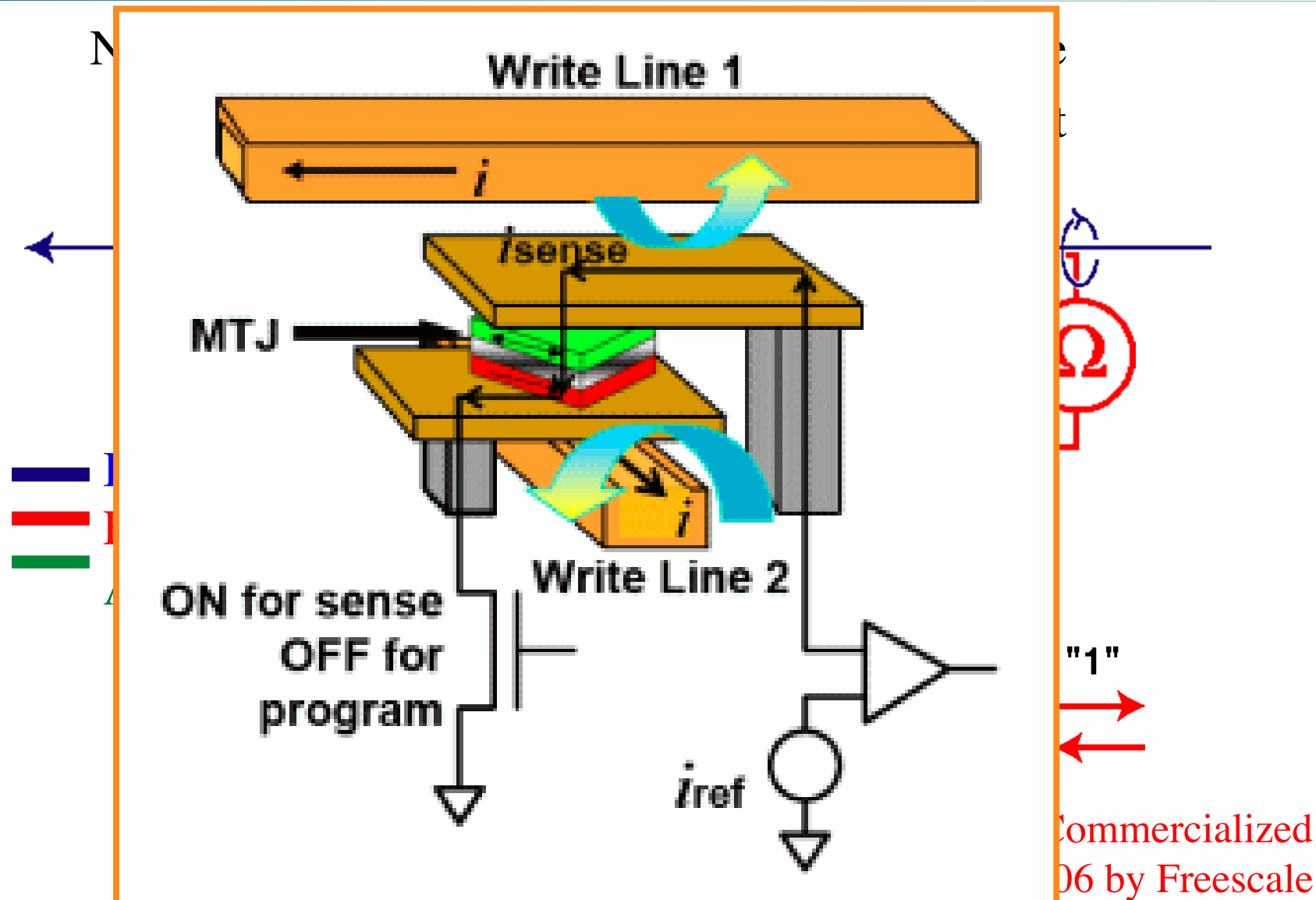
Non-volatile, highly integrated solid-state device

Each TMR element represents one bit



Commercialized
2006 by Freescale

Application of TMR: Magnetic RAM



Advanced switching concept

Giant or tunneling magnetoresistance (GMR, TMR):

“The magnetization state controls to the electric current flow”

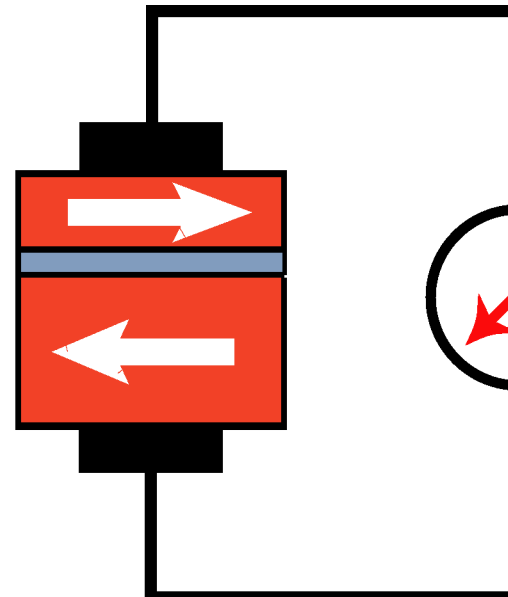
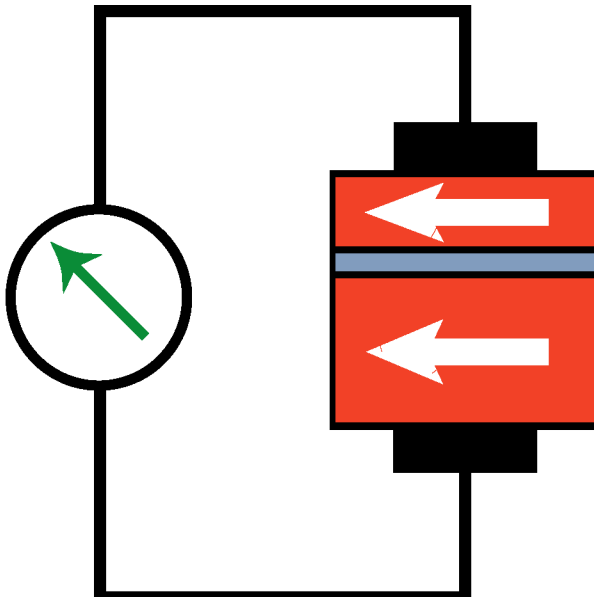
Parallel alignment

⇒ low resistive

Antiparallel alignment

⇒ high resistive

$R_P = \text{low}$
 $I_P = \text{high}$

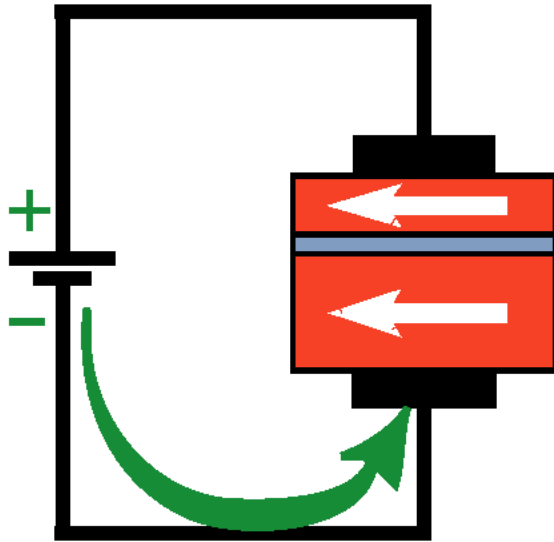


$R_{AP} = \text{high}$
 $I_{AP} = \text{low}$

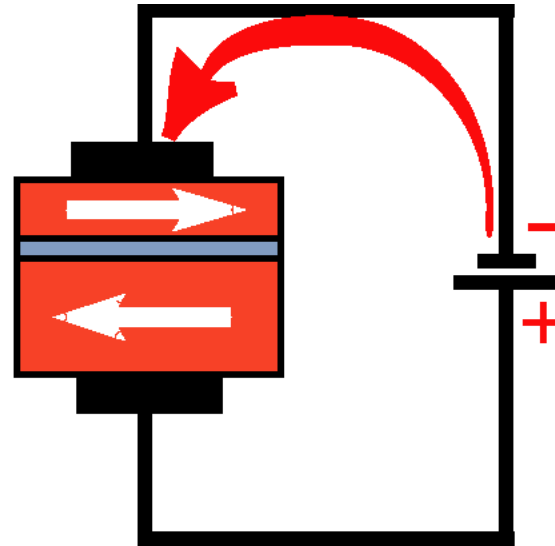
Advanced switching concept

Apply Newton's third law "*Actio = Reactio*" to GMR/TMR:
"*The electric current flow controls the magnetization state*"

Negative current
⇒ parallel alignment



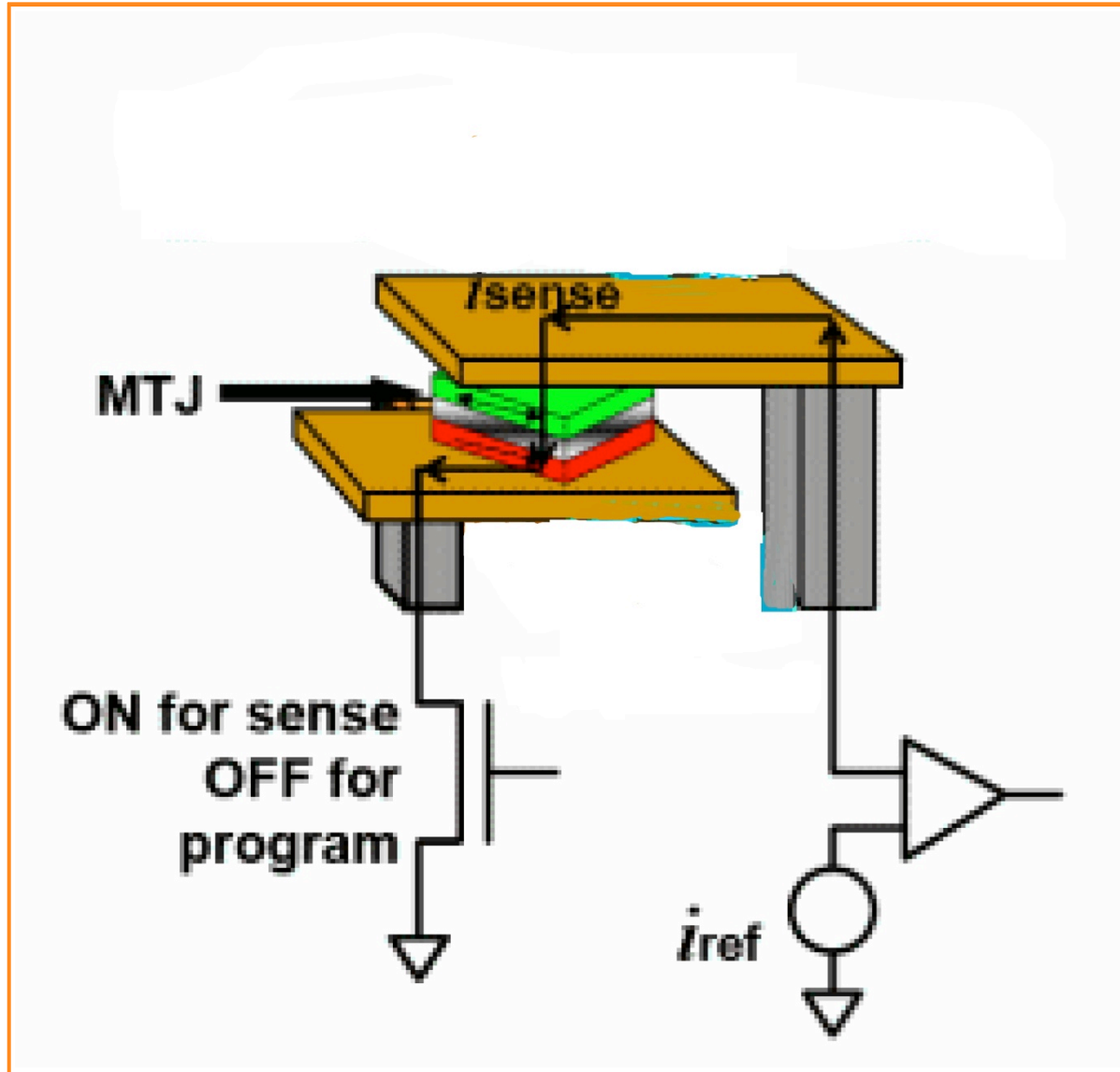
Positive current
⇒ Antiparallel alignment



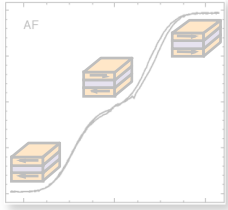
⇒ Current-induced magnetization switching
by spin-transfer torque

J.C. Slonczewski, J. Magn. Magn. Mater. **159**, L1 (1996); L. Berger, Phys. Rev B **54**, 9353 (1996)

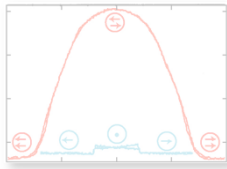
Magnetic random access memory (MRAM)



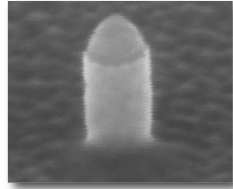
Introduction



Interlayer exchange coupling



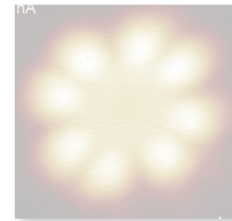
Giant and tunneling magnetoresistance



Current-induced magnetization dynamics



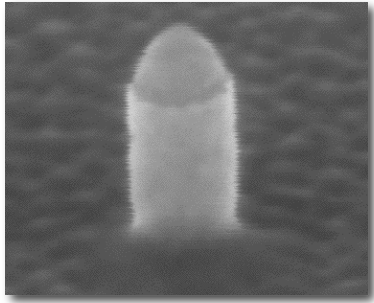
Pure spin current



Magnetic molecules

Conclusions

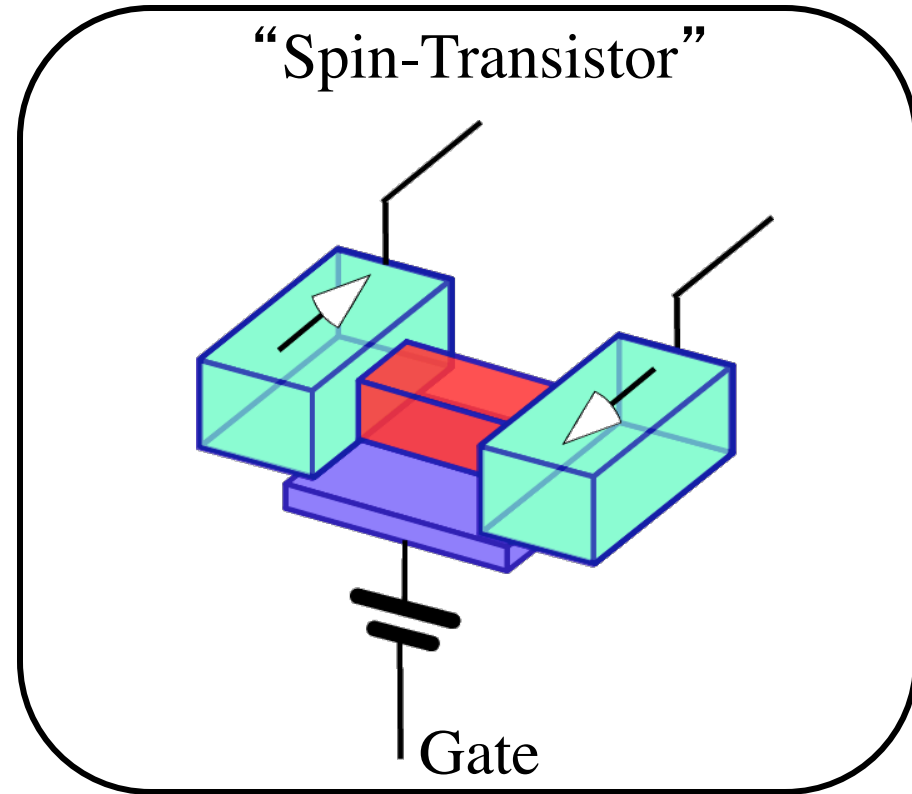
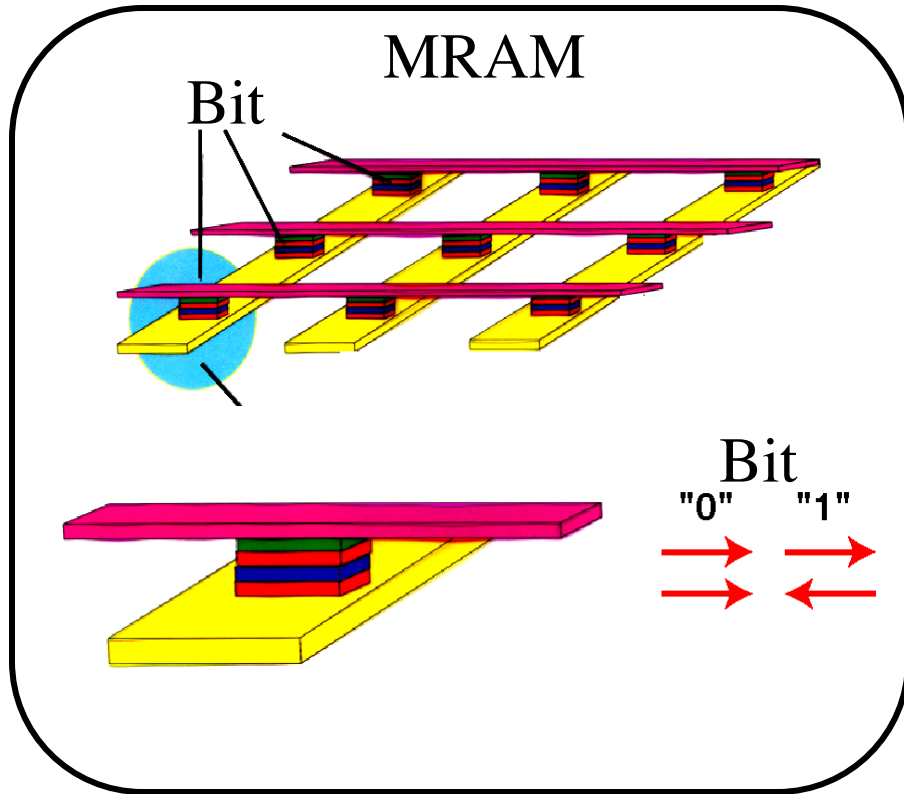
Outline: Current-induced magnetization dynamics



- Need for advanced magnetic switching concept
- Phenomenology of spin-transfer torque (STT)
“Current-induced magnetization switching”
- Physical picture for STT
- Current-driven magnetization dynamics
“Extended Landau-Lifshitz-Gilbert equation”
“Spin-torque oscillators (STO)”
- STT in non-uniform magnetization structures

Advanced switching concept for spintronic devices

Spintronic devices employ the electron spin for data storage and processing.

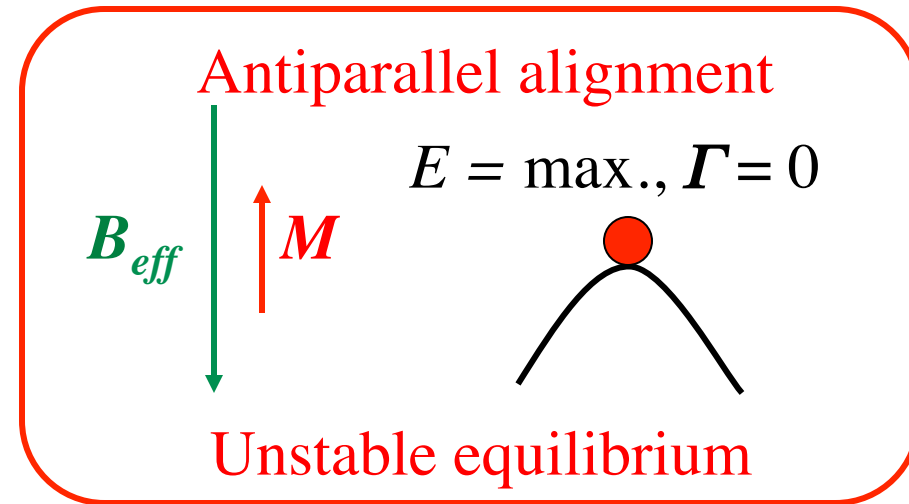
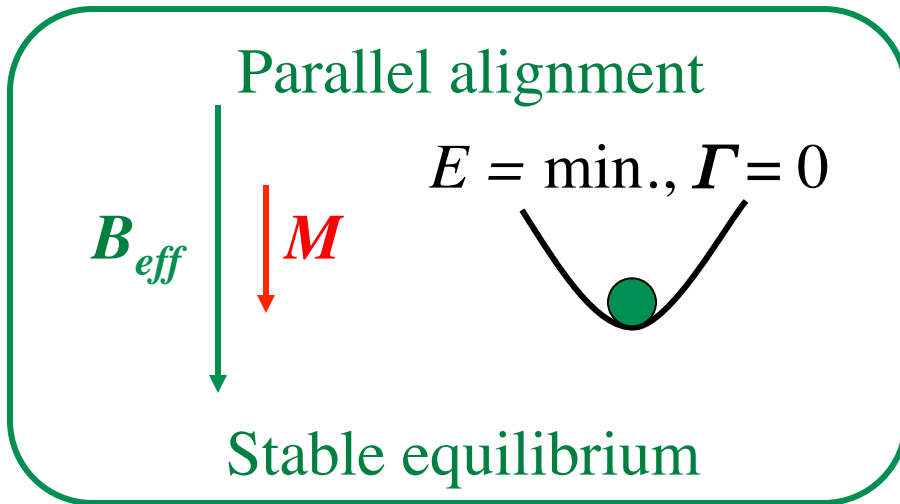


Manipulation of the magnetic state of ferromagnetic nano-scale objects, *e.g.* electrodes, is of crucial importance.

Conventional field-induced magnetization switching

Consider a constant magnetization \vec{M} within a certain volume. The effective field \vec{B}_{eff} gives rise to the energy density E and a torque $\vec{\Gamma}$:

$$E = -\vec{M} \cdot \vec{B}_{eff} \quad ; \quad \vec{\Gamma} = -(\vec{M} \times \vec{B}_{eff})$$

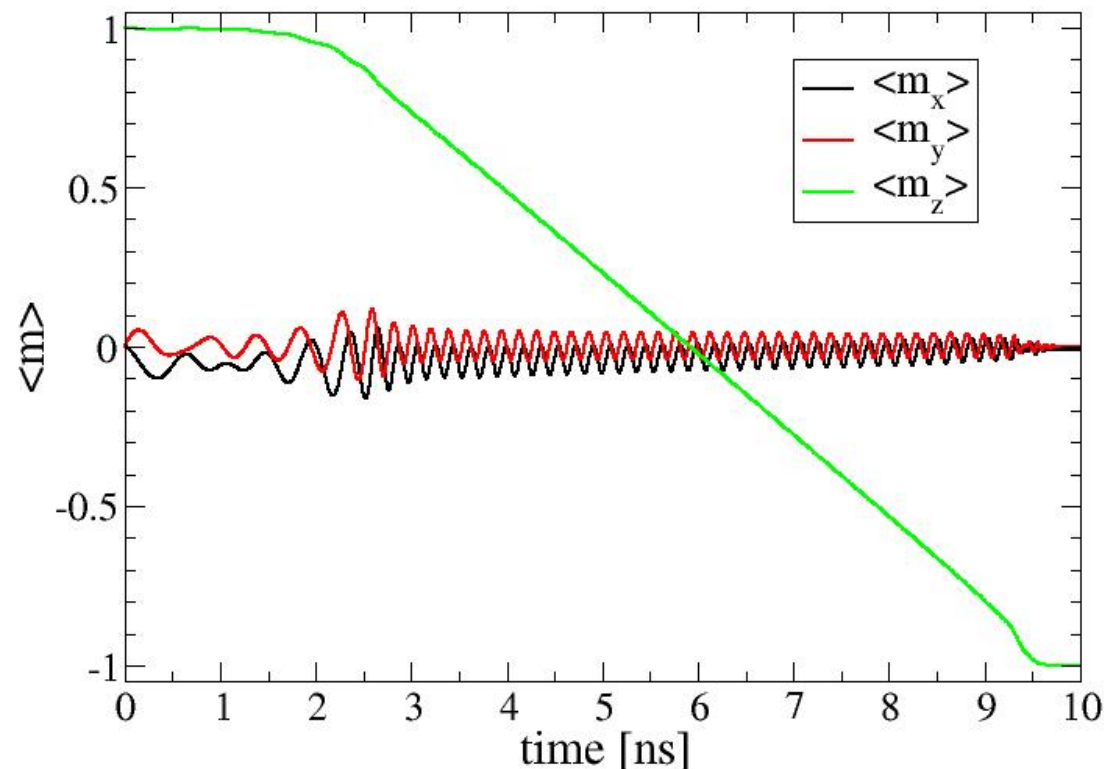


Conventional switching by applying an antiparallel field depends on perturbations (temperature, edges, magnetic inhomogeneities)
 \Rightarrow Slow, energetically inefficient, spatially incoherent

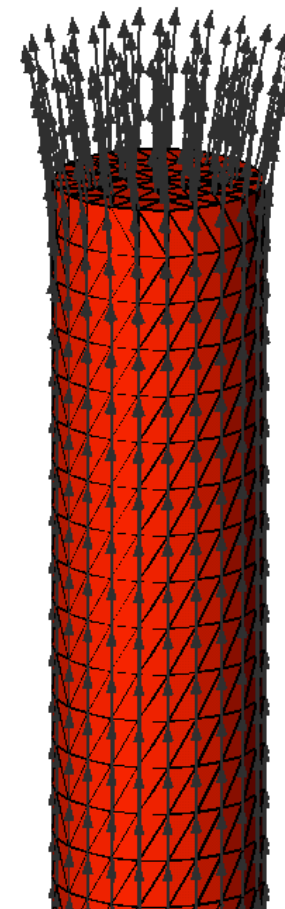
Conventional switching of a thin Ni nanowire

Ni wire, 40 nm diameter, 1 μm length, $\alpha = 0.1$ H = 200 mT.

$t = 0 \dots 4.5$ ns



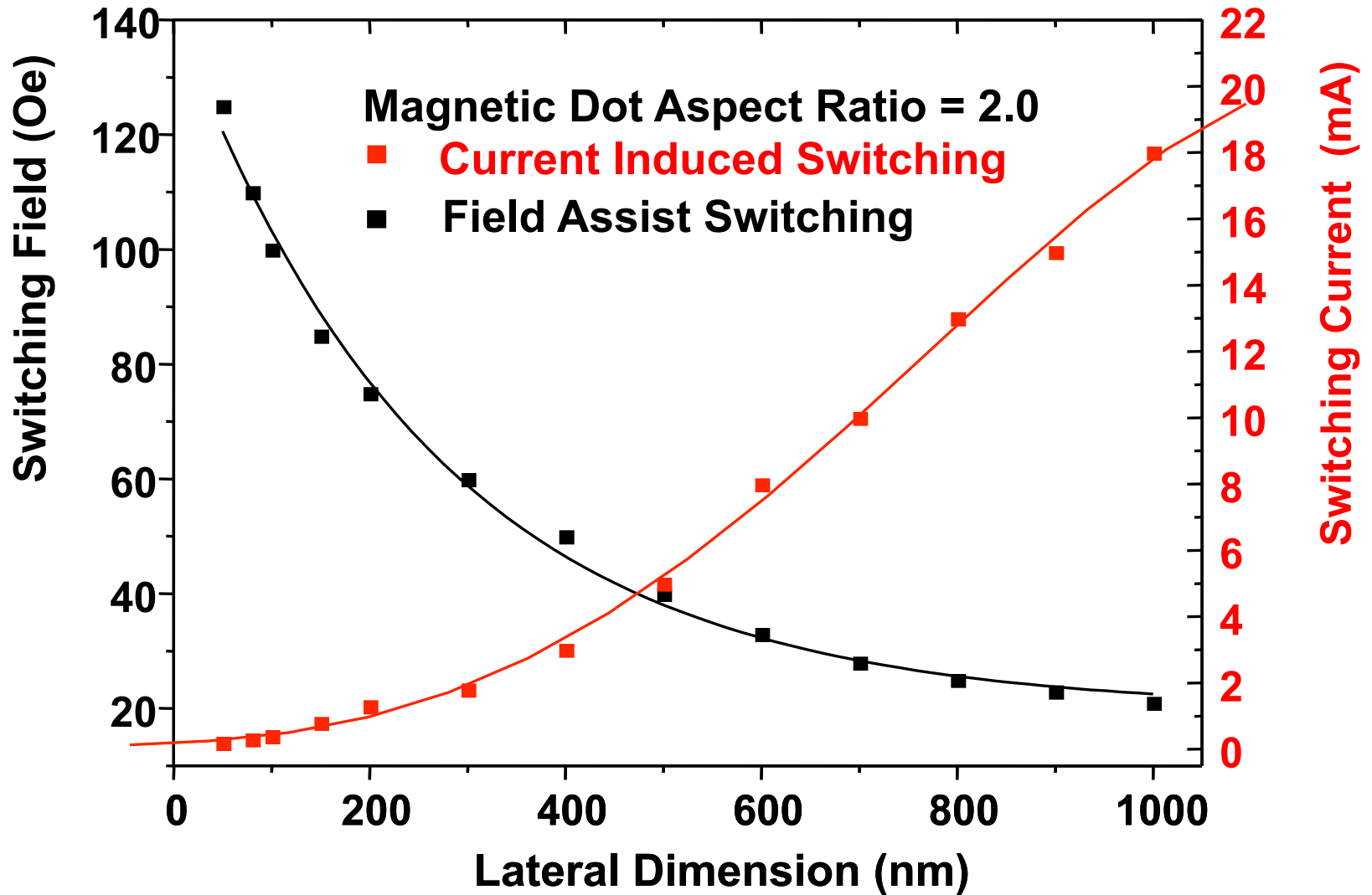
H_{ext} ↓



Nucleation, propagation, precession, ringing
⇒ slow, inefficient, incoherent

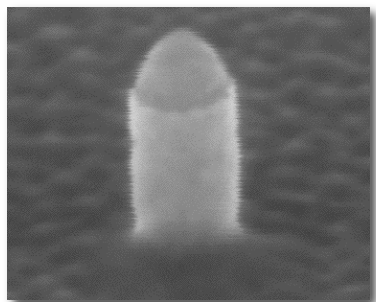
R. Hertel, J. Magn. Magn. Mater. **249**, 251 (2002).

Field-induced *versus* current-induced writing of MRAM cells



Kamel Ounadjela, Cypress Semiconductor

Outline: Current-induced magnetization dynamics



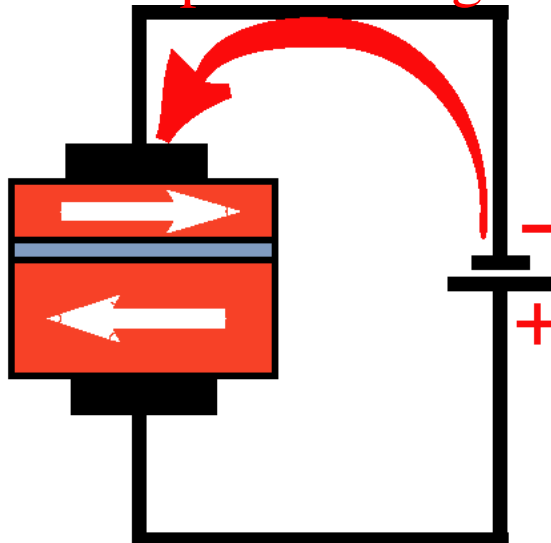
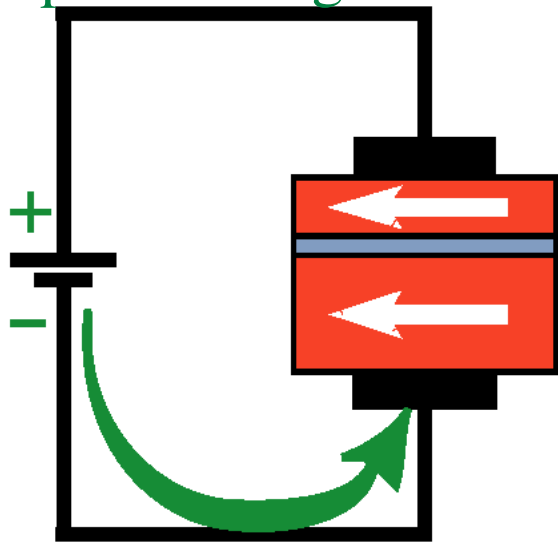
- Need for advanced magnetic switching concept
- Phenomenology of spin-transfer torque (STT)
“Current-induced magnetization switching”
- Physical picture for STT
- Current-driven magnetization dynamics
“Extended Landau-Lifshitz-Gilbert equation”
“Spin-torque oscillators (STO)”
- STT in non-uniform magnetization structures

Current-induced magnetization switching

The polarity of the electric current flow controls the magnetization state.

Negative current
⇒ parallel alignment

Positive current
⇒ Antiparallel alignment



100 nm
contact diameter

Electron flux

⇒ parallel

⇒ antiparallel

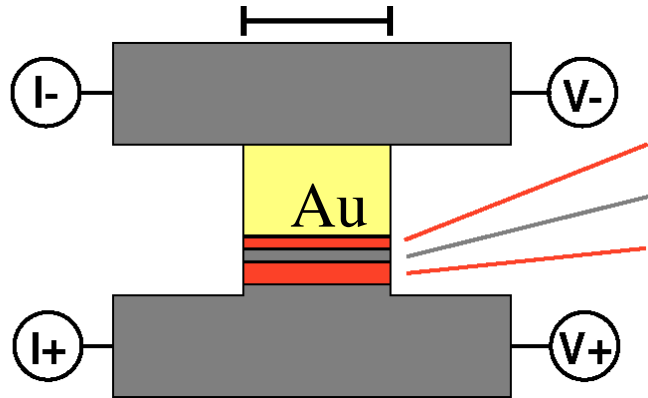
High current densities: $>10^7$ A/cm² or several mA per (100 nm)²

J.C. Slonczewski, J. Magn. Magn. Mater. **159**, L1 (1996); L. Berger, Phys. Rev B **54**, 9353 (1996)

E.B. Myers *et al.*, Science **285**, 867 (1999); J.A. Katine *et al.*, Phys. Rev. Lett. **84**, 3149 (2000)

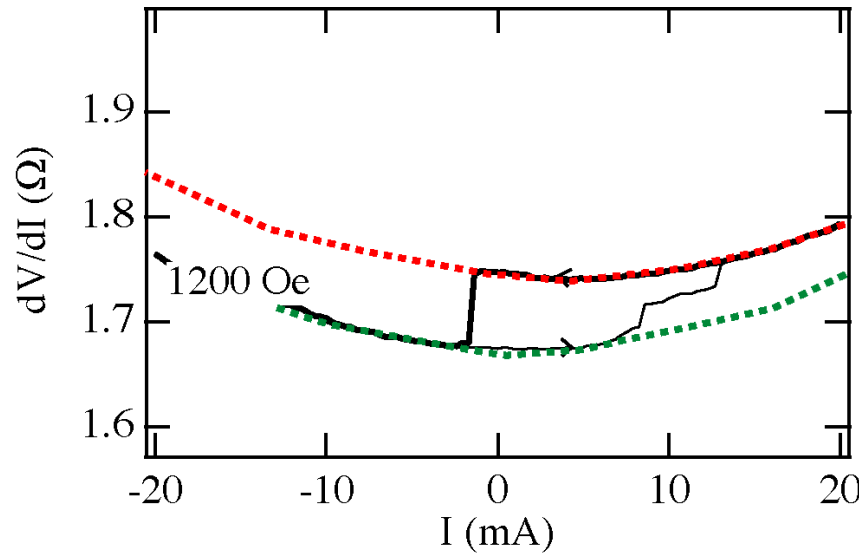
Pioneering work by the Cornell group

Columnar structure (“nanopillar”) and measurement via GMR effect:
 $\varnothing = 130 \text{ nm}$



Sputtered, polycrystalline system:
2.5 nm Co: thin, “free” FM layer
6.0 nm Cu: spacer
10.0 nm Co: thick, “fixed” FM layer

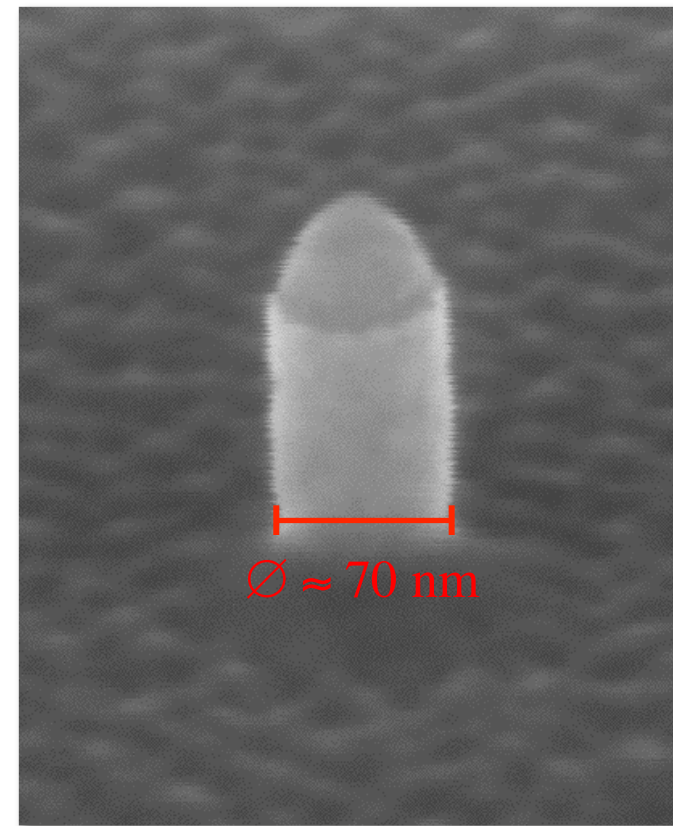
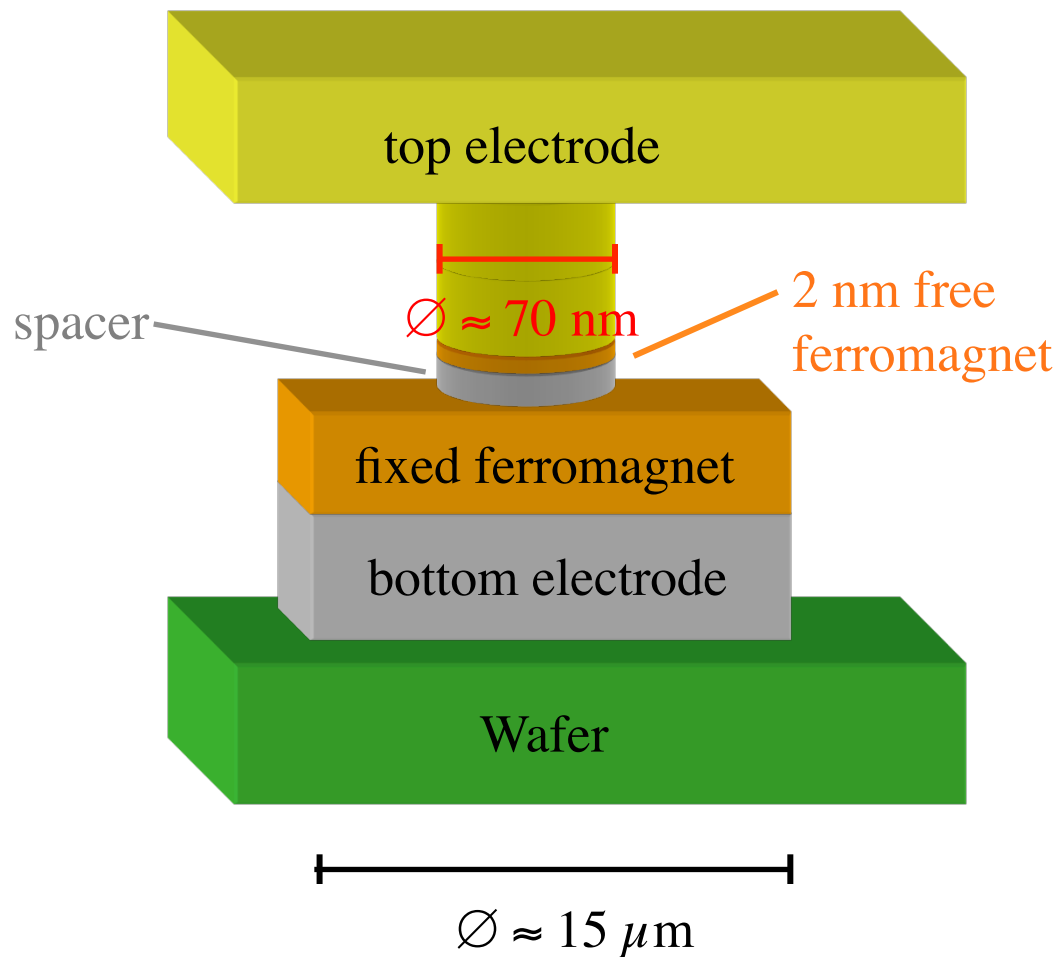
low resistive,
parallel state for
negative current



high resistive,
antiparallel state for
positive current

E.B. Myers *et al.*, Science **285**, 867 (1999); J.A. Katine *et al.*, Phys. Rev. Lett. **84**, 3149 (2000)

Nanopillars for spin-transfer torque effects

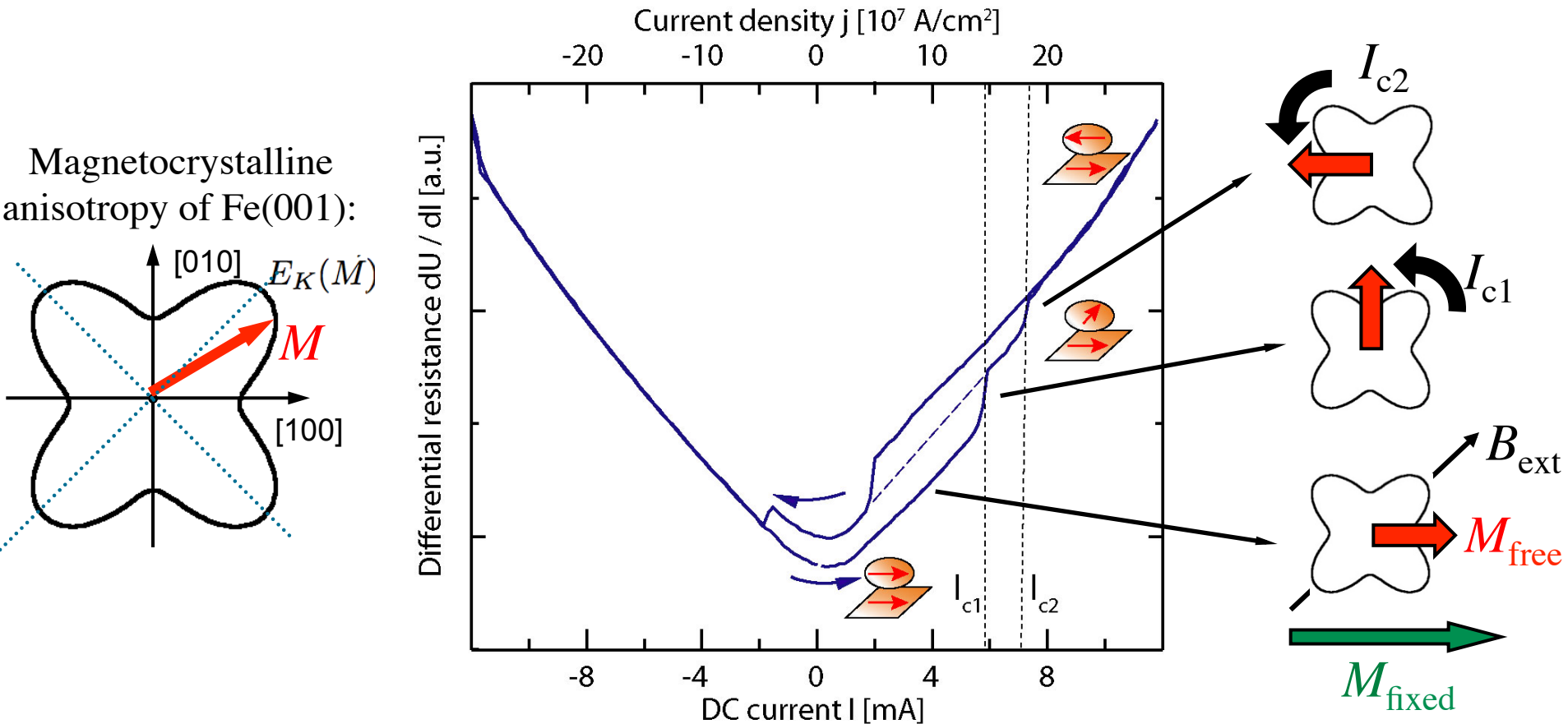


SEM micrograph

R. Lehndorff, D.E. Bürgler *et al.*, Phys. Rev. B **76**, 214420 (2007);
H. Dassow, D.E. Bürgler *et al.*, Appl. Phys. Lett. **89**, 222511 (2006)

Interplay between crystalline anisotropy and STT

2 nm Fe / 6 nm Ag / 20 nm Fe at 5 K; $B_{\text{ext}} = 7.9$ mT along hard axis



⇒ Precise control of magnetization alignment by current

R. Lehndorff, D.E. Bürgler *et al.*, Phys. Rev. B76, 214420 (2007)

Switching by Oersted field of current?

The current ($\approx 10^7$ A/cm²) gives rise to a circular magnetic field, which favors a vortex-like magnetization state in the small magnetic elements.

BUT:

- The vortex state is symmetric with respect to the current polarity
 - The maximum Oersted field at the edge scales like $\alpha I/d$
 - The spin-torque transfer (STT) scales like $\beta I/d^2$
(current I , contact diameter d)

STT exceeds Oersted field ($\beta I/d^2 > \alpha I/d$) for d below $1 \mu\text{m}$

Contact diameters of several 100 nm ...

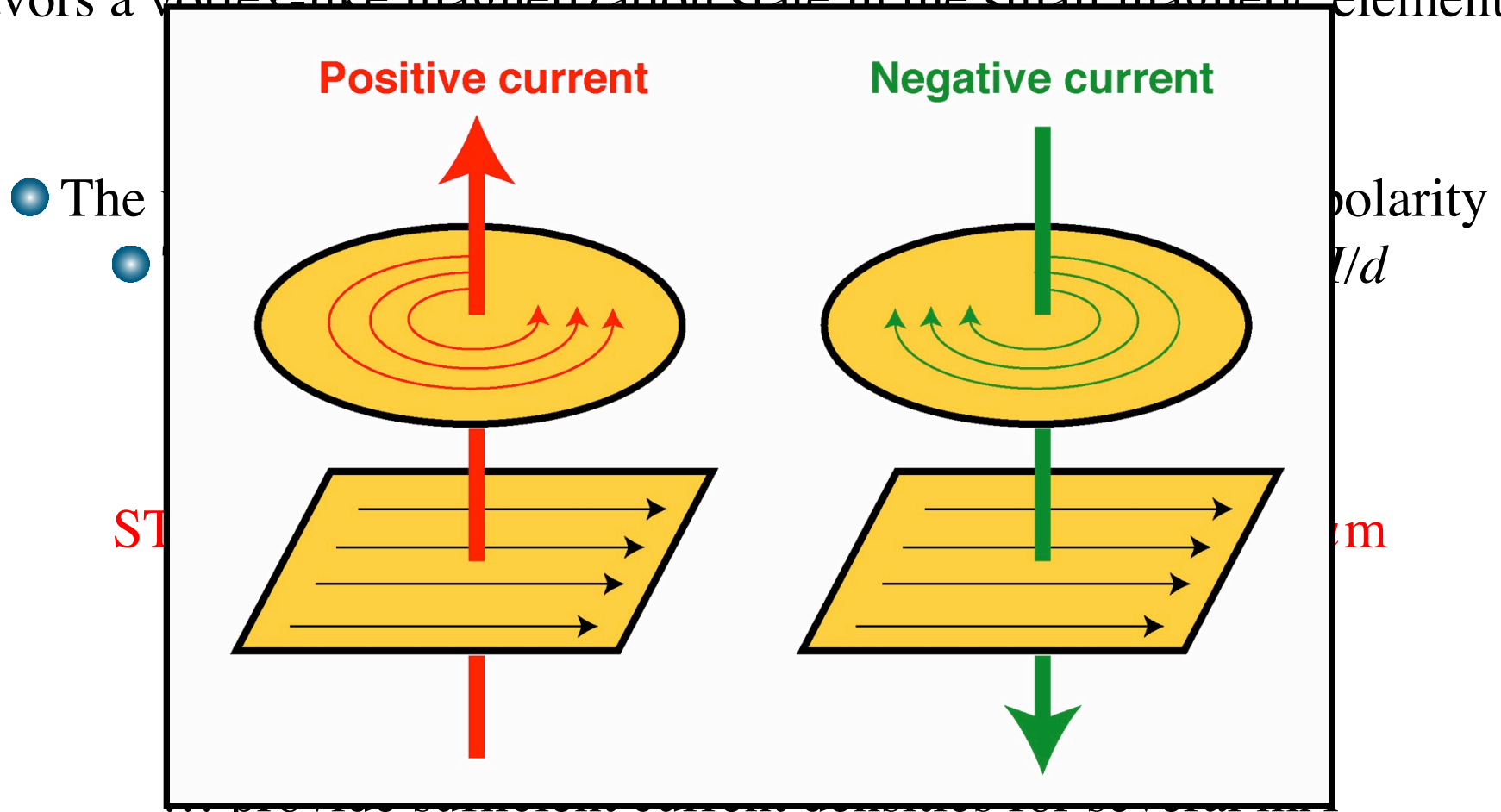
... are needed to overcome Oersted fields

... provide sufficient current densities for several mA

... are feasible with electron-beam lithography

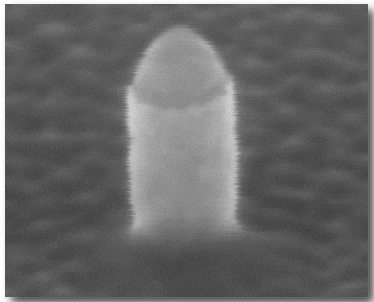
Switching by Oersted field of current?

The current ($\approx 10^7$ A/cm²) gives rise to a circular magnetic field, which favors a vortex-like magnetization state in the small magnetic elements.



... are feasible with electron-beam lithography

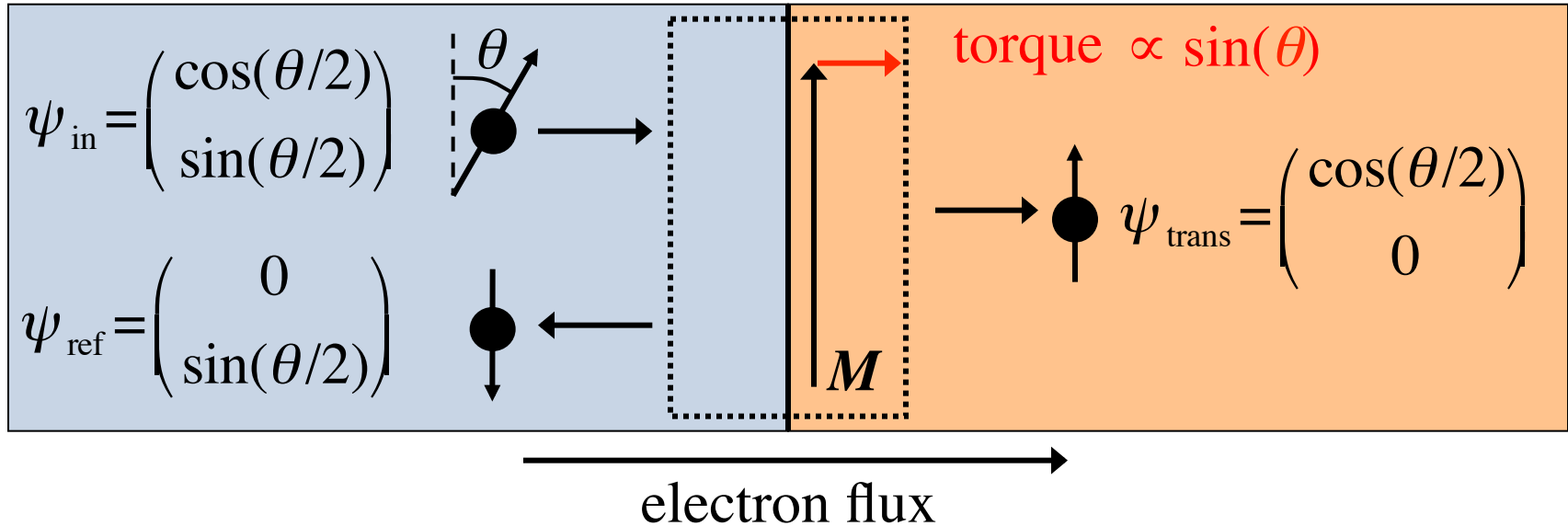
Outline: Current-induced magnetization dynamics



- Need for advanced magnetic switching concept
- Phenomenology of spin-transfer torque (STT)
“Current-induced magnetization switching”
- **Physical picture for STT**
- Current-driven magnetization dynamics
“Extended Landau-Lifshitz-Gilbert equation”
“Spin-torque oscillators (STO)”
- STT in non-uniform magnetization structures

Absorption of transversal spin component I

Consider a polarized current entering from a **non-magnet** into a **ferromagnet**. The spin-split DOS gives rise to spin-dependent transmission and reflection at the interface:



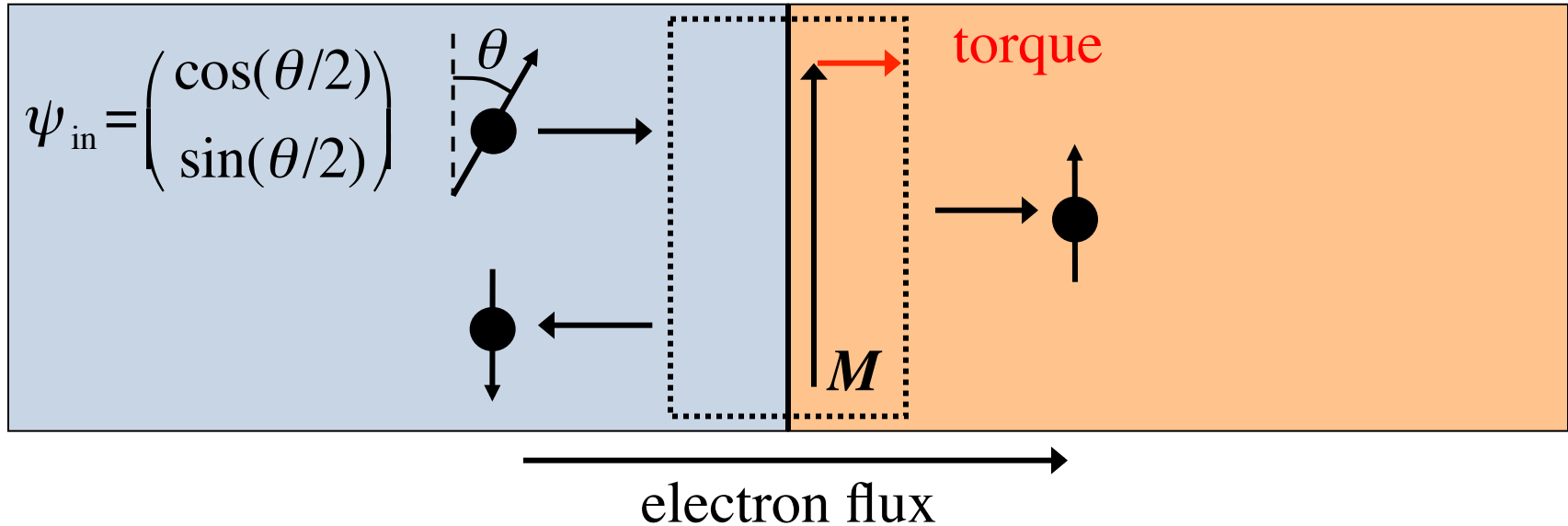
Transversal spin moment is absorbed and acts as a torque on the magnetization \Rightarrow **Spin filtering**

Spinors for ideal spin filtering, *e.g.* for a half-metallic ferromagnet

M. Stiles and A. Zangwill, Phys. Rev B **66**, 014407 (2002)

Absorption of transversal spin component I

Consider a polarized current entering from a **non-magnet** into a **ferromagnet**. The spin-split DOS gives rise to spin-dependent transmission and reflection at the interface:



Transversal spin moment is absorbed and acts as a torque on the magnetization \Rightarrow **Spin filtering**

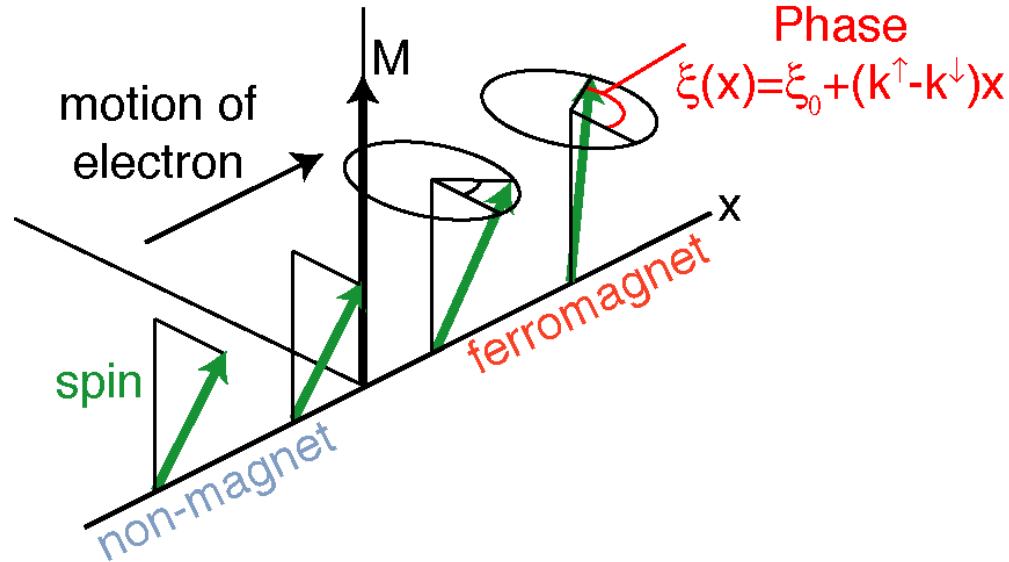
In realistic cases, spin filtering absorbs about 50% of the transversal spin component. The other 50% are transmitted or reflected.

M. Stiles and A. Zangwill, Phys. Rev B **66**, 014407 (2002)

Absorption of transversal spin component II

Spin-up and spin-down waves of the transmitted electrons have in the ferromagnet different k vectors, k^\uparrow and k^\downarrow .

⇒ Each spin precesses in space and acquires a k -dependent phase ξ



Summing over all k , different ξ reduce the transversal spin component

⇒ Absorption of the transversal spin component due to spatial spin precession in the ferromagnet

M. Stiles and A. Zangwill, Phys. Rev B **66**, 014407 (2002)

Absorption of transversal spin component III

Quantum-mechanically, a reflected or transmitted spin is rotated by some k -dependent angle

Summing over all k , different rotation angles reduce the transversal spin component

⇒ Absorption of the transversal spin component due to spin rotation of reflected and transmitted electrons

All three effects together

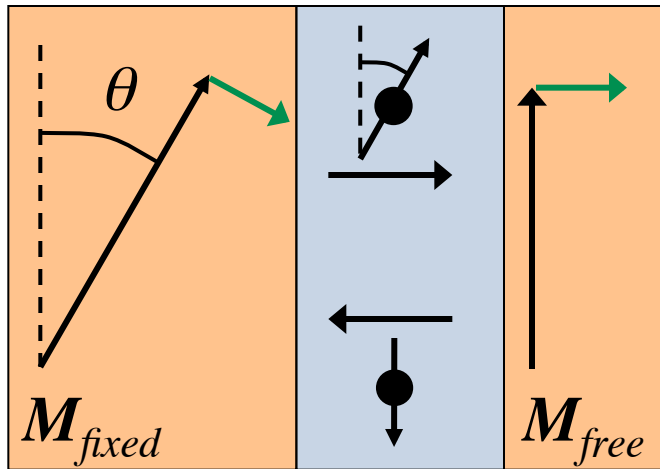
–(i) spin filtering, (ii) spin precession, and (iii) spin rotation– completely absorb near the interface the transversal spin component of the incident current, which acts as a torque on the magnetization

M. Stiles and A. Zangwill, Phys. Rev B **66**, 014407 (2002)

Physical picture

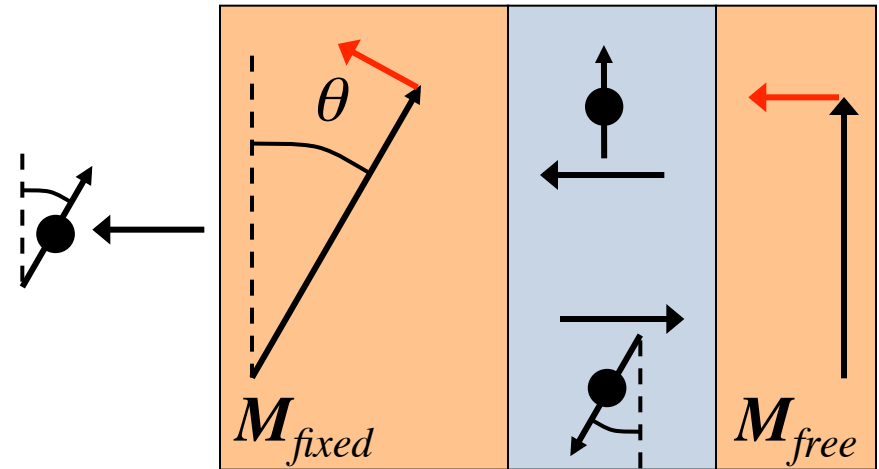
A second FM layer with tilted magnetization polarizes the incident current. One layer (M_{free}) is easier to switch than the other (M_{fixed}):

electron flux



M_{free} rotates towards M_{fixed}
 \Rightarrow stabilization of
parallel alignment

electron flux



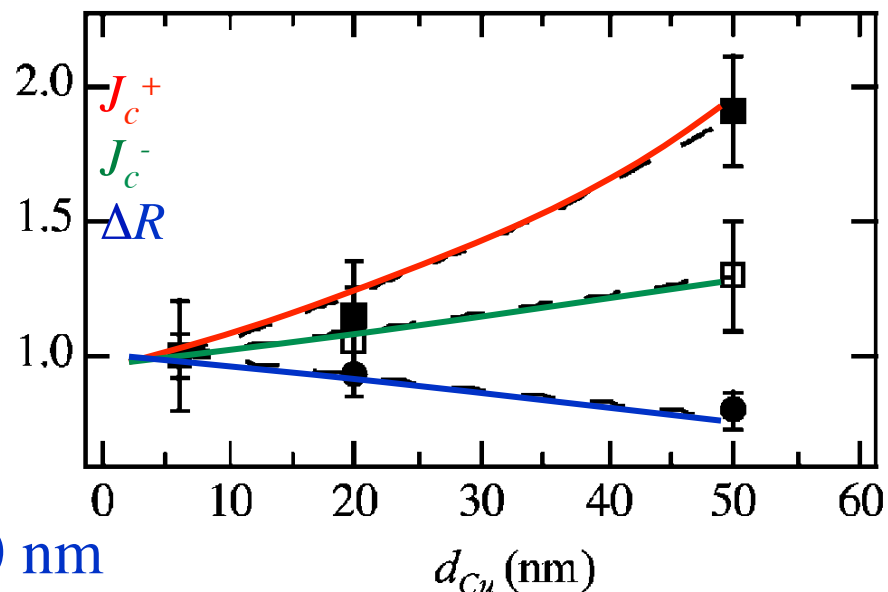
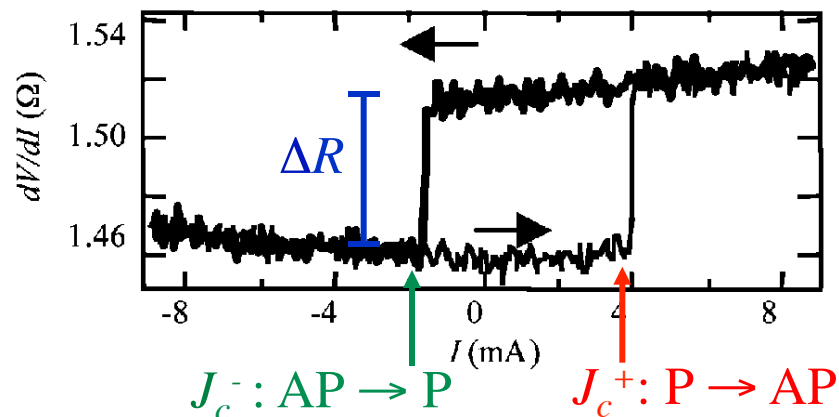
M_{free} rotates away from M_{fixed}
 \Rightarrow destabilization of
antiparallel alignment

Note importance of reflected current and asymmetry of FM layers

X. Waintal *et al.*, Phys. Rev. B **62**, 12317 (2000)

Confirmation of picture: Dependence on spacer thickness

Spin-flip scattering in the spacer reduces the spin-torque transfer efficiency g and requires larger critical current densities J_c^+ , J_c^- .



$$\Delta R \propto \exp(-d_{Cu}/\lambda) \quad \Rightarrow \quad \lambda = 190 \pm 20 \text{ nm}$$

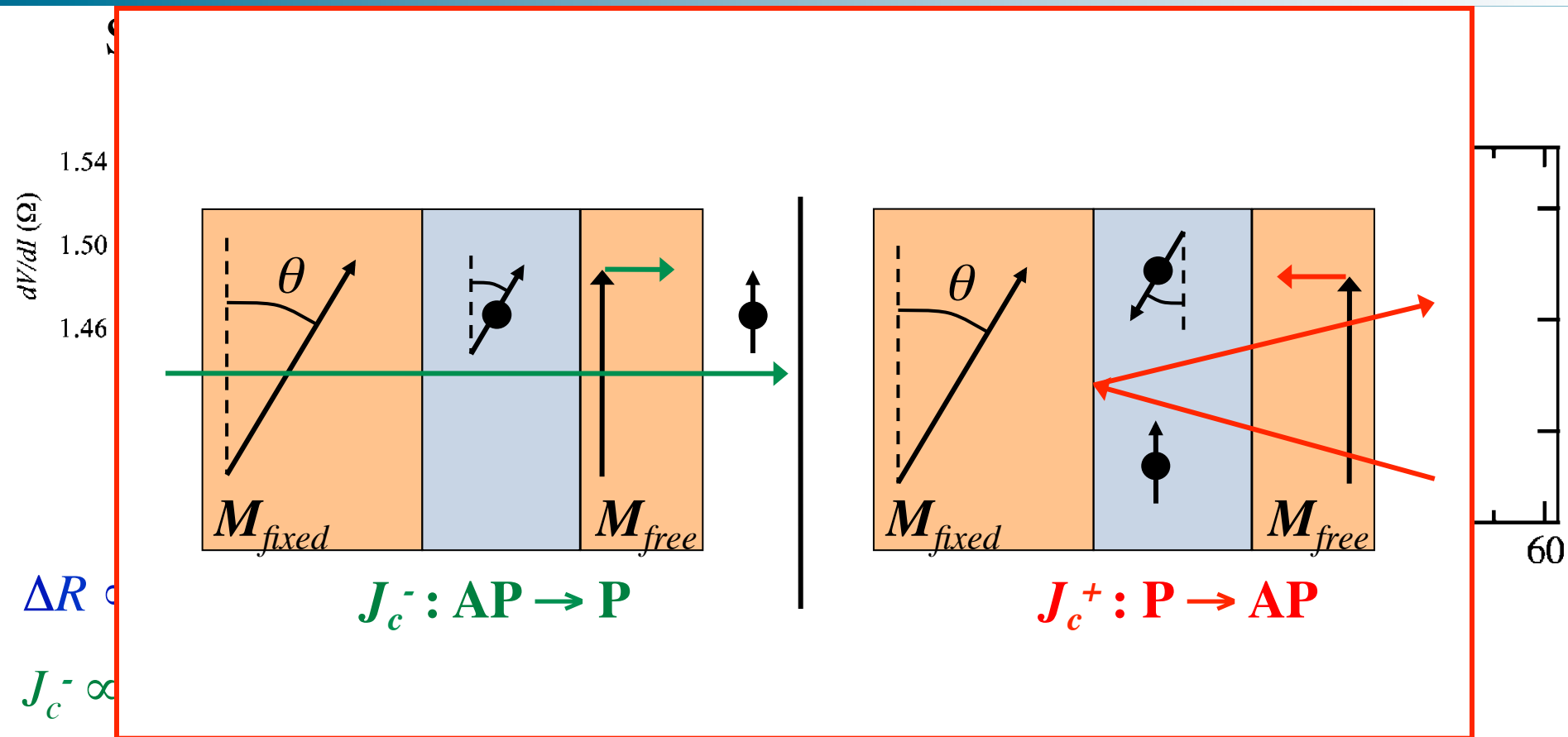
$$J_c^- \propto \exp(d_{Cu}/\lambda) \quad \Rightarrow \quad \lambda = 170 \pm 40 \text{ nm}$$

$$J_c^+ \propto \exp(2d_{Cu}/\lambda) \quad \Rightarrow \quad \lambda = 140 \pm 30 \text{ nm} \quad (70 \pm 20 \text{ nm without factor 2)}$$

Reflected electron must cross the spacer layer twice!

F.J. Albert *et al.*, Phys. Rev. Lett. **89**, 226802 (2002)

Confirmation of picture: Dependence on spacer thickness



$J_c^+ \propto \exp(2d_{Cu}/\lambda) \Rightarrow \lambda = 140 \pm 30 \text{ nm} (70 \pm 20 \text{ nm without factor 2})$

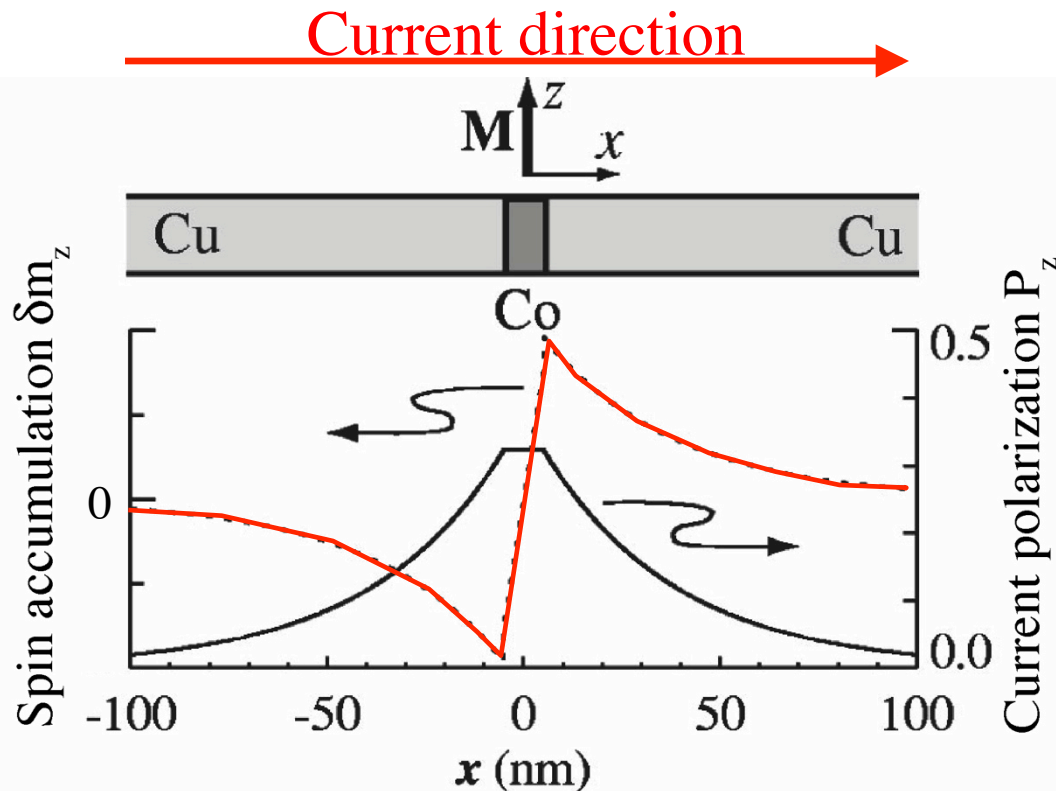
Reflected electron must cross the spacer layer twice!

F.J. Albert *et al.*, Phys. Rev. Lett. **89**, 226802 (2002)

Role of diffusive transport

Above consideration is correct for any spin-polarized current:

- Ballistic current due to drift motion in an electric field
- Diffusive current due to spin accumulation δm_z

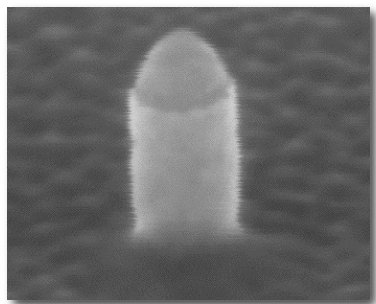


Spin accumulation δm_z decays due to spin-flip scattering over distances given by the spin scattering length λ

\Rightarrow gradient in δm_z

\Rightarrow diffusive spin-polarized current

Outline: Current-induced magnetization dynamics



- Need for advanced magnetic switching concept
- Phenomenology of spin-transfer torque (STT)
“Current-induced magnetization switching”
- Physical picture for STT
- **Current-driven magnetization dynamics**
“Extended Landau-Lifshitz-Gilbert equation”
“Spin-torque oscillators (STO)”
- STT in non-uniform magnetization structures

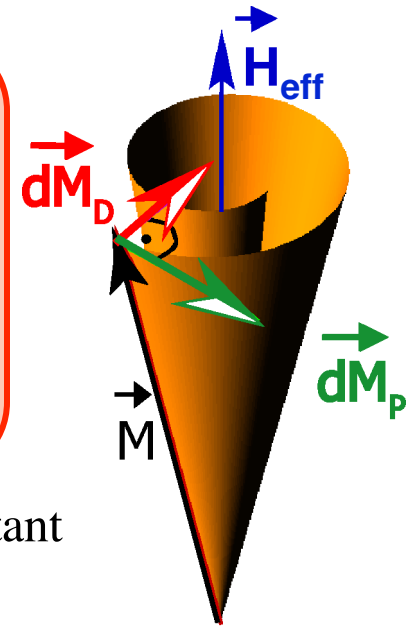
Landau-Lifshitz-Gilbert (LLG) equation

Landau-Lifshitz-Gilbert equation describes the motion of \vec{M} in \vec{H}_{eff} :

$$\frac{d\vec{M}}{dt} = -\frac{\gamma}{1+\alpha^2} [\vec{M} \times \vec{H}_{\text{eff}}] - \frac{\alpha\gamma}{M_s(1+\alpha^2)} \vec{M} \times [\vec{M} \times \vec{H}_{\text{eff}}] ; \vec{H}_{\text{eff}} = -\frac{1}{\mu_0} \frac{\delta E_{\text{tot}}}{\delta \vec{M}}$$

Precession around H_{eff}
with Larmor frequency
of typically several GHz
(e.g. Fe, Co, Ni)
 $\Rightarrow \tau \approx 0.1 \text{ ns}$

Damping towards H_{eff}
with a typically time
constant (for $\alpha = 0.001$)
of several ns



μ_0 : permeability of vacuum

α : phenomenological damping constant

γ : gyromagnetic ratio

M : saturation magnetization

L. Landau and E. Lifshitz, Phys. Z. Sowjetunion **8**, 153 (1935)

T. L. Gilbert, PhD thesis (1956); T. L. Gilbert, IEEE Trans. Magn. **40**, 3443 (2004)

Extended Landau-Lifshitz equation

The spin-transfer torque can be written as:

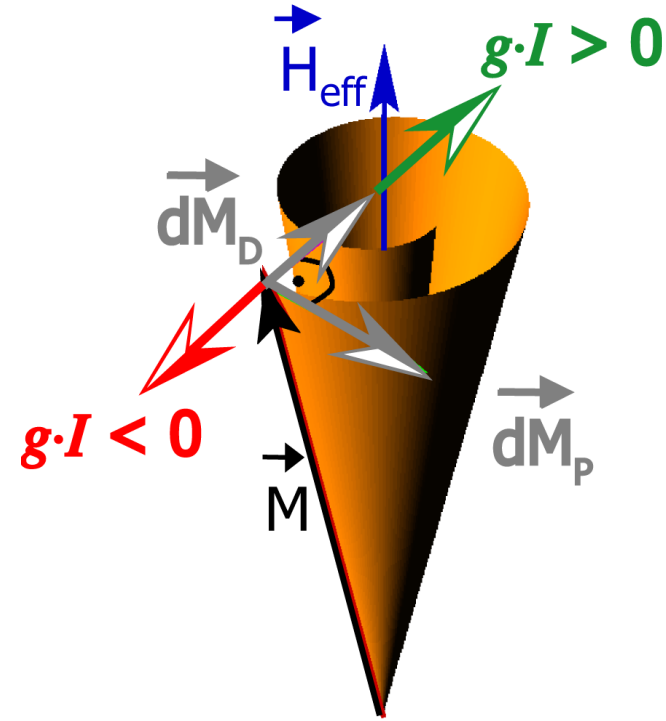
$$\frac{d\vec{M}_{\text{free}}}{dt} = \frac{I}{A} \cdot g(\theta) \cdot \vec{M}_{\text{free}} \times \left[\vec{m}_{\text{free}} \times \vec{m}_{\text{fixed}} \right] ; \quad \vec{m}_{\text{free, fixed}} = \frac{\vec{M}_{\text{free, fixed}}}{M_S}$$

$g(\theta)$ is the material-dependent efficiency of the spin-transfer effects

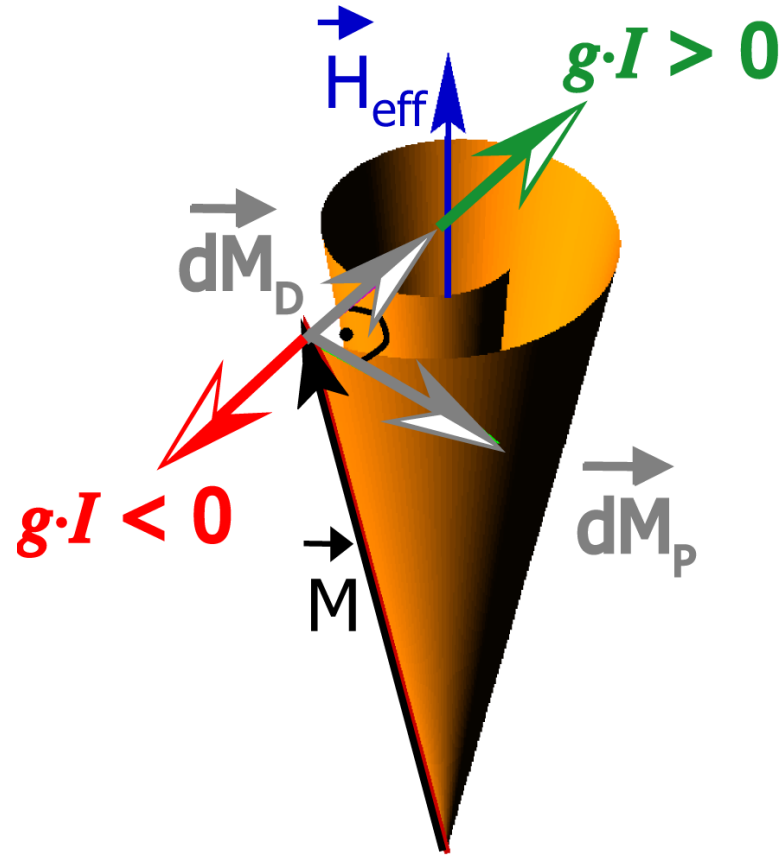
J.C. Slonczewski, J. Magn. Mater. **159**, L1 (1996)

Compare to LLG damping term:

$$\frac{d\vec{M}}{dt} = -\frac{\alpha\gamma}{M_S(1+\alpha^2)} \vec{M} \times \left[\vec{M} \times \vec{H}_{\text{eff}} \right]$$



Spin-transfer torque

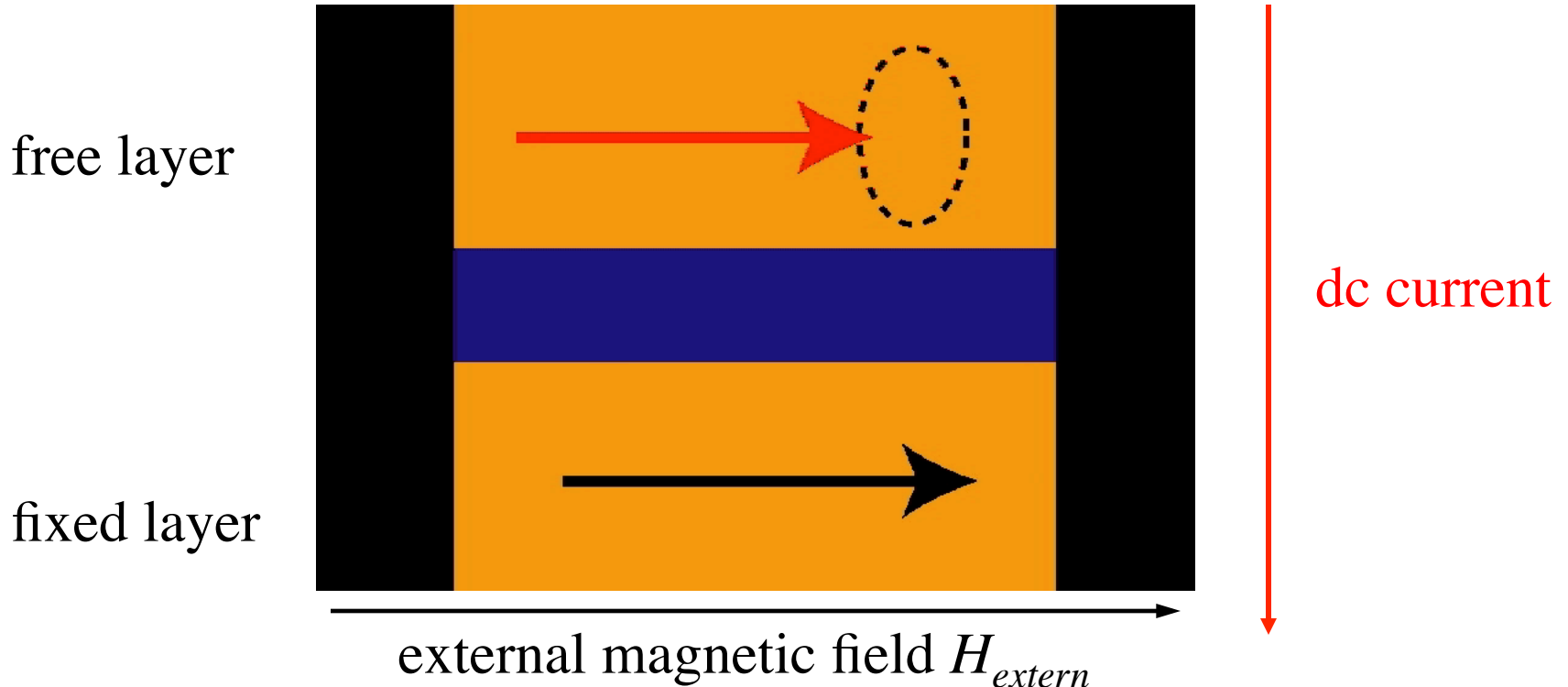


Depending on the **polarity of I** and **$sign(g)$** , the spin-transfer torque increases or compensates the intrinsic damping.

Microwave oscillations driven by spin-polarized currents

Spin-transfer torque can excite oscillatory motions of M_{free} with frequencies of several GHz.
⇒ GHz voltage signal due to GMR

⇒ dc currents in magnetic nanostructures give rise to microwave signals



Microwave oscillations driven by spin-polarized currents

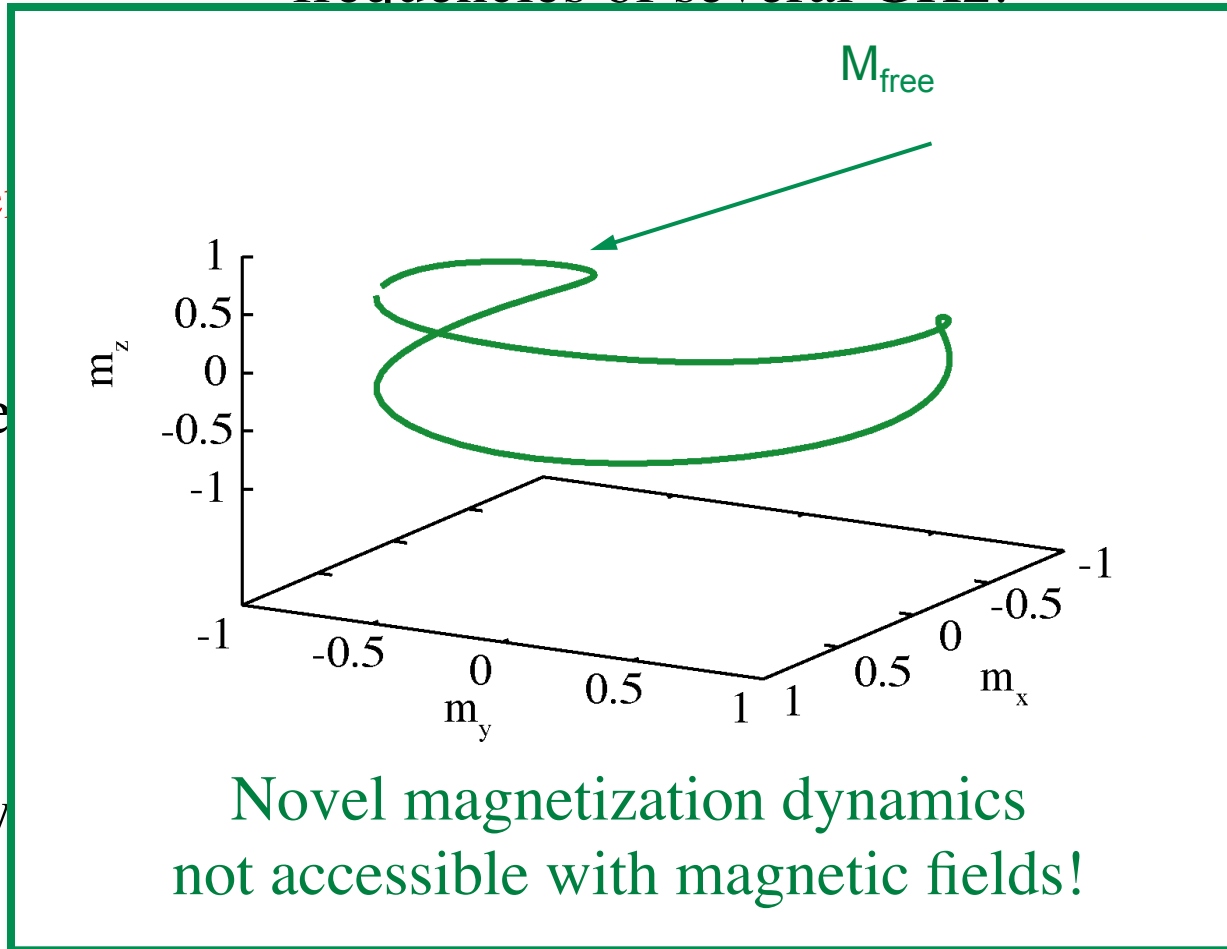
Spin-transfer torque can excite oscillatory motions of M_{free} with frequencies of several GHz.

⇒ dc current

wave signals

free layer

fixed layer

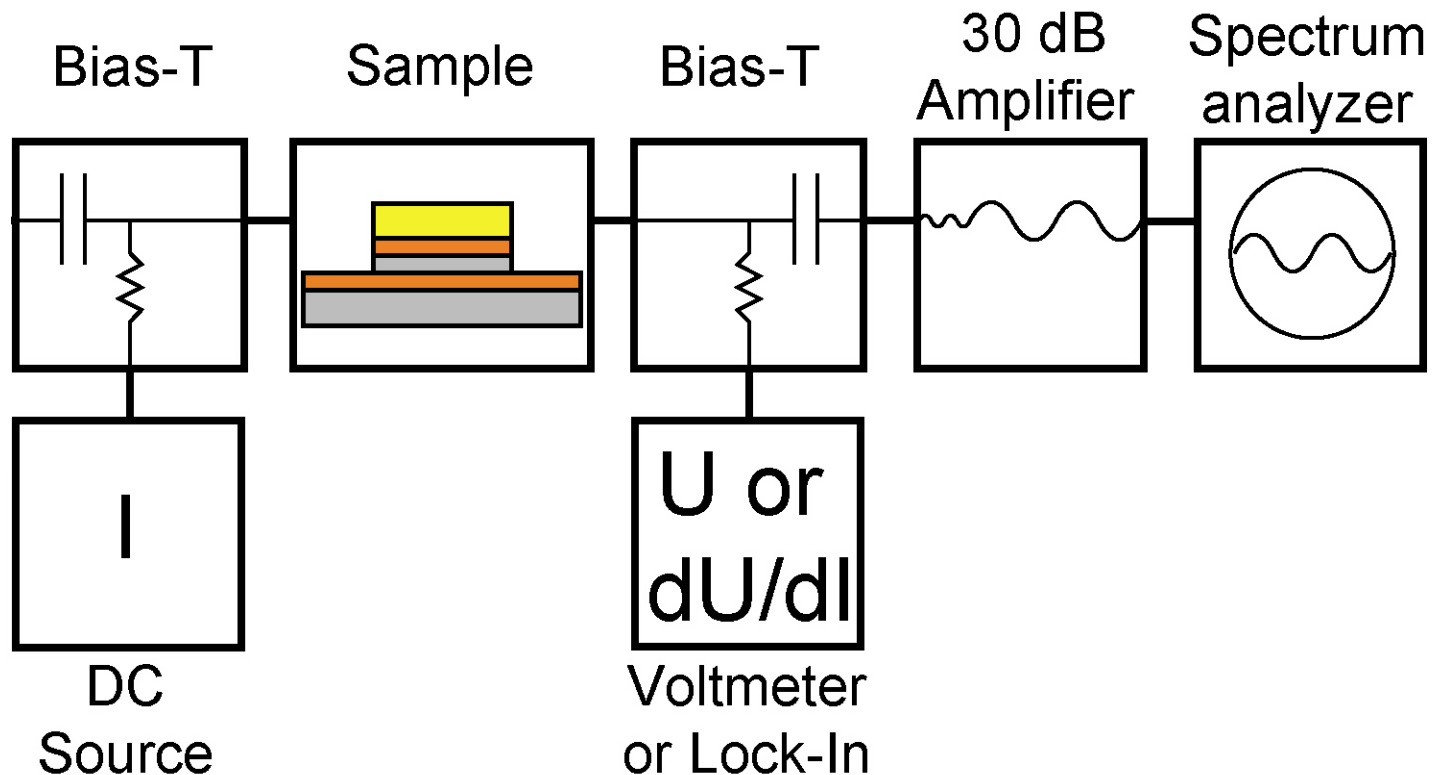


ac current

Novel magnetization dynamics
not accessible with magnetic fields!

external magnetic field H_{extern}

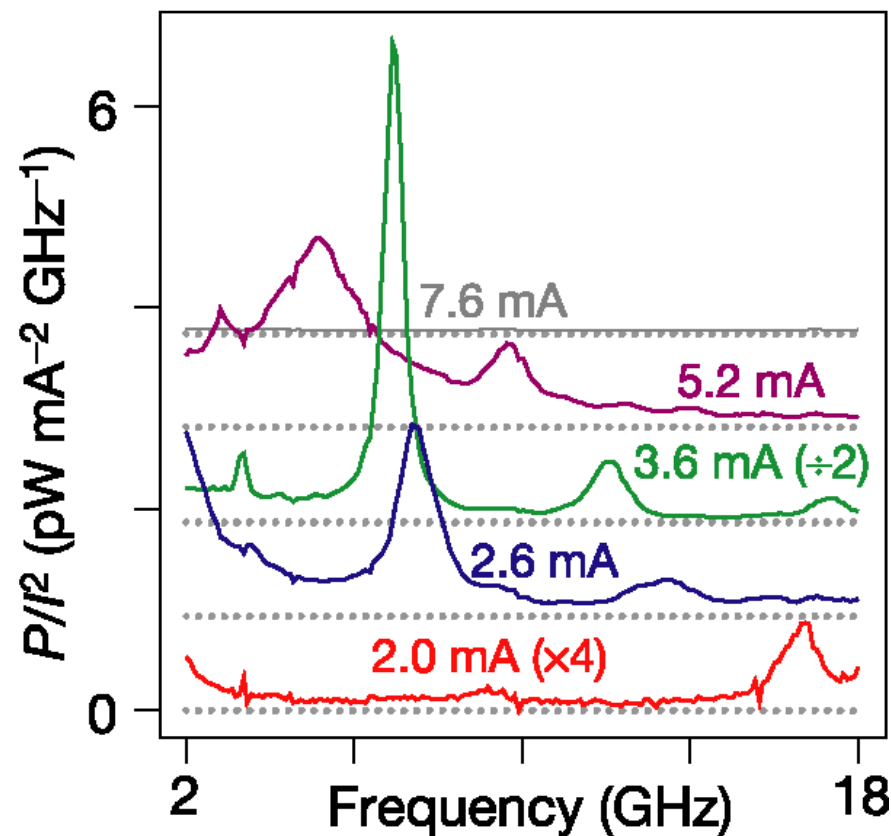
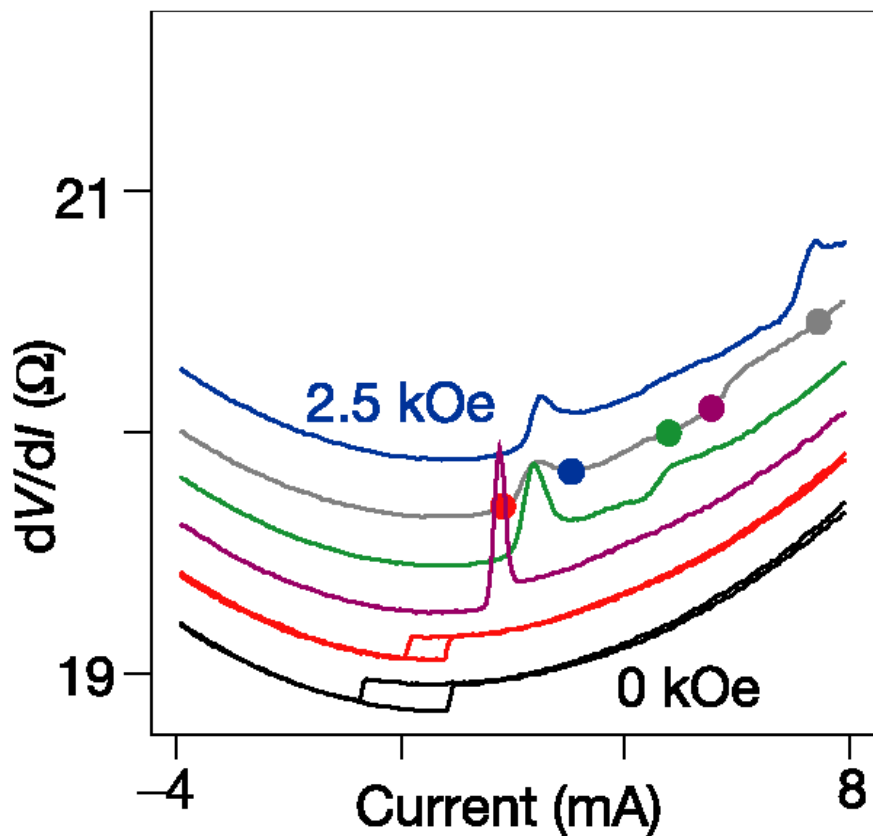
Wiring diagram for HF measurements



Setup similar to Kiselev *et al.*, Nature **425**, 380 (2003)

Pioneering work by the Cornell group

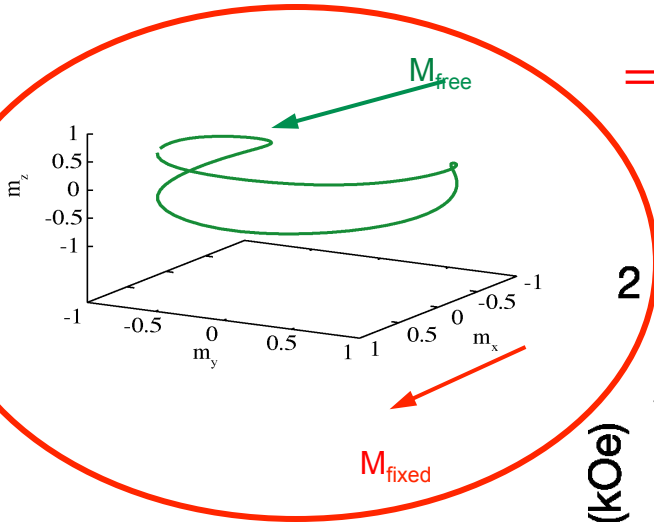
First observation of current-driven magnetization dynamics



S.I. Kiselev *et al.*, Nature **425**, 380 (2003)

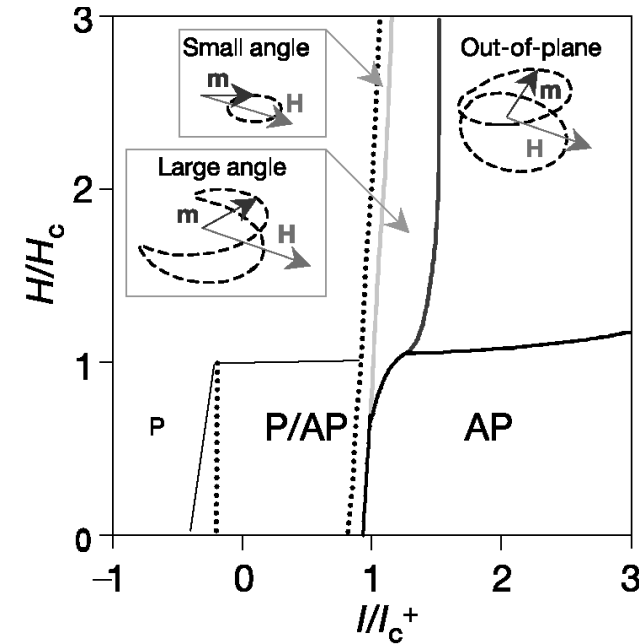
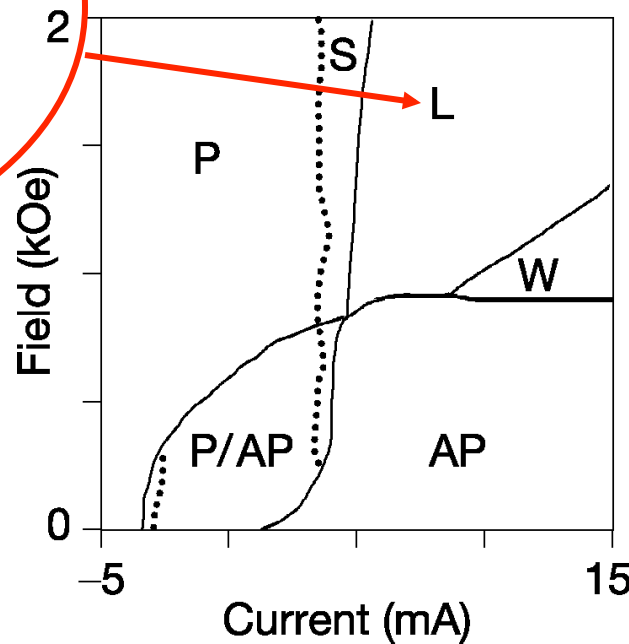
Current-driven magnetization dynamics: Macrospin model

Oscillatory motion of M_{free} and the $H-I$ phase diagram can qualitatively be understood by applying the extended LLG to a macrospin:



⇒ much larger “precession angles” than in FMR
 ⇒ new type of magnetization dynamics

R. Lehdorff, D.E. Bürgler *et al.*,
 IEEE Trans. Magn. **44**,
 1951 (2008)



S.I. Kiselev *et al.*, Nature **425**, 380 (2003)

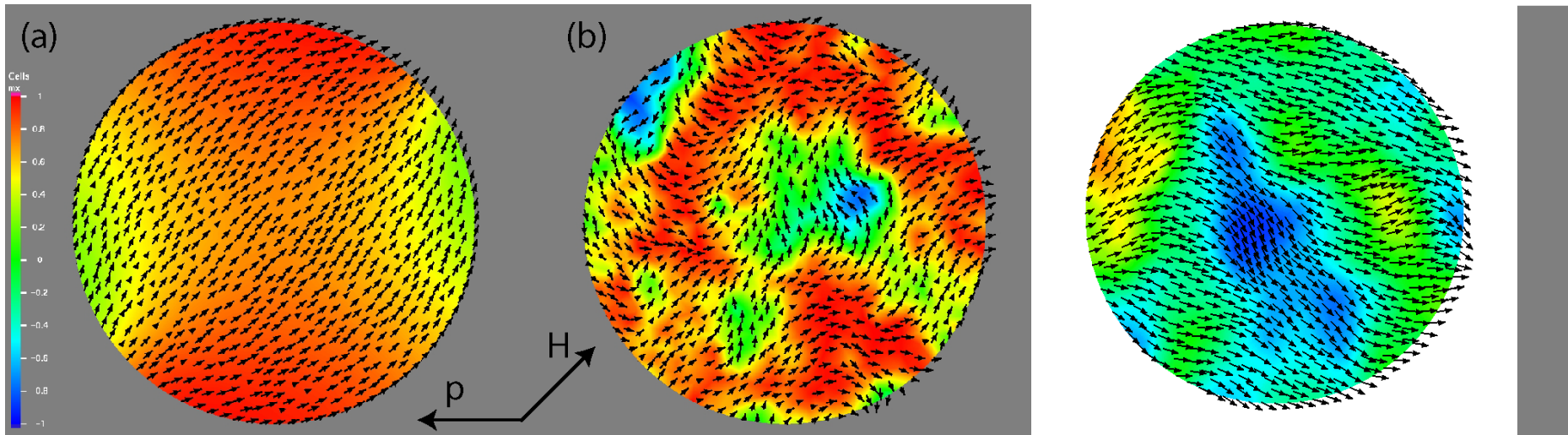
FEM micromagnetic simulation

2 nm-thick Fe nanomagnet with \varnothing 150 nm
50 mT external field along Fe(110), $\alpha = 0.02$
 5×10^7 A/cm², 30% spin-polarization

t = 0 ns

t = 5.4 ns

t = 8.3 ns



⇒ Very inhomogeneous magnetization structures

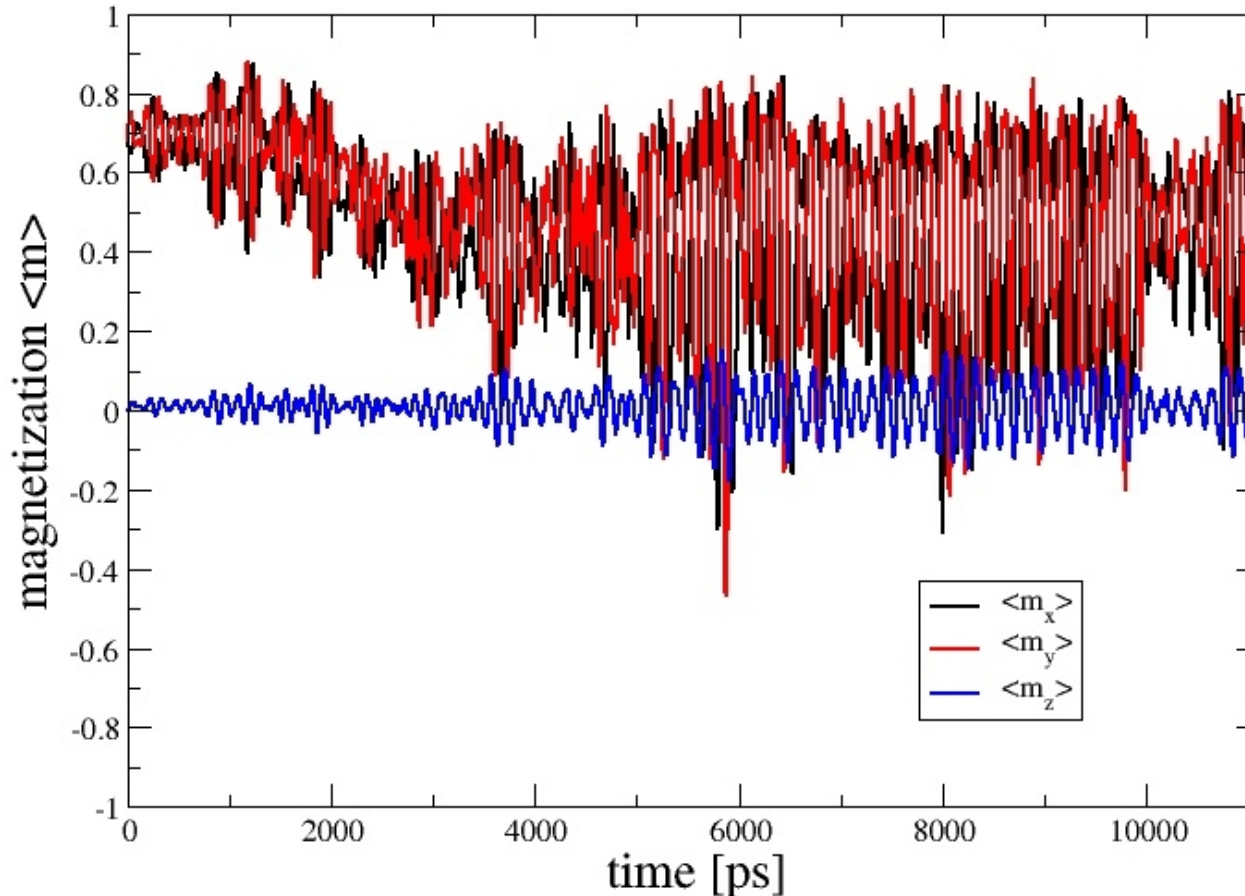
⇒ Different from what we know from field-induced dynamics

R. Hertel *et al.*, Forschungszentrum Jülich;

K.-J. Lee *et al.*, Nature Materials **3**, 877 (2004)

FEM micromagnetic simulation

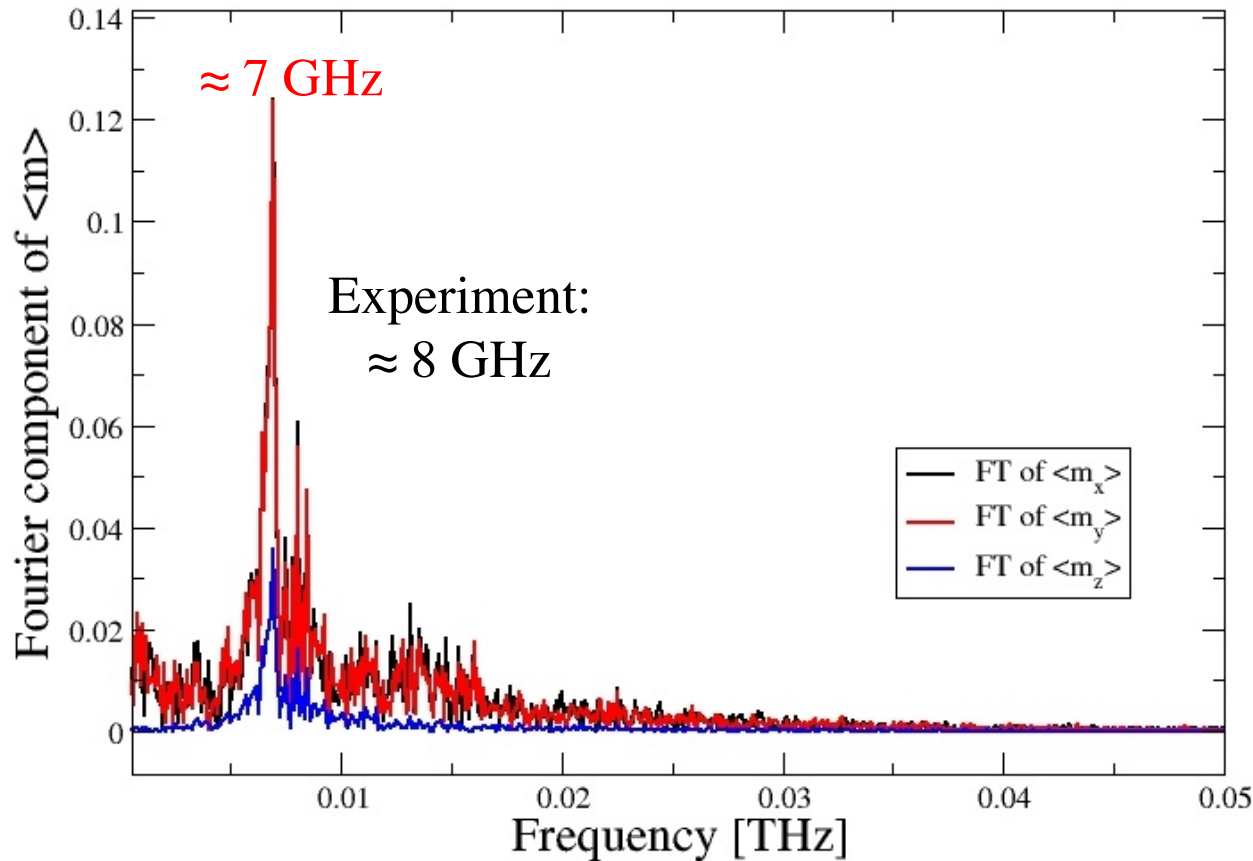
Time evolution of spatially averaged magnetization components



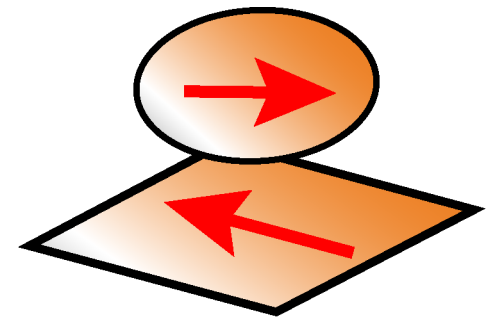
⇒ Oscillations with strongly varying amplitude

FEM micromagnetic simulation

Fourier transform of spatially averaged components



Fe nanomagnet:
2 nm-thick, \varnothing 150 nm
50 mT along Fe(110)
 $5 \times 10^7 \text{ A/cm}^2$, $P = 30\%$
 $\alpha = 0.02$

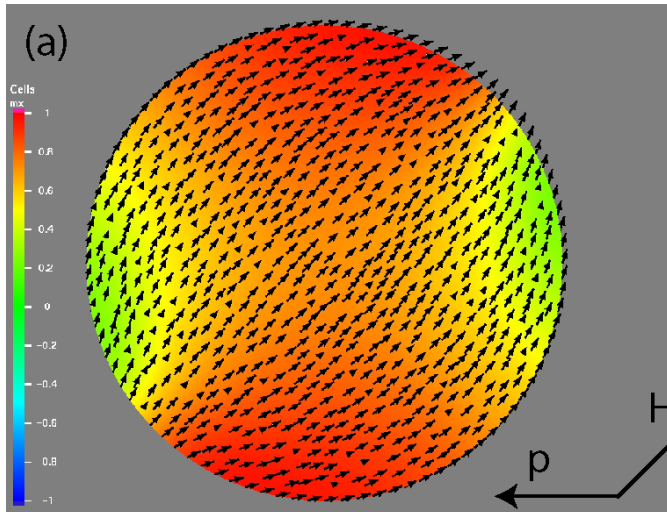


\Rightarrow Clearly visible peaks in Fourier spectrum

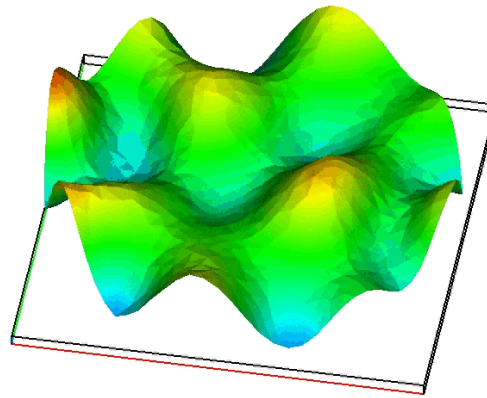
FEM micromagnetic simulation

2 nm-thick Fe nanomagnet with \varnothing 150 nm
50 mT external field along Fe(110), $\alpha = 0.02$
 5×10^7 A/cm², 30% spin-polarization

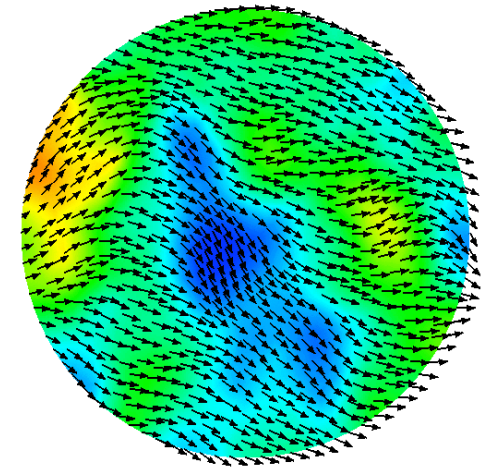
$t = 0$ ns



FTT filtered



Full magnetization

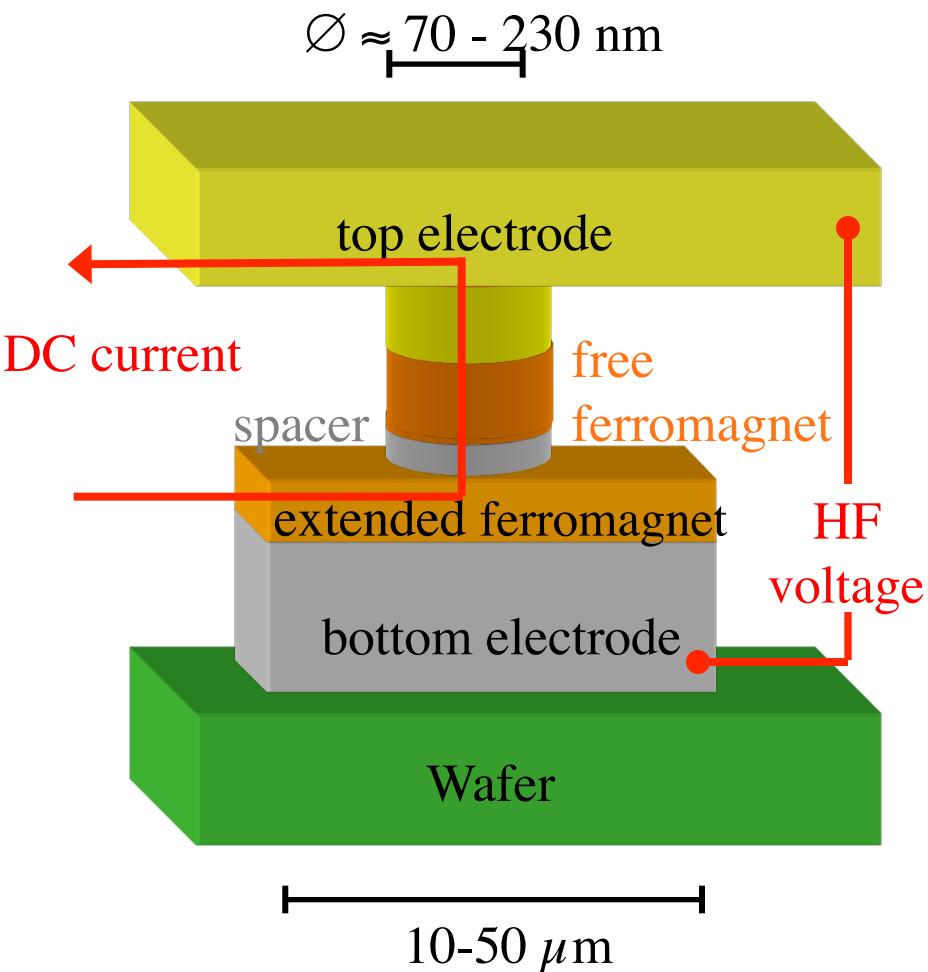


⇒ Very inhomogeneous magnetization structures

⇒ Constant supply of energy provided by the current
is converted into spin waves, which incoherently superimpose

R. Hertel *et al.*, Forschungszentrum Jülich; K.-J. Lee *et al.*, Nature Materials **3**, 877 (2004)

Spin-torque oscillator (STO)



Excitation of free ferromagnet
due to spin-transfer torque

Spin-torque oscillators (STO) as
microwave sources:

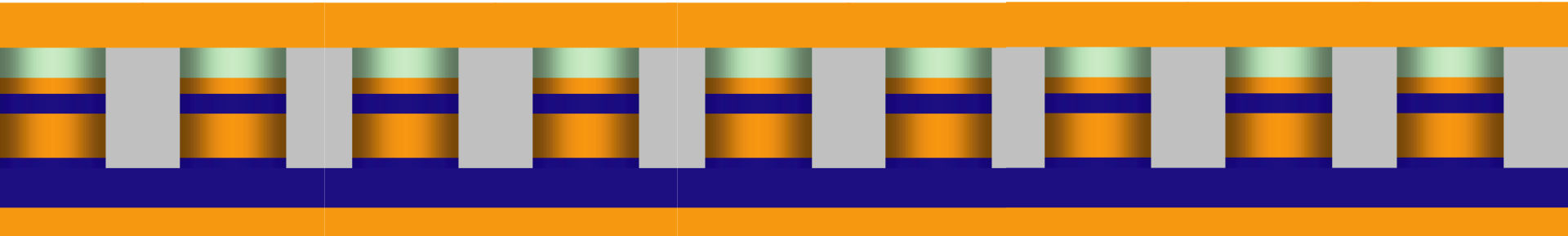
- solid-state realization
- nano-scale
- tunable by field and current
- RT operation
- envisaged for applications in
communication and
quantum information technology

BUT: **Output power** needs to be
significantly increased:

- **Optimizing** STOs properties
- **Synchronization** of many STOs

IDEA:

Create an **array of coupled and thus coherently oscillating STNOs**:
 N oscillators produce up to N^2 -fold output power
due to coherency



Coupling via

- magnetic interaction (spin-waves) in common magnetic layer

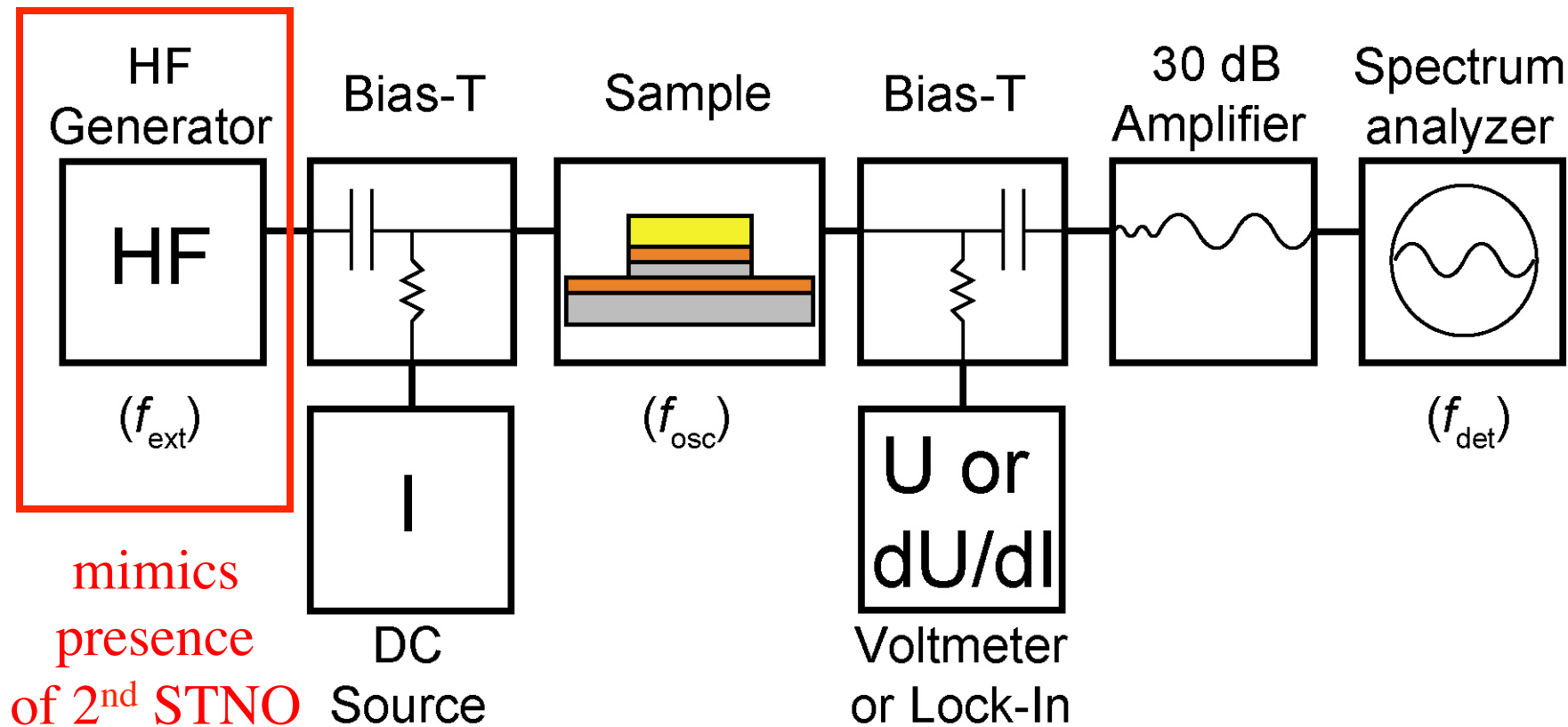
S. Kaka et al., Nature 437, 389 (2005)

F.B. Mancoff et al., Nature 437, 393 (2005)

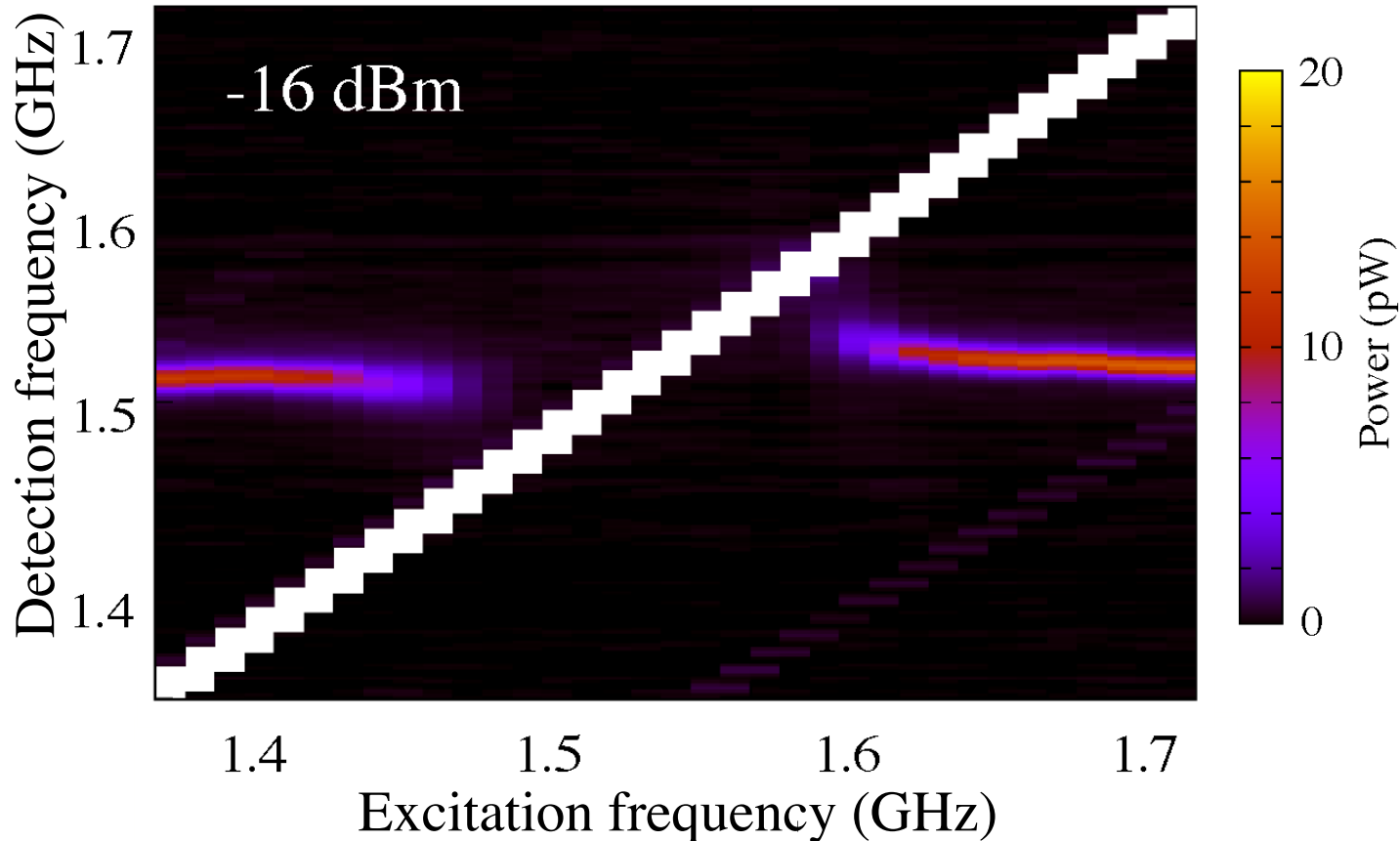
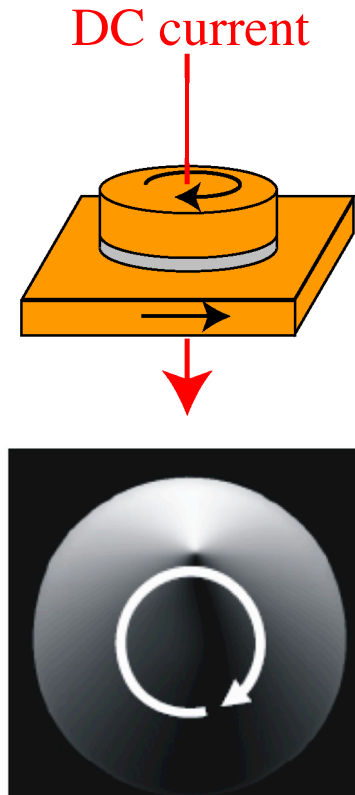
- electric interaction (microwaves) in common electrodes

-J. Grollier et al., Phys. Rev. B 73, 060409 (2006)

Wiring diagram for injection locking



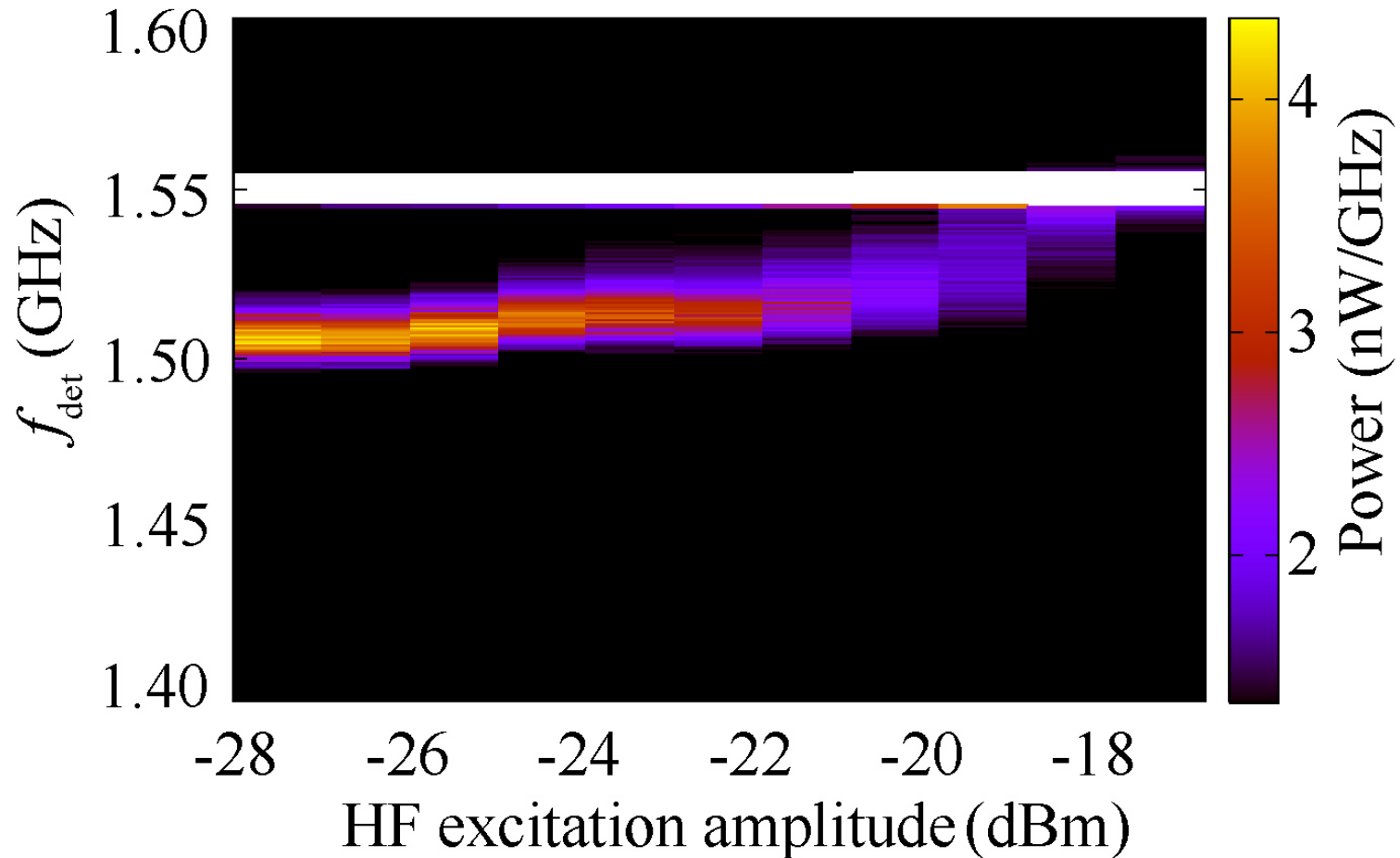
Phase-locking of gyrotropic motion to external HF signal



Vortex STNO phase-locks to the externally applied HF signal in a rather large frequency range of about 100 MHz

R. Lehdorff, D.E. Bürgler *et al.*, Appl. Phys. Lett. **97**, 142505 (2010)

Frequency versus external HF amplitude



Estimated HF power emitted from STNO: 0.4 nW

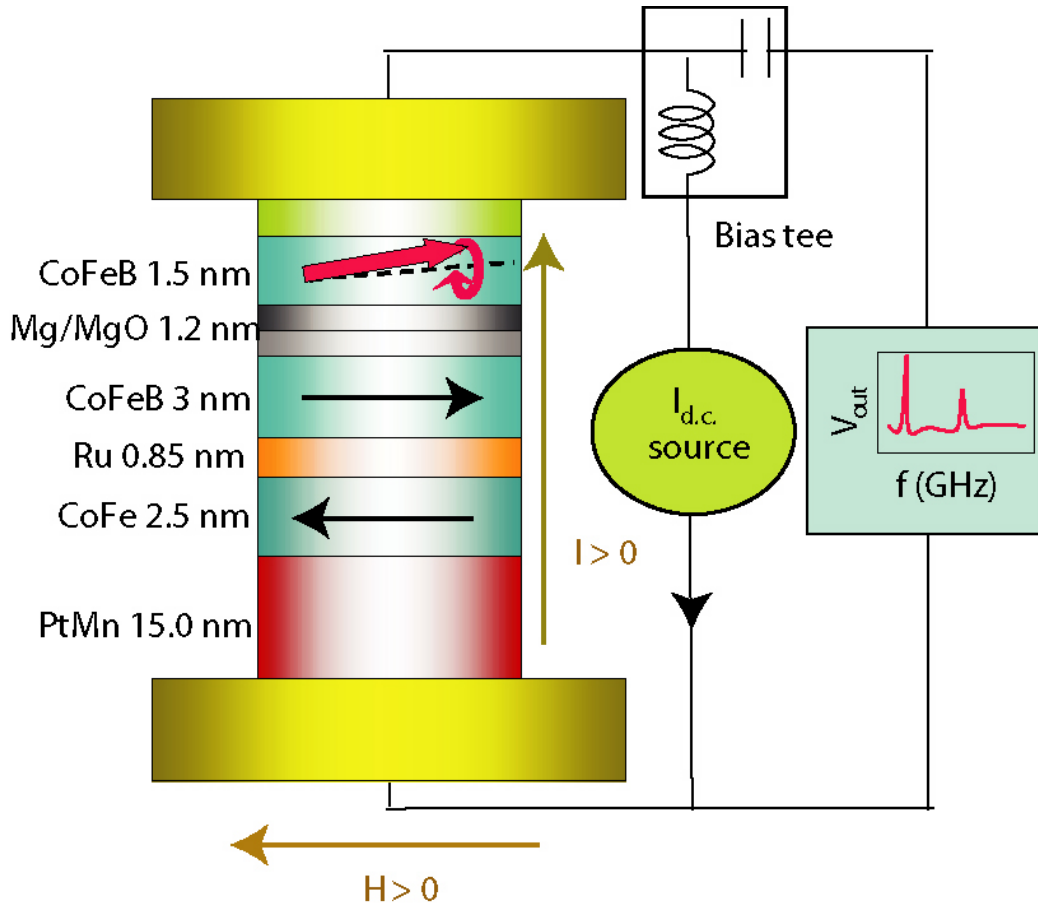
Estimated external HF power required for phase-locking: 1.3 μ W

R. Lehdorff, D.E. Bürgler *et al.*, Appl. Phys. Lett. **97**, 142505 (2010)

TMR-based spin-torque nano-oscillator

HF output power scales with $(\text{MR-ratio})^2$

\Rightarrow Use TMR instead of GMR



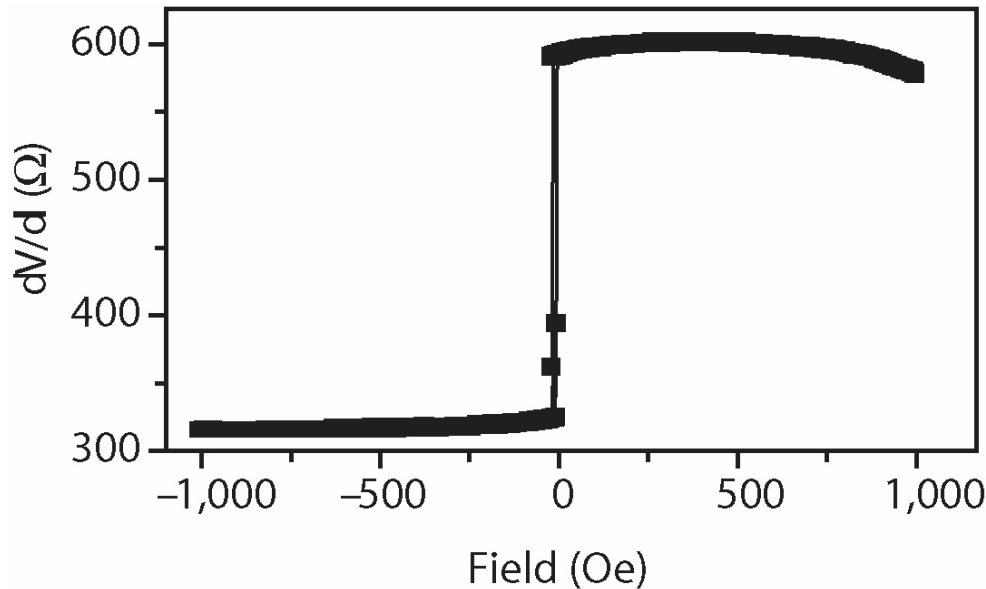
- Elliptical cross-section
160 nm x 70 nm

- $RA = 4 \Omega\mu\text{m}^2$

A.M. Deac *et al.*, Nature Physics 4, 803 (2008)

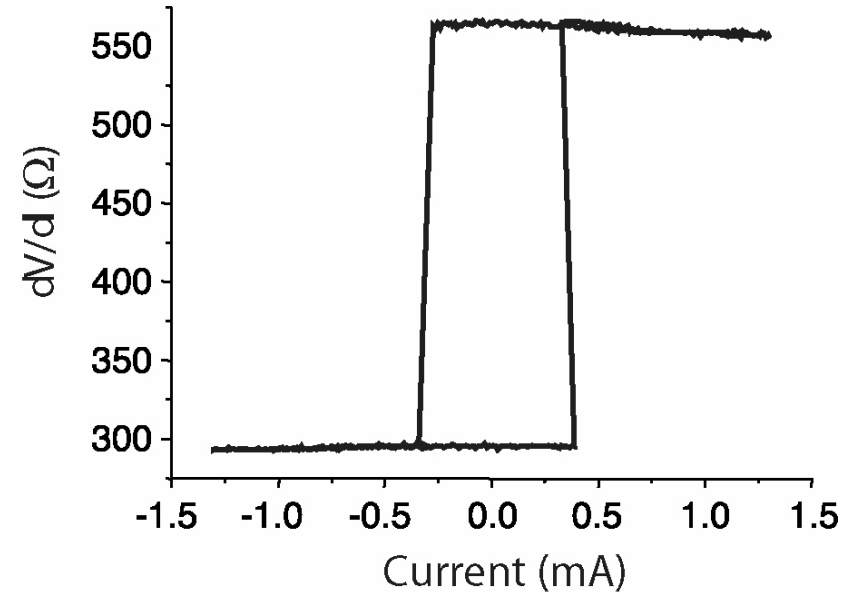
TMR-based spin-torque nano-oscillator

Field-induced switching:



● 110% TMR ratio

STT-induced switching:



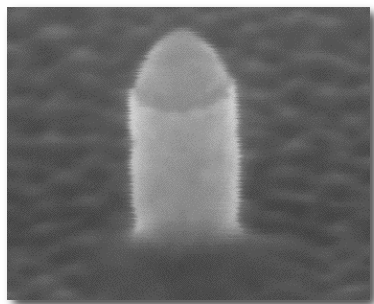
● Critical current density:
 $3 \times 10^6 \text{ A/cm}^2$

● Maximum output power: $0.48 \mu\text{W}$

(although a significant fraction is lost due to poor impedance matching)

A.M. Deac *et al.*, Nature Physics 4, 803 (2008)

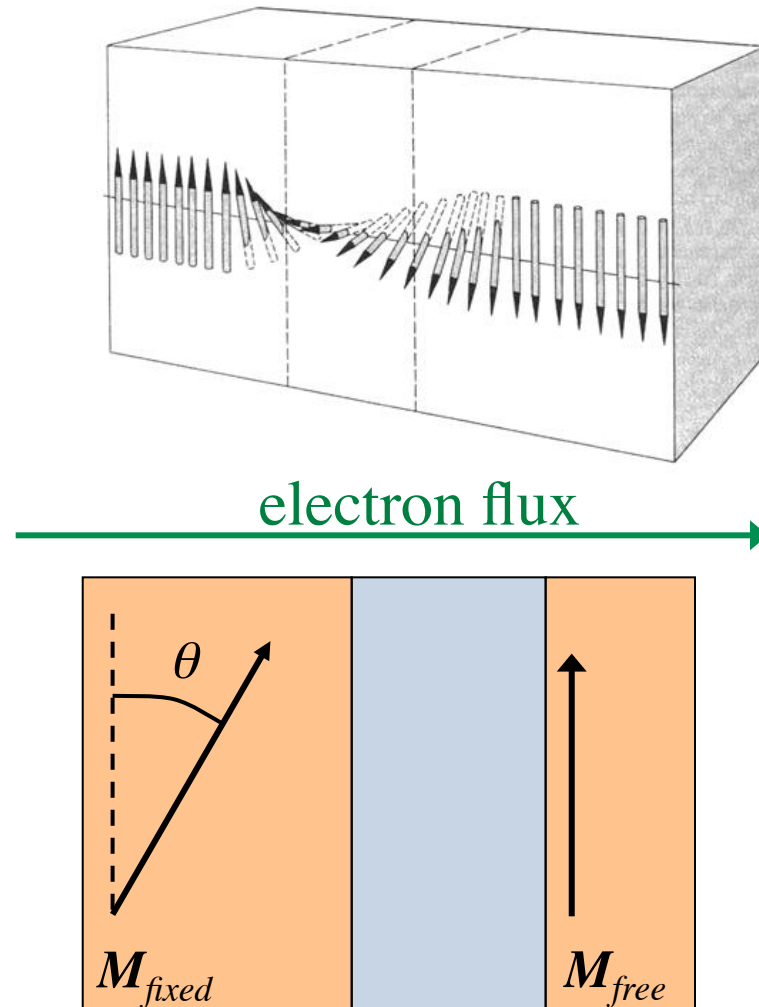
Outline: Current-induced magnetization dynamics



- Need for advanced magnetic switching concept
- Phenomenology of spin-transfer torque (STT)
“Current-induced magnetization switching”
- Physical picture for STT
- Current-driven magnetization dynamics
“Extended Landau-Lifshitz-Gilbert equation”
“Spin-torque oscillators (STO)”
- STT in non-uniform magnetization structures

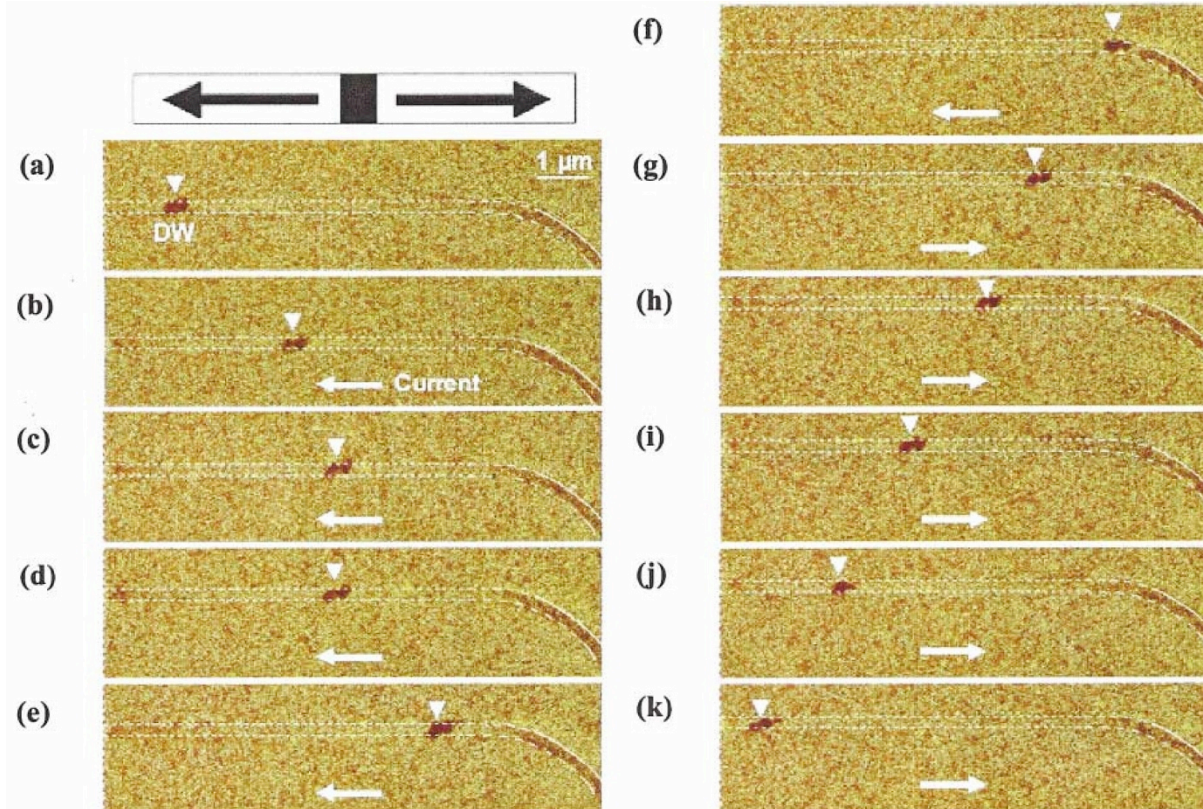
Current-driven domain wall motion

Domain walls are intrinsically non-uniform magnetization structures



Current-driven domain wall motion

MFM observation of current-induced domain wall motion



Here, arrows indicate the technical current direction

Current pulses: $1.2 \times 10^8 \text{ A/cm}^2$, $0.5 \mu\text{s}$

A. Yamaguchi *et al.*, Phys. Rev Lett. **92**, 077205 (2004)

STT term in continuous limit

STT acting on a magnetization distribution $\vec{M}(\vec{x})$ due to a current given by the current density \vec{j} and polarization P :

$$\left(\frac{d\vec{M}}{dt} \right)_{\text{STT}} = -(\vec{u} \cdot \nabla) \cdot \vec{M} + \frac{\beta}{M_s} \left[\vec{M} \times (\vec{u} \cdot \nabla) \cdot \vec{M} \right] ; \quad \vec{u} = -\frac{\mu_B P}{e M_s} \vec{j}$$

Slonczewski-like
in-plane
adiabatic

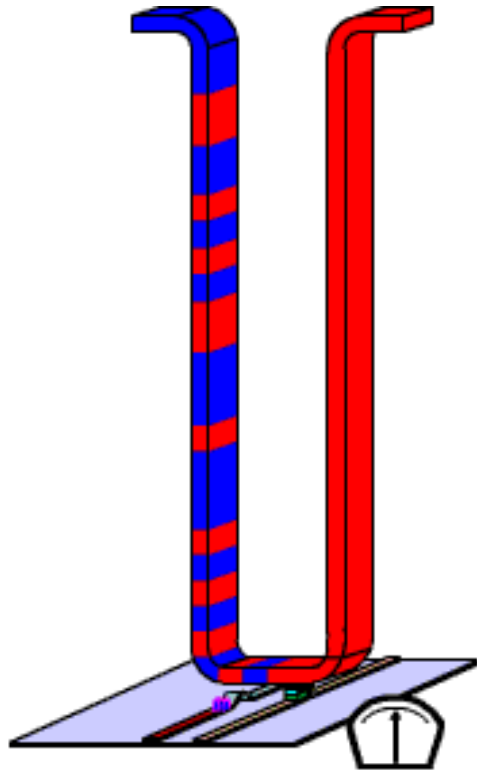
field-like
out-of-plane
non-adiabatic

\Rightarrow Non-adiabatic STT is required to explain experimental observation of current-induced domain wall motion

A. Thiaville *et al.*, Europhys. Lett. **69**, 990 (2005)

Current-driven domain wall motion: Racetrack memory

current

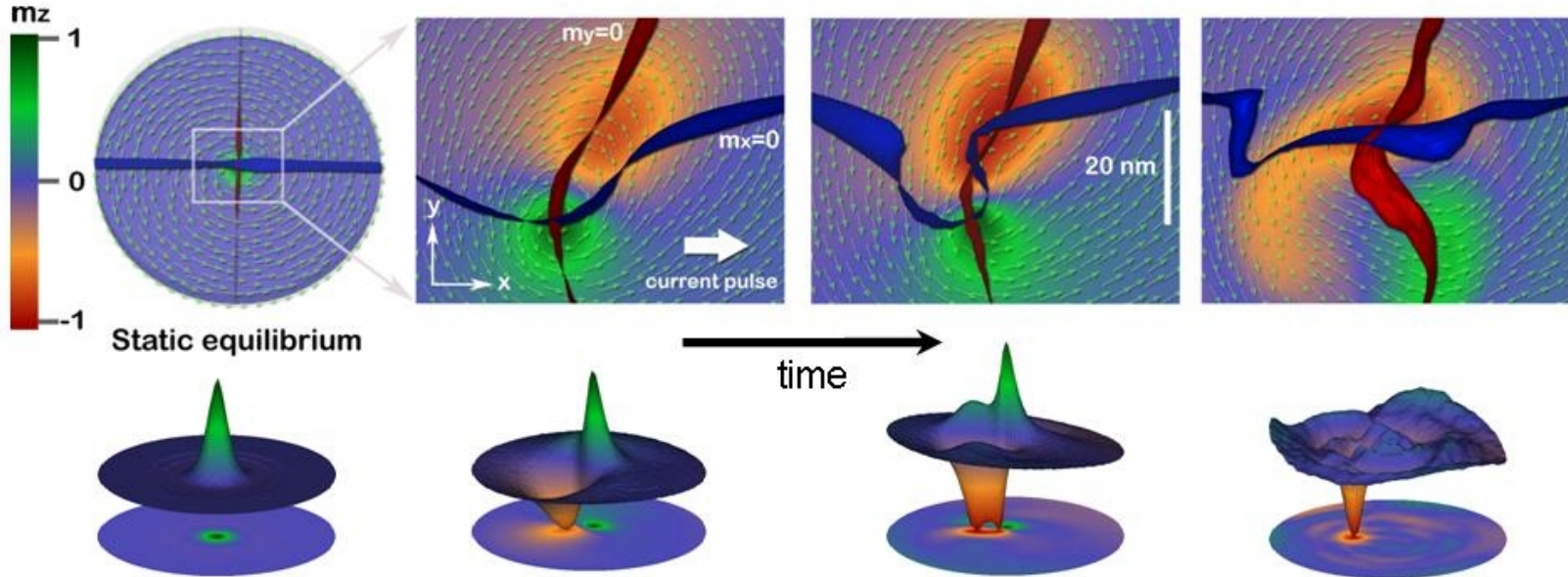
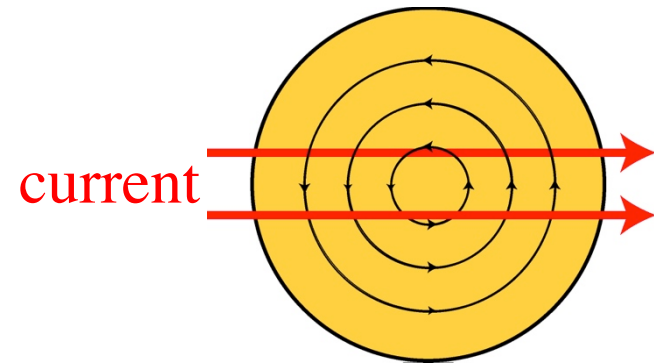


- powerful storage-class memory
- solid-state device
- cost and storage capacities rivaling that of HDDs
- but much improved performance and reliability

Current-driven vortex core switching

Current pulses applied to magnetic vortices can

- excite the gyrotropic mode of the vortex
- switch the core polarization



Simulation: Liu *et al.*, Appl. Phys. Lett. **91**, 112501 (2007)

Experiment: K. Yamada *et al.*, Appl. Phys. Lett. **93**, 152502 (2008)

STT and GMR in metallic antiferromagnets

PHYSICAL REVIEW B 73, 214426 (2006)

Theory of spin torques and giant magnetoresistance in antiferromagnetic metals

A. S. Núñez,^{*} R. A. Duine,[†] Paul Haney,[‡] and A. H. MacDonald[§]

Department of Physics, The University of Texas at Austin, 1 University Station C1600, Austin, Texas 78712-0264, USA

(Received 26 April 2006; published 14 June 2006)

PRL 100, 226602 (2008)

PHYSICAL REVIEW LETTERS

week ending
6 JUNE 2008

Spin-Transfer Torques in Antiferromagnetic Metals from First Principles

Yuan Xu, Shuai Wang, and Ke Xia

State Key Laboratory for Surface Physics, Institute of Physics, Chinese Academy of Sciences, P.O. Box 603, Beijing 100080, China

(Received 15 August 2007; published 3 June 2008)

PHYSICAL REVIEW B 75, 174428 (2007)

Ab initio giant magnetoresistance and current-induced torques in Cr/Au/Cr multilayers

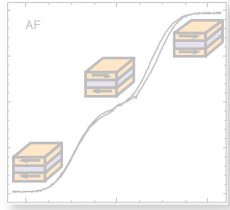
P. M. Haney,^{1,*} D. Waldron,^{2,†} R. A. Duine,^{3,‡} A. S. Núñez,^{4,§} H. Guo,^{2,||} and A. H. MacDonald^{1,¶}

Conclusions on STT

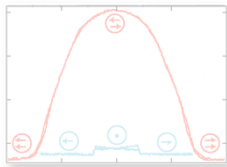
- STT is understood in terms of **spin momentum transfer** and **angular momentum conservation**
- Current-induced STT enables a **novel, highly non-linear magnetization dynamics**
- Current-induced magnetization switching and STOs are of **high technological relevance**

Overview

Introduction



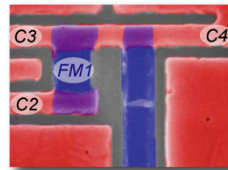
Interlayer exchange coupling



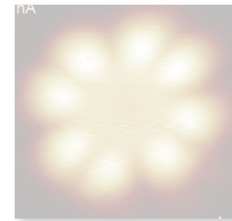
Giant and tunneling magnetoresistance



Current-induced magnetization dynamics



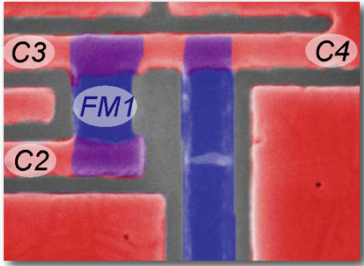
Pure spin current



Magnetic molecules

Conclusions

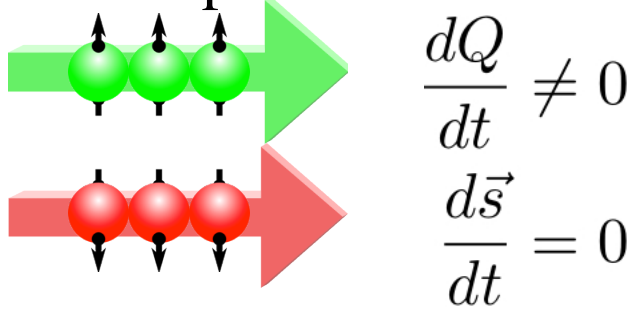
Outline: Pure spin current



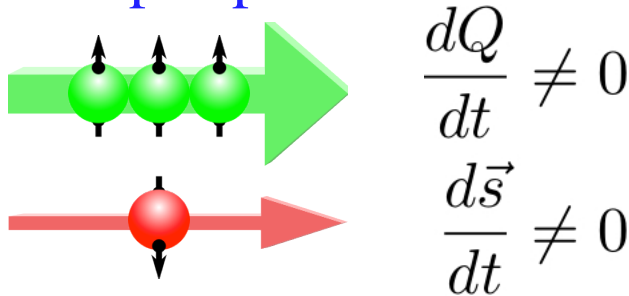
- What is a pure spin current?
- Generation and detection of pure spin currents in lateral spin-valves (LSV)
- Example: In-situ FIB fabrication of LSV
- Pure spin current induced magnetization switching

Pure spin currents

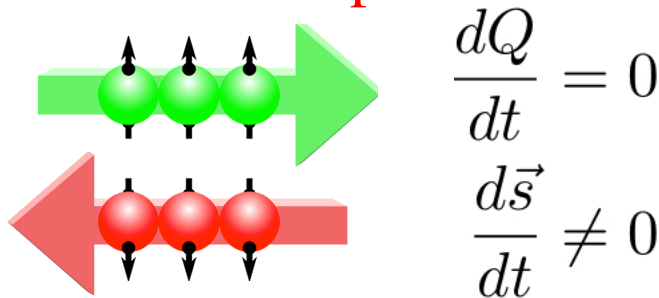
Unpolarized current:



Spin-polarized current:



Pure spin current:

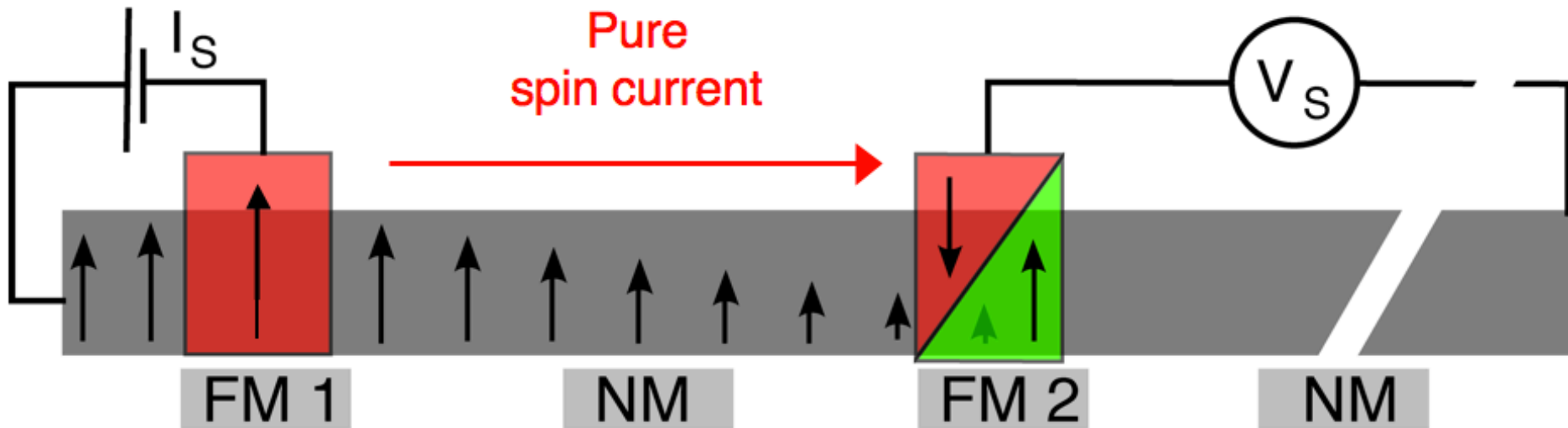


- transport spin momentum
- without (net) charge motion
- do not give rise to Oersted fields
- do not create resistive voltage drops
- do not produce Joule heating

⇒ Potential to significantly reduce
power dissipation of
(spin-)electronic devices

Generation and detection of pure spin currents

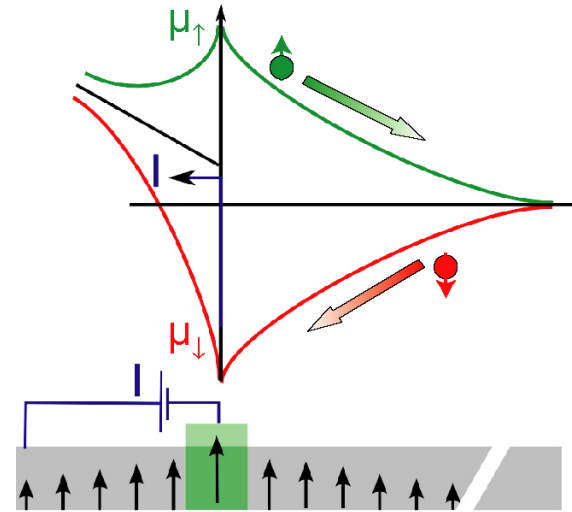
Non-local transport measurement in a “lateral spin valve”



M. Johnson and R. H. Silsbee, Phys. Rev. Lett. **55**, 1790 (1985); F. J. Jedema *et al.*, Nature **410**, 345 (2001)
Y. Ji *et al.*, Appl. Phys. Lett. **85**, 6218 (2004); T. Yang *et al.*, Nat. Phys. **4**, 851 (2008)

Pure spin currents in lateral spin-valves (LSV)

Generation:



Spin accumulation
at FM/NM interface

⇒ splitting of

chemical potential $\mu_{\uparrow, \downarrow}$

⇒ diffusion of spins

due to $\nabla \mu_{\uparrow, \downarrow}$

Diffusion of electrons:

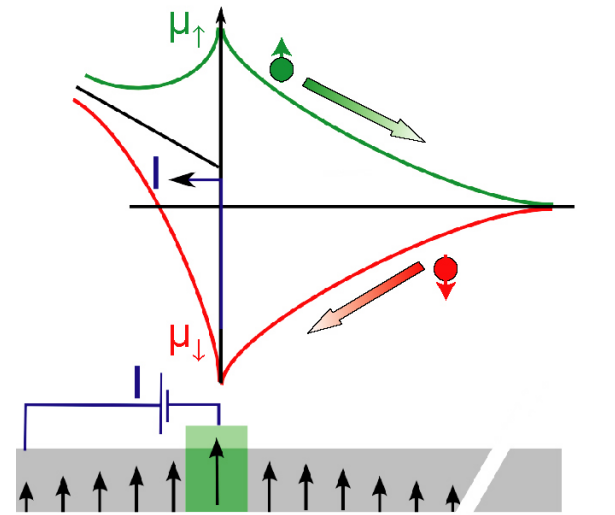
Motion of electrons is due to
diffusion driven by Fermi velocity
distribution (rather than temperature)

⇒ “Non-dissipative” flow of
pure spin current

F. Casanova *et al.*; Phys. Rev. B **79**, 184415 (2009)

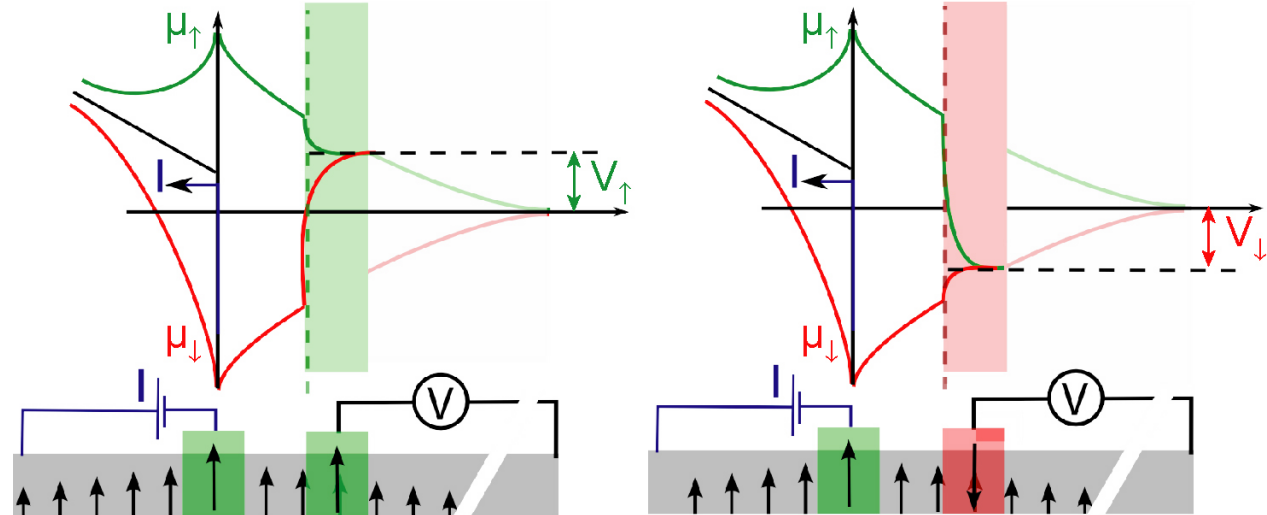
Pure spin currents in lateral spin-valves (LSV)

Generation:



Spin accumulation
at FM/NM interface
⇒ splitting of
chemical potential $\mu_{\uparrow, \downarrow}$
⇒ diffusion of spins
due to $\nabla \mu_{\uparrow, \downarrow}$

Detection:



Detection of spin accumulation with a FM
probe located within the spin diffusion length:

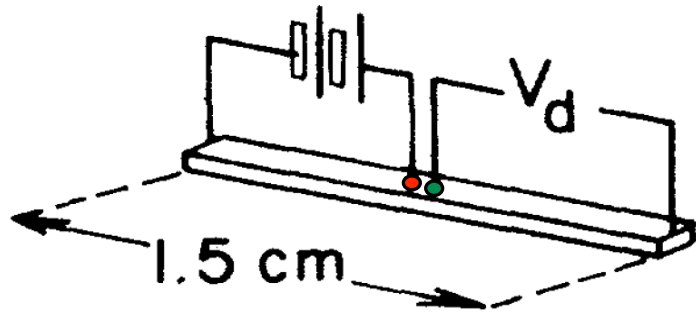
Parallel alignment:
⇒ Probe potential
adjusts to μ_{\uparrow}

Antiparallel alignment:
⇒ Probe potential
adjusts to μ_{\downarrow}

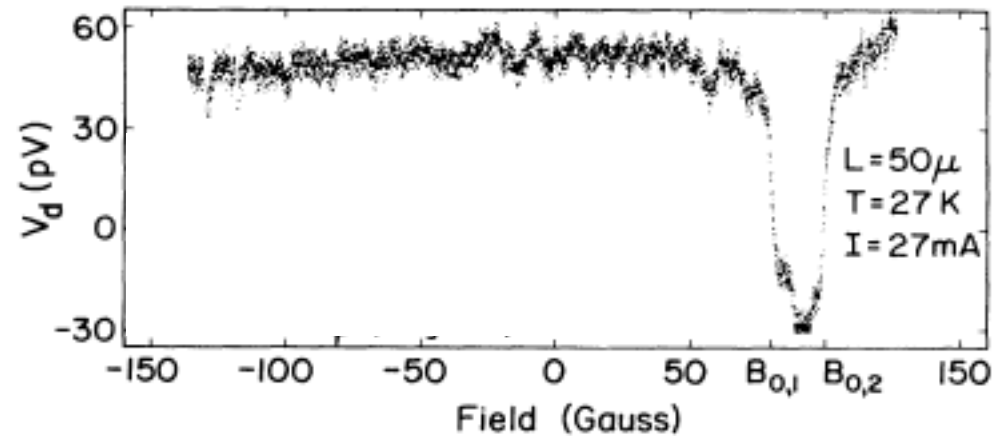
F. Casanova *et al.*; Phys. Rev. B **79**, 184415 (2009)

First observation of pure spin currents

M. Johnson and R. H. Silsbee, Phys. Rev. Lett. **55**, 1790 (1985)



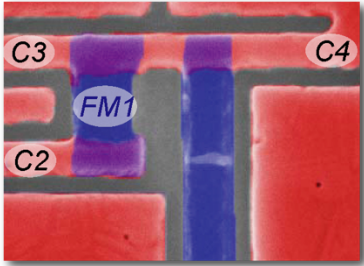
- Pure Al bulk material
- Permalloy **injector** and **detector**



F. J. Jedema *et al.*, Nature **410**, 345 (2001);

Y. Ji *et al.*, Appl. Phys. Lett. **85**, 6218 (2004); F. Casanova *et al.*; Phys. Rev. B **79**, 184415 (2009)

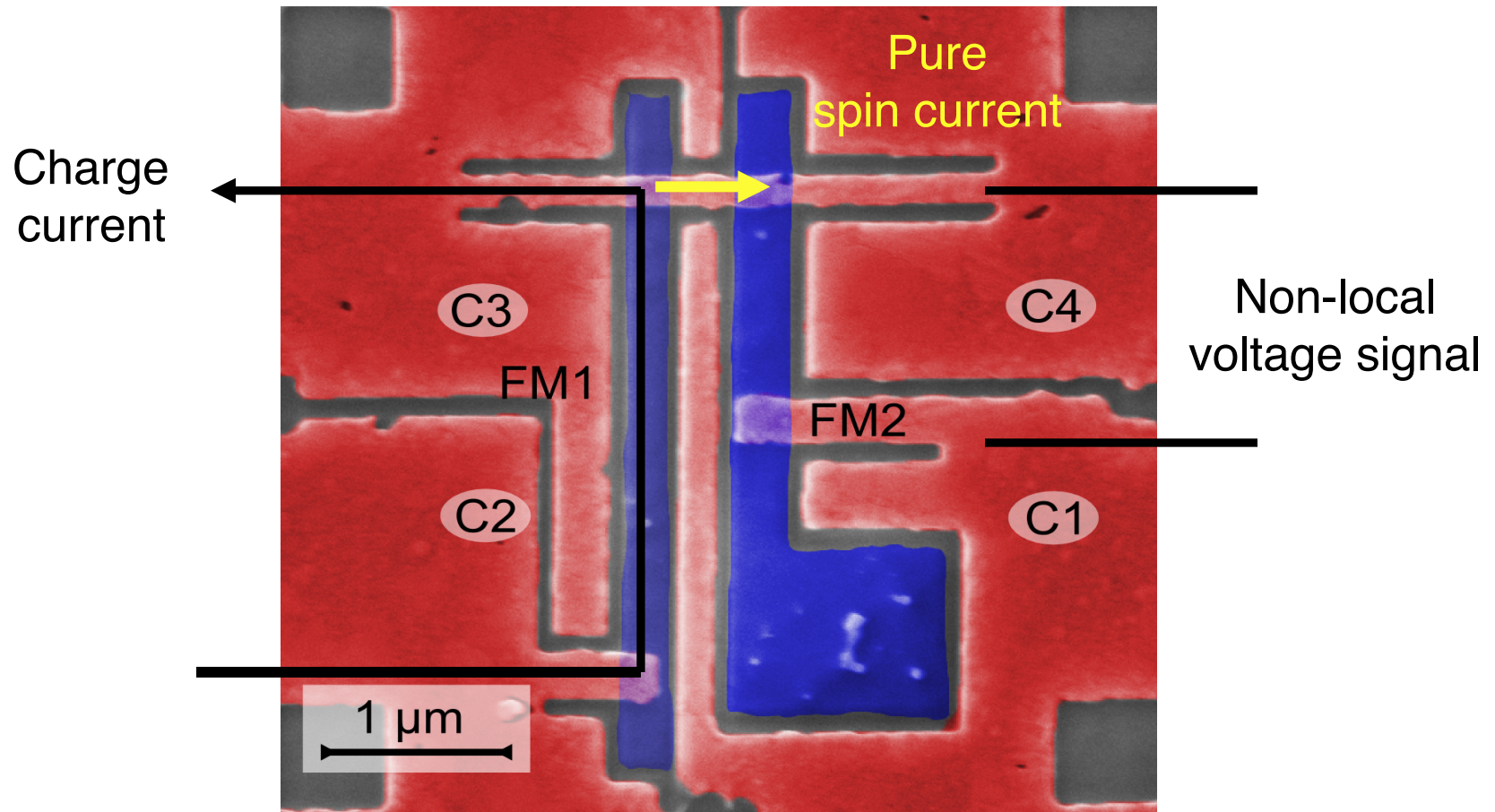
Outline: Pure spin current



- What is a pure spin current?
- Generation and detection of pure spin currents in lateral spin-valves (LSV)
- Example: In-situ FIB fabrication of LSV
- Pure spin current induced magnetization switching

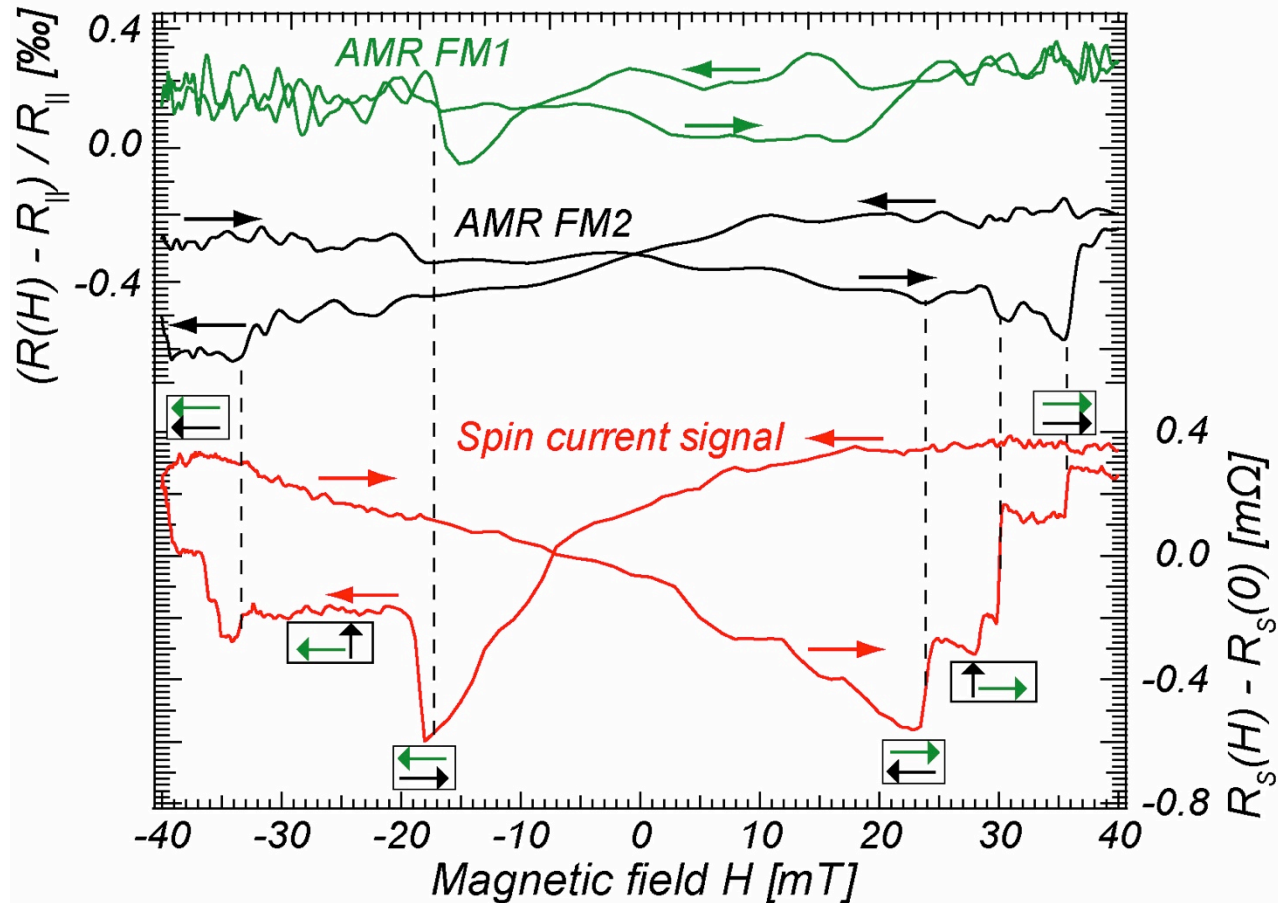
In-situ focused ion-beam (FIB) fabrication of a LSV

In-situ SEM of lateral spin-valve with topmost FM layers



J. Mennig, D.E. Bürgler *et al.*, J. Appl. Phys. **111**, 07C504 (2012)

AMR and spin signal of LSV



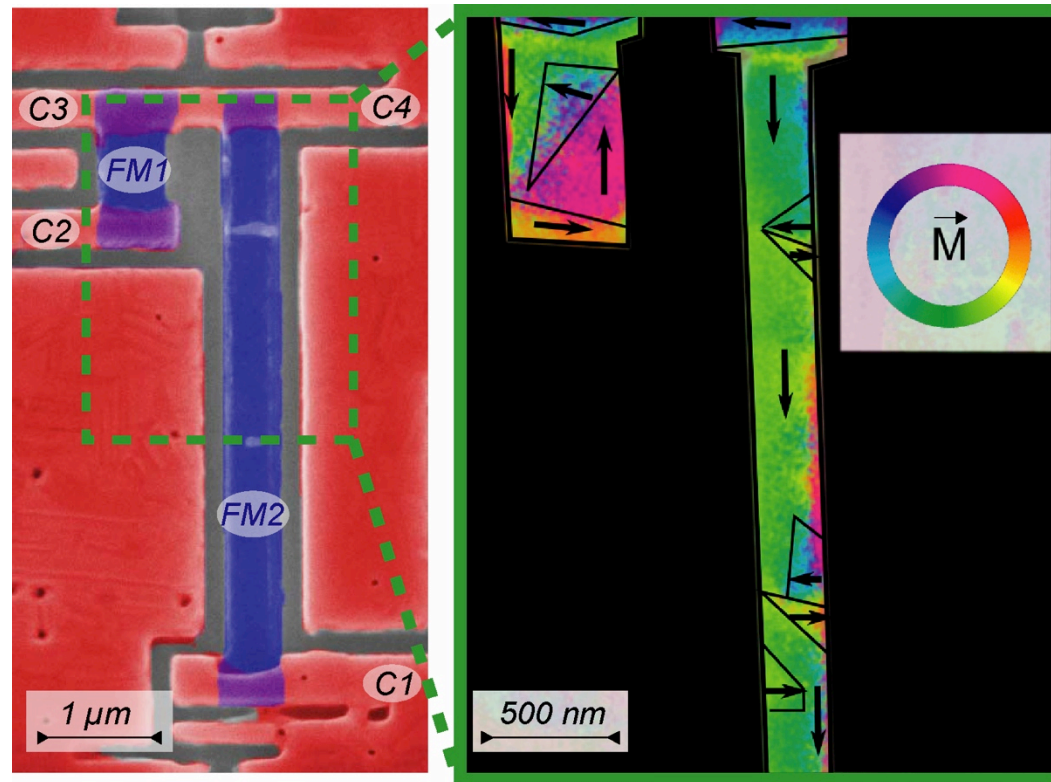
\Rightarrow Switching fields of AMR and R_s are correlated (dashed lines)

$\Rightarrow R_s$ of up to 0.9 m Ω indicates clean interfaces

J. Mennig, D.E. Bürgler *et al.*, J. Appl. Phys. **111**, 07C504 (2012)

SEM and SEMPA of LSV with wide FMs

Width of FMs (480 nm for FM1 and 350 nm for FM2) is larger than the typical lateral size of the FIB-induced roughness

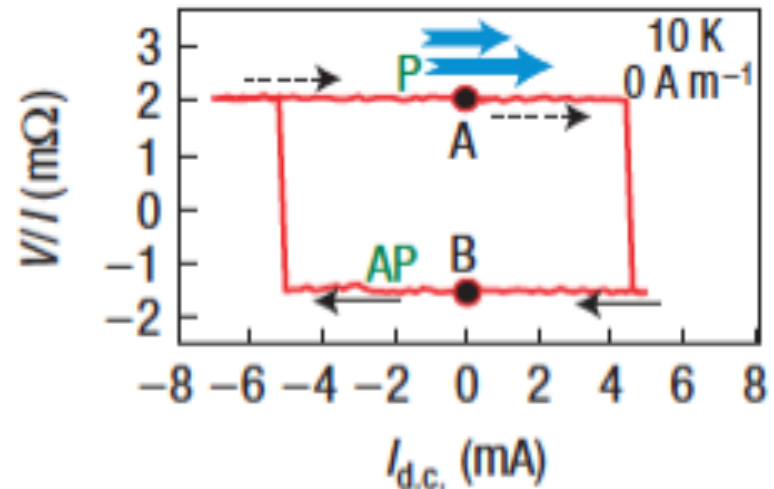
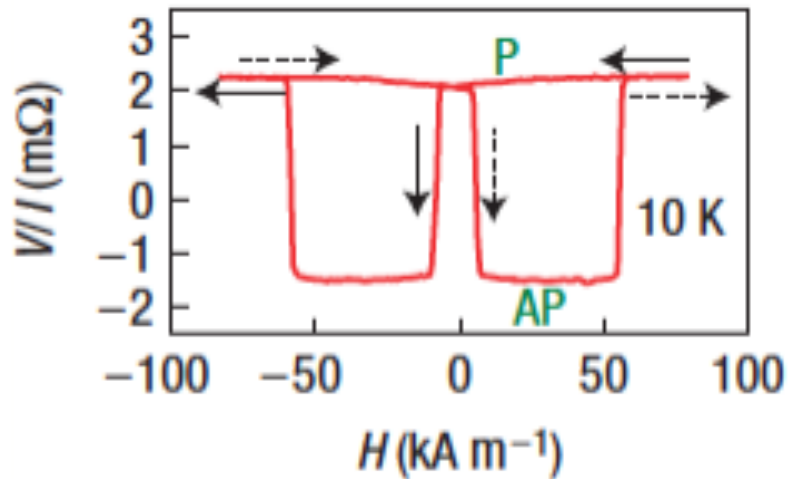
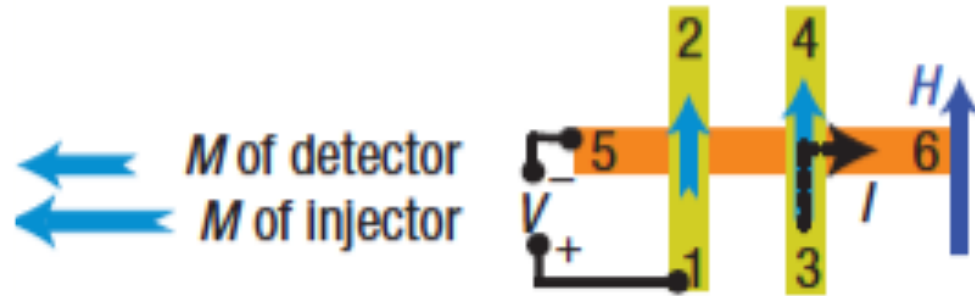
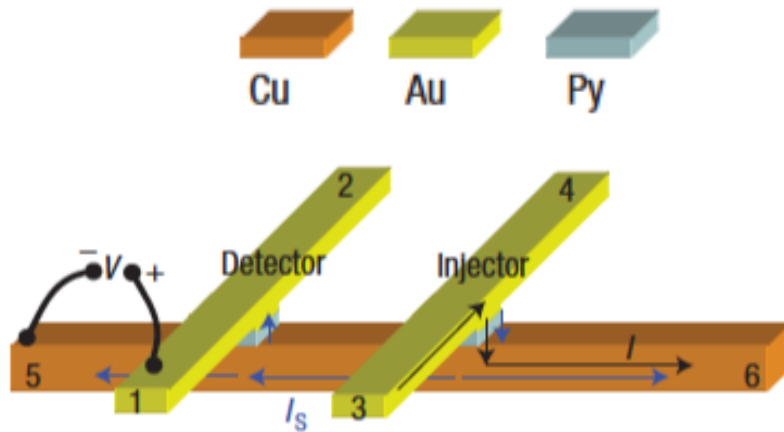


- ⇒ Landau-like magnetization pattern in the left Co element
- ⇒ Almost single-domain state in the right Co element

J. Mennig, D.E. Bürgler *et al.*, J. Appl. Phys. **111**, 07C504 (2012)

Pure spin current induced magnetization switching

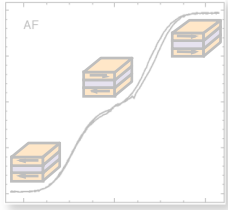
Injector and detector are Py nanomagnets ($80 \times 170 \text{ nm}^2$ and $75 \times 170 \text{ nm}^2$)



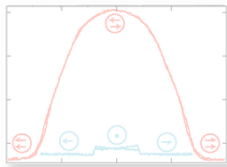
T. Yang *et al.*, Nature Physics 4, 851 (2008)

Overview

Introduction



Interlayer exchange coupling



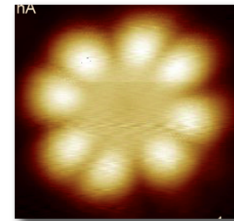
Giant and tunneling magnetoresistance



Current-induced magnetization dynamics



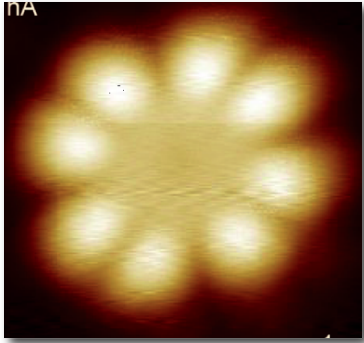
Pure spin current



Magnetic molecules

Conclusions

Outline: Magnetic molecules



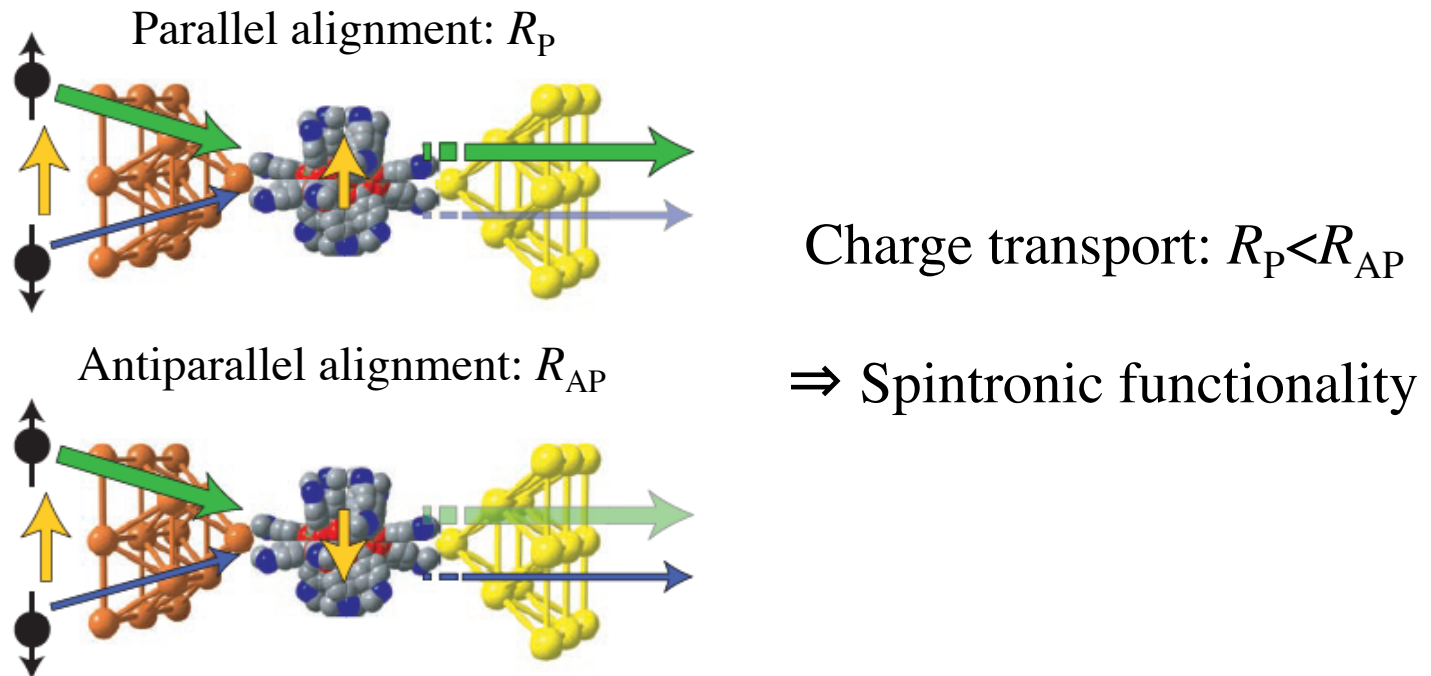
- Why magnetic molecules?
- Challenges of the interface between molecule and substrate/electrode
- Example: Nd phthalocyanine double-decker (NdPc_2) molecules on $\text{Cu}(100)$

Molecular spintronics

Combines molecular electronics and spintronics
to exploit the rich diversity and functionality of molecules and
the spin degree of freedom for novel nanoelectronic device concepts

Example of spintronic functionality:

SMM in ferromagnet/non-magnet junction



L. Bogani und W. Wernsdorfer, Nat. Mat. 7, 179 (2008)

Realization of molecular spintronics

Molecules need to be supported

- How do molecules adsorb on surfaces?
 - Do they decompose upon deposition?
- What is their adsorption geometry and site?

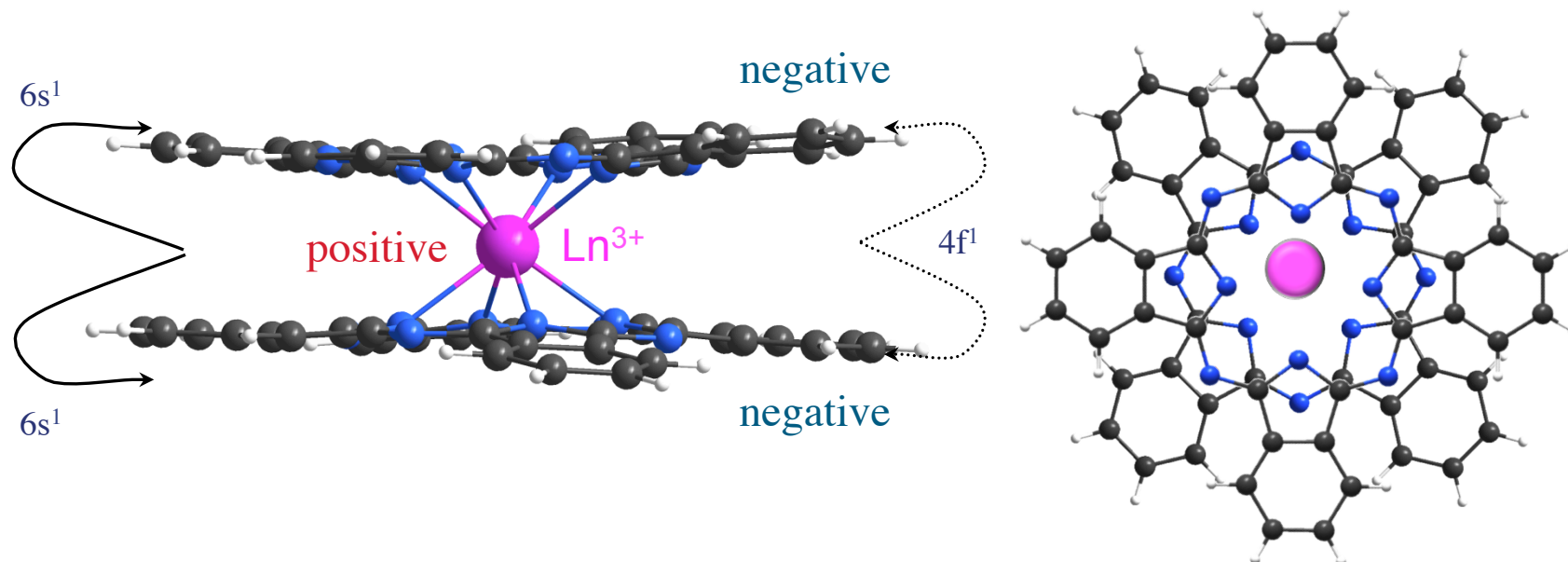
Adsorption properties on substrates

Molecules need to be electrically contacted

- Role of metal-molecule interaction?
- Impact of metal-molecule hybridization?
- Impact of metal surface on magnetic moment?
- Do the “magnetic” orbitals contribute to charge transport?

Electronic structure of adsorbed/contacted molecules

Lanthanide double-decker phthalocyanines (LnPc_2)



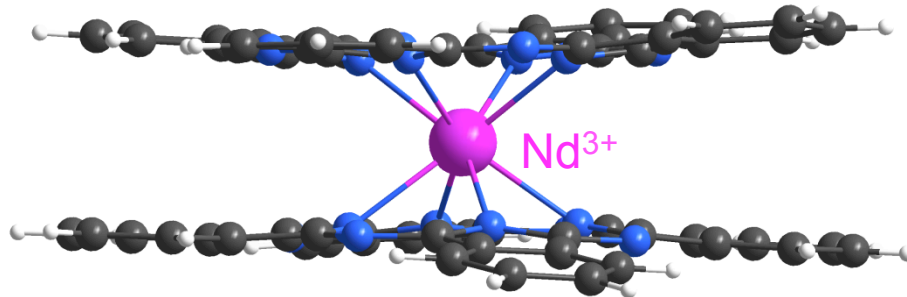
- Intramolecular interaction between the Pc ligands and the central Ln ion is mainly of electrostatic nature
- Relative angle of 45° between the two Pc ligand
- Some LnPc_2 , e.g. TbPc_2 , DyPc_2 , and HoPc_2 [1,2] are known to be SMMs with blocking temperatures of several tens of Kelvin
- Accessing Tb 4f-states in TbPc_2 by STM is not possible [3]

[1] Ishikawa *et al.*, *J. Phys. Chem. B* **108**, 11265 (2004);

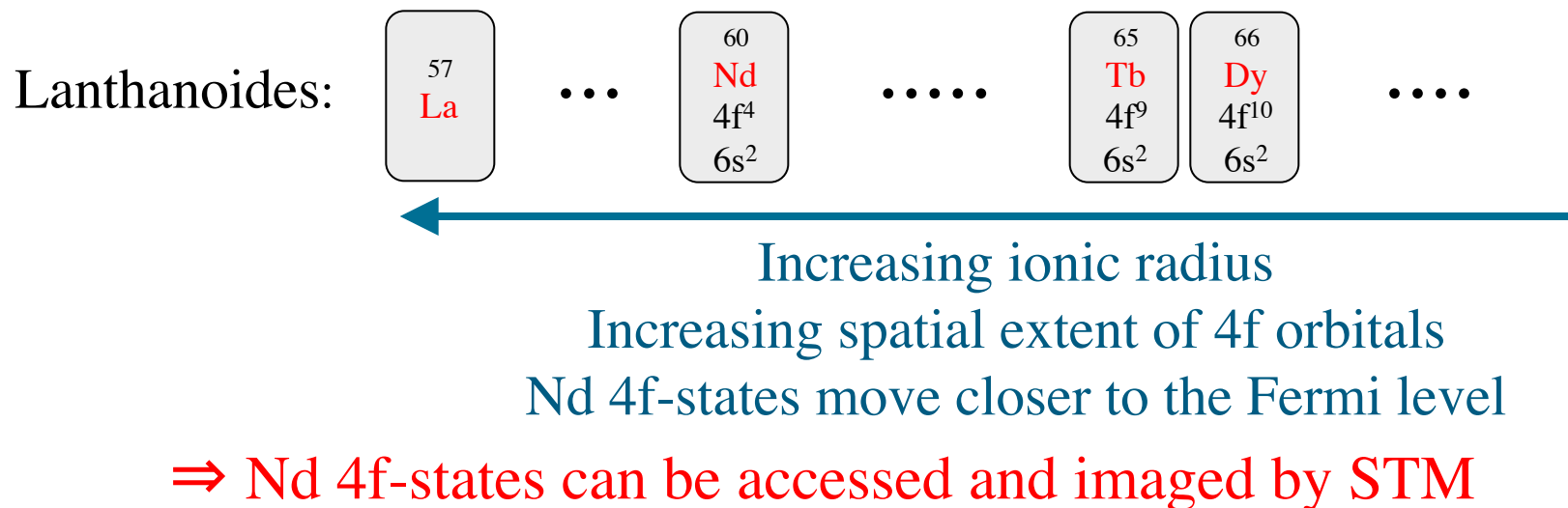
[2] F. Branzoli *et al.*, *J. Am. Chem. Soc.* **131**:4387 (2009); [3] Schwöbel *et al.*, *Nat. Commun.* **3**, 953 (2012)

“bis(phthalocyaninato)-neodymium(III)”

Neodymium double-decker phthalocyanine (NdPc₂)

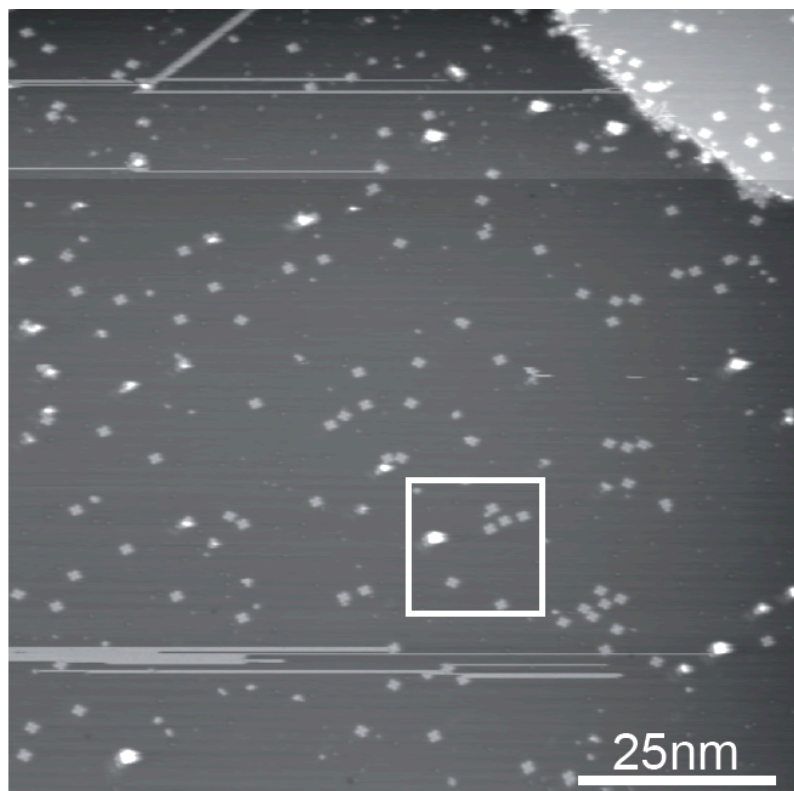


- NdPc₂ is a promising SMM, but has not examined under this aspect

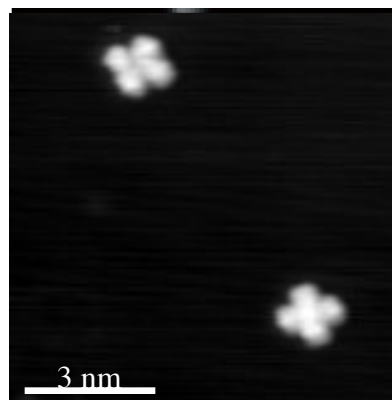


NdPc₂ on Cu(100)

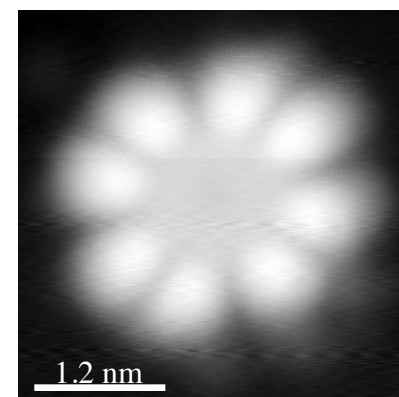
- Molecules sublimated at 850 K
metal substrate held at 300 K
- STM in UHV and at 4 K; etched W tips
- Bias voltage modulation (30 mV, 2.7 kHz)
for dI/dV -spectra and dI/dV -maps



low  high



Single-decker



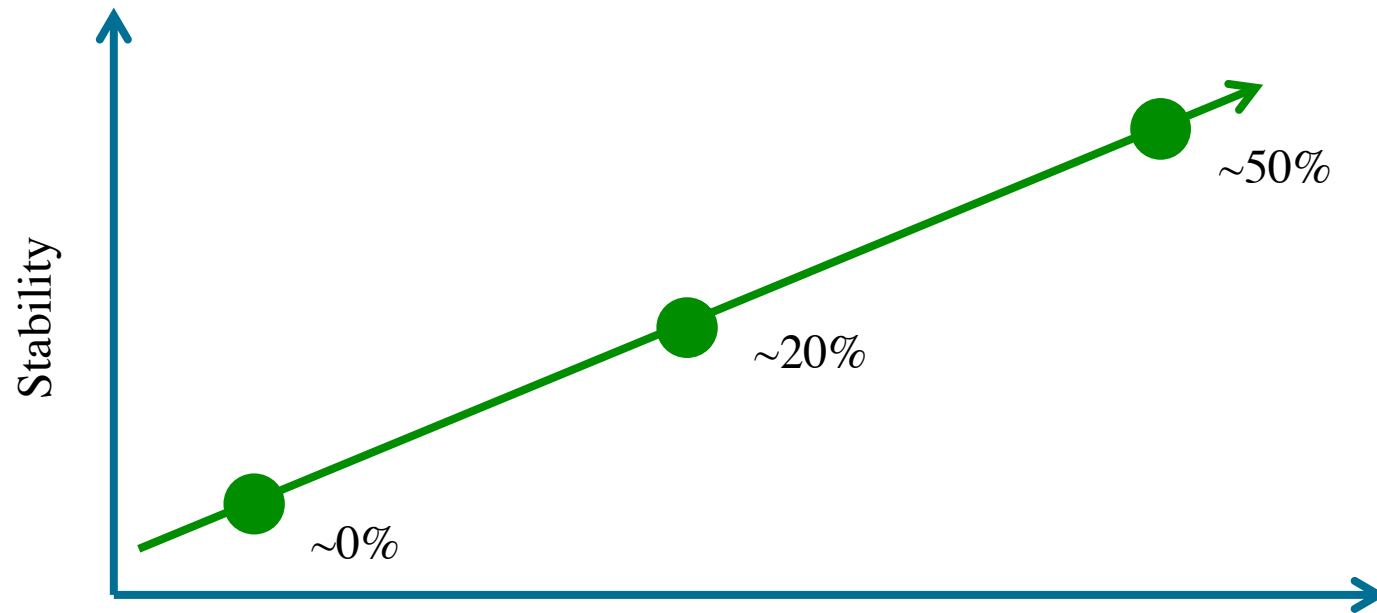
Double-decker

2 types of molecules, each in 2 orientations:

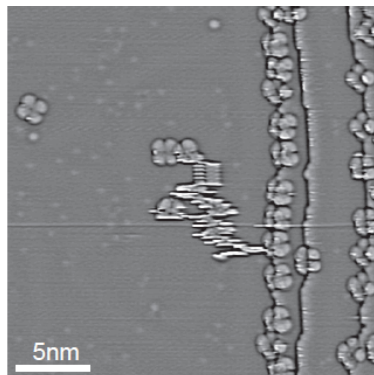
⇒ Double-decker (NdPc₂) and single-decker (NdPc, Pc)

⇒ NdPc₂ molecules break up upon deposition

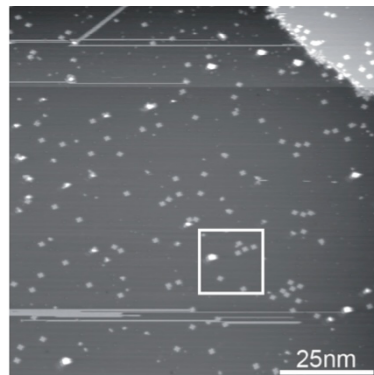
Substrate dependent adsorption



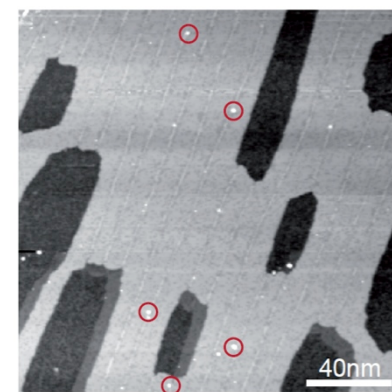
Au(111)



Cu(100)



Fe/W



S. Fahrendorf, D.E. Bürgler *et al.*, SPIN 4, 1440007 (2014)

Substrate dependent adsorption and decomposition rate

Destabilizing contributions:

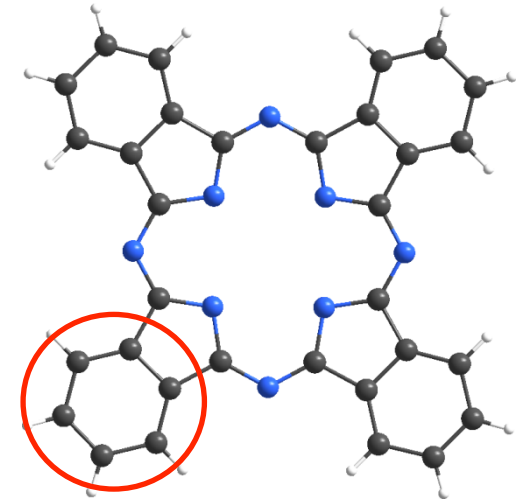
- Thermal energy in the crucible (~ 70 meV)
- Kinetic energy (~ 70 meV)
- Adsorption energy (substrate dependent):

Benzene as model system:

- Benzol on Au(111) : -0.55 eV [1]
- Benzol on Cu(100) : -0.68 eV [2]
- Benzol on Fe/W(110) : -0.98 eV [3]

⇒ Adsorption energy is dominant and depends on the substrate material

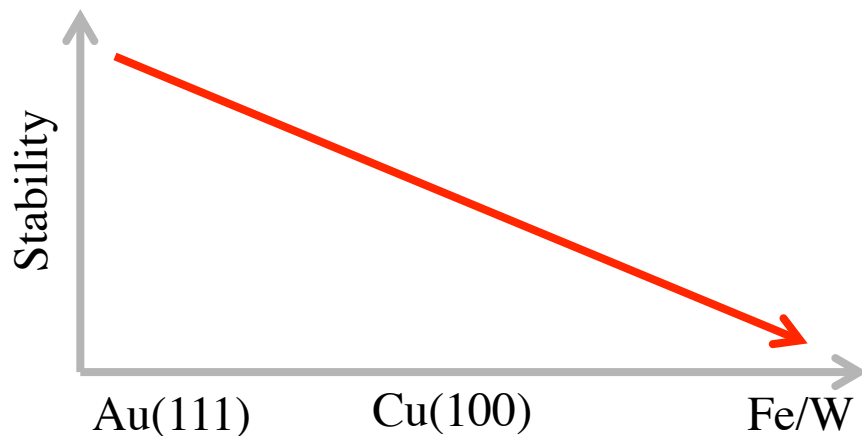
- [1] K. Toyoda *et al.* Surface Science **603**, 2912(2009);
[2] N. Lorente *et al.* Phys. Rev. B **68**, 155401 (2003);
[3] N. Atodiresei *et al.* Phys. Rev. B **84**, 172402 (2011)



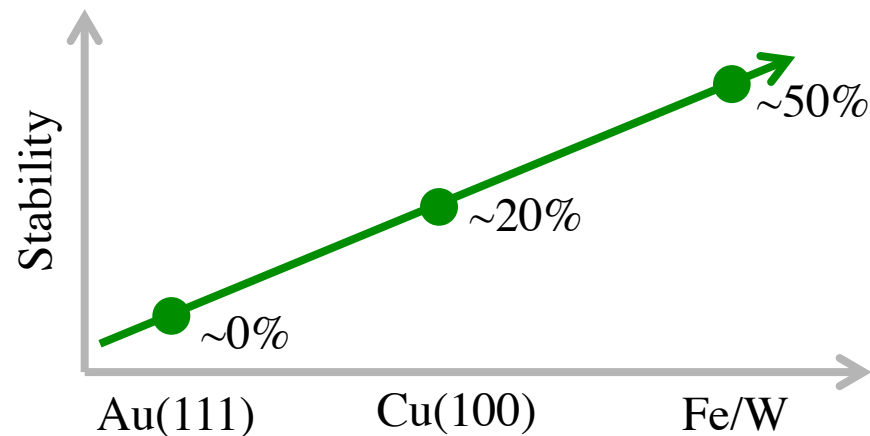
benzene-like

Substrate dependent adsorption

Expected trend

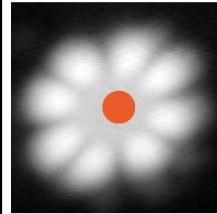
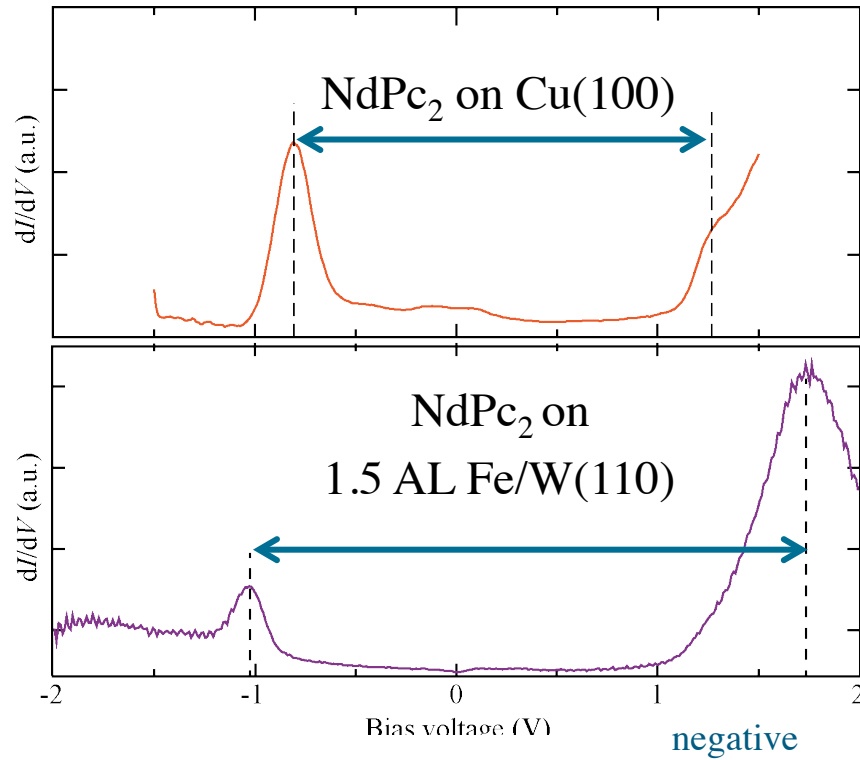


Measured trend

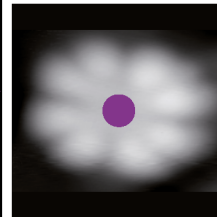


What mechanism stabilizes the molecules
on more reactive surfaces?

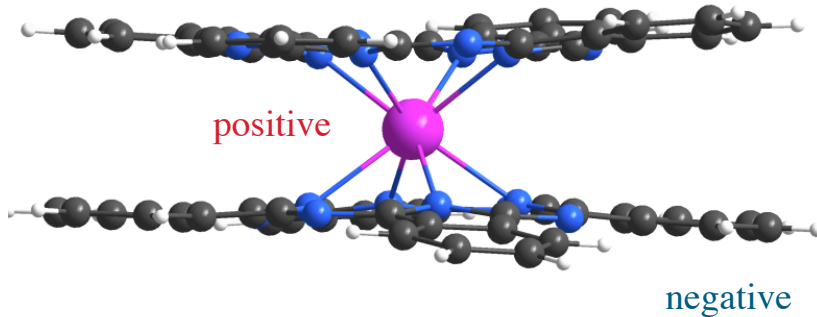
Stabilizing mechanism



Larger bonding-antibonding splitting for NdPc₂ on Fe/W



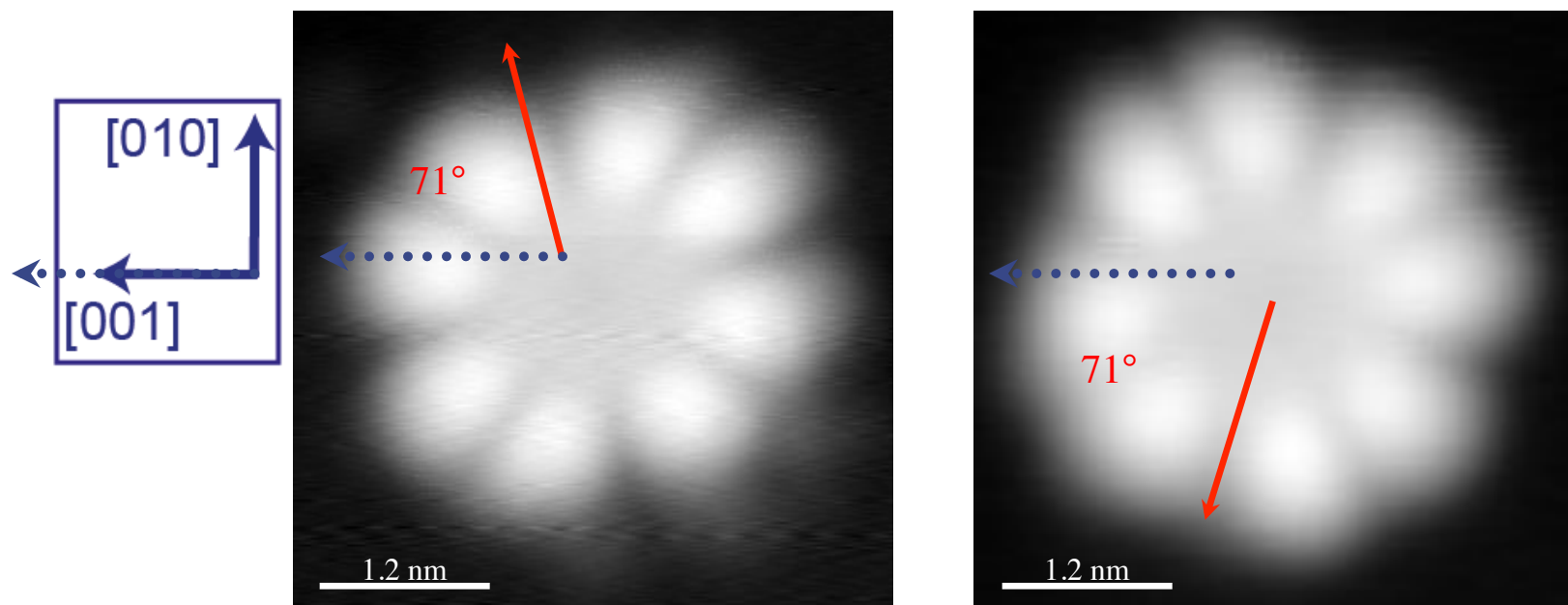
⇒ Stronger intramolecular bonding



Stronger interaction with substrate
⇒ Enhanced charge transfer to the molecule, i.e. the lower Pc
⇒ Increased stability of the molecule

S. Fahrendorf, D.E. Bürgler *et al.*, SPIN 4, 1440007 (2014)

Double-decker NdPc₂ on Cu(100)

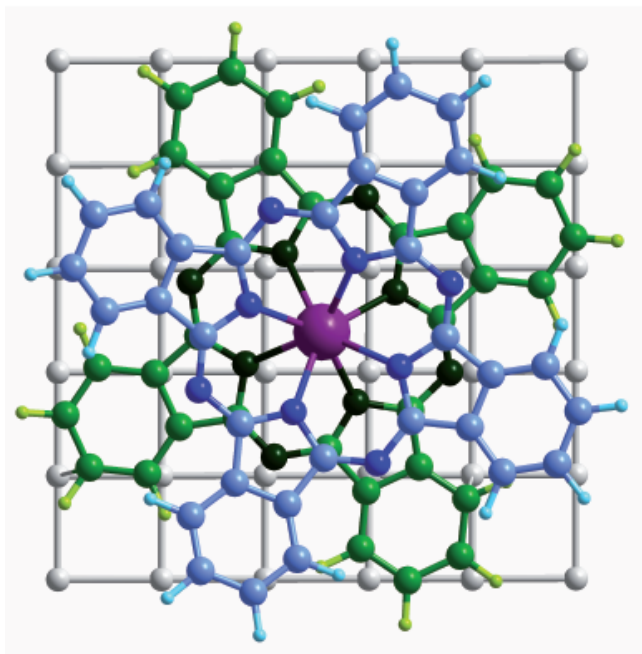


Upper ligand is imaged and its axes are rotated with respect to [001] axis by $\pm(71\pm 2)^\circ$

Consider twist between ligand Pc: $\pm(26+45)^\circ = \pm 71^\circ$

\Rightarrow Absorption position is determined by the binding of lower Pc to the substrate

NdPc₂ on Cu(100): Calculations



- NdPc₂ on 5 layer of Cu
- GGA+U calculations ($U=2.2$ eV)
- Including van-der-Waals forces

Optimized and relaxed structure:

- NdPc₂ center above Cu hollow site
- Two symmetric and degenerate positions

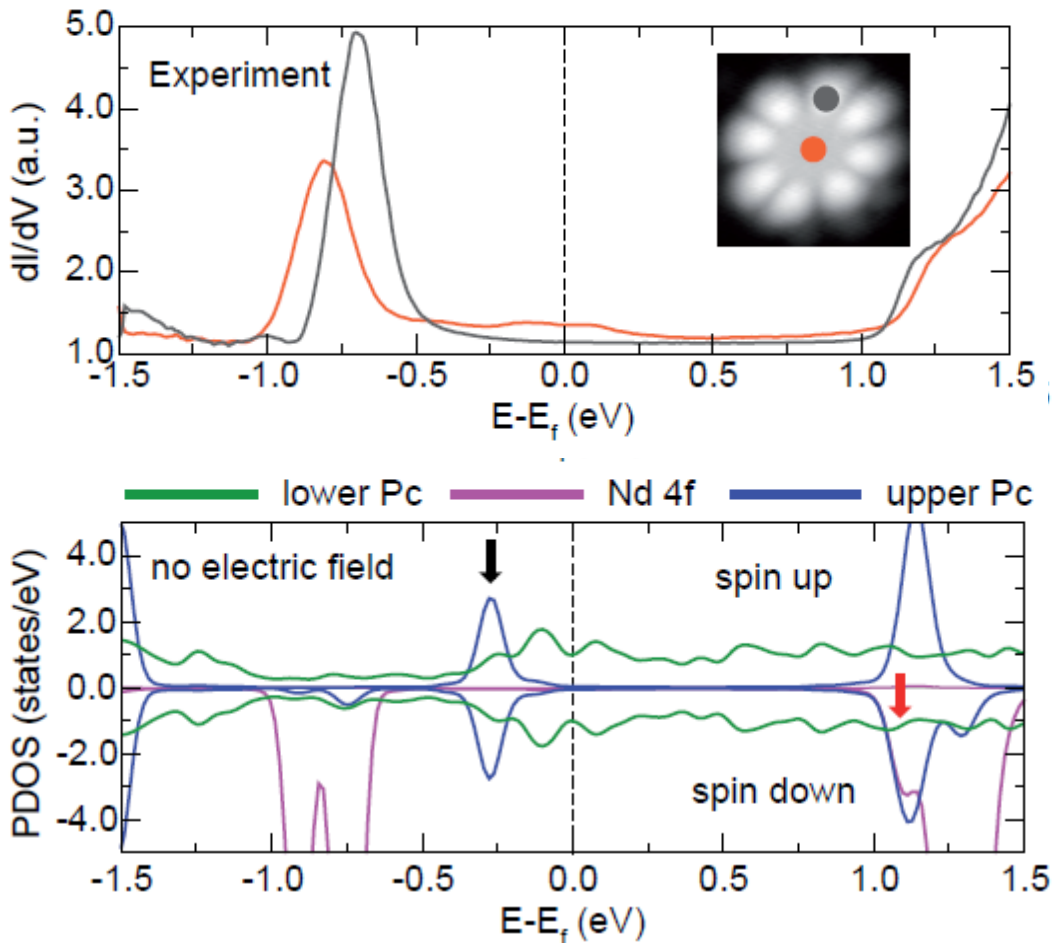
We calculate:

- Contours of constant DOS
- Local DOS versus V
- Maps of DOS at given V_{bias}

We measure:

- > STM topography
- > dI/dV -curves
- > dI/dV -maps at V_{bias}

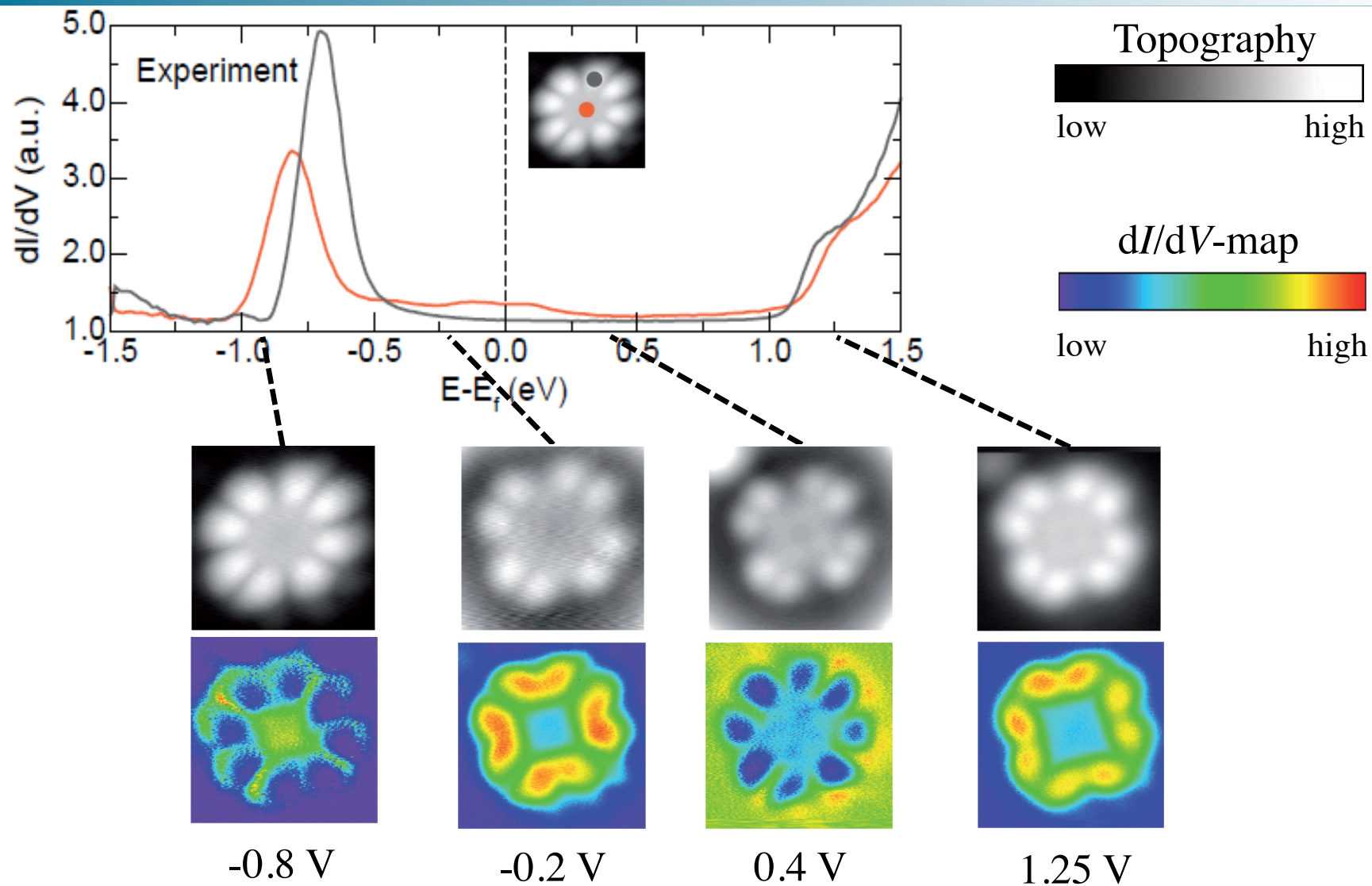
NdPc₂ on Cu(100)



- ⇒ Direct detection of spin-polarized 4f-states
- ⇒ Lower Pc strongly hybridizes with substrate
- ⇒ Upper Pc keeps sharp molecular-type states

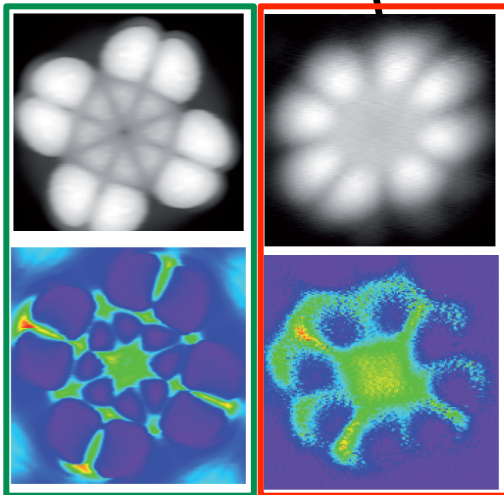
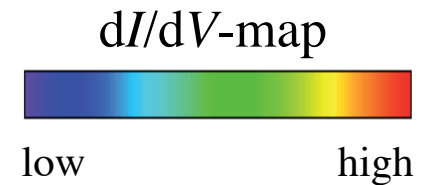
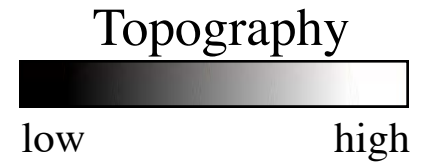
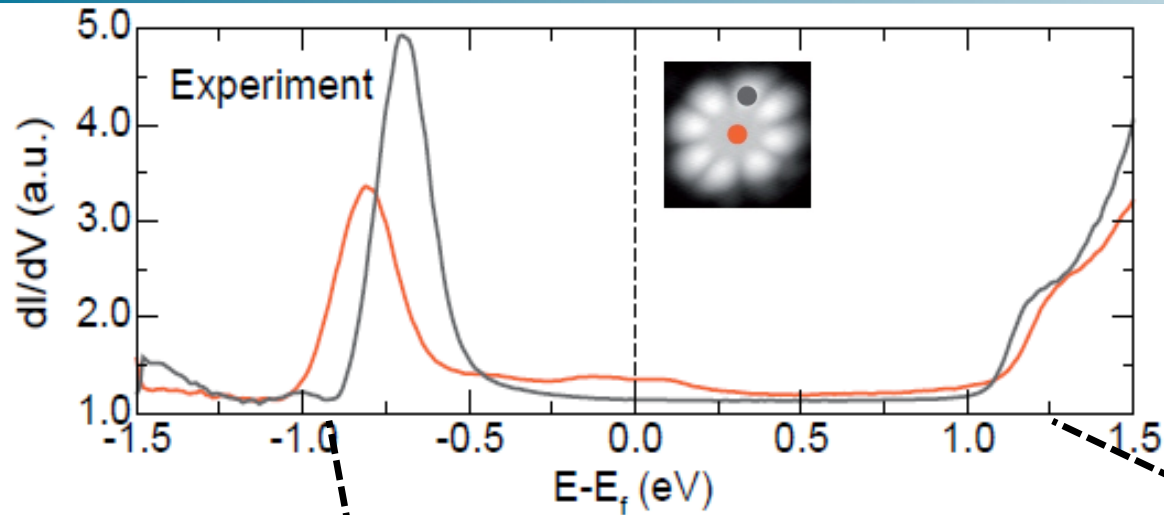
S. Fahrenndorf, D.E. Bürgler *et al.*, Nature Commun. 4, 2425 (2013)

NdPc₂ on Cu(100)



S. Fahrenndorf, D.E. Bürgler *et al.*, Nature Commun. 4, 2425 (2013)

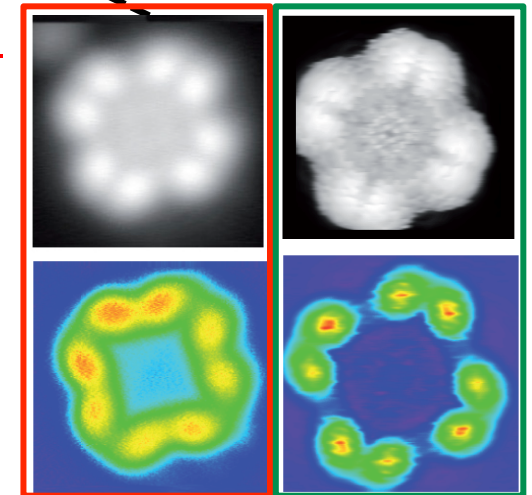
NdPc₂ on Cu(100)



Theory / Experiment

⇒ Direct detection of spin-polarized Nd 4f-states by STM

⇒ Prospects for electrical manipulation/detection of molecular spin



Experiment / Theory

S. Fahrenndorf, D.E. Bürgler *et al.*, Nature Commun. 4, 2425 (2013)

The “History” of Spintronics

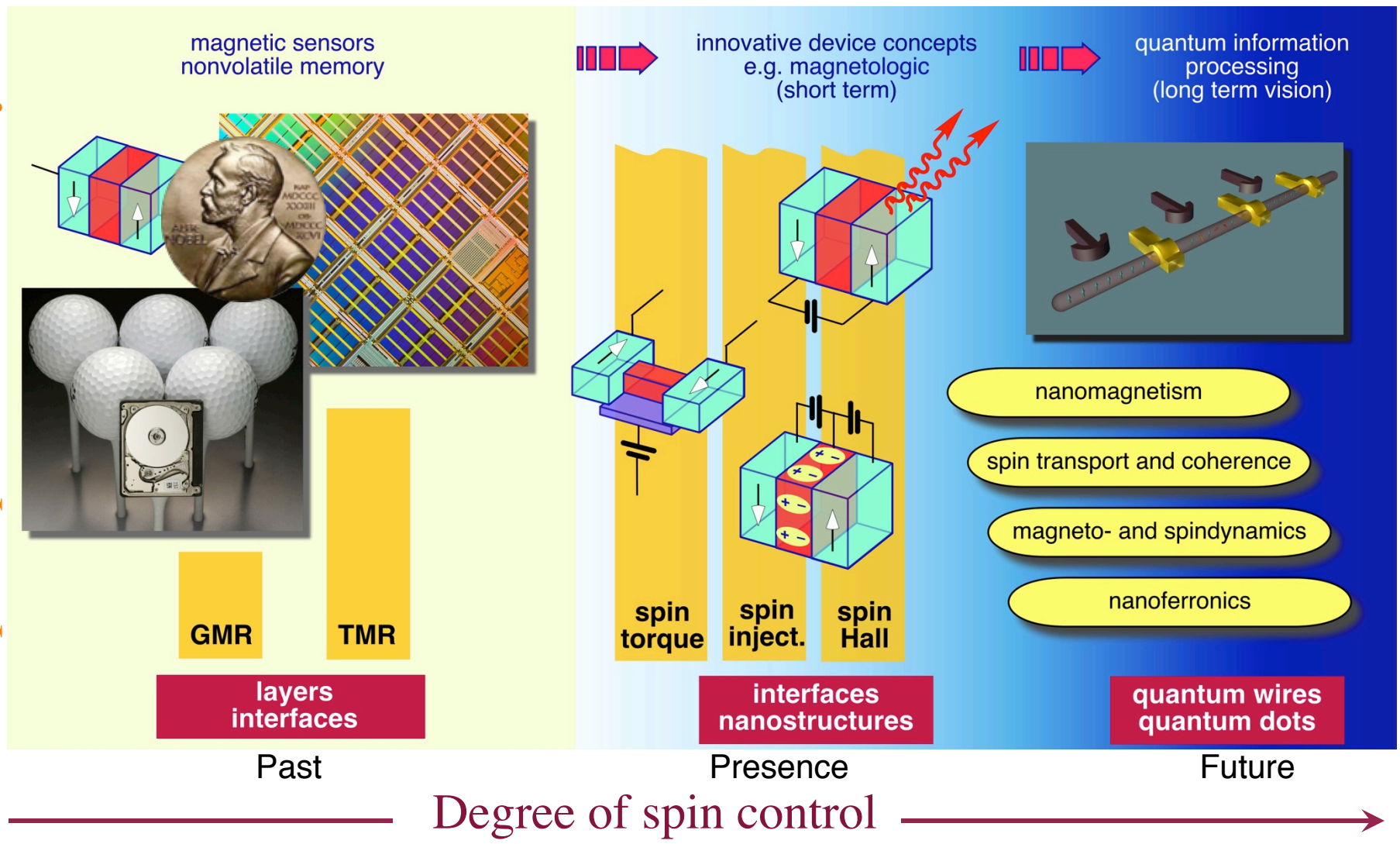
- 1986 Discovery of magnetic interlayer exchange coupling (Grünberg)
- 1988 Discovery of GMR (Grünberg, Fert)
- 1995 Realization of TMR at room temperature (Miyazaki, Moodera)
- 1996 Prediction of spin-transfer effects (Slonczewski, Berger)
- 1998 First commercial harddisks with GMR sensors (IBM)
- 2000 Experimental observation of spin-transfer effects (Cornell)
- 2001 Commercial harddisks with AFC media (IBM)
- 2004 Giant TMR across epitaxial MgO barriers (Parkin, Yuasa)
- 2006 Commercialization of MRAM based on TMR (Freescale)
- 2007 Demo: MRAM based on giant TMR and spin-transfer (Hitachi)

... short transfer times from basic research to
applications in mass markets

... there is more to come: *e.g.* quantum information technology

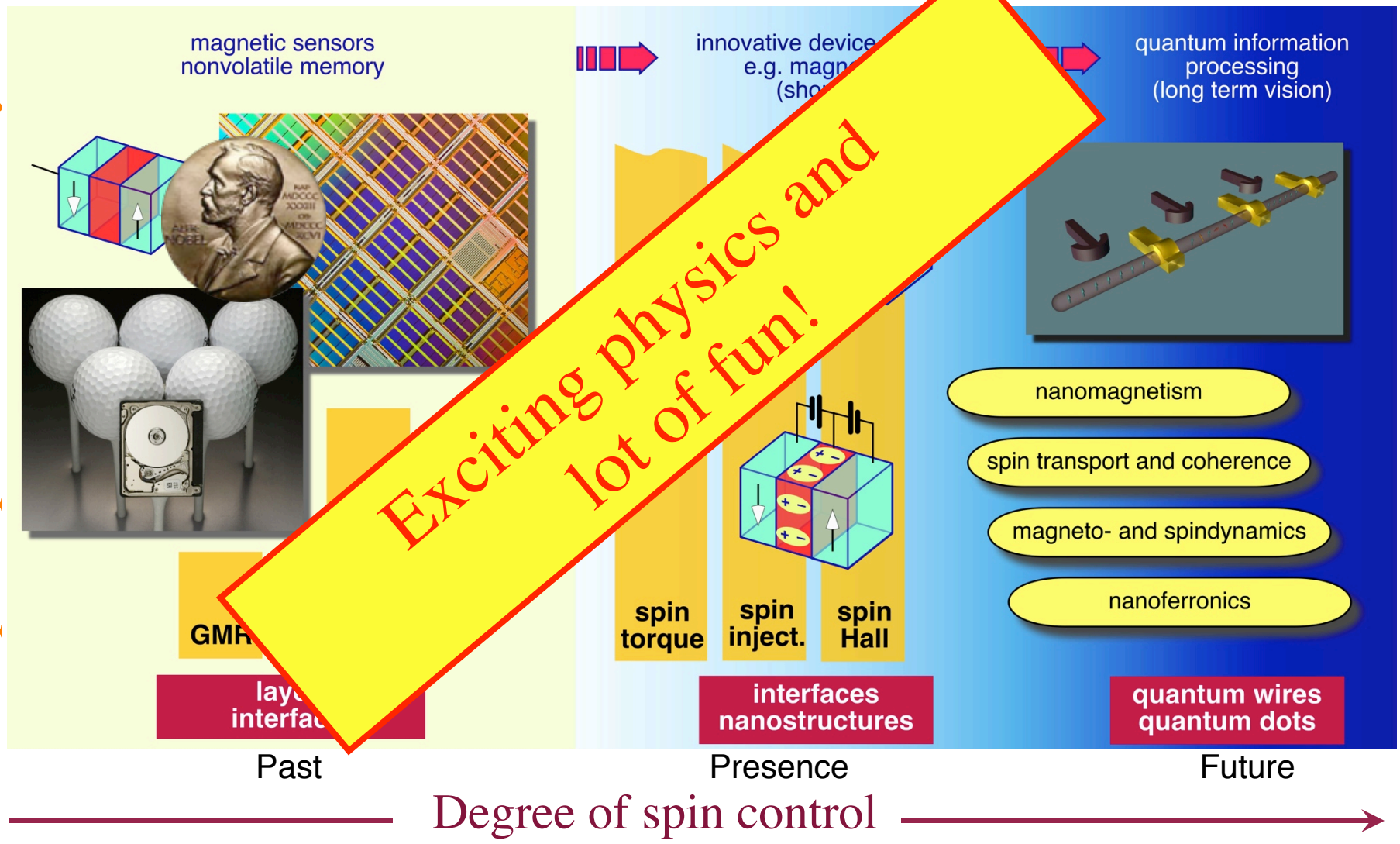
Future of Spintronics

Spin-dependent functionality



Future of Spintronics

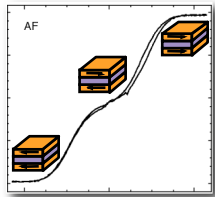
Spin-dependent functionality



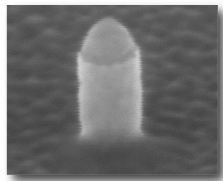
Take-home message

Spintronics relies on **manipulating and detecting magnetization states** of nm-sized FM objects

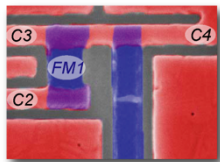
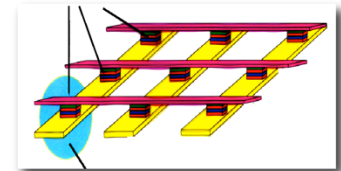
Spin-transfer processes enable such functionalities:



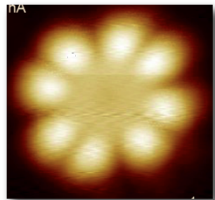
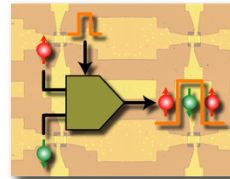
- Established: **GMR** and **IEC** in HDD



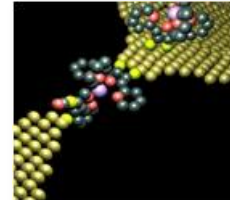
- Currently: **Spin-transfer torque** in MRAMs



- Future: **Pure spin currents** in low-dissipation devices



- Future: **Magnetic molecules** in molecular transistors and in artificial neuronal magnetic networks



Thanks ...

- Sarah Fahrendorf, Julius Mennig, Saban Tirpanci, Frank Matthes, Peter Grünberg, Claus M. Schneider (FZ Jülich)
- Ronald Lehndorff (now Sensitec Mainz Germany)
- Volker Sluka, Alina Deac (now Helmholtz-Zentrum Rossendorf)
 - Zbigniew Celinski (Colorado Springs, USA)
 - Sebastian Gliga, Attila Kákay (FZ Jülich)
 - Riccardo Hertel (now CNRS Strasbourg, France)
- Claire Besson, Paul Kögerler (RWTH Aachen and FZ Jülich)
- Nicolae Atodiresei, Vasile Caciuc, Stefan Blügel (FZ Jülich)